SYNTHESIS OF BIO-LUBRICANT BASE STOCKS FROM WASTE OIL

Thesis submitted in partial fulfilment of the requirements for the degree of

DOCTOR OF PHILOSOPHY

by

Atanu Kumar Paul

(Roll No.: 136107004)

Department of Chemical Engineering

Indian Institute of Technology Guwahati

Guwahati–781039

Assam, India

February 2022

SYNTHESIS OF BIO-LUBRICANT BASE STOCKS FROM WASTE OIL

Atanu Kumar Paul

DEDICATED

TO

MY PARENTS

DEPARTMENT OF CHEMICAL ENGINEERING

INDIAN INSTITUTE OF TECHNOLOGY GUWAHATI

STATEMENT

I do hereby declare that the content embodied in this thesis entitled "SYNTHESIS OF BIO-LUBRICANT BASE STOCKS FROM WASTE OIL" is the result of investigations carried out by me at Department of Chemical Engineering, Indian Institute of Technology Guwahati, Guwahati, India, under the guidance of Prof. Vaibhav V. Goud. In keeping with the general practice of reporting scientific observations, due acknowledgements have been made wherever the work described is based on the findings of other investigators.

Atanu Kumar Paul

Date: 28.02.2022

Atanu Kumar Paul

DEPARTMENT OF CHEMICAL ENGINEERING

INDIAN INSTITUTE OF TECHNOLOGY GUWAHATI

CERTIFICATE

This is to certify that the thesis entitled **"SYNTHESIS OF BIO-LUBRICANT BASE STOCKS FROM WASTE OIL"** submitted by **Mr. Atanu Kumar Paul (Roll No.: 136107004)**, a research scholar in the Department of Chemical Engineering, Indian Institute of Technology Guwahati, for the award of the degree of Doctor of Philosophy, is a record of the original research work carried out by him under my supervision and guidance. The thesis has fulfilled all requirements as per the regulations of the institute and in my opinion has reached the standard needed for submission. The work documented in this thesis have not been submitted to any other University or Institute for the award of any degree.

Prof. Vaibhav Vasant Goud

Professor
Department of Chemical Engineering
Indian Institute of Technology Guwahati
Guwahati - 781039, Assam, India.

Date: 28.2.22

Acknowledgements

I consider myself blessed to have an incredible journey of Ph.D. at Indian Institute of Technology Guwahati (IIT Guwahati). This was all made possible by the guidance, motivation and love of a lot of people who hold immense value in my life.

First and foremost, I would like to express my deepest gratitude to my supervisor Professor Vaibhav V. Goud, for his continuous support during my Ph.D. studies and research, for his patience and motivation, and for imparting his immense knowledge. Also, I would like to thank Prof. Goud for giving me this golden opportunity to work in his laboratory and take care of all the facilities to carry out my research. His guidance helped me throughout the time of my research and my writing of this thesis. His suggestions, encouragement and support were crucial to the completion of my Ph.D. thesis. Without his precious support, it would not be possible to complete this research. I am grateful for his advice, great ideas and scientific discussions, which are part of this thesis. Being a part of the Bioenergy research group is an invaluable learning experience for me both scientifically and personally. The tremendous support, valuable suggestions, and encouragement are the main factors behind shaping my thesis work.

I would also like to thank Prof. Jaya Narayan Sahu of the University of Stuttgart in Stuttgart, Germany (abroad examiner) and Prof. Satya Narayan Naik of the Indian Institute of Technology Delhi in Delhi, India (Indian examiner) for their thorough assessment of my thesis and insightful suggestions. I would also like to extend my gratitude to the members of my Doctoral Committee, Prof. Vimal Katiyar (Chairman), and Prof. Kaustubha Mohanty of the Department of Chemical Engineering, and Prof. Debasish Das of the Department of Biosciences & Bioengineering, for their valuable suggestions throughout this journey. Also, I want to extend my thanks to the members of the comprehensive examination committee, Prof. Kaustubha Mohanty, Prof. Mahuya De, and Dr. Pankaj Tiwari, for their constructive evaluation. I want to thank the present

and former Heads of the Department, Prof. Vijay S. Moholkar, Prof. Bishnupada Mandal, and Prof. Anugrah Singh, and other faculty members for their support and guidance. Also, I want to thank the technical and non-technical staff of our department for helping me in numerous ways and making my life easy in the department. I would also like to express my gratitude to Prof. Aloke Kumar Ghoshal for supporting me in the initial days of my research work. I want to acknowledge the Department of Chemical Engineering, the Centre for Sustainable Polymers (formerly Centre of Excellence for Sustainable Polymers (CoE-SusPol)), the School of Energy Science and Engineering (formerly Centre for Energy), and the Department of Mechanical Engineering for providing the infrastructure needed for my research work. I would also like to acknowledge the Central Instrumentation Facility (CIF), IIT Guwahati, and Guwahati Biotech Park for providing high-end instruments to execute some of the experiments.

I also want to express my gratitude to my teachers, Prof. Kartik Chandra Ghanta, M.Tech. thesis supervisor at National Institute of Technology Durgapur (NIT Durgapur), Prof. Gopinath Halder, former head of the Department of Chemical Engineering at Durgapur Institute of Advanced Technology and Management (DIATM) and current head of the Department of Chemical Engineering at NIT Durgapur, Dr. Bimal Das, B.Tech. thesis supervisor at DIATM, and Prof. Ananta Kumar Das, former head of the Department of Chemical Engineering at DIATM, for their constant help and support.

I earnestly thank my seniors, juniors, interns, and labmates—Dr. Venu Babu Borugadda (thank you so much for everything), Dr. Swaroopa Rani Dasari, Dr. Amrita Difusa, Dr. Devendra Kumar Maravi, Dr. Garima Srivastava, Dr. Narendra Naik Deshavath, Dr. Dipsikha Kalita, Dr. Dipesh Kumar, Dr. Machhindra S. Bhalerao, Ms. Sutapa Das, Mr. Sukumar Purohit, Ms. Nongmaithem Debeni Devi, Dr. Mood Mohan, Mr. Abebe Moges, Mr. Pravin G. Suryawanshi, Mr. Sajan Babhare,

Ms. Kakali Borah, Dr. Jyoti Kainthola, Ms. Rituparna Addy, Mr. Prasenjit Barman, Ms. Pushpita Das, Mr. Rupjyoti Bhuyan, Mr. Tapan Sharma, Mr. Akash, Mr. Ankit Patidar, Mr. Vikas Kumar, Mr. Rahul Tiwari, Mr. Ravichandra C. Patil, Mr. Omkar Desai, Mr. Shubham Jain, Mr. Rupesh Kumar, Ms. Sumee Sharma, Ms. Angana Chaudhuri, Ms. Shrishti Dewangan, Dr. Minakshi Gohain, Ms. Shipra Goswami, Dr. Ali Shemsedin Reshad, Dr. Amit Baran Das, Dr. Abhishek Shukla, Dr. Robinson Timung, and Mr. Chitta Ranjan Barik—for providing a collaborative research environment. I sincerely appreciate the help, guidance, and love received from all of them.

I would like to thank all my batchmates—Dr. Gourhari Chakraborty, Dr. Basudhrity Banerjee, Dr. Narendren S., Dr. Shasanka Sekhar Borkotoky, Dr. Randeep Singh, Dr. Monika, Dr. Melaku Tesfaye, Dr. Pallab Das, Dr. Babul Prasad, Ms. Medha Mili, Dr. Kibrom Alebel Gebru, Dr. Abdisa Jabesa, Dr. Anand Bharti, Dr. Badri Vishal, Dr. Geeta Kumari, Dr. Jitendra Singh Rawat, Dr. Maneesh Poddar, and Dr. Pavan Krishna Kanchi—with whom I have spent a wonderful time here at IIT Guwahati. From academic conversations to recreational activities, we have been there for each other always.

I want to thank all the individuals who supported me throughout my time at this institute and contributed significantly to the outcome of this dissertation; their time and effort are greatly appreciated. I am immensely thankful to all these people and others who have made my stay in Guwahati a memorable and enjoyable journey. I thank them all for being there for me always and for providing an amicable work environment.

I would like to give my special thanks to the team members of the group "১৩ পার্বণ Tero Parbon, IIT Guwahati", "LUBDHAK" (Bengali performing arts group), Advaya (PG cultural fest of IITG), and Cobra Seven (cricket team of Brahmaputra hostel) which kept me active and happy in many ways during my stay in IITG.

My next thanks go to my alma mater, IIT Guwahati, which gave me an opportunity to embark on this delicate endeavour of learning with ample facilities and with an equally enchanting bounty of nature which I experienced throughout the Northeast of India. I am so overwhelmed by the beauty of this campus that I have no words to describe it.

Next, I would like to thank the funding agencies that provided me with the financial support to conduct my research. I am grateful to the Ministry of Education (formerly Ministry of Human Resource Development (MHRD)) for the fellowship during my Ph.D. studies.

"Freindshipp is beyond all relations of flesh and blood, because it is less materiall."—John Evelyn

I have been very fortunate to have some great friends; they are more likely to be my family. I would love to thank Sujoy da, Mandar da, Supriyo da, Suman da, Mitali di, Ardhendu da, Suman da (Saha), Biplab da, Arvind bhaiya, Rahul bhaiya, Rajkumar da, Chandan da, Riddhi di, Madhubanti di, Jayato da, Zunipa di, Anuj da, Biswajit, Shamik, Bubai, Richa, Runa, Abhishek, Bhaskar, Tatai, Arundhati, Tapas, Moumita, Tripti, Anand, Junior Bhaskar, Arunangshu, Abhradip, Tanushree, Rana, Dooradarshi, Jinat, Surabhi, Sushma, Kajal, Jinesh, Siddharth, Pradip, Barnali, Rima, Bhargav, Sohanbir, Saptarshi, Poulomee, and Sunandita, for their support, care, and love.

Finally, and most importantly, I would like to remember my parents and family for their never-ending love, support, and patience. It is their numerous personal sacrifices that have enabled me to reach this juncture in life. Simple thanks is not enough to convey my deep respect and gratitude towards my family.

Thanks to the Lord, the Almighty, for showering Her/His/Its grace on me at every step.

Atanu Kumar Paul

Abstract

Lubricants are oils that are often used in machines to reduce friction. Most lubricants and functional fluids in the present day are made entirely from petrochemical or mineral sources. Rising concerns about the environmental effects of mineral-based lubricants have prompted research into biodegradable lubricants. Vegetable oils have excellent biodegradability and rheological properties at higher operating temperatures, but poor cold flow characteristics. Several methods have been attempted to solve these technological challenges, including altering fatty acid structure and genetic modification. Bio-lubricant base stocks derived from waste soybean cooking oil and its methyl esters are ideal for hydraulic and transmission applications as an alternative to traditional lubricants. Three modelling methods, namely, Response Surface Methodology (RSM), Artificial Neural Network (ANN), and Genetic Algorithm (GA) have been applied to optimise the process parameters to maximise the product yield. Additionally, thermal degradation kinetics of the prepared product have also been attempted in this study.

Waste soybean cooking oil was used to prepare a bio-lubricant base stocks via structural modification of unsaturated fatty acids. An optimisation of the effect of process parameters on maximum oxirane oxygen content (OOC) was studied. Interaction among the process parameters, such as C=C bonds to H_2O_2 molar ratio, catalyst loading, and reaction time, was examined. Here, the main focus is to establish optimum OOC conditions using sulphuric acid (H_2SO_4) as the homogeneous acid catalyst. Optimum OOC of epoxidised waste soybean cooking oil (EWSCO) was found to be 4.69 mass % under the experimental conditions of 60 °C temperature, 6 h of reaction time, 1.5 g of catalyst loading and 1:2 molar

ratio of C=C bonds to H_2O_2 molar ratio. The formation of the resultant epoxide product was confirmed with the help of Fourier transform infrared (FTIR) spectroscopy (at 844 cm^{-1}) and nuclear magnetic resonance (NMR) spectroscopy (at δ = 2.8 to δ 3.1 ppm) analysis. ANN modelling and GA optimisation were also performed on identical data sets. According to the findings of this study, chemically modified WSCO derivatives could also be used as potential bio-lubricant base stocks.

Methyl esters of waste soybean cooking oil (WSCOME) were used to prepare bio lubricant base stocks via structural modification of unsaturated fatty acids (in situ epoxidation). Similar optimisation tools were used by WSCOME to predict the optimum conversion of unsaturated fatty acids to oxirane oxygen content (OOC). The optimum OOC of the epoxidised waste soybean cooking oil methyl esters (EWSCOME) was found to be 4.92 mass % under the experimental conditions of 60 °C temperature, 4.14 h of reaction time, 1.95 g of catalyst loading, and a 1:2.21 molar ratio of unsaturation to H_2O_2. The product formation (EWSCOME) was confirmed by FTIR spectroscopy and NMR analysis. After successful optimisation by the RSM technique, the ANN and GA methods were also applied to verify the optimum results.

Rheological properties were measured at temperatures ranging from 25–100 °C and shear rates ranging from 5–300 s^{-1}. The viscosity of epoxidised waste soybean cooking oil and its methyl esters showed Newtonian flow behaviour in the studied temperature range. Different shear rates (5–100 s^{-1}, 5–300 s^{-1}, 100–300 s^{-1}) were studied to understand the shear rate dependency of the oils. The dynamic viscosities of the EWSCO and EWSCOME were found to be dependent on fatty acid composition, unsaturation, and temperature. Based on the viscosity (EWSCO, 278 cSt; EWSCOME, 12 cSt) and viscosity index (EWSCO, 164;

EWSCOME, 151), it was deduced that the prepared epoxides could complement the standard lubricants (ISO VG) in the market.

Thermal characteristics and kinetics parameters of samples were determined by using a thermogravimetric analyser under non-isothermal conditions. Samples were prepared by increasing the temperature up to 800 °C at different heating rates of 10, 20, 30, and 50 °C/min, in an inert atmosphere of nitrogen. WSCO was found to be thermally stable up to 200 °C whereas WSCOME was thermally unstable up to 100 °C. The data showed that the degradation of the prepared bio-lubricant samples took place at temperatures ranging from 200–500 °C due to the breakage of the weak chemical bonds. The data obtained at various temperatures was used to calculate kinetic parameters such as activation energy (E) and pre-exponential factor (A) using three techniques: Friedman, Kissinger-Akahira-Sunose (KAS), and Flynn-Wall-Ozawa (FWO). The activation energies of WSCO, WSCOME, EWSCO, and EWSOME as determined by the above-mentioned methods were found to be 171, 51, 140, and 86 kJ/mol, respectively. The most probable model for the degradation of EWSCO agrees with the phase boundary controlled (contracting volume) (R3) model, and the thermal degradation process of EWSCOME responds to a mechanism involving phase boundary controlled (contracting area) (R2) model.

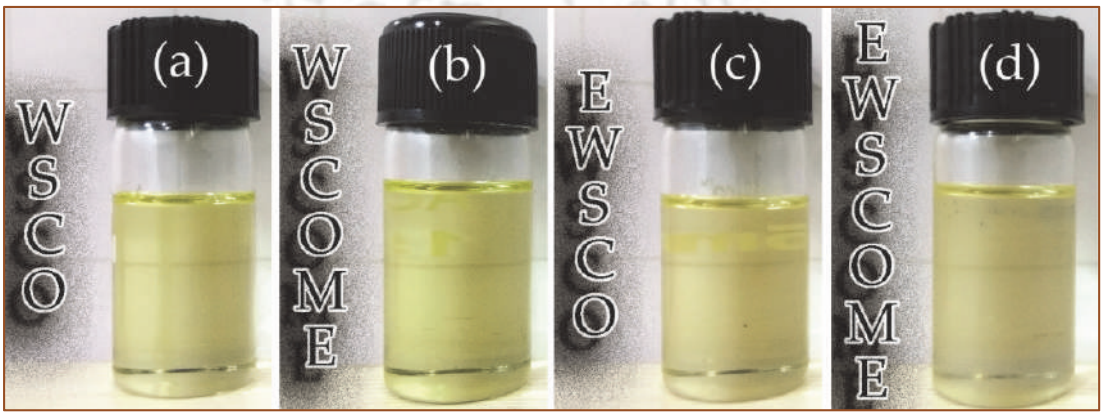

Prepared Bio-lubricant Base Stocks

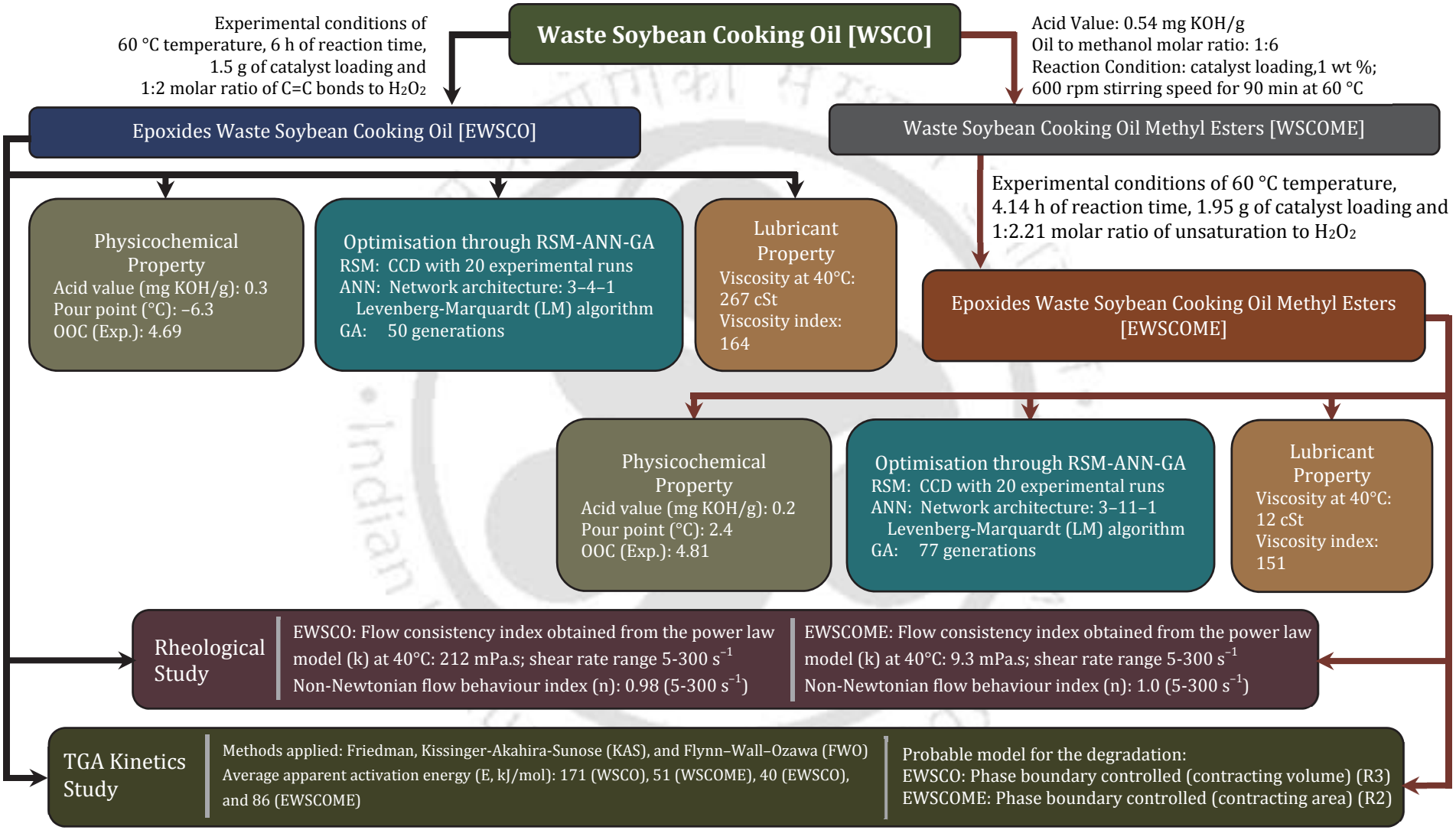

Graphical Abstract of PhD Thesis Work

Table of Contents

List of Tables

List of Figures

Chapter V

Chapter VI

Abbreviations

AIER — Acidic Ion Exchange Resin

ANN — Artificial Neural Network

ANOVA — Analysis of Variance

ARE — Average Relative Error

ASTM — American Society for Testing and Materials

AV — Acid Value

$Ba(OH)_2 \cdot 8H_2O$ — Barium Hydroxide Octahydrate

CAGR — Compound Annual Growth Rate

CCD — Central Composite Design

CH_3COOH — Glacial Acetic Acid

CV — Calorific Value

DMC — Double–Metal Cyanide

DOE — Design of Experiments

DSC — Differential Scanning Calorimetry

DTG — Differential Thermogravimetric

EABS — Sum of Absolute Errors

EC — Ethyl Cellulose

ERSO — Epoxidised Rapeseed Oil

ESBO — Epoxidised Soybean Oil

ESO — Epoxidised Soybean Oil

EWSCO — Epoxides of Waste Soybean Cooking Oil

EWSCOME — Epoxides of Waste Soybean Cooking Oil Methyl Esters

FAME — Fatty Acid Methyl Esters

FFA — Free Fatty Acid

FP — Flashpoint

FTIR — Fourier Transformed Infrared Spectroscopy

FWO — Flynn-Wall-Ozawa

GA — Genetic Algorithm

GCMS — Gas Chromatography–Mass Spectrometry

H_2O_2 — Hydrogen Peroxide

H_2SO_4 — Sulphuric Acid

HHV — Higher Heating Value

HOSBO — High Oleic Soybean Oil

HOSO — High Oleic Sunflower Oil

HSO — Hydrogenated Soybean Oil

HSR — High Shear Rate

HYBRID — Hybrid Fractional Error Function

IIT — Indian Institute of Technology

ISO VG — International Organization for Standardization Viscosity Grade

KAS — Kissinger-Akahira-Sunose

KBr — Potassium Bromide

KOH — Potassium Hydroxide

KV — Kinematic Viscosity

LSR — Lower Shear Rate

MPSD — Marquardt's Percent Standard Deviation

MSE — Mean Square Error

MW — Molecular Weight

NaOH — Sodium Hydroxide

NMR — Nuclear Magnetic Resonance

OOC — Oxirane Oxygen Content

OOT — Oxidative Onset Temperature

OS — Oxidative Stability

PE — Processing Elements

PP — Pour Point

RBOT — Rotary Bomb Oxidation Test

RI — Refractive Index

RMSE — Root Mean Square Error

RPVOT — Rotating Pressure Vessel Oxidation Test

RSM — Response Surface Methodology

RSSOT — Rapid Small Scale Oxidation Test

RT — Room Temperature

SAE — Society of Automotive Engineers

SBO — Soybean Oil

SD — Standard Deviation

TFATE — Trimethylolpropane Fatty Acid Triester

TFMO — Thin Film Micro Oxidation

TG — Thermogravimetric

TGA — Thermogravimetric Analysis

TMP — Trimethylolpropane

UFA — Unsaturated Fatty Acid

USA — United states of America

VI — Viscosity Index

WCO — Waste Cooking Oil

WCOFAME — Waste Cooking Oil Fatty Acid Methyl Esters

WLF — Williams-Landel-Ferry

WSCO — Waste Soybean Cooking Oil

WSCOME — Waste Soybean Cooking Oil Methyl Esters

Notations

A_i — Atomic Weight of Iodine

A_o — Atomic Weight of Oxygen

A_{OH} — Atomic Weight of Hydroxyl Group

$CDCl_3$ — Deuterated Chloroform

E — Activation Energy (kJ/mol)

f(α) — Temperature Independent Function of Conversion or The Reaction Model

G_{exp} — Experimental α–glycol Value

G_{the} — Theoritical α–glycol Value

IV_o — Initial Iodine Value

n — Order of Reaction Model

OO_{exp} — Experimental Oxirane Oxygen Content

OO_{the} — Theoretical Oxirane Oxygen Content

R — Gas Constant ($8.314\,J/mol/K$)

R^2 — Regression Coefficient

t — Time (min)

T — Temperature (°C)

T_f — Degradation Offset Temperature (°C)

T_o — Onset Temperature (°C)

T_i — Degradation Initiation Temperature (°C)

T_p — Maximum Degradation Temperature (°C)/ Temperature for Maximum Rate of Mass Loss

τ — Shear Stress (Pa)

γ — Shear Rate (s^{-1})

n — Non-Newtonian Flow Behaviour Index

β — Heating Rate (°C/min)

α — TGA Conversion of Oil/Bio-lubricant (wt %)

k — Flow Consistency Index Obtained from Power Law Model ($mPa.s^n$)

k_{exp} — Average Dynamic Viscosity Obtained from Experiment (mPa.s)

Units

% — Percentage

°C — Degree Centigrade

°C/min — Degree Centigrade Per Minute

cp — Centipoise

cSt — Centistoke

g — Gram

gI_2/100 g — Grams of Iodine Per 100 g

h — Hour

kg — Kilogram

kg/m^3 — Kilogram Per Cubic Metre

kHz — Kilo Hertz

kJ/mol — Kilo Joule Per Mole

m.Pa.s — Millipascal Second

m^3 — Cubic Metre

mg KOH/g — Milligrams of KOH Per Gram

min — Minute

MJ/kg — Mega Joule Per Kilogram

mL/min — Millilitre Per Minute

mw — Milliwatt

Pa.s — Pascal Second

vol % — Volume Percentage

wt % — Weight Percentage

µL — Microlitre

CHAPTER I

Introduction and Literature Review

Motivation

Current Scenario

Objectives

Thesis Organisation

Introduction and Literature Review

This chapter provides a quick overview to conventional lubricants, and the need for alternative lubricants as well as the limits of these alternatives. Aside from that, this section will cover the current state and future prospects of bio-lubricants in India, as well as data on potential renewable resources accessible in India and their application in a variety of areas (chemistry, chemical composition). Subsequently, the review focuses on some of the research and experimental work that relates to possible structural modifications for lubricant base oil production. Following this, a summary of the conclusions made in these studies will be providing further research direction, and the contribution of the research topic to the chosen field has been elaborated. Finally, the objectives and the organisation of this thesis are summarised.

1.1. Introduction

A steady increase in the use of eco-friendly consumer products like lubricants has occurred due to strict government regulations and increased public awareness for a pollution-free environment. There are wide ranges of lubricant base oils in current use, including mineral oils, synthetic oils, re-refined oils, and vegetable oils. Among these, mineral oils are the most commonly used—predominantly they consist of hydrocarbons, and also contain some sulphur and nitrogen compounds with traces of a number of metals. Due to their inherent toxicity and

non-biodegradable nature, they pose a constant threat to ecology and vast groundwater reserves (Lathi and Mattiasson, 2007).

In general, the chemical contamination of water has a remarkable negative influence on public opinion. Many coastal oil contamination instances have been recorded in recent years. For this reason, special attention is being paid to protecting the environment against pollution exerted by lubricants and hydraulic fluids originated from fossil fuels (Tornero and Hanke, 2016).

Industry and automobile sectors have been using lubricants extensively for their machinery and instruments, and as a result, the demand for lubricants is growing by 1.6% per year (Sharma and Dalai, 2013). Particularly, they consist of around 70–99% of base fluids (base stocks) and 30–1% of additives (to increase the performance properties). Currently, liquid lubricants, in the lubricant market, are the predominant form for various industrial and automotive applications. However, they are constantly being introduced into some distinct applications, such as hydraulic fluids, lubricants for the food industry, sewage treatment plants, and lubrication of maintenance equipment in some of the sensitive areas. Among various liquid lubricants, engine oils and hydraulic fluids are highly used and are in demand for specific requirements like thermo-oxidative stability, low-temperature properties, and a wide range of viscosity (Dave and Patel, 2017; Hwang and Erhan, 2006; Salimon et al., 2011; Salimon and Salih, 2010).

Due to these environmental threats, mineral-based lubricants are usually not considered as eco-friendly. Further, biodegradability has become one of the main parameters in both the selection of base stocks and the overall preparation of the

lubricants. Thus, replacing mineral base oils with eco-friendly products is one of the ways to decrease the unfavourable effects (low biodegradability) on the ecosystem caused by using traditional lubricants (Lathi and Mattiasson, 2007). Moreover, the lubricant industry has been trying to prepare biodegradable lubricants with better performance properties than those introduced from fossil resources. Thus, vegetable oils/plant seed oils and their esters are perceived to be alternatives to mineral oils for use as lubricant base oils due to certain inherent technical properties and biodegradable nature (Jain and Suhane, 2012). Compared to mineral oils, vegetable oils possess advantageous properties such as high viscosity index, high flash point, and low volatility. However, besides these positive impacts, vegetable oils also exhibit better tribological performance than conventional lubricants (Kodali, 2014). In addition, they show superior performance properties to conventional lubricants in terms of anti-wear and fatigue resistance, and also have good compatibility with fluid additives (Lathi and Mattiasson, 2007; Padmaja et al., 2012). Nevertheless, edible and non-edible oils cannot be used as lubricants directly in their present form due to poor low-temperature performance, and low oxidative and thermal stability (Anand and Chhibber, 2006). There are a number of methods to improve these undesired properties, such as genetic modification of fatty acid profile of vegetable oils, direct addition of antioxidants, viscosity modifiers, pour point depressant to vegetable oils, emulsification of vegetable oils, and chemical modification of vegetable oils (Nagendramma and Kaul, 2012; Salimon et al., 2010; Soni and Agarwal, 2014). Among these methods, chemical modification (Figure 1.1) is the most promising approach with great potential to improve significant

physico-chemical properties such as thermo-oxidative stability and pour point (McNutt and He, 2016).

Chemical modifications of vegetable oils without sacrificing favourable physico-chemical characteristics and lubricity include transesterification, hydroxylation with various alcohols such as methanol, 2-propanol, 1-butanol, and 2-ethyl hexanol (2-EH), hexanoylation with hexanoic anhydride, selective hydrogenation of polyunsaturated (C=C) fatty acids, and conversion of the unsaturated fatty acid to oxirane oxygen via epoxidation (Bepari et al., 2017; Borugadda and Dalai, 2018; Borugadda and Goud, 2019; Huang et al., 2017; Khodadadi et al., 2020). Among these, epoxidised oil received special attention due to the high reactivity of oxirane rings and a wide range of feasible reactions. This allows the synthesis of fully saturated esters with improved stability; hence, epoxidation is an innovative approach for the conversion of vegetable oils into useful bio-lubricant base stocks (Campanella et al., 2008; Erhan et al., 2008).

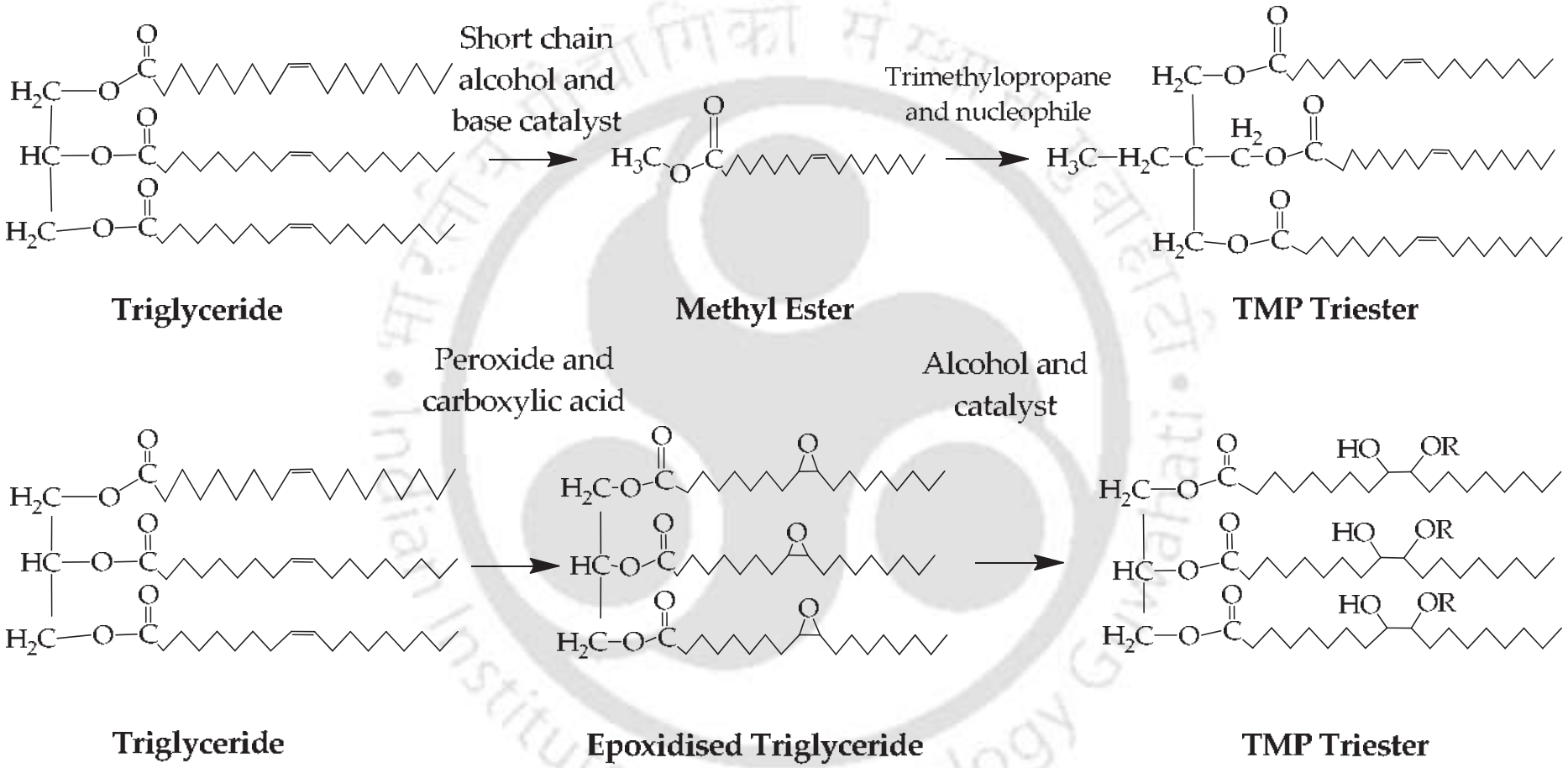

Figure 1.1. Reaction pathway of the chemical modification method a) esterification/transesterification, b) epoxidation/ring opening. Adapted from (McNutt and He, 2016).

In most instances, edible oils have been used for epoxide synthesis; however, they are also a part of the human nutrition chain and are not economical for commercialisation. Hence, low-priced raw materials, such as used/waste cooking oils, can be considered as a promising alternative to substitute the edible refined oils (Luque and Melero, 2012). In India, production of bio-lubricant from non-edible oilseeds has vast potential due to the huge production of WCO annually and of other non-edible oils such as Karanja (*Pongamia pinnata)*, Neem (*Melia azadirachta)*, Mahua (*Madhuca indica)*, Linseed (*Linium usitatissimum*), Castor oil (*Ricinus communis*), and Rice bran oil (*Oryza sativa*)(Czerwik-Marcinkowska et al., 2020; Karmakar et al., 2021; Le et al., 2018; Reshad et al., 2015; Talaghat et al., 2020). In a developing country like India, bio-lubricants are being given serious consideration as future potential energy sources. Few selected reports in the literature (Zhang et al., 2020) showed a green and efficient strategy for preparing octylated branched bio-lubricant from waste cooking oil (WCO). The esterification of unsaturated fatty acids (UFAs) with 2-ethylhexanol using substrates (*Candida sp.* 99-125) was carried out, for which the reaction scheme is shown in Figure 1.2. The obtained product showed excellent lubricant properties, such as a low pour point of -61 °C, high viscosity index of 149, and high thermal-oxidation stability (onset temperature of 326 °C and oxidative onset temperature of 312 °C). Another study reported that the conventional mineral oil-based lubricants could be substituted by bio-lubricants prepared from vegetable oils that have high oleic acid content (Mungroo et al., 2008). Thus, chemical modification of double bond (unsaturation) offers an appropriate method for producing commercial value-added fuels, chemicals, and lubricants from renewable raw materials (Borugadda et al., 2017). Figure 1.3 shows the molecular structure of a typical triglyceride molecule for structural modification via

epoxidation to prepare bio-lubricant base stocks. This allows the production of fully saturated esters with improved stability against oxidative attack and thus is an innovative approach for converting native oils, including the epoxidised oil, into useful base fluids for lubricants.

Furthermore, due to high price of virgin oils, the end product price also remains high. Therefore, in order to minimise the end product cost, non-edible oils and waste oils which do not have any commercial value in the market can be used to prepare lubricant base stocks. Hence, the present study was proposed with the intention of modifying the fatty acid structure to formulate lubricant base oil with improved performance properties. Prepared lubricating oil from renewable sources is also known as bio lubricant base oils, due to its biodegradable nature.

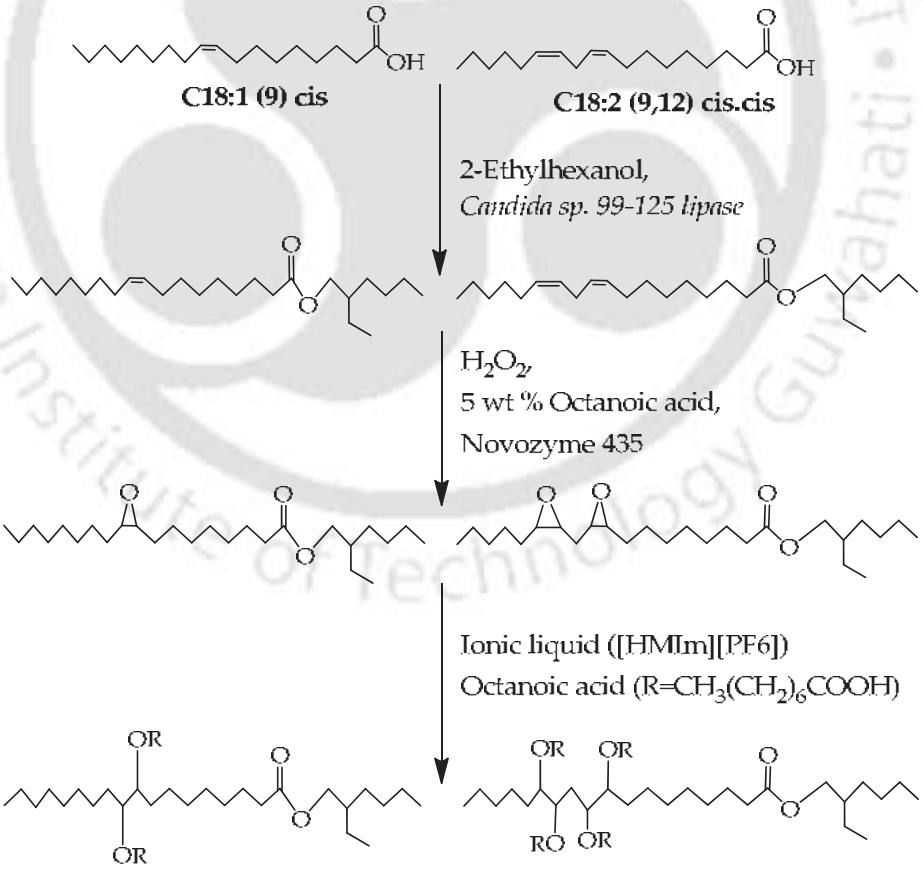

Figure 1.2. The specific scheme for the preparation of octylated branched bio-lubricant. Adapted from (Zhang et al. 2020).

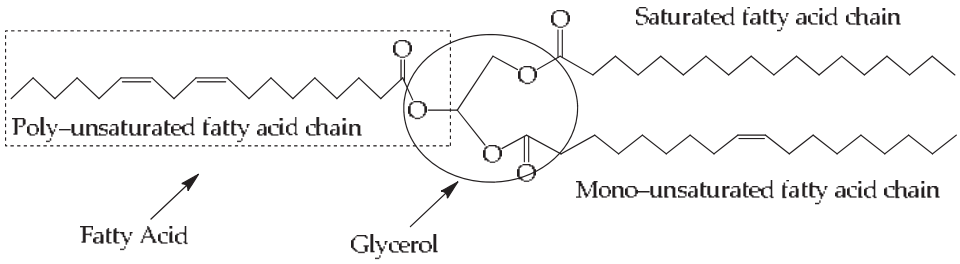

Figure 1.3. Molecular structure of a typical triglyceride molecule, three fatty acids (saturated, mono-unsaturated and poly unsaturated) are connected to glycerol as a backbone.

1.2. Literature

1.2.1. Current Scenario

At present, the growth in global lubricant demand will be aided by the current expansion of the automobile industry, manufacturing, and other industrialised activities. From the prior information from various lubricant industries across the globe, it was found that the global lubricant market has undergone remarkable changes during the past ten years ("Bio-lubricants market," 2020). International demand for lubricants has continued at around 35 million tonnes per year ever since 1991. It was recorded that 37.4 million tonnes of lubricants were consumed worldwide during 2004, with 53% being automobile lubricants, 32% being industrial lubricants, 10% being process oils, and 5% being marine oils (Nagendramma and Kaul, 2012). Later, in 2005, 37.9 million tonnes, and in 2007, 41.8 million tonnes of lubricants were used worldwide, and limited data was presented to the market for 2008 (Mobarak et al., 2014).

Today, market demands for lubricants are increasing due to factors such as environmental compatibility, reduced emissions, greater occupational safety, and above all, superior performance (including longer lifetime and energy efficiency)

(Bolina et al., 2021). The global volume of lubricants, especially engine oils and hydraulic fluids, used in various industrial applications, is remarkable (about 40 Mt/year). Demand for lubricants in the United States is about 2.8 billion gallons (2006), mainly on account of process oils and high-performance lubricants (Mang and Wilfried, 2017). Most of these products (e.g. general industrial oils, engine oils, transmission and hydraulic fluids, gear oils, and greases) are still based on mineral oils. Concerns about environmental pollution caused by many chemicals, including lubricants, have created a growing worldwide trend of promoting new environmentally friendly products. In Europe, some 1.1 million tonnes per year of used lubricating oils (representing 20% of total market) are not traceable. It has been estimated that about 600,000 tonnes of total–loss lubricants–including chainsaw oils, mould release oils, two–stroke engine oils, chassis and wheel flange greases–are released into the environment every year in the European Union alone (Quinchia et al., 2009; Stempfel, 1998); for others release estimates and recommendation reported elsewhere (Battersby, 2000). Whatever the precise figures are, approximately 50% of all lubricants used worldwide end up somehow in the environment via total-loss applications, evaporation, spillage or accidents (Schneider, 2006). Estimates for the loss of hydraulic fluids are even higher (70–80%) (Carnes, 2004). Currently, over 95% of these materials are mineral oil-based or synthetic oils. Mineral oils are toxic for mammals, fish, and bacteria. A major portion of oils and fats for human consumption comes from plants and animals. The world production of edible oils is made up of 71% vegetable oils, 26% animal fat, and 2% fats from marine species (Sharma and Biresaw, 2016). It is estimated that soybean oil, for example, comes from nearly one-third of the world's oilseeds, with almost one-half produced in the United States. The technology for bio-based lubricants, initially referred to as biodegradable lubricants, was based on

vegetable oils with minor chemical modification and performance-enhancing additives. Since vegetable oils generally face inherent challenges in industrial lubricant uses, their performance properties must therefore be carefully studied (Bart et al., 2013). Bio-lubricants can typically be made from plant oils such as rapeseed, soybean, sunflower, palm and coconut, wax esters, and plant polymeric carbohydrates. Since the cost of a lubricant is considerably higher than that of an equal volume of fuel, the use of oleo-chemicals as raw materials for lubricants makes good economic sense (Honary and Richter, 2011). Successful replacement of petroleum-based lubricants with bio-lubricants requires overcoming a number of technical, developmental, and marketing hurdles. Global lubricant sales reached $126.5 billion in 2019 ("Lubricants market size," 2021), and its production is estimated to be 43.87 million tonnes in 2022 at an annual growth rate of 2.4% ("Lubricants market size," 2021). China leads the rankings in the market of lubricants worldwide in 2019 (7.3 million tonnes), followed by the USA (6.05 million tonnes), India (1.7 million tonnes), Japan (1.35 million tonnes), Russia (1.3 million tonnes), Brazil (1.1 million tonnes), and Germany (1.0 million tonnes) ("Market volume of lubricants worldwide," 2021).

The global bio-lubricants market size is projected to grow from USD 2.0 billion in 2020 to USD 2.4 billion by 2025, at a compound annual growth rate (CAGR) of 4.1% between 2020 and 2025 ("Bio-lubricants market," 2020) as shown in Figure 1.4. The demand for bio-lubricants can be attributed to the growing environmental awareness, adoption of stringent regulations, and increasing acceptance of bio-lubricants in industries. On the basis of base oil, the vegetable oil segment is projected to be the largest market for bio-lubricants. The dominant market position of the vegetable oil segment can be attributed to its high biodegradability, low toxicity, and high lubricity. The growth can also be

attributed to the abundant availability of vegetable oil seeds which are used as raw materials.

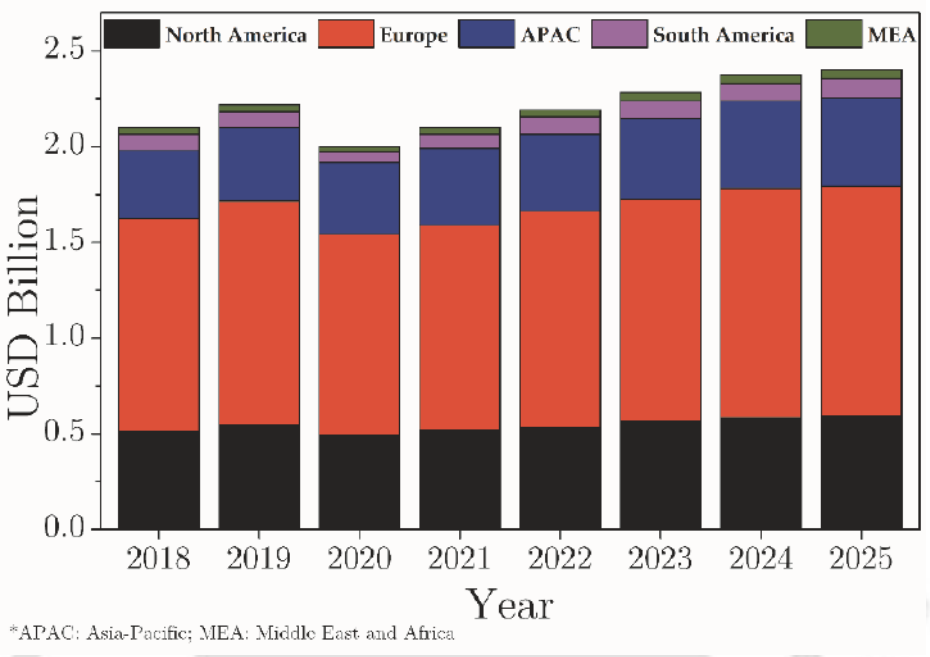

Figure 1.4. Bio-lubricants market by region. Adapted from ("Bio-lubricants market," 2020).

1.2.2. Chemical Composition and Chemistry of Vegetable Oils

Vegetable oils can be categorised as edible and non-edible; they are part of a big family of chemical compounds known as fats or lipids. Currently, they have become more appealing because they are made from renewable resources, are adaptable to the ecosystem, and are compatible to use in diverse fields as feedstocks to synthesise value-added products. Chemically speaking, vegetable oils and animal fats are triesters of glycerol with fatty acids, commonly called triglycerides, which are hydrophobic in nature (Luque and Melero, 2012; Sharma and Biresaw, 2016). Triglycerides, which constitute vegetable oil matrix, are derived from different carboxylic acids, and they vary in the nature of the alkyl

chain attached to glycerol (Mang and Wilfried, 2017). All types of existing triglycerides have been used throughout the ages as foods, fuels, lubricants, and starting materials for other chemicals. This wide utility results from the unique chemical features and physical properties of triglycerides (Honary and Richter, 2011). A generalised triglyceride structure has been shown in Figure 1.5, where R_1, R_2, R_3 are different fatty acids attached to the glycerol molecule.

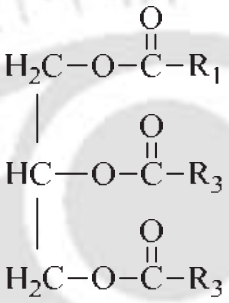

Figure 1.5. Schematic structure of triglyceride molecule.

Thus, the physical and chemical properties of vegetable oil are mainly contributed by fatty acid composition and distribution, which is 90% fatty acids to 10% glycerol (Honary and Richter, 2011; Sharma and Biresaw, 2016). Fatty acids have a polar head and a hydrocarbon chain; these hydrocarbon chains of fatty acids contain one or more unsaturated double bonds. The position of double bonds and their relative position with respect to the carbon atom of the polar head group (carbonyl carbon) provide fatty acids their characteristic properties (Honary and Richter, 2011). Naturally, vegetable oil triglycerides contain fatty acids that range from 14 to 22 carbons with various degrees of saturation and unsaturation (Fox and Stachowiak, 2007).

Plant oils have another factor that is related to the viscosity and melting point of the oil (Honary and Richter, 2011). The length of the carbon chain making up

a molecule has a large effect on its physical properties. The longer the chain is, the higher the viscosity and melting or boiling point are. This factor is due to the presence of one or more double bonds between carbon atoms making up the carbon chain of the fatty acids (Conceição et al., 2005; Saalah et al., 2017). Plant oils typically have one, two, or three double bonds between carbon atoms that make up the fatty acid chain of the oil. In general, as the degree of unsaturation increases, the melting point decreases (Gapinski et al., 1994).

This property of plant oils is important, considering the gelling properties of lubricants. Unsaturated plant oils remain in the liquid state at lower temperatures than saturated hydrocarbons do (Lathi and Mattiasson, 2007). Applications like cooking and some forms of lubricants require solid fats rather than liquids. To remedy this situation, manufacturers use hydrogen to "saturate" unsaturated plant oils. Eliminating the double bonds in plant oils greatly increases their melting points, thus converting them to solids at room temperature (Fox and Stachowiak, 2007). Basically, hydrogen gas in the presence of a catalyst is added to the double bonds in plant oils converting them to saturated fats. The effect is to create a solid out of a liquid oil. This process increases the longevity of the oil in frying applications and could also be helpful in creating more stable vegetable oil-based lubricants (Honary and Richter, 2011). But this complete saturation of double bonds results in poor low-temperature fluidity. Therefore, a limiting situation is reached beyond which further improvement in high- and low-temperature stability cannot be obtained. This restricts the use of triglyceride molecules in industrial applications, operating under a broad temperature range. Thus, chemical modification is compulsory to improve certain performance limitations of ester-based lubricant base oils without impairing their tribological and environmentally relevant properties. Among all the feasible chemical

modifications, a reaction involved at the fatty acid hydrocarbon chain (i.e. epoxidation) has gained much significance. Epoxide can be defined as cyclic ethers which consist of three membered rings; according to IUPAC norms, epoxide is also termed as oxirane ring. The mechanism of epoxidation and product formation is mainly determined by oxidants and catalysts (Bart et al., 2013). Mechanism involved in the formation of oxirane ring is shown in Figure 1.6.

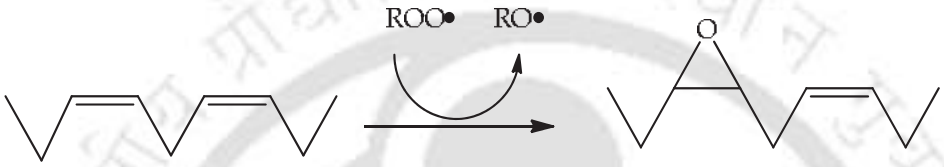

Figure 1.6. Mechanism involved in the formation of oxirane ring.

The epoxidation of olefins can be classified by the reaction mechanism into Jacobsen–Katsuki (Manganese salen complexes and iron-porphyrin catalyst), sharpless asymmetric, shi, prilezhaev reaction (peracid catalyst), and enzymatic epoxidation (Chua et al., 2012). However, every method has its advantages and disadvantages in terms of selectivity, catalyst life, yield, and product separation; yet, purification remained as a shortcoming in these systems. From the prior literature, it was noticed that, above all the process, epoxidation by prilezhaev reaction gained much significance since it is leading to low oxirane degradation and higher selectivity (depending on the catalyst and feedstock). There are four significant categories of epoxidation processes based on the type of catalyst used during epoxidation: conventional sulphuric acid, acidic ion exchange resin (AIER), chemoenzymatic, and metal-catalysed epoxidation (Tan and Chow, 2010).

The structure of an epoxide group of fatty acid molecules is represented by the carbon-carbon-oxygen ring, as shown in Figure 1.7.

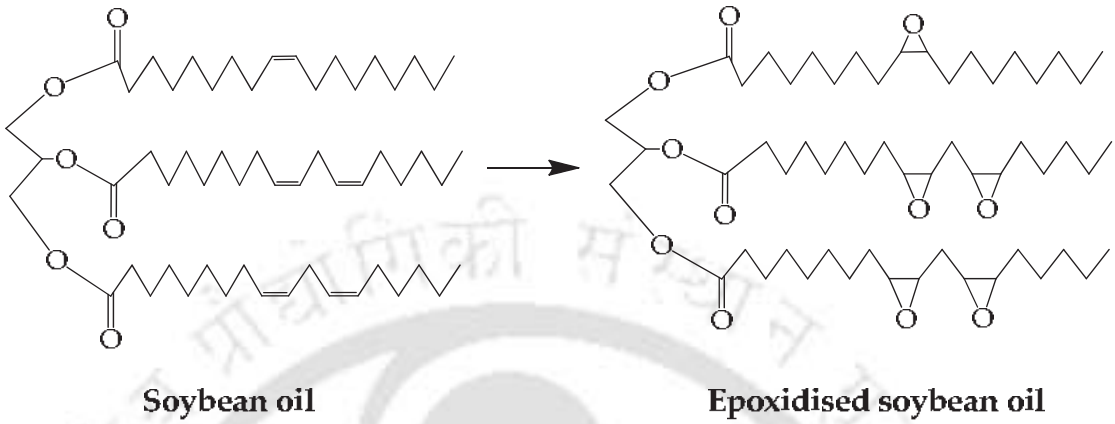

Figure 1.7. Chemical structure of the fatty acids presents in the Soybean oil and epoxidised soybean oil. Adapted from (Karadeniz et al., 2015).

The structure of epoxides derived from natural triglycerides is located along a hydrocarbon chain so that each carbon of the cyclic ether bears an alkyl substituent. To use epoxides for a specific application, they should maintain their physical, chemical, and structural integrity at all storage conditions (Bart et al., 2013). The epoxidised derivatives can be used as lubricant base fluids due to their excellent lubricity and higher thermo-oxidative stability compared to their structurally unmodified feedstock (Adhvaryu et al., 2005; Honary and Richter, 2011; Sharma and Biresaw, 2016).

Wu et al., (2000) studied the application of epoxidised rapeseed oil (ERSO) as a biodegradable lubricant base stocks. The main objective was to avoid the unsaturation (C=C) in rapeseed oil and increase the oxidative and thermal stability by epoxidation. During the study, they have observed that the epoxidation treatment has no adverse effect on the biodegradability of the base stocks. Epoxidised rapeseed oil has superior oxidative stability, and it can be

improved further by adding antioxidants. The result obtained in this study showed significant improvement in the density and viscosity of ERSO compared with rapeseed oil. This may be due to an increase in molecular weight, polarity, and intermolecular forces. Moreover, the three-membered oxirane ring could form polyester or polyether material due to tribo-polymerisation, which is tribologically effective in reducing friction.

Adhvaryu and Erhan, (2002) studied the performance of epoxidised soybean oil (ESBO) over soybean oil (SBO) and genetically modified high oleic soybean oil (HOSBO) in certain high-temperature lubricant applications. The study showed that C=C unsaturation in the fatty acid chain is responsible for the instabilities. Epoxidation enhanced the thermal and oxidative behaviour relative to soybean oil. The presence of C=C unsaturation in the soybean oil was replaced with the epoxy group. The result of the study showed that ESBO had maximum oxidative stability (OS) of 188 °C. They also investigated the oxidative stability at various additive concentrations, and 0.5 wt % of additive concentration showed maximum OS. However, other important properties such as boundary lubrication and deposit forming tendency showed improved performance. Similarly, the coefficient of friction was more for ESBO than for SBO and HOSBO.

Adhvaryu et al., (2005) prepared a synthetic lubricant base fluid with improved temperature stability via chemical modification of epoxidised soybean oil (ESBO). The reactions were carried out in two steps: (i) synthesis of dihydroxylated soybean oil from ESBO with $HClO_4$, and (ii) reaction of acetic, butyric, and hexanoic anhydride with the dihydroxylated product. The reaction products were confirmed by NMR and FTIR spectroscopy, oxidative stability was determined from the Thin Film Micro Oxidation (TFMO) method, while pour point and low-

temperature properties were measured by ASTM methods. From the above testing methods, it was observed that thermal and oxidative stabilities, viscosity, volatility, and other lubricant base oil properties were improved for the ESBO compared to SBO. The study concluded that the removal of unsaturation in the SBO by converting it into epoxide significantly improved the thermal and oxidative stability of SBO. In addition, it was observed that the presence of multiple double bonds in the vegetable oil fatty acid chains accelerates oxidative degradation.

Recently, Li and Wang, (2015) derived the bio-lubricants from waste cooking oil with improved oxidation stability and enriched low-temperature properties via epoxidation, esterification by methanol, and transesterification by iso-octanol, iso-tridecanol and iso-octadecanol. Among all the transesterified products, iso-octadecanol derived bio-lubricants showed improved results in terms of kinematic viscosity (KV), pour point (PP), and oxidation onset temperature (OOT), which were found to be 43 cSt, 24 °C and 194 °C respectively. Investigation on the tribological properties suggested that transesterified products showed improved performance than WCO.

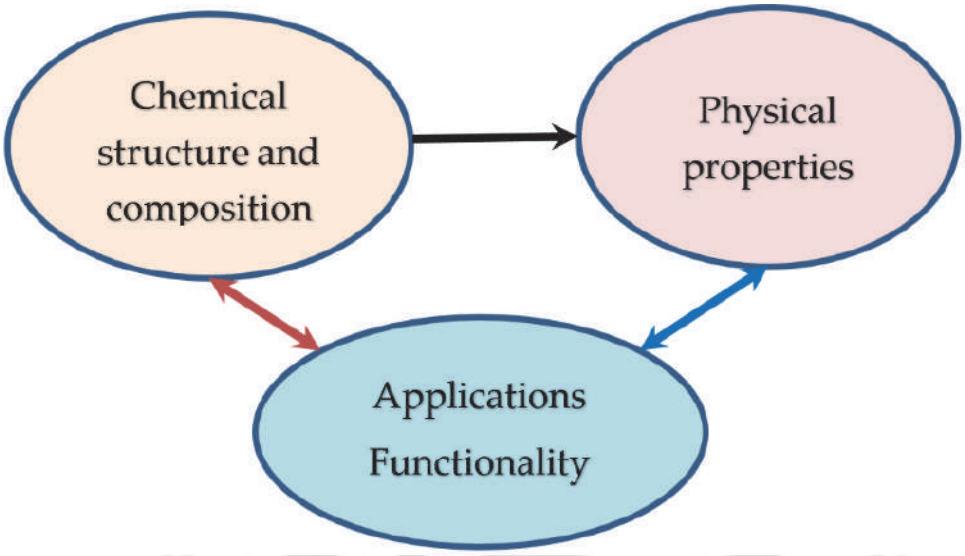

Figure 1.8. Properties vs functionality of chemical structures for lubricant application. Adapted from (Bart et al., 2013).

The main chemical composition of biodegradable lubricants consists of (i) triglycerides (e.g. rapeseed oil, sunflower oil); (ii) esters of (modified) vegetable oils; (iii) semi-saturated, transesterified ester oils with natural fatty acids (e.g. trimethylolpropane trioleate); (iv) (partially bio-based) fully saturated, synthetic esters based on chemically modified vegetable oils or mineral oil (e.g. diisotridecyladipate); (v) polyglycols; and (vi) Poly-α-olefin (Boyde, 2002). In fact, natural oils and fats, consisting of more or less unsaturated triglycerides, such as castor oil, palm oil, rapeseed oil, soybean oil, sunflower oil, tallow, lard, and sperm oil with excellent tribological qualities (low friction coefficient, good wear protection) are historically well documented for their lubrication properties (Rudnick and Shubkin, 1999). However, their range of use is generally limited by lower stability against thermal-oxidative and hydrolytic stress, and partly inferior cold flow properties. These limits can be improved in several ways, e.g. by chemical or genetic modification or by additivation (Bart et al., 2013).

Table 1.1. Physical properties and reaction conditions of epoxidised vegetable oil/non edible oil/waste oil and their derived fatty acids.

Sl. No.	Reactants	Products	Catalyst	Reaction Conditions	Viscosity at 40 °C (cSt)	Viscosity at 100 °C (cSt)	Viscosity Index	Pour Point (°C)	Oxidative/Thermal Stability	Yield (%)	Reference
1	Methyl linolenate and H_2O_2	Epoxidised methyl linolenate	Formic acid	—	308	19.3	63	–7.5	Oxidative onset temperature: 131.2 °C	85	(Sharma et al., 2007)
2	Methyl linoleate and H_2O_2	Epoxidised methyl linoleate	Formic acid	—	14.3	3.5	132	–1.5	Oxidative onset temperature: 180.3 °C	95	(Sharma et al., 2007)
3	Methyl oleate and H_2O_2	Epoxidised methyl oleate	Formic acid	—	8.0	2.5	151	0	Oxidative onset temperature: 189.75 °C	97	(Sharma et al., 2007)
4	Oleic acid, formic acid, and H_2O_2	Epoxidised oleic acid	Sulphuric acid	4 °C, 2 h	—	—	45.44	0	FP: 113.11 °C	—	(Salih et al., 2011)
5	Canola oil, acetic acid, and H_2O_2	Epoxidised canola oil	Amberlite IR–120H	65 °C, 8 h	151	—	—	10	Thermal stability: 320 °C	—	(Madankar et al., 2013)
6	Jatropha oil, formic acid, and H_2O_2	Epoxidised jatropha oil	H_2SO_4	10 °C for 2 h while H_2O_2 added, then 60 °C until complete	146.5	18.2	139	0	RBOT: 20 min, FP: 288 °C	96	(Sammaiah et al., 2014)
7	Canola oil, acetic acid, and H_2O_2	Epoxidised canola oil	Sulfated–SnO_2 Catalyst	70 °C, 6.5 h	114	19	141	9	Oxidative induction time: 60 h	—	(Somidi et al., 2014)

8	Thumba oil, formic acid, and H_2O_2	Epoxidised thumba oil	—	5–10 °C, before adding H_2O_2 and heating to 60 °C for 7 h	216.9	22.7	128	–3	RBOT: 20 min	—	(Kamalakar et al., 2015)
9	Canola oil, acetic acid, H_2O_2	Epoxidised canola oil	Amberlite IR–120H	65 °C, 8 h	—	—	—	9	Thermal stability: 319 ℃	—	(Sharma et al., 2015)
10	Passion fruit oil, formic acid, and H_2O_2	Epoxidised passion fruit oil	—	30 °C, 3 h	185.65	—	—	—	RSSOT: 16.89 min	—	(Silva et al., 2015)
11	Moringa oil, formic acid, and H_2O_2	Epoxidised moringa oil	—	30 °C, 3 h	80.37	—	—	—	RSSOT: 24.57 min	—	(Silva et al., 2015)
12	Canola biodiesel, acetic acid, H_2O_2	Epoxidised biodiesel	Amberlite IR–120H	65 °C, 8 h	—	—	—	0	Thermal stability: 160 ℃	—	(Sharma et al., 2015)
13	Bintaro seeds, acetic acid, H_2O_2	Polyol	Sulphuric acid	—	818.83	54.35	111.36	23.89	—	92.42	(Daniel et al., 2019)
14	Octyloleate (OO), performic acid, 1-octanol,	Octyl 9-epoxyoleate (OEO)	Hexane, formic acid	25 °C, 900 rpm, 24 h	16.3	3.9	148	–15	Oxidative stability: 106 min	94.0	(Marques et al., 2020)

	hydrogen peroxide										
15	Soybean oil, formic acid, hydrogen peroxide	Epoxidised soybean oil	Was not used	60 °C, 1000 rpm, 4 h	210 (38 °C)	—	—	—	—	91.9	(Olivieri et al., 2020)
16	Acetic acid, hydrogen peroxide, peracetic acid	Epoxidised *Euphorbia lathyris* oil	Sulphuric acid	20 °C, 4.5 h	141.19	12.93	187	2.14	—	—	(Singh et al., 2021)

Note: RPVOT, Rotating Pressure Vessel Oxidation Test; RBOT, Rotary Bomb Oxidation Test; RSSOT, Rapid Small Scale Oxidation Test; — not available or not required

Table 1.2. Physical properties and reaction conditions of lubricants derived from fatty acid methyl esters.

Sl. No.	Reactants	Product	Catalyst	Reaction Conditions	Viscosity at 40 °C (cSt)	Viscosity at 100 °C (cSt)	Viscosity Index	Pour Point (°C)	Oxidative/ Thermal Stability	Yield (%)	Reference
1	High oleic palm ME and TMP	TMP triesters	Sodium methoxide	120–150 °C, 0.3 mbar, 45 min	45.5–50.7	9.2–10	183–200	(–37) to (–9)	—	—	(Yunus et al., 2005)
2	Sunflower oil and octanol	FA–n–octyl esters	Fe–Zn double–metal cyanide (DMC) complexes	170 °C, 8 h	7.93	2.74	226	–3	23 min (RBOT)	98	(Sreeprasanth et al., 2006)
3	Jatropha and TMP	TMP triesters	Sodium methoxide	150 °C, 10 mbar, 3 h	4.90	8.71	180	–6	—	>80	(Tinia et al., 2009)
4	Valeric acid TMP	Valeric acid TMP ester	Silica–sulphuric acid	70 °C molar ratio of	9.5	2.5	80	–75	—	—	(Kerman et al., 2011)

				3:1, toluene							
5	Castor biodiesel and TMP	TMP triesters	Amberlyst 15 ionic exchange resin	120 °C, 0.01 bar	20.94	4.46	127	—	—	—	(Kerman et al., 2011)
6	Castor biodiesel and TMP	TMP triesters	Sodium methoxide	120 °C, 0.01 bar	11.28	3.10	141	—	RPVOT: 150 min (Butylated hydroxytoluene hydroxytoluene added)	—	(Kerman et al., 2011)
7	Pentaerythritol and oleic acid	Pentaerythritol tetraoleate ester	Ion exchange resin, Indion-130	110 °C, 6 h toluene solvent	63.08	12.00	190	–24	—	—	(Nagendramma, 2011)
8	Jatropha ME and TMP	TMP triesters	Sodium methoxide	150 °C, 55 min	42.57	9.37	183	–6	325 °C	—	(Resul et al., 2012)
9	Palm ME and TMP	TMP triesters	Calcium methoxide	180 °C, 50 mbar, 8 h	—	—	—	—	—	92.38	(Masood et al., 2012)
10	Castor biodiesel and TMP	TMP triesters	Dibutyltin dilaurate	170 °C, 0.01 bar	287.2	26.13	119	–27	RPVOT: 43 min (Butylated hydroxytoluene added)	89.7	(Da Silva et al., 2013)
11	Rapeseed ME and NPG/TMP/PE	NPG/TMP/PE triesters	C Antarctica lipase	150, 200, 50 h	7.8–38.2	2.7–8.4	205–224	(–31.3) to (–18)	Δv : 90.1–147.1 ΔA_c : 2.9–7.7	98	(Gryglewicz et al., 2013)

12	Rubber ME and NPG/TMP /PE	NPG/TMP/ PE triesters	p–Toluensulphonic acid	135–140 °C, until theoretical reaction complete	23.1–62.6	5.9-12.6	206-222	(–15) to (–3)	10–15 min (RBOT) FP: 266–308 °C	94.5–96.5	(Kamalakar et al., 2013)
13	Soybean oil and various alcohols	n–alcohol–esters	Sulfated zirconia catalysts	140 °C, 4 h	10.3–432.7	3.0–34.4	45–195	—	—	>80	(Oh et al., 2013)
14	Canola biodiesel ME and TMP	TMP triesters	Sodium methoxide	110 °C, 1 mbar, 5 h	40.5	7.8	204	–66	Induction time: 0.74 h	90.9	(Sripada et al., 2013)
15	WCO ME and TMP	TMP triester	KOH	128 °C, 200 Pa, 1.5 h	36.60	8.44	204	–8	FP: 240 °C	85.7	(Wang et al., 2014)
16	Palm ME and TMP	TMP triesters	Sodium methoxide	140 °C, 25 mbar, 25 min, oscillatory flow reactor at 1.5 Hz with 20 nm amplitude	47.1	9.0	176	–2	355 °C Degradation temperature	94.6	(Koh et al., 2014)
17	Thumba ME, xylene and NPG/TMP /PE	NPG/TMP/ PE triesters	p–Toluensulphonic acid	135–140 °C, until complete	20.65–60.26	5.45–11.89	209–220	(–12) to (–3)	10–15 min (RBOT) FP: 270–318 °C	89–95	(Kamalakar et al., 2015)

18	Tilapia oil ME, toluene, formic acid, aqueous H_2O_2	Epoxidised methyl esters		60 °C, 350 rpm, 12 h	7.4	—	—	9	~230 °C	94.0	(Valle et al., 2018)
19	Palm stearin methyl esters	Epoxidised palm stearin methyl esters	Lipase as biocatalyst	H_2O_2/C=C molar ratio of 1.51 mol, 4.34 h, 52 °C, enzyme concentration of 6.4 wt %, and acetic acid/C=C molar ratio of 0.163:1	—	—	—	—	—	98.9	(Afifah et al., 2021)
20	Jatropha oil, soybean oil, formic acid, hydrogen peroxide	Epoxidised fatty acid	—	70 °C, 700 rpm, 5 h	28.95 (Jatropha) 31.02 (Soybean)	7.23 (Jatropha) 6.97 (Soybean)	168.94 (Jatropha) 159.27 (Soybean)	<–18 (Jatropha) <–18 (Soybean)	—	—	(Pindit et al., 2021)

Note: RPVOT, Rotating Pressure Vessel Oxidation Test; RBOT, Rotary Bomb Oxidation Test; RSSOT, Rapid Small Scale Oxidation Test; FP, Flashpoint; — not available or not required.

1.2.3. Rheological Study

In case of oils, consistency, flow properties, or viscosity are key parameters for lubrication efficiency and the application of lubricants. These are the terms that appear in nearly all lubricant specifications. Viscosity is also the only lubricant property adopted into the design process for hydrodynamic and elasto-hydrodynamic lubrication (Mang and Wilfried, 2017). Viscosity is one of the most critical checks to be performed during automotive engine oil operations. Lubricant oils are graded at different temperatures based on their viscosity (Pirro et al., 2016). Viscosity depends on temperature and reduces with increased temperature. Suitable viscosity range is therefore very important for different domestic and industrial applications. The viscosity index is an indicator of temperature–viscosity variance (Bolina et al., 2021).

Epoxidised oil is an epoxidised derivative of a mixture of esters of glycerol with various saturated and unsaturated fatty acids (Borugadda et al., 2017). The viscosity of the unmodified oil decreased with an increase in the unsaturated fatty acid (UFA) content. However, the viscosity of epoxidised oils increased slightly as the level of epoxidation increased (Borugadda and Goud, 2018). The rheological properties of epoxides can be evaluated by analysing the effects of epoxidation degree and the chemical structure of epoxide. Unmodified plant oils (i.e. soybean, sunflower, passion fruit, moringa, rapeseed, coconut) have low viscosity (~50 cSt) at 40 °C, and they are considered as Newtonian fluids (Fox and Stachowiak, 2007). However, when unmodified oils are chemically modified via epoxidation, hydrogenation, esterification, and transesterification, their viscosity could be increased dramatically, suitable for domestic and industrial applications (McNutt and He, 2016). Triglycerides may be changed to provide

various functional classes at different functionality levels (Khot et al., 2001). As a consequence of chemical modification, the polarities of triglyceride molecules change, which may have a broad influence on rheology (Berry and Fox, 2006; Guo et al., 2002). Further, viscosity depends on the operating temperature; with an increase in temperature, viscosity would reduce. To simplify the classification of lubricants according to their application, viscosity grades are introduced, which are now internationally accepted. ISO viscosity grades (ISO VG) apply to industrial lubricants, while Society of Automotive Engineers (SAE) classifications apply to the automotive engine and gear oils (Mang and Wilfried, 2017).

García-Zapateiro et al., (2013) studied the thermal and tribological characteristics of a variety of estolides obtained from both oleic and ricinoleic acids using different acid–catalysts. They found that the lubricants prepared via sulphuric acid catalyst influences friction and wear. Campanella et al., (2010) reported the production of polyols with branched ether and ester compounds from epoxidised vegetable oils pertaining to temperate climate crops such as soybean, sunflower, and high-oleic sunflower oils for bio-lubricant applications. Further, Erhan and Perez, (2002) analysed physical, chemical, and kinetics data for cottonseed, corn, safflower oils-derived base stocks. They have found promising results in oxirane content, iodine value, peroxide value, and thermal and kinetics data. The study reported that genetically modified high-oleic vegetable oils performed better than unmodified vegetable oils in terms of thermal and oxidative stabilities.

Likewise, Wang et al., (2014) reported the use of Trimethylolpropane fatty acid triester (TFATE) as a bio-lubricant synthesised by transesterification of fatty acid methyl esters from waste cooking oil with trimethylolpropane. In addition, TFATE's properties met the requirements of ISO VG 32. Viscosity is one of the

most important parameters for a lubricant that controls the thickness of the film. Insufficient lubrication can occur if the viscosity is not within the specified range, resulting in high friction and excessive wear. However, a high viscosity also must be accompanied by a high pressure–viscosity coefficient (Ciannamea and Ruseckaite, 2018). Low viscosity can cause oil film failure at high temperatures and high loads, whereas high viscous lubricant can cause excessive heat generation, resulting in oxidation, sludge/varnish build-up, and excessive fuel consumption. At 100 °C, multigrade engine oils are graded according to their viscosity. For industrial use, the viscosity range is 30–240 cSt. Since the viscosity range of vegetable oils/waste oils is very low, to improve its viscosity range, it is important to find acceptable chemical modifications. Limited literature is available on rheological model fitting on waste oil as well as bio-lubricant base stocks (Hernández-Sierra et al., 2019; Libor, 1991; Sun et al., 2011b). Among the different rheological models like Andrade equation (Frenkel, 1930), modified Williams-Landel-Ferry (WLF) (Sun et al., 2011b), Arrhenius relationship (Borugadda and Goud, 2014a), and Herschel-Bulkley (Enweremadu and Mbarawa, 2009), power–law model (Borugadda and Goud, 2014a; Sun et al., 2011b; Xu and Qu, 2009) has gained more popularity due to its simplicity and fewer assumptions.

Table 1.3. Parameters applied for rheological studies of mineral and bio-lubricants.

Sl. No.	Test Fluid/Bio-lubricant	Temperature	Shear Rate	Viscosity Range	Equipment	Observation and Application	Reference
1	Engine oils SAE 15W–40, SAE 20W–40, SAE 20W–50 and SAE 25W–50	–20 to 20 °C	3 to 60 rpm	~1250–32 mPa.s (SAE 15W–40) ~2750–40 mPa.s (SAE 20W–40) ~2250–180 mPa.s (SAE 20W–50) ~4250–60 mPa.s (SAE 25W–50)	Brookfield synchro-lectric viscometer	Multigrade engine oils SAE 15W–40 and SAE 20W–40 are expected to behave as Newtonian fluids at temperatures higher than about 5℃. These oils behave as dilatant fluids at temperatures lower than about 5℃.	(Tanveer et al., 2006)
2	Soybean, sunflower, high oleic sunflower and castor oils with ethylene–vinyl acetate copolymer	25 to 120 °C	5 to 1000 s^{-1}	~0.0544–0.0056 Pa.s (SOY) ~0.0583–0.0053 Pa.s (SO) ~0.0650–0.0064 Pa.s (HOSO) ~0.52–0.0113 Pa.s (CO)	Rotational controlled strain rheometer, model ARES (Rheometric Scientific, UK)	Viscosity increments up to 330–420% respecting the original oil. Bio-lubricant applicable for gearboxes and four-strokes engine	(Quinchia et al., 2010)
3	Soybean oil based bio-lubricant	30 to 80 °C	—	~ 39–9 mPa.s (Soybean oil) ~ 52–10 mPa.s (hydrogenated soybean oil) ~ 288–28 mPa.s (epoxidised soybean oil)	Brookfield controlled-stress rheometer and ultra rheometer	Soybean oil, the hydrogenated soybean oil and the epoxidised soybean oil mixture used as engine bio-lubricants. Dynamic viscosity as follows at 40 ℃ is 28 (SO), 33 (HSO), and 156 mPa.s (ESO).	(Ting and Chen, 2011)

4	Castor, rapeseed, soybean, sunflower and high oleic sunflower oils with viscosity modifier and pour point depressant additives	–40 to 25 °C	10 s^{-1}	~ 103–100 Pa.s (CO) ~ 4–0.05 Pa.s (RO) ~ 40–0.04 Pa.s (SO) ~ 10–0.05 Pa.s (HOSO)	TA controlled–strain rheometer	Additives used as viscosity modifiers, such as ethyl cellulose (EC), also induce a delay in high oleic sunflower oil (HOSO) crystallisation, producing a similar effect to pour point depressant (PPD), besides increasing the viscosity.	(Quinchia et al., 2012)
5	Cottonseed, soybean, groundnut and castor oils and their blends	30 to 80 °C	—	Viscosity in Redwood second ~75.73–24.28 (CSO) ~78.83–26.28 (SOY) ~81.92–22.21 (GO) ~609.22–89.67 (CO)	Redwood viscometer no. 1	Viscosity of soybean oil blends with castor oil was found to be higher among this other vegetable oil blends.	(Talkit et al., 2012)
6	Rubber seed oil	40 to 100 °C	—	~8–3 cSt (2–ethylhexyl esters of rubber fatty acids (R2–EtHE)) ~23–6 cSt (NPG esters of rubber fatty acids (RNPGE)) ~38–7 cSt (TMP esters of rubber	ASTM D445	PE, TMP and NPG esters of rubber fatty acids exhibited higher viscosities, which were found in the range of ISO VG 22, 32 and 68 respectively, while that of 2-ethylhexyl esters of rubber fatty acids was found in the range of ISO VG 7 which is due to more number of acyl groups in case of polyol esters. All the esters exhibited higher viscosity indices in the range of 187–206.	(Kamalakar et al., 2013)

				fatty acids (RTMPE)) ~63–13 cSt (PE esters of rubber fatty acids (RPEE))			
7	Jatropha oil	—	—	~174–20 cSt (JBL0) ~130–19 cSt (JBL10) ~121–18 (JBL20) ~96–16 (JBL30) ~82–14 (JBL40) ~68–13 (JBL50)	—	Jatropha oil blended bio–lubricant with the commercial lubricant SAE 40.	(Shahabuddin et al., 2013)
8	Castor oil–based ionic liquid micro–emulsions	0 to 100 °C	—	~ 780–20 mm^2/s	NDJ–5S viscometer	VI for emulsions (220), for CO (90). Friction and wear tests: micro emulsions have a low friction coefficient, and smaller wear scar diameters are formed compared with the commercially available lubricant 400SN. Tremendous potential as renewable bio–lubricant base stocks.	(Wang et al., 2013)
9	DXT III, MG 20W-50, MC	20 to 50 °C	10 to 100 s^{-1}	~0.24–0.06 Pa.s (DXT III)	Anton–Paar rheometer (MCR302)	Five different industrial lubricating oils are considered as sample for this study with varying	(Vasishth et al., 2014)

	20W–50, EP 90 and SAE 20W–50			~0.45–0.22 Pa.s (MG 20W-50) ~0.46–0.15 Pa.s (MC 20W-50) ~0.51–0.23 Pa.s (EP 90) ~0.61–0.20 Pa.s (SAE 20W–50)		shear rate and varying temperature and it was shown that some of them obey Reynolds' equation.	
10	Waste cooking oil methyl esters epoxide	28 to 100 °C	0 to 500 s^{-1}	~23–4 cSt	Anton–Paar rheometer (MCR 301)	Kinematic viscosity increases 121% from ME to epoxide (4.71 cSt to 10.42 cSt) at 40℃. A possible substitute for the conventional lubricant base stocks.	(Borugadda and Goud, 2016a)
11	Epoxidised waste cooking oil (EWCO) and waste cooking oil fatty acid methyl esters (WCOFAME)	25 to 100 °C	0 to 500 s^{-1}	29.63–9.65 cSt (Hydroxylated WCO) 10.57–2.9 cSt (Hexanoylated WCO) 16.76–4.99 cSt (Hydroxylated WCOFAME) 8.33–1.09 cSt (Hexanoylated WCOFAME)	Anton–Paar rheometer (MCR 301)	Hexanoylated WCO and WCOFAME are following the SAE20W40, AG 100, ISO VG 32, 46, 68 and 100 standards.	(Borugadda and Goud, 2019)
12	Castor oil and epoxidised cellulose pulp	25 to 150 °C	Frequency range: 0.03–100 rad/s	Wear diameters (μm) and friction factor	Controlled-stress rheometer (Anton Paar	The pulp samples with the higher epoxy indices were more compatible with castor oil; decreasing the friction coefficient	(Cortés-Triviño et al., 2019)

				values at 25 ℃ and 95 ℃. ~ 400 – 431 μm ; ~384–446 (OECPN-1) ~ 416 – 431 μm ; ~373–446 (OECPN-5) ~ 440 – 436 μm ; ~434–433 (OECPN-20) ~ 481 – 500 μm ; ~408–394 (Castor oil)	Physica MCR 501)	in the mixed lubrication region. The cellulose pulps modified with aromatic epoxides used as thickening agents were more efficient in protecting the metal surface and led to smaller wear scar diameters as a consequence.	
13	Sunflower, soybean, jatropha, and waste cooking oils	28 to 100 °C	0–140 s^{-1}	18–3 mPa.s (Sunflower bio-lubricant) 36–6 mPa.s (Soybean bio-lubricant) 27–5 mPa.s (Jatropha bio-lubricant) 44–5 mPa.s (Waste oil bio-lubricant)	Brookfield DV-II	Viscosity indexes of the ethylene glycol di–esters (EGDEs) were found to be higher than 140 for the waste oil and 311 for Jatropha oil. Rheological behaviours of the EGDEs behave as Newtonian fluids.	(Attia et al., 2020)

— not available or not required

1.2.4. Optimisation of Reaction Processes Using RSM, ANN, and GA

Various techniques have been proposed and used to optimise industrial processes (Aghbashlo et al., 2021). The classical technique of one parameter at a time is time-consuming, and is not effective for the identification of interactions as well as for the predictions of parameters involved in the process. Nowadays, mathematical methods such as response surface methodology (RSM) (Azaman et al., 2010) and artificial neural network (ANN) (Ebrahimpour et al., 2008; Haider et al., 2008) are commonly used for modelling and optimisation of processes. RSM is based on a collection of statistical and mathematical techniques (Gul et al., 2021). This technique is useful in developing, improving and optimising processes in which a response of interest is influenced by several independent variables, and the objective is to optimise this response (Talib et al., 2019). Besides analysing the effects of independent variables, this experimental methodology generates a mathematical model, which can be used to describe the process for better understanding (Kumar et al., 2020). Before applying the RSM, some preliminary studies are needed, such as the selection of the experimental design which includes variable selection, and selecting the range of parameters, etc. (Bezerra et al., 2008). If the number of variables is too large, screening of the significant variables shall be carried out first, prior to the selection of appropriate optimisation design. Various experimental designs may be used for RSM optimisation (Haider et al., 2008). RSM has many advantages over the conventional single parameter optimisation technique, but it is not applicable to all optimisation and modelling studies (Okpalaeke et al., 2020). The major drawback of RSM is the need for a second-order polynomial to fit the data. All systems containing curvature such as symmetrical or non-symmetrical bell-shaped curves may not be explained well by the second-order polynomial (Cornish-Bowden, 2001).

Data-driven machine learning (ML) technology is a promising alternative to traditional modelling approaches to deal with the nonlinear, uncertain, complex, and multivariate nature of biodiesel/bio-lubricant systems (Aghbashlo et al., 2021). Among the available ML techniques, artificial neural network (ANN) technology is the most widely used method in biodiesel/bio-lubricant research (Aghbashlo et al., 2021; Gul et al., 2021; Hajar and Vahabzadeh, 2014; Karimmaslak et al., 2021; Soufi et al., 2015). ANN is a powerful modelling technique that has several advantages over conventional modelling techniques, including the ability to model without making assumptions about the nature of phenomenological mechanisms, the ability to comprehend the mathematical background of the process, and the ability to learn linear and nonlinear relationships between variables directly from a set of examples (Basheer and Hajmeer, 2000). Hence, the ANN approach is briefly introduced and described in the following section.

ANNs are computational models formed from hundreds of single units, called artificial neurons, inspired by biological neurons and connected with coefficients (weights) which constitute the neural structure (Lahiri and Ghanta, 2008). These neurons are sometimes called processing elements (PE) as they process information. These weights are just like the synaptic activity in a biological neuron. The weights of the inputs are summed, and the threshold subtracted to determine the activation of the neuron (Noorossana et al., 2009). The other important capability of neural networks is that they can learn the input–output relationship through training (Lahiri and Ghanta, 2008). ANN analysis is quite flexible as regards to the amount and form of the training (experimental) data, which makes it possible to use more informal experimental designs than with statistical approaches (Noorossana et al., 2009). A neural network does not need

any model or screening before the development of a network. Neural networks may be applied to designed data or on the data that is not statistically designed. Sufficient data with all possible operating conditions of input variables are needed to develop a neural network. A network model is then constructed according to the system's behaviour (Lahiri and Ghanta, 2009). The constructed model may be used for predictions and other applications within the assessed operating conditions. Since the regression analysis is dependent on predetermined statistically significant levels, the less significant factors are not included in the model. ANN uses all the data, making the model more accurate. A neural network can perform tasks that cannot be performed by linear programming. If an element of the neural network fails, the network can still continue to perform the task owing to its parallel nature, and there is no need for reprogramming (Gul et al., 2021). The main disadvantage of ANN is the requirement of training in order to operate. A neural network needs to be emulated because the architecture is different from that of microprocessors, where high processing time is required for a large network. (Puig-Arnavat and Bruno, 2015) Different architectures may also be involved in ANN, which requires different types of algorithms (Hajar and Vahabzadeh, 2014). The development of accurate models for a biological reaction on chemical and physical bases is still a critical challenge, mainly due to the non-linear nature of the biochemical network interactions. The use of advanced non-linear data analysis techniques such as ANN has been applied in various areas such as food science (Razmi-Rad et al., 2007), biotechnology (Ghaffari et al., 2006), chemical processes (Basheer and Hajmeer, 2000), equipment development (Noorossana et al., 2009), and biochemical engineering (Haider et al., 2008). Comparative studies of ANN and RSM for fermentation processes employing wild strains have been reported (Dasari et al., 2009). Quite an increasing number of

researchers around the globe have started to employ RSM and ANN as tools to predict and optimise biodiesel as well as bio-lubricant synthesis processes, as found in the following examples of work: bio-lubricant production using Novozym 435 and castor oil substrate (Hajar and Vahabzadeh, 2014), performance and exhaust emissions of a SI two-stroke engine with bio-lubricants (Soufi et al., 2015), biodiesel production from castor oil (Banerjee et al., 2017), microwave mediated production of FAME from waste cooking oil (Selvaraj et al., 2019), sustainable green lubricants by advance transesterification process (Gul et al., 2020), and optimisation of sustainable production of cotton bio-lubricant (Gul et al., 2021). The results and data from the implementation of RSM and ANN are superior in their sensitivity analysis. A schematic illustration of the analogy between a biological neuron and an artificial neuron is shown in Figure 1.9.

Further, very scanty information exists in the literature on the use of WCO for epoxide synthesis with RSM and ANN. Reported literature described the chemoenzymatic route for mono-epoxidation of linoleic acid using RSM and D-optimal design to optimise the process parameters. They found that hydrogen peroxide (H_2O_2) has a significant effect on the degree of epoxidation (Abdullah et al., 2014; Salih et al., 2011). Similarly, literature reported the enzymatic epoxidation of *Sapindus mukorossi* seed oil by perstearic acid, and the process was optimised by RSM with Box-Behnken design techniques (Sun et al., 2011a).

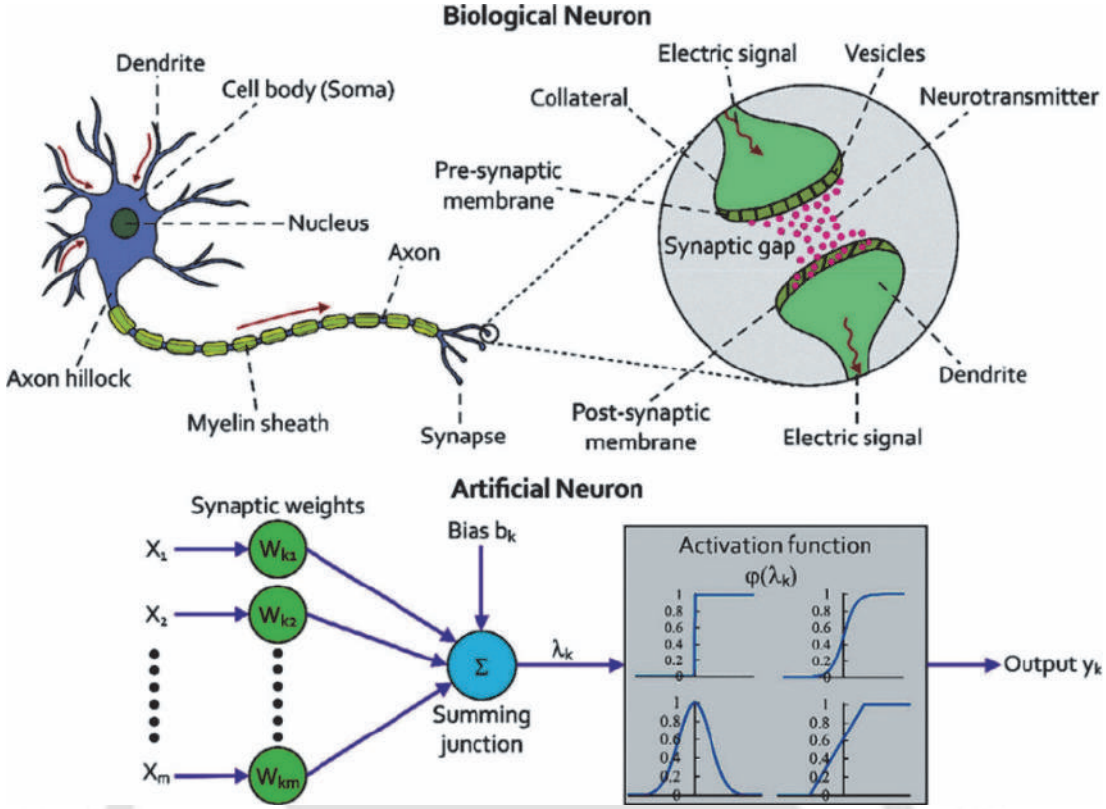

Figure 1.9. A schematic illustration of the analogy between a biological neuron and an artificial neuron. Adapted from (Aghbashlo et al., 2021; Basheer and Hajmeer, 2000; Elsheikh et al., 2019).

A genetic algorithm (GA) is a straightforward and powerful general-purpose stochastic optimisation method inspired by the Darwinian evolution of population genetics (Okpalaeke et al., 2020). It is subjected to duplicate, crossover the alteration, in a particular environment where only the fittest can survive (Srivastava et al., 2018). GA preferably combines with genetic operators to create an artificial survival of fittest obtained from given search space to form a very robust mechanism that is suitable for a variety of optimisation problems (Kana et al., 2012). The input data of GA creates an initial population (set off a possible solution) either indiscriminately or by learning through experience (heuristically). The less fit individuals in the population die, and to search other points in space,

some variations are introduced into the new population by using idealised recombination (translational) operators (e.g. crossovers, mutation) (Bhatti et al., 2011). As a result, over the course of a generation, the population with the best fit survives. In other words, the optimal condition that is most suited for the situation will be generated globally (Bhatti et al., 2011; Srivastava et al., 2018). GA technique as well as ANN–GA coupled method is successfully applied to the product optimisation and to improve the overall system in several studies—modelling study on pectin extraction from *Helianthus annuus* (sunflower) heads (Muthusamy et al., 2019), decanol proportional effect prediction model as an additive in palm biodiesel for diesel engine (Kumar et al., 2020), ferric sulphate catalysed esterification of Neem (*Azadirachta indica*) seed oil (Okpalaeke et al., 2020), prediction of performance and emission parameters of Kusum (*Schleichera oleosa*) biodiesel-based diesel engine (Singh et al., 2020), nano-catalytic heterogeneous reactive distillation for algal biodiesel production (Mondal et al., 2021), the correlation between fatty acid composition of biodiesel with the fuel properties, effects of using biodiesel–ethanol blends on the performance and emission characteristics of a diesel engine (Shirneshan et al., 2021), predicting the optimal conditions for biodiesel synthesis from *Chrysophyllum albidum* seed oil (Onukwuli et al., 2021a), engine performance with waste soya oil-based biodiesel (Onukwuli et al., 2021b), optimisation of performance and emission of compression ignition engine fueled with propylene glycol and biodiesel–diesel blends (Karimmaslak et al., 2021), etc. From the above discussion, it appears that there are no reports available in the literature on bio-lubricant base stocks synthesis from waste oil using optimisation techniques ANN and GA. Figure 1.10 shows the number of studies that dealt with the use of data-driven machine learning (ML) technology in biodiesel research.

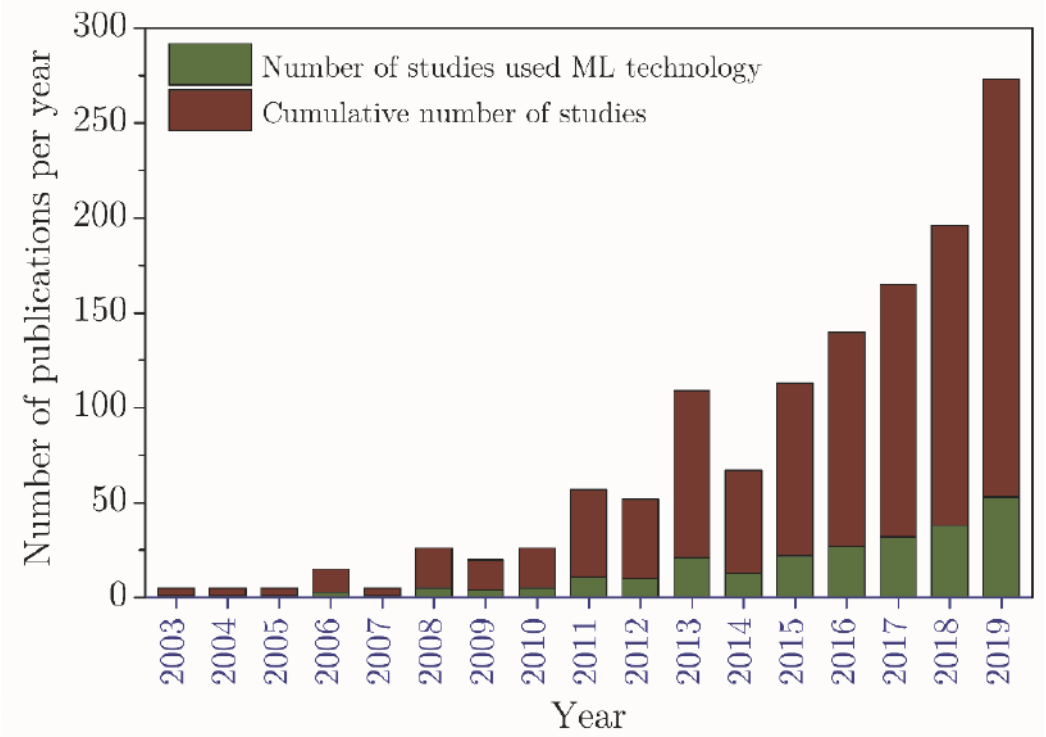

Figure 1.10. The number of studies that dealt with the use of data driven machine learning (ML) technology in biodiesel research. Adapted from (Aghbashlo et al., 2021).

1.2.5 TGA Kinetics

Thermal degradation of thermally unstable oils, fuels, and bio-lubricants may form a troublesome amount of insoluble degradation products such as gums and sediments. Thermal analysis can be useful for the selection of fuel or bio-lubricants for high-temperature applications and also be useful for storage of the same for extended durations depending on environmental conditions (Roy et al., 2020). The thermal characteristics of biodiesel/bio-lubricant vary as per feedstock composition and feedstock processing technique. For this reason, it is imperative to determine and improve the thermal stability of biodiesel as well as bio-lubricant and its feedstock (Elmelawy et al., 2021). The interplay of thermal degradation characteristics and kinetics parameters of biodiesel/bio-lubricant and

its feedstock is not fully understood. The knowledge of thermochemical conversion and chemical kinetics is required for the process design and optimisation of thermochemical processes for biodiesel/bio-lubricant production (Suryawanshi and Goud, 2021; Vuppaladadiyam et al., 2019). Thermal analysis is a widely used technique to evaluate solid-state decomposition processes' kinetics parameters and has also been used for liquid fuels. There are reports of this technique applied to sunflower oil (De Souza et al., 2004), palm oil (Nik et al., 2005), cottonseed oil-derived biodiesel (Souza et al., 2007), and corn-derived biodiesel (Dantas et al., 2007a).

Kinetics parameters of sunflower oil obtained by non-isothermal thermogravimetry by the Coats and Redfern, Madhusudanan, Horowitz and Metzger, and Van Krevelen methods were dependent on the antioxidant used, and in these studies, sunflower oil shows thermal stability up to ~200 °C (De Souza et al., 2004). Kinetics study of Jatropha bio-lubricant showed overall second-order kinetics with a rate constant of 0.18 (% wt/wt min °C)$^{-1}$ and activation energy of 1.65 kJ/mol (Resul et al., 2012). Thermal degradation of biodiesel and its feedstock oil was studied through thermogravimetric analysis. The kinetics parameters were evaluated via the model-free approach, and the reaction order is determined by the Avrami theory (Li et al., 2015). Biolubricant from melon-based methyl esters shows second-order reaction kinetics, and it gives the best fit for modelling the transesterification reaction. The estimated value of activation energy for the transesterification of melon methyl esters (MME) with TMP was 34 kJ/mol (Menkiti et al., 2016). Kinetics of thermal degradation of test bio-lubricant (Karanja oil derived bio-lubricant base oil) was studied under a heating rate of 10 °C/min and nitrogen flow rate of 50 mL/min, and a first-order reaction with two steps weight loss was reported (Sharma et al., 2019).

Similarly, Moringa oil methyl esters synthesis followed by thermal degradation kinetic showed an overall reaction order of two and a reaction rate constant of 0.20465 L/mol/s (Oladipo et al., 2020). Well-fitted kinetics plot of waste cooking oil methyl esters suggested that the reaction followed pseudo-first-order kinetics. Moreover, corresponding signs of thermodynamic parameters implied that the reaction follows an endothermic nonspontaneous pathway (Roy et al., 2020). The kinetics of biodiesel prepared from underutilised sandbox seeds followed a unimolecular pseudo-second-order rate law with the reaction rate of 0.0016 L/mol.min at 35 °C. The activation energy and frequency factor was calculated as 11 kJ/mol and 0.1362 L/mol.s, respectively (Oraegbunam et al., 2020). Transesterification of sunflower oil followed by the kinetics study of transesterified product demonstrated that the reaction followed a pseudo-first-order reaction rate with a rate constant of 0.01558/min at 64 °C. The activation energies of this reaction calculated using both Eyring–Polanyi (for liquids) and Arrhenius (for gases) relationships were found to be 59 kJ/mol and 62 kJ/mol, respectively (Salmasi et al., 2020). Thermal degradation kinetics study of Trimethylolpropane (TMP) fatty acid trimester suggested that the transesterification process of OME with TMP was based on three distinct elementary reversible series-parallel reaction mechanisms (Elmelawy et al., 2021). Another report on kinetics study of waste cooking oil (sunflower oil) methyl esters revealed that the reaction was kinetically controlled by pseudo-first-order. The activation energy was estimated to be 21 kJ/mol which indicates that it is not an energy-intensive process (Naeem et al., 2021).

1.3. Knowledge Gap

Bio-lubricants are now available for numerous applications, with performance in competition with that of mineral oil-based products (ranging from worse to comparable and sometimes even better). Lubricant base fluids based on renewable raw materials have been reviewed in the recent past (Pavlovicova and Cvengros, 1999; Schneider, 2006; Wagner et al., 2001; Zwinselman et al., 2000). Therefore, the present text describes the advanced technologies for lubricant production from waste oils based on the technical and scientific literature up to late 2020, and makes some recommendations for the future. Consumer acceptance of renewable lubricants depends on how well they perform during high-temperature oxidation and in low-temperature applications. Previously, a wide variety of (chemically modified) vegetable oils has been evaluated in terms of their thermal, oxidation, and low-temperature behaviour for their potential use as base fluids for industrial and automotive lubrication. This text traces recent developments in lubricant base stocks of vegetable oil (waste oil) origin, putting emphasis on structure–property relations as a means for improved product design. According to the author's knowledge, a combined approach of RSM optimisation and ANN modelling has never been explained for the synthesis of bio-lubricant base stocks from waste cooking soybean oil and its methyl esters. The application of both RSM and ANNs could be helpful to optimise and analyse different key process parameters that strongly influence the reaction mechanism to develop a phenomenological numerical model. Furthermore, the combination of RSM and ANN techniques could be employed as a novel and economical approach for the design of different industrial processes.

From the available literature review on the synthesis of bio-lubricants and other findings, it is found that the field lacks a lot of information. The major limitations in the field are highlighted below.

- So far, only a few oils are compared with the conventional lubricant base stocks, and also this was done mostly in European countries; however, there is little information about Indian lubricant base stocks in this regard.
- European countries started bio-lubricant synthesis and replaced 5% of their conventional base stocks with bio-lubricants, but there is no contribution from India in this field to date.
- Minimal information is available on optimising process parameters of transesterification and on epoxidation reaction of WSCO through RSM and artificial neural network (ANN).
- Although a significant amount of research has been conducted to characterise lubricant base stocks, no study has been reported on the detailed rheological characteristics of the lubricant base stocks.
- TGA Kinetics study of lubricant base stocks has not been established.

1.4. Objectives

Considering the knowledge gap in the current literature, the following objectives are formulated to prepare bio-based lubricant from waste soybean cooking oil and waste soybean cooking oil methyl esters. Major focus has been given on improving the thermal-oxidative stability, rheological properties, and other important properties of the produced lubricants. Based on the study of the latest literature, this Ph.D. thesis targets the fulfilment of the following major objectives.

1. *In situ* epoxidation of waste soybean cooking oil for the synthesis of bio-lubricant base stocks: process parameter optimisation and comparison with Response Surface Methodology (RSM), Artificial Neural Network (ANN), and Genetic Algorithm (GA)
2. Synthesis of waste soybean cooking oil methyl esters and its epoxidation for the synthesis of bio-lubricant base stocks via Response Surface Methodology (RSM), Artificial Neural Network (ANN), and Genetic Algorithm (GA)
3. Studies on the rheological properties of epoxides of waste soybean cooking oil (EWSCO) and waste soybean cooking oil methyl esters epoxides (EWSCOME)
4. Studies on degradation kinetics of waste soybean cooking oil epoxides (EWSCO) and waste soybean cooking oil methyl esters epoxides (EWSCOME)

1.5. Organisation of the Thesis

The doctoral thesis is organised into seven chapters as follows:

Chapter 1: Introduction and review of literature

In this chapter, the current scenario, literature studies, objectives, and organisation of the thesis are discussed in detail.

Chapter 2: Materials and methods

In this chapter, the discussion is made on materials and methodology used for experiments in this thesis work. This chapter aims to provide

detailed transesterification and epoxidation reaction process for bio-lubricant production. This chapter also addresses various characterisation techniques used to estimate physico-chemical and thermal properties, and discusses quantification of the raw materials and produced products.

Chapter 3: *In situ* epoxidation of waste soybean cooking oil for the synthesis of bio-lubricant base stocks: process parameter optimisation and comparison with Response Surface Methodology (RSM), Artificial Neural Network (ANN), and Genetic Algorithm (GA)

Waste soybean cooking oil (WSCO) was used to prepare bio-lubricant base stocks via structural modification of unsaturated fatty acids (in situ epoxidation). Optimisation of the effect of process parameters on maximum oxirane oxygen content (OOC) was studied using the RSM technique. Interaction among the process parameters such as C=C bonds to H_2O_2 molar ratio, catalyst loading, and reaction time was examined by ANOVA using the Design-Expert software. The main focus of this chapter is on establishing optimum OOC conditions using sulphuric acid (H_2SO_4) as the homogeneous acid catalyst. Optimum OOC of epoxidised waste soybean cooking oil (EWSCO) was found to be 4.69 mass % under the experimental conditions of 60 °C temperature, 6 h of reaction time, 1.5 g of catalyst loading, and 1:2 molar ratio of C=C bonds to H_2O_2. The standard methods evaluated the significant physico-chemical properties of the bio-lubricant base stocks prepared at the optimum conditions. Further, ANN modelling and genetic algorithm (GA) optimisation

were carried out using identical data sets. The outcomes of this study revealed that the chemically modified WSCO derivatives could also act as potential bio-lubricant base stocks.

Chapter 4: Synthesis of waste soybean cooking oil methyl esters and its epoxidation for the synthesis of bio-lubricant base stocks via Response Surface Methodology (RSM), Artificial Neural Network (ANN), and Genetic Algorithm (GA)

In this study, artificial neural networks (ANNs) and response surface methodology (RSM) techniques were used to optimise and predict the maximum oxirane oxygen content (OOC) of waste soybean cooking oil methyl esters (WSCOME). WSCOME bio-lubricant base stocks was prepared using the same technique as that discussed in Chapter 3. The optimum OOC of epoxidised waste soybean cooking oil methyl esters (EWSCOME) was found to be 4.92 mass % under the experimental conditions of 60 °C temperature, 4.14 h of reaction time, 1.95 g of catalyst loading, and 1:2.21 molar ratio of unsaturation to H_2O_2. The formation of EWSCOME was confirmed by FTIR spectroscopy (at 843 cm^{-1}) and NMR spectroscopy (at δ = 2.8 to δ 3.1 ppm) analysis. Several physico-chemical properties of the prepared bio-lubricant were also measured by the standard techniques. Lastly, it was concluded that the prepared EWSCOME could be used as a probable bio-lubricant base stocks.

Chapter 5: Studies on the rheological properties of epoxides of waste soybean cooking oil (EWSCO) and waste soybean cooking oil methyl esters epoxides (EWSCOME)

In this study, the rheological properties of epoxidised waste soybean cooking oil and its methyl esters were evaluated by varying the temperature and shear rate to understand their rheological behaviour for bio-lubricant applications. Further, the power law model was used to fit the outcomes of rheological studies. In conclusion, viscosity and viscosity index properties of epoxidised waste soybean cooking oil and its methyl esters were compared with that of the standard lubricants (viscosity grade) to identify the proper area of application. To the best of our knowledge, this is the first report on the rheological study of EWSCO and EWSCOME for lubricant applications.

Chapter 6: Studies on degradation kinetics of waste soybean cooking oil epoxides (EWSCO) and waste soybean cooking oil methyl esters epoxide (EWSCOME)

In this chapter, thermal characteristics and kinetics parameters of waste soybean cooking oil (WSCO), waste soybean cooking oil methyl esters (WSCOME), epoxide of waste soybean cooking oil (EWSCO), and epoxide of waste soybean cooking oil methyl esters (EWSCOME) were determined by thermogravimetry analysis under non-isothermal heating conditions. A series of experiments was performed by increasing the temperature up to 800 °C at different heating rates of 10, 20, 30, and 50 °C/min in an inert (nitrogen) atmosphere. The mass loss curves showed that the degradation of the prepared bio-lubricant samples occurred mainly in the range of 200–500 °C, due to the breakage of the weak chemical bonds, leading to the formation of smaller molecules of volatile organic compounds and

gaseous products. Further, a detailed reaction mechanism of prepared bio-lubricant base stocks was discussed.

Chapter 7: Overall conclusions and scope for future work

This chapter summarises the appropriate conclusions of this work, based on all the characterisations and investigations. This chapter also provides some useful recommendations for future research in the relevant field.

CHAPTER II

Materials and Methods

Materials

Methods

Procedures

Physico-chemical Characterisations of Feedstocks and Products

Chapter II

Materials and Methods

This chapter discusses the experimental methods and procedures used to conduct the two primary processes: i) transesterification process for waste soybean cooking oil (WSCO), and ii) epoxidation of WSCO and waste soybean cooking oil methyl esters (WSCOME). During transesterification and epoxidation process, response surface methodology (RSM) with central composite design (CCD) was applied for parameter optimisation. ^{1}H NMR, GC-MS, TGA, and acid value are extensively used for evaluation of methyl esters formation during transesterification process. Furthermore, physico-chemical characterisation of the feedstocks and products for their suitability for respective applications was elaborated in detail in this chapter.

2.1. Materials

Waste soybean cooking oil was collected from hostel mess, IIT Guwahati, India. Hydrogen peroxide (H_2O_2, 30 % v/v), sulphuric acid (H_2SO_4, 98 % v/v) were purchased from Rankem, and glacial acetic acid (CH_3COOH, 99-100 %) was supplied by Merck India Ltd. All the other reagents were analytical grade and were used as received. Chemicals such as methanol (99%), sodium hydroxide (NaOH) pellet, barium hydroxide octahydrate ($Ba(OH)_2 \cdot 8H_2O$) (97%), sulphuric acid (98%), hexane (95%), ethanol (99.9%), and phenolphthalein were procured from Merck India Ltd. Diesel was obtained from the local fuel station.

2.2. Methods

2.2.1. Base Catalysed Transesterification of WSCO

Waste soybean cooking oil (fish fried soybean oil) was collected from hostel mess, IIT Guwahati, Guwahati, India. After collection, oil was used without any further purification to prepare methyl esters. The obtained oil was measured for its acid value (AV) and was recorded to be 0.54 mg KOH/g. Hence, single step transesterification procedure was followed at 1:6 oil to methanol molar ratio, 1 wt % catalyst loading, 600 rpm stirring speed for 90 min at 60 °C reaction temperature to prepare waste soybean cooking oil methyl esters (WSCOME) (Borugadda and Goud, 2014a).

After transesterification, the methyl esters conversion was confirmed by ^{1}H NMR spectral techniques. The physico-chemical properties of prepared methyl esters were determined using standard ASTM, AOCS official methods and are discussed in the respective chapters.

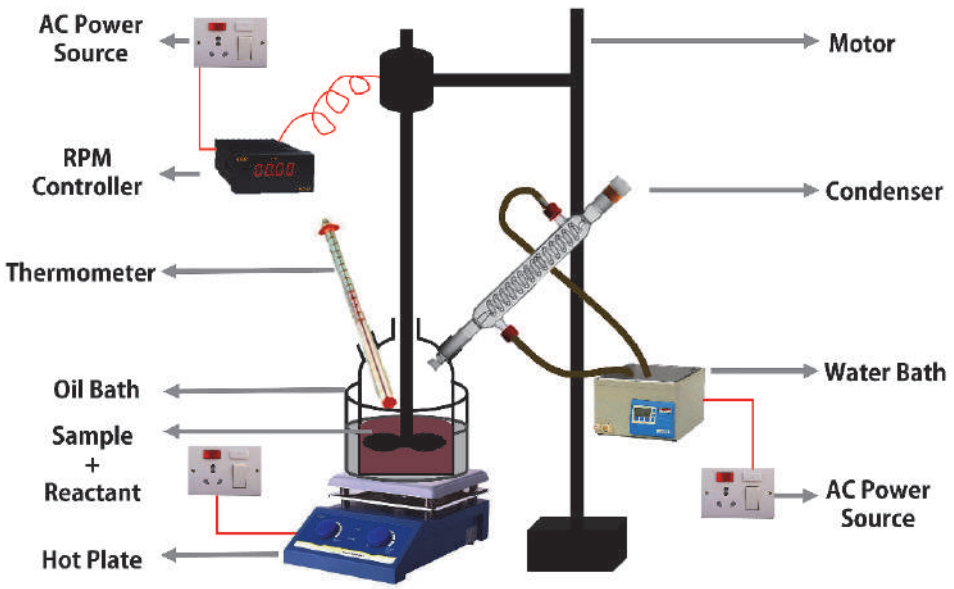

Figure 2.1. Schematic diagram of transesterification reaction setup.

2.2.2. Methyl Esters Synthesis

Transesterification reactions of WSCO were carried out using mechanical agitation technique on applying optimum reaction conditions stated above at section 2.2.1. The transesterification reactions were carried out in a 500 mL specially designed 3 mm thick glass reactor with condenser on the top. This reaction setup was kept in a temperature controlled water bath. After that, direct transesterification reactions were carried out using base catalyst (KOH) because of low (less than 1) free fatty acid value (WSCO:0.27). The physico-chemical and rheological properties of the produced methyl esters (WSCOME) was estimated.

2.2.3. Epoxidation Reaction Procedure

The reaction was carried out in a three necked glass reactor of 250 mL capacity, with a plane bottom, having a baffle. The reactor was provided with an overhead glass stirrer having five-blade down-flow impeller. The reactor also had a condenser for reflux. The entire reactor assembly was placed in a heating water bath. The preliminary experimental studies were performed to figure out the optimum range for each process parameter. During the experimentations, WSCO, hydrogen peroxide and glacial acetic acid amounts were measured in a molar ratio; sulphuric acid was consumed in terms of wt %. Initially, WSCO was heated to 60 °C temperature, and then glacial acetic acid and H_2SO_4 were added. H_2O_2 was later added drop-wise to the reaction mixture. Stirring speed of 1100–1500 rpm was kept to ensure uniform mixing. After complete addition of H_2O_2, the reaction was continued for the desired time duration. Estimation of OOC was carried out for final epoxide product after each run.

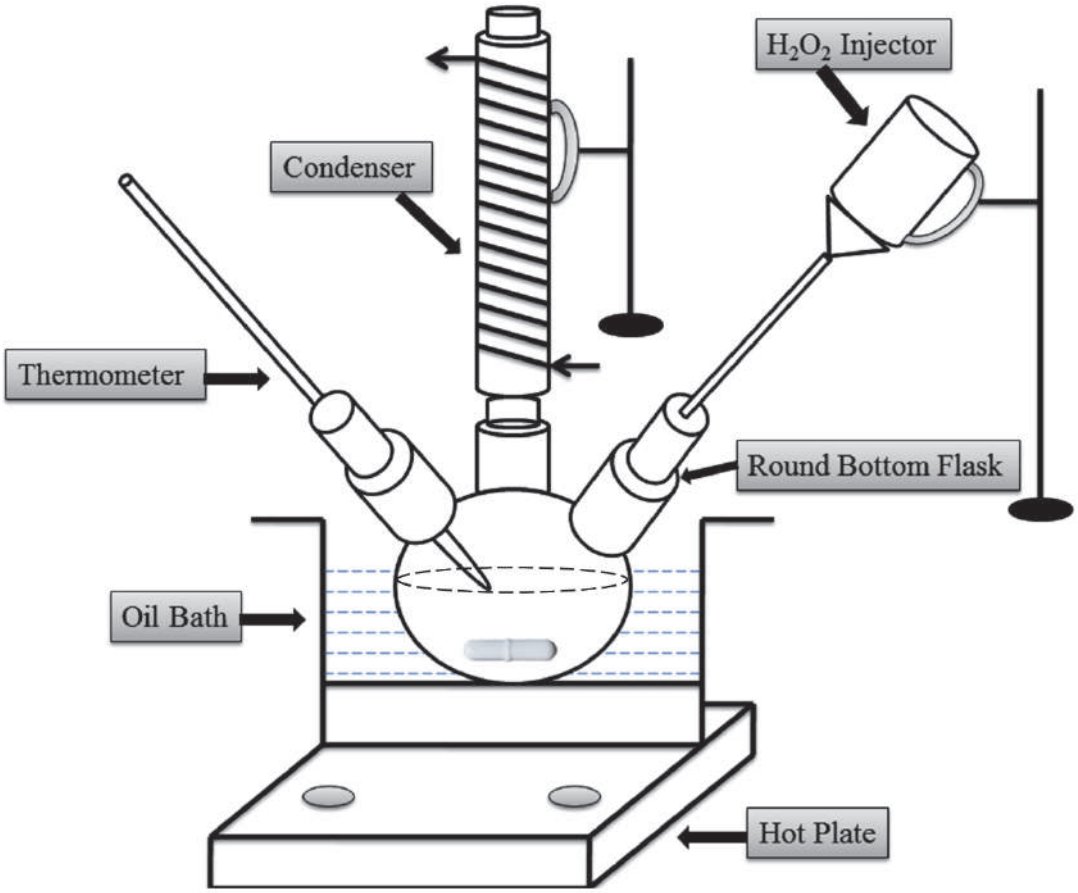

Figure 2.2. Schematic diagram of epoxidation reaction setup.

2.3. Physical and Chemical Properties of WSCO and EWSCO

The Wijs' Method (AOCS Tg 1-64, 1997) was used to determine the iodine value, which in turn indicates the unsaturation content of oil. Acid value (AV) and free fatty acid (FFA) content of WSCO and its epoxide were determined according to the AOCS official method (Te 1a-64, 1997). Density and specific gravity were found out using a specific gravity bottle. Refractive index (RI) was measured using a refractometer (ABBE Refracto meter). The samples were analysed for the moisture content by Kerl-Fischer auto titrator.

2.3.1. (Alpha) α- glycol Content

α -glycol content enables to know the presence of hydroxyl groups in epoxide. It was determined by the method reported by May (1973) and Weiss (1970), based on the oxidation of glycol with benzyltrimethylammonium periodate in a non-aqueous medium. The following expression was used for the estimation of α-glycol content of epoxide product.

$$\alpha-\text{Glycol content (moles/100g)} = \frac{(V_B - V_S)\times N}{20\times W} \quad (2.1)$$

where V_B, volume of $Na_2S_2O_3$ solution consumed for the blank test, mL;

V_S, volume of $Na_2S_2O_3$ solution consumed by the oil/FAME epoxide or ring opened sample, mL;

N, normality of $Na_2S_2O_3$ solution;

W, weight of epoxide product, g

The relative percentage conversion to α-glycol was calculated from the following expression:

$$\text{Relative percentage conversion to } \alpha-\text{glycol} = (G_{\exp}/G_{the})\times 100 \quad (2.2)$$

Where, $G_{\exp}$ is the experimentally obtained α-glycol and G_{the} is the theoretically obtainable maximum $\alpha-$glycol, which was determined from the following expression:

$$G_{the} = \left[\frac{(IV_0/2\times A_i)}{100+(IV_0/2\times A_i)2\times A_{OH}}\right]\times 100 \quad (2.3)$$

Where, A_{OH} (= 17) is the atomic weight of hydroxyl group.

2.3.2. Fourier Transformed Infrared Spectroscopy (FTIR)

FTIR spectra for sample and their epoxide were recorded on a Shimadzu Fourier Transform Infrared Spectrophotometer (IR Affinity 1, Shimadzu, Japan) equipped with a KBr beam splitter. The confirmation of WSCO and EWSCO spectra's was carried out using the FTIR technique using standard procedure. A normal scanning range of 400–4000 cm^{-1} was employed for 30 repeated scans at a spectral resolution of 4 cm^{-1} with a pair of KBr crystals in thin film. The spectra was recorded in transmittance mode.

2.3.3. ^1H NMR Spectroscopy

^1H NMR spectrum of WSCO and their epoxides was recorded using 600 MHz Nuclear Magnetic Resonance (NMR) Spectrometer (Make: Bruker). Samples were dissolved in 400 μl deuterated chloroform ($CdCl_3$) and transferred to 5-mm NMR tube. The deuterated chloroform chemical shift peak at 7.26 ppm was used as an internal reference. Typical parameters used were, spectral width: 4800 Hz; time domain data points: 32 K; flip angle: 90 °C; relaxation delay: 5 s; spectrum size: 32 K points; and line broadening for exponential window function: 0.3 Hz.

2.3.4. Iodine Value (g I_2/100 g)

The iodine value (IV) can be defined as mass of iodine in grams consumed by 100 grams of oil/ME/epoxide; it measures the amount of unsaturation (double bonds) present in the sample. IV greatly influences the oxidation and aging process, and higher iodine value signifies more unsaturation content. In this study, IV was determined according to the Wijs method (AOCS Tg 1-64, 1997).

2.3.5. Oxirane Oxygen Content (OOC)

The oxirane oxygen content was determined by AOCS Method (Cd-9, 120) II.D.20 (HBr method) using hydrobromic acid solution in glacial acetic acid. Theoretical oxirane oxygen (OO_{th}) and relative percentage conversion to oxirane were calculated from the following expressions.

Theoretical oxygen oxirane content $$OO_{th} = \left[\frac{(IV_0 / 2A_i)}{100 + (IV_0 / 2A_i)A_0}\right] A_0 \times 100 \quad (2.4)$$

Where, A_i and A_0 are the atomic weights of iodine and oxygen respectively, and IV_0 is the initial iodine value of the WSCO.

Relative percentage conversion to Oxirane = $$\left[\frac{OO_{ex}}{OO_{th}}\right] \times 100 \quad (2.5)$$

Where OO_{ex} is the experimentally determined content of oxirane oxygen, and OO_{th} is the theoretically maximum oxirane oxygen content.

2.3.6. Acid Value and Free Fatty Acid Content

Acid value (AV) is defined as the amount of potassium hydroxide (in mg) required for neutralising 1 g of sample. Half of the AV is always considered as free fatty acid content in the sample (FFA); AV and FFA were calculated according to AOCS official method (Te TA-64,1997).

Phenolphthalein solution was used as an indicator for titration. Acid value was calculated using the following expression:

$$Acid\ Value = \frac{Volume\ of\ the\ titrant\ (ml) \times N \times 56.10}{Mass\ of\ the\ sample\ (\mathrm{g})} \quad (2.6)$$

Where, N is the normality of accurately standardised sodium hydroxide solution.

2.3.7. Calorific Value (CV, MJ/kg)

The calorific value (CV) or higher heating value (HHV) can be defined as the energy released in the form of heat when one gram of testing substance undergoes complete combustion with oxygen under standard conditions. The CV was determined according to ASTM D2015-85 standard method. The calorific value is a characteristic for each substance; higher is the calorific value, more is the heat energy produced when unit amount of oil/FAME is burnt.

2.3.8. Chemical (Fatty Acid) Composition of Feedstocks by Gas Chromatography

The fatty acid composition of WSCO was determined using Nucon 5765 gas chromatograph equipped with a flame ionisation detector (Nucon Engineers, Delhi, India) and fused silica capillary column BPX-70, 60 m × 0.25 mm × 0.25 µm (SGE, India). The column temperature was programmed to increase from 180 °C to 240 °C at 4 °C/min. The detector and injector temperatures were fixed at 240 °C and 230 °C, respectively. The carrier gas used was nitrogen (40 psi) at a flow rate of 45 mL/min; air and hydrogen flow rates were 30 mL/min and 300 mL/min, respectively. The sample injection volume was 1.0 µL with a split flow of 60 mL/min.

2.3.9. Cold Flow Properties by Differential Scanning Calorimetry (DSC)

Pour point (PP, °C) was measured to determine the low temperature flow properties, and it was a rough indication of the lowest temperature at which sample is promptly pumpable. In this study, PP was also determined by adopting differential scanning calorimetry technique (DSC, 1 star e system, Mettler Toledo). Three to five milligrams sample was taken in a 40 µL sealed pan under

the nitrogen flow rate of 40 mL/min. A temperature program with four sequential active steps was used, in which the sample was heated from room temperature (RT) to 50 °C at 5 °C/min at constant heating rate; then it was held at 50 °C for 5 min (isothermal condition) to homogenise the sample. After that, the sample was cooled from 50 °C to (-30 °C) at 5 °C/min and continued at the same temperature for 5 min for complete crystallisation. Thereafter, the sample was heated from (-30 °C) to 50 °C at a heating rate of 5 °C/min. DSC measurements were repeated twice, and the average values are reported here.

2.3.10. Density (kg/m³)

The density (ρ) of a material is defined as its mass per unit volume. Densities were determined at 25 °C using a specific gravity bottle according to ASTM D4052 method. Density was calculated using the following expression:

$$Density\,(kg/m^3) = \frac{Mass\ (kg)}{Volume\ (m^3)} \tag{2.7}$$

2.3.11. Kinematic and Dynamic Viscosity (Rheological Experiments)

Rheological analysis of all the samples was performed using Interfacial Rheometer (Anton-Paar Model: MCR 301) by varying temperature from 25–100 °C and shear rate in the range of 5–300 s^{-1}. The thermostatic water bath was used to control the working temperature within the set range of 40–100±0.1 °C. Diesel, methyl esters and epoxides samples (~ 2 mL) were stored in different Eppendorf tubes and ~ 0.6 mL volume of each sample was used for rheology experiments. A rheometer with plate (PP 50, Dia.: 50 mm) and plate (INSET I-PP 80/SS, Dia.: 80 mm) system was used. The sample temperature was maintained constant within ±0.1 °C. The measurements were triplicated and the average values are

reported. The maximum uncertainties of viscosity determinations were found to be less than ±1%.

2.3.12. Moisture Content

Moisture content was determined using Karl fisher auto-titrator; it is a qualitative parameter which influences the storage life. High moisture content may serve as a medium for microbial growth. Microbial growth in the oil may lead to damage of fuel/storage tank and supports emulsion formation.

2.3.13. Thermal and Oxidative Stability by Thermogravimetric Analysis

Thermal and oxidative stability study was carried out in a non-isothermal mode in TGA-4000 (PerkinElmer, USA) thermogravimetric analysis (TGA) instrument to identify the temperature regimes where predominant weight losses (and hence transformations) occur. TGA was conducted in N_2—an insight could be gained to analyse the effect of atmosphere on various temperature regimes. The conventional heating rate (10 °C/min) was adopted, and temperature programming was from room temperature (25 °C) to 800 °C. Less than ten milligrams of sample was taken in a silica crucible (900 µL) and was heated in an inert atmosphere (Nitrogen, 40 mL/min) to determine thermal stability, and oxygen/air atmosphere (100 mL/min) was used to define oxidative stability. The onset temperature (thermal stability, OT, °C) and oxidation onset temperature (oxidative stability, OOT, °C) were calculated from a plot of weight % versus temperature (°C) for each run. In kinetics study, four different heating rates, namely 10 °C/min, 20 °C/min, 30 °C/min, and 50 °C/min, were employed.

2.3.14. Refractive Index (RI)

The RI was measured using refracto meter (ABBE Refracto meter); it is the degree of deflection of a beam light that occurs when it passes from one medium to the other. The refractive index value increases with the degree of unsaturation. This value indicates the presence of long chain un-saturated fatty acids in the sample.

2.4. Response Surface Methodology

Response Surface Methodology (RSM), Central Composite Design (CCD) is a widely used technology for intellectual experimental design and process optimisation in the absence of mechanistic information. During this century, many scientists and researchers are attracted towards RSM to optimise the process variables in various reactions. RSM was used not only to get optimum process variables but also to observe the interaction among the process variables; it was developed by Box and Wilson. It was originated from design of experiments (DOE) to optimise the experimental process parameters (i.e. factors) for conducting laboratory experiments and collecting the data (theoretically). Then the data can be used to develop an empirical model which relates the process response to the process parameters; afterwards, the model helps to search for better process response, which is validated through laboratory experiment(s). All the above procedure iterates until an optimal process is identified or the limit on experimental resources is reached. CCD helps in investigating linear, quadratic, cubic and cross-product effects of process variables in an experiment. RSM has got various applications in almost every area of scientific research and engineering practice, including the development of chemical and biochemical processes (Abdullah et al., 2014; Chi et al., 2012; Sun et al., 2011a).

In general, many different experimental designs exist, but they differ largely in purpose, number of experiments, and experimental setup. Each design has its own advantages and disadvantages. Factorial designs are widely used to inquire main effects and interactions between the parameters. When each factor is varied over two levels, factorial design can be employed. Two-level (fractional) factorial design cannot be used if quadratic terms are important for describing the response accurately. Expansion of factorial design to three or more can be done but number of experiments will increase drastically. A fractional factorial design with three variables is illustrated in Figure 2.3a. Central Composite Design (CCD) was an alternative to expanding the factorial design, and is a widely used design for optimisation of process parameters. This design consists of two level factorial design and additional axial points, and is shown in Figure 2.3b. In CCD, the factorial points will contribute in estimating the interaction terms, and the axial points will contribute in estimating the quadratic terms.

Box-Behnken designs are based on incomplete three level factorial designs; graphically this can be visualised in a cube that consists of centre point and the middle point of the edges, shown in Figure 2.3c. In this method, no factorial points or face points are present; these designs should be used in cases where one is not interested in predicting responses at the extremes. Box-Behnken designs for the three factors cannot determine as this always will have the value zero. Doehlert designs are another type of design which is used only in rare conditions. All the above designs are rotatable, i.e. there is equal prediction precision in all directions. But Doehlert design is not rotatable, and it has its own advantages like high efficiency and requirement of few experiments. In this design, the number of studied levels may differ from factor to factor. The general rule in this design is that the variables with the strongest effects are studied in the highest

number of levels in order to obtain most information from the system (Chi et al., 2012). A Doehlert design with three variables is shown in Figure 2.3d.

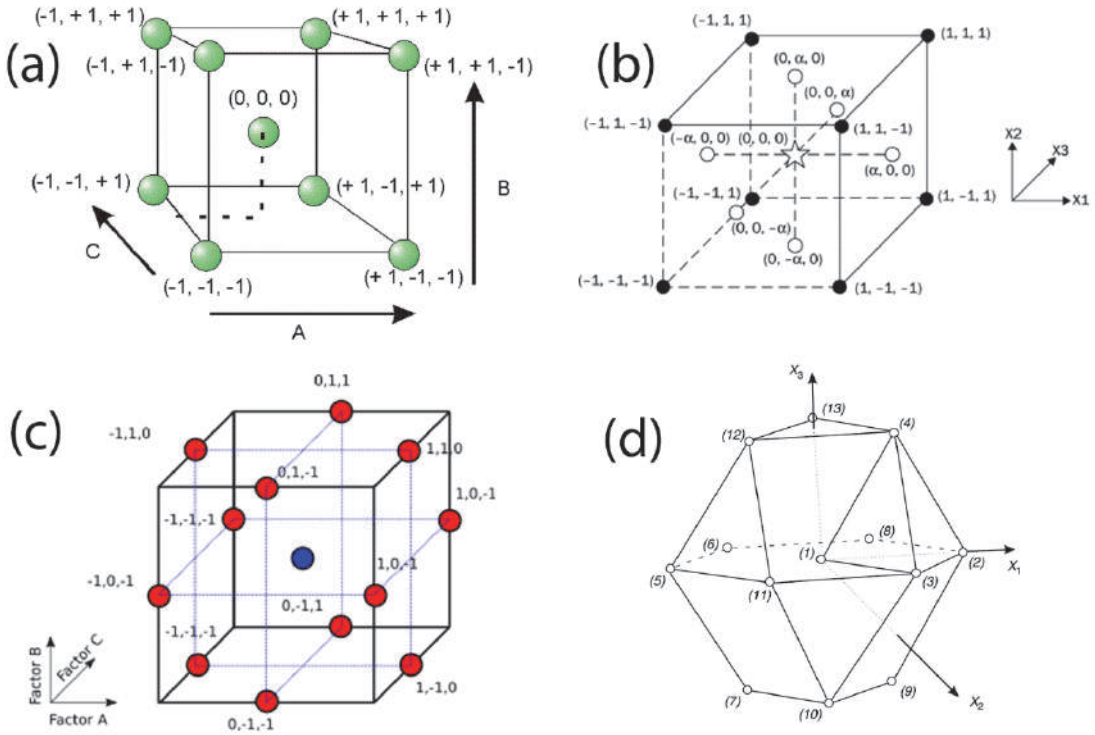

Figure 2.3. RSM design; a) Fractional factorial design with three variables, b) Full factorial design with three variables, c) Box-Behnken design, d) Doehlert design.

RSM is an advanced optimisation technique adopted in the present scenario for various applications, due to its trustworthiness, ease of analysis of results, clarity in data analysis, and the advantage of getting more information in short time. In this study, WSCO epoxidation reaction process parameters were optimised by using Response Surface Methodology, and full factorial Central Composite Design technique was used to study the interaction among the process variables.

RSM was employed to ensure the robustness in optimising the process conditions and formulating a response surface model for the preparation of epoxidised waste

soybean cooking oil (EWSCO) which can be a potential alternative to conventional lubricant base stocks. CCD was used to design the experiments, and the statistical analysis was performed with the aid of the DOE (trail version 7.0.1). In addition to reducing the number of experimental runs, DOE can also help in studying the effect of individual process parameters on the response. Synthesis process of the epoxide was followed as reported in section 2.2.3. Based on the outcomes of the preliminary studies, a three level, three factorial CCD was employed in this study. Tables in respective chapters show the independent process parameters and their levels selected to optimise the process conditions for the epoxidation of WSCO. Full factorial CCD for three variables was used to obtain the combination of values that maximise the response (OOC)—a total of 20 experiments have been employed in this work to evaluate the effect of three independent variables on epoxidation of WSCO. These 20 experimental runs were obtained based on the following conventional design formula:

$$N = 2^n \text{ (factorial point runs)} + 2n \text{ (axial point runs)} + K \text{ (centre point runs, 6)}, \quad (2.8)$$

Where 'n' is number of process parameters.

A general equation of factorial design analysis will look like the equation below (Antony, 2014).

$$y_i = \beta_0 + \beta_1 Z_{1i} + \beta_2 Z_{2i} + \beta_3 Z_{1i} Z_{2i} + e_i \quad (2.9)$$

y_i = outcome score for the ith unit

β_0 = coefficient for the intercept

β_1 = mean difference on factor 1

β_2 = mean difference on factor 2

β_3 = interaction of factor 1 and factor 2

Z_{1i} = dummy variable for factor 1

Z_{2i} = dummy variable for factor 2

e_i = residual for the ith unit

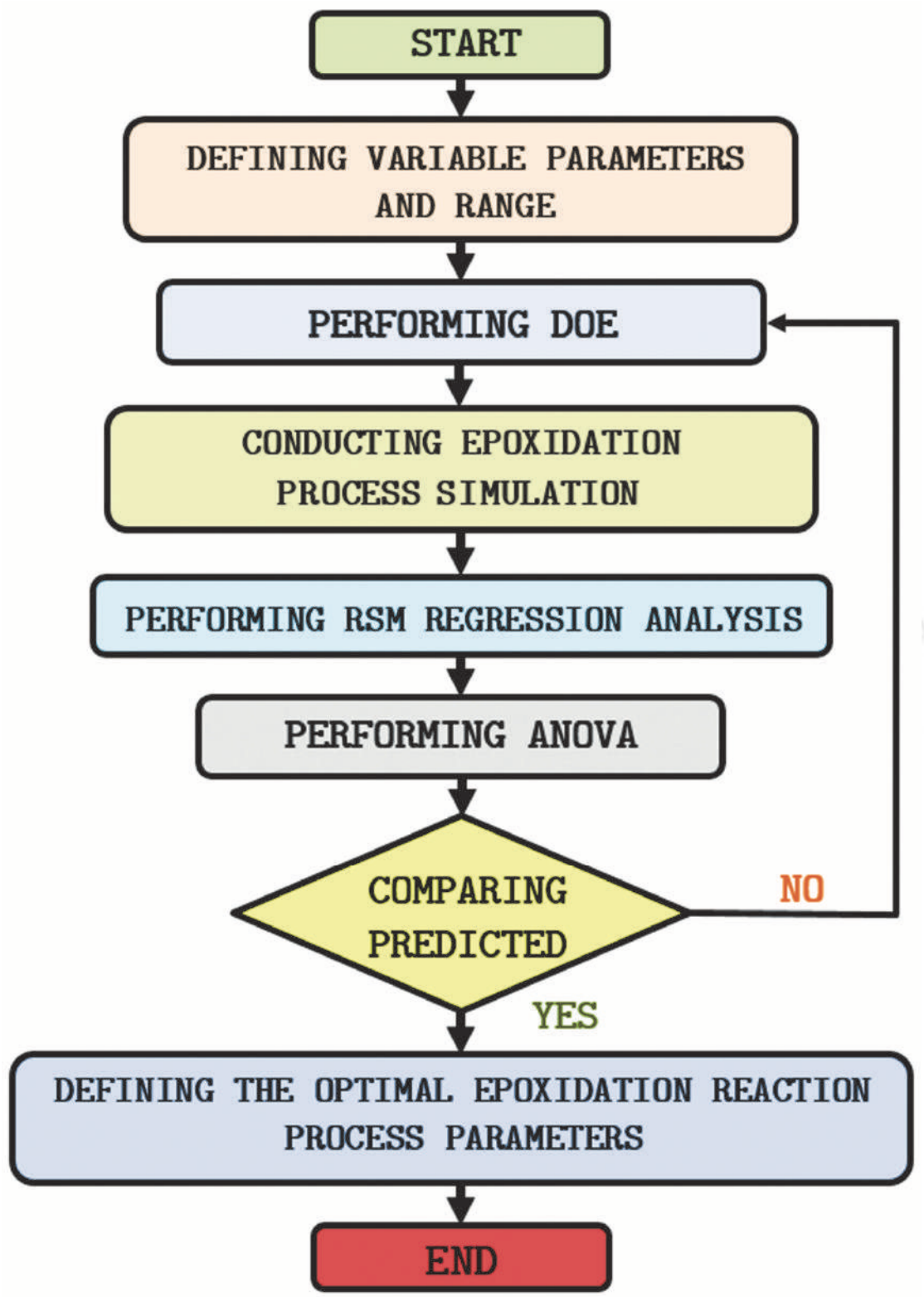

Figure 2.4. Flowchart for Response Surface Methodology (RSM). Adapted from (Hazwan et al., 2017).

2.5. Artificial Neural Network

The artificial neural network can be used for polynomial regression model as an alternative to statistical model as it can predict complex nonlinear model. ANN having extremely interconnected structure, consists of a large number of simple processing elements called neurons, which are organised in different layers in the network (an input layer, an output layer, and all other intermediate units, called hidden layers) (Shanmugaprakash and Sivakumar, 2013). In this work, a three-layered feedforward neural network was used. Log-sigmoid transfer function (log sig) was used as a hidden layer transfer function, the linear transfer function (purelin) was used as an output layer transfer function, and Levenberg–Marquardt algorithm was used as the overall training method (algorithm) (Garciaa-Gimeno et al., 2003; Prakash Maran and Priya, 2015a, 2015b).

The sigmoid transfer function was given by

$$Y_i = \frac{1}{(1+\exp(-net_i))} \tag{2.10}$$

The linear activation function is used as output layer activation function

$$Y_i = (net_i) \tag{2.11}$$

Where, Y_i is the output from node i and net_i is the input to the node $i = \sum w_i \times x_i$

The back propagation algorithm (BPA) and Levenberg-Marquardt (LM) were used for network training. MATLAB (version R2014b (8.4.0.150421)) mathematical software was used to model the system by artificial neural network

toolbox (version 8.2.1). The input variables were oil/ME to H_2O_2, oil/ME:H_2SO_4 ratio, and time. Oxirane oxygen content is used as a target (Mohamed et al., 2013).

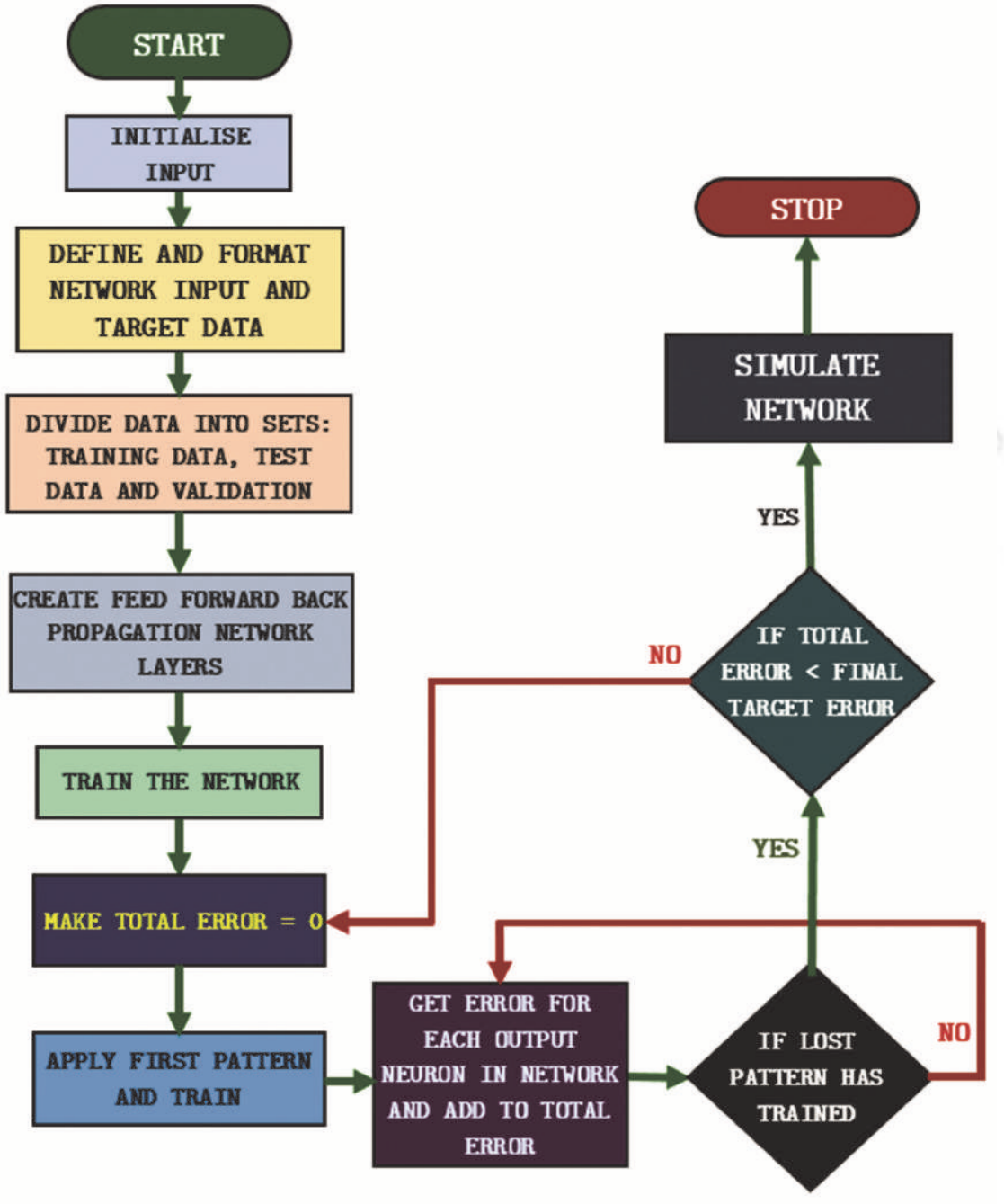

Figure 2.5. Flowchart for Artificial Neural Network (ANN). Adapted from (Karthic et al., 2013).

2.6. Genetic Algorithm

Genetic algorithm (GA) is a class of heuristic optimisation methods. GA mimics the process of natural evolution by modifying a population of individual solutions. Design points are represented by chromosomes. The method randomly selects individuals from the current population to be parents and uses them to produce the children for the next generation. Over consecutive generations, the population approaches an optimal solution because "good" parents produce "good" children. The "bad" points are eliminated from the generation. GA can be applied to solve a variety of optimisation problems in many applications that are not suited for conventional optimisation methods, including problems in which the objective function is discontinuous, non-differentiable, or nonlinear. GA has the potential to reach the global optimal solution if it does not stick at a local optimal solution. Since GA is a probabilistic approach, different solutions could be generated by different runs. Therefore, multiple runs are required to verify the optimal solution. A GA flowchart is shown in Figure 2.6.

On the other hand, genetic algorithm (GA) is a stochastic method mostly associated with the simulation of biological heredities and evolutionary processes. Each desirable solution to a set of problems is taken as an "individual" among the population, and each individual is coded as a character string. GA applies its unique selection, crossing, and mutagenesis operators on a random population to compute a new one, eventually introducing some diversity to the algorithm (Garciaa-Gimeno et al., 2003). An interesting trait of GA is that the algorithm can avoid a one-point optimal search usually associated with gradient descent or LM back propagation. Instead, GA is capable of global optimum exploration of the design space (Ghaffari et al., 2006).

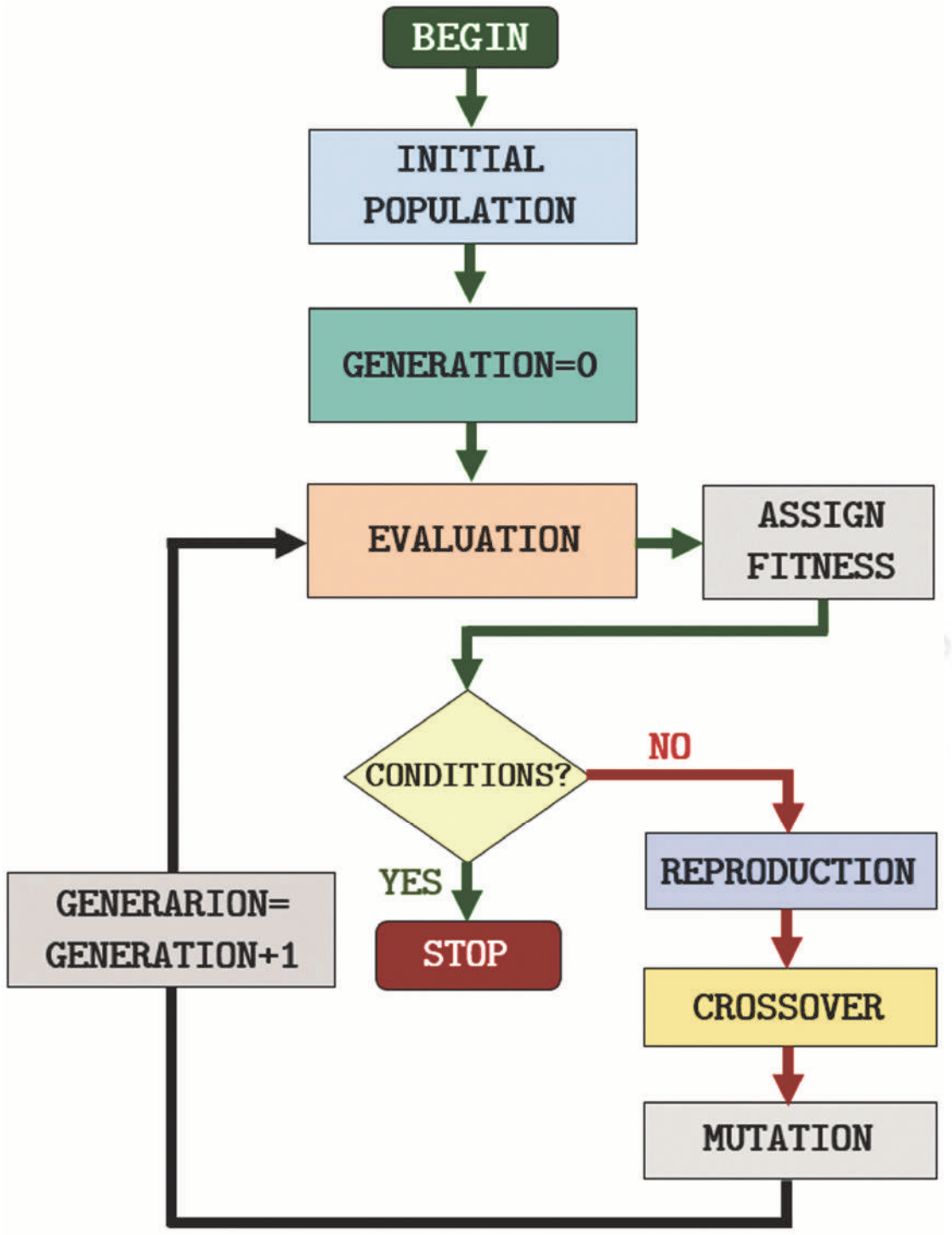

Figure 2.6. Flowchart showing working principle of GA. Adapted from (Deb, 2011).

2.7. Kinetics Analysis

The kinetics data of thermal degradation of WSCO, WSCOME, epoxide of waste soybean cooking oil (EWSCO), and epoxide of waste soybean cooking oil methyl esters (EWSCOME), was obtained in the form of percentage of mass available over the time and temperature from thermogravimetric analysis at different heating rates. The kinetics parameters such as apparent activation energy, pre-exponential factor and kinetics model for thermal degradation mechanism of selected liquid compounds were determined as per the recommendations of the ICTAC Kinetics Committee (Vyazovkin et al., 2014, 2011) as described in following paragraph.

Thermogravimetric kinetics of epoxides (bio-lubricant) was shown in this study. The overall process can be represented by the following reaction schemes, where Volatiles refers to the sum of condensable gases and non-condensable gases (Equation (2.12)).

Bio-lubricant = Solid residue + Volatiles (2.12)

The selected liquid compound on thermal degradation formed another intermediate liquid product which subsequently degraded to form volatiles. Therefore, for this case, the whole thermal degradation reaction can be written as $A(l) \rightarrow B(g)$. The rate equation for this reaction can be represented as

$$Rate \propto [A]^n \text{ or } Rate = k \times f(\alpha) \text{ or } \frac{d\alpha}{dt} = k \times f(\alpha) \quad (2.13)$$

$\frac{d\alpha}{dt}$ is degradation rate, α is fractional conversion, and $k$is the rate constant.

Rate constant k is represented as a function of temperature according to Arrhenius equation

$$k = A T^{m} e^{\left(\frac{-E}{RT}\right)} \text{ or } k = A e^{\left(\frac{-E}{RT}\right)} \quad (2.14)$$

where T is absolute temperature, A is pre-exponential or frequency factor, E is apparent activation energy, R is the gas constant ($8.314\,J/mol/K$).

Fractional conversion α at any time t is computed from TG data as

$$\alpha = \frac{m_i - m_t}{m_i - m_f} \quad (2.15)$$

where m_i is the initial mass of sample, m_t is the mass of sample residue at temperature T during the thermal decomposition, and m_f is the final mass residue of the sample when the experiment is completed.

For non-isothermal kinetics analysis, the linear heating rate $\left(\beta \text{ or } \frac{dT}{dt}, ^{\circ}C/\min\right)$ was applied to heat the sample, which can be represented as $T = T_0 + \beta t$, where T_0 is initial temperature and T is temperature at time t (Khawam and Flanagan, 2005; Yancey and Vyazovkin, 2015). The previously defined term $d\alpha/dt$ is isothermal reaction rate, which was transformed into non-isothermal reaction rate $d\alpha/dT$ as shown in Equation (2.16).

$$\frac{d\alpha}{dT} = \frac{d\alpha}{dt} \times \frac{dt}{dT} \quad (2.16)$$

Equation (2.16) can be written as,

$$\frac{d\alpha}{dT} = \frac{d\alpha}{dt} \times \frac{1}{\beta} \quad (2.17)$$

The non-isothermal reaction rate equation can be written as Equation (2.18)

$$\frac{d\alpha}{dT} = \frac{k \times f(\alpha)}{\beta} \tag{2.18}$$

$$\frac{d\alpha}{dT} = \frac{A}{\beta} \times e^{-\frac{E}{RT}} \times f(\alpha) \tag{2.19}$$

The Equation (2.19) represents the differential form of non-isothermal reaction rate, which can be transformed into integral form as Equation (2.20).

$$g(\alpha) = \int \frac{d\alpha}{f(\alpha)} = \frac{A}{\beta} \int e^{-\frac{E}{RT}} \times dT \tag{2.20}$$

2.7.1. Arrhenius method

The final rate equation of Arrhenius method can be obtained as follows:

$$\ln\left(\frac{d\alpha}{dt}\right) - n\ln(1-\alpha) = \ln\left(\frac{A}{\beta}\right) - \frac{E}{RT} \tag{2.21}$$

According to Equation (2.21), the plot of $\ln\left(\frac{d\alpha}{dt}\right) - n\ln(1-\alpha)$ versus $\frac{1}{T}$ should give a straight line for the appropriate value of reaction order n. The activation energy and pre-exponential factor of each of the active degradation stages were calculated from the related slope $\left(-\frac{E}{R}\right)$ and interception $\ln\left(\frac{A}{\beta}\right)$ in final plots, respectively.

As per the recommendations from ICTAC committee, iso-conversional methods are used for kinetics analysis in present work. Among the few commonly used non-isothermal kinetics methods from literature, Kissinger-Akahira-Sunose (KAS) (Sbirrazzuoli et al., 1997) and Flynn-Wall-Ozawa (FWO) (Flynn and Wall, 1966; Ozawa, 1965) are broadly applicable model-free iso-conversional methods (Khawam and Flanagan, 2006).

2.7.2. Iso-conversional Methods ("Model Free" Approach)

The iso-conversional method is used to calculate the activation energy (E) at different conversion rates (α) without any prior modelistic assumptions (Pal and Katiyar, 2017). The main advantage of this method is that it does not require any previous knowledge of reaction mechanisms. In this study, the most common established "model free" methods like Friedman method, Kissinger-Akahira-Sunose (KAS), and Flynn-Wall-Ozawa (FWO) have been used to calculate kinetics parameters at different heating rates. Models are generally classified based on the graphical shape of their isothermal curves ($\alpha vs t$ or $d\alpha/dt\ vs\ \alpha$) or on their mechanistic assumptions (Khawam and Flanagan, 2006).

2.7.2.1. Friedman Method

This method is a useful iso-conversional method for calculation of activation energy. The method can be written as

$$\ln\frac{d\alpha}{dt} = \ln\left[\frac{d\alpha}{dT}\right] = \ln\left[Af(\alpha)\right] - \frac{E}{RT} \tag{2.22}$$

Graphs are plotted between $\ln\left[\frac{d\alpha}{dT}\right]$ vs $\frac{1}{T}$ for constant conversions, and from the slope of the linear lines, activation energy can be calculated (Friedman, 1964).

2.7.2.2. Kissinger-Akahira-Sunouse Method

KAS method is based on Murray and White approximation for temperature integral (Kissinger, 1957).

$$\frac{d\alpha}{f(\alpha)} = \frac{A}{\beta}\exp\left[-\frac{E}{RT}\right]dT \tag{2.23}$$

This method utilises the initial condition of $\alpha = 0$ and $T = T_0$ for obtaining the expression below

$$g(\alpha) = \int_0^{\alpha} \frac{d\alpha}{f(\alpha)} = \frac{A}{\beta} \int_{T_0}^{T} \exp\left[-\frac{E}{RT}\right] dT = \frac{AE}{\beta R} p\left[\frac{E}{RT}\right] \tag{2.24}$$

The KAS method can be written as given below

$$ln\left(\frac{\beta}{T^2}\right) = -\left(\frac{E}{RT}\right) + ln\left(\frac{AR}{E\, g(\alpha)}\right) \tag{2.25}$$

This method is based on Coats-Redfern approximation (Aboulkas and Harfi, 2008). The assumption of this method is that A, f(α) and E are independent of temperature T. A and E are also assumed to be independent of conversion. In this method, plots have been made between $\ln(\beta / T^2)\ vs\ 1/T$. Straight lines are obtained at each conversions, and from the slope of these lines, activation energy (E) can be calculated.

2.7.2.3. Flynn-Wall-Ozawa Method

This method is an integral iso-conversional method, based on Doyal's linear approximation (Opfermann and Kaisersberger, 1992). The equation comes from Arrhenius rate equation. The FWO equation can be expressed as given below

$$\ln \beta = \ln\left[\frac{AE}{R\, g(\alpha)}\right] - 5.331 - 1.052\frac{E}{RT} \tag{2.26}$$

In this method, graph was plotted between $\ln \beta\ vs\ 1/T$ for every sample. Straight lines should be obtained at various conversions in different heating rates. The slopes of these lines can be utilised to calculate the activation energy (E) (Flynn and Wall, 1966; Ozawa, 1965).

2.7.3. Master Plot Method for Mechanistic Analysis

The mathematical model to describe the thermal degradation mechanism was determined using master plots defined by Criado (Criado, 1978). The LHS of Equation (2.27) was created by using experimental data and compared with the plots drawn using theoretical models given in Table 2.1. All models used for solid-state kinetics cannot be used for liquid phase thermal degradation kinetics, however few models such as first-order reaction model (F1), autocatalytic models (A1, A2, A3), and contracting geometry models (R2, R3) can be used to describe the liquid phase kinetics.

$$\left(\frac{T}{T_{0.5}}\right)^2 \times \frac{(d\alpha/dt)}{(d\alpha/dt)_{0.5}} = \frac{f(\alpha)\times g(\alpha)}{f(\alpha)_{0.5}} \tag{2.27}$$

2.7.4. Determining Reaction Models and Pre-Exponential Factors from Model-Free Methods

The aforementioned model-free methods (e.g., iso-conversional) allow one to evaluate the activation energy without determining the reaction model. However, this should not be understood to imply that the model-free methods cannot be used for determining the reaction models. Both reaction model and pre-exponential factor can be readily determined when using model-free methods subject to one important condition. Here, model and pre-exponential factor were determined by using the compensation effect method. For this purpose, the E_i and A_i values are used to determine the 'a' and 'b' parameters of the compensation effect. Then, substitution of the model-free activation energy into

compensation equations gives a model-free estimate for the pre-exponential factor, A_0. Then, from the knowledge of E_0 and A_0, the kinetics model was determined.

$$\ln A_i = aE_i + b \tag{2.28}$$

The parameters a and b depend on the heating rate. The invariant kinetics parameters, $ln\ A_{inv}$ and E_{inv} are evaluated from several sets of b_j and a_j obtained at different heating rates β_j as follows:

$$b_j = lnA_{inv} + E_{inv}a_j \tag{2.29}$$

$$ln\ A_0 = aE_0 + b \tag{2.30}$$

$$f(\alpha) = \beta\left(\frac{d\alpha}{dT}\right)_a \left[A_0\, exp\left(\frac{-E_0}{RT_\alpha}\right)\right]^{-1} \tag{2.31}$$

Table 2.1. Some of the kinetics models for liquid state thermal degradation.

Code	Reaction Model	$f(\alpha) = 1/k \times d\alpha/dt$	$g(\alpha) = kt$
F1	First order	$(1-\alpha)$	$-\ln(1-\alpha)$
F2	Second order	$(1-\alpha)^2$	$-(1-\alpha)^{-1}$
Fn	n^{th} order	$(1-\alpha)^n$	$1-(1-\alpha)^{1-n}/1-n$
P2	Mampel power law (n = 1/2)	$2\alpha^{1/2}$	$\alpha^{1/2}$
P3	Mampel power law (n = 1/3)	$3\alpha^{2/3}$	$\alpha^{1/3}$
P4	Mampel power law (n = 1/4)	$4\alpha^{3/4}$	$\alpha^{1/4}$
A1	Nucleation and growth (Avrami-Erofeyev)	$1.5(1-\alpha)[-\ln(1-\alpha)]^{1/3}$	$[-\ln(1-\alpha)]^{2/3}$
A2	Nucleation and growth (Avrami-Erofeyev)	$2(1-\alpha)[-\ln(1-\alpha)]^{1/2}$	$[-\ln(1-\alpha)]^{1/2}$
A3	Nucleation and growth (Avrami-Erofeyev)	$3(1-\alpha)[-\ln(1-\alpha)]^{2/3}$	$[-\ln(1-\alpha)]^{1/3}$
A4	Nucleation and growth (Avrami-Erofeyev)	$4(1-\alpha)[-\ln(1-\alpha)]^{3/4}$	$[-\ln(1-\alpha)]^{1/4}$
R1	Phase boundary controlled reaction (One dimensional movement)	1	α
R2	Contracting geometry (Area)	$2(1-\alpha)^{1/2}$	$1-(1-\alpha)^{1/2}$
R3	Contracting geometry (Volume)	$3(1-\alpha)^{2/3}$	$1-(1-\alpha)^{1/3}$
D1	1-D diffusion	$1/2\alpha$	α^2
D2	2-D diffusion (Valensi equation)	$[-\ln(1-\alpha)]^{-1}$	$(1-\alpha)\ln(1-\alpha)+\alpha$
D3	3-D diffusion (Jander equation)	$3/2(1-\alpha)^{2/3}[1-(1-\alpha)^{1/3}]^{-1}$	$[1-(1-\alpha)^{1/3}]^2$
D4	3-D diffusion (Ginstling-Brounshtein)	$3/2[(1-\alpha)^{1/3}-1]^{-1}$	$(1-2\alpha/3)-(1-\alpha)^{2/3}$

CHAPTER III

In Situ Epoxidation of Waste Soybean Cooking Oil (WSCO) for Synthesis of Bio-lubricant Base Stocks: Process Parameter Optimisation and Comparison with Response Surface Methodology (RSM), Artificial Neural Network (ANN), and Genetic Algorithm (GA)

Effect of Process Parameters on Epoxidation of WSCO

Optimisation of Epoxidation of WSCO using RSM, ANN & GA

Physico-chemical Characterisation of EWSCO

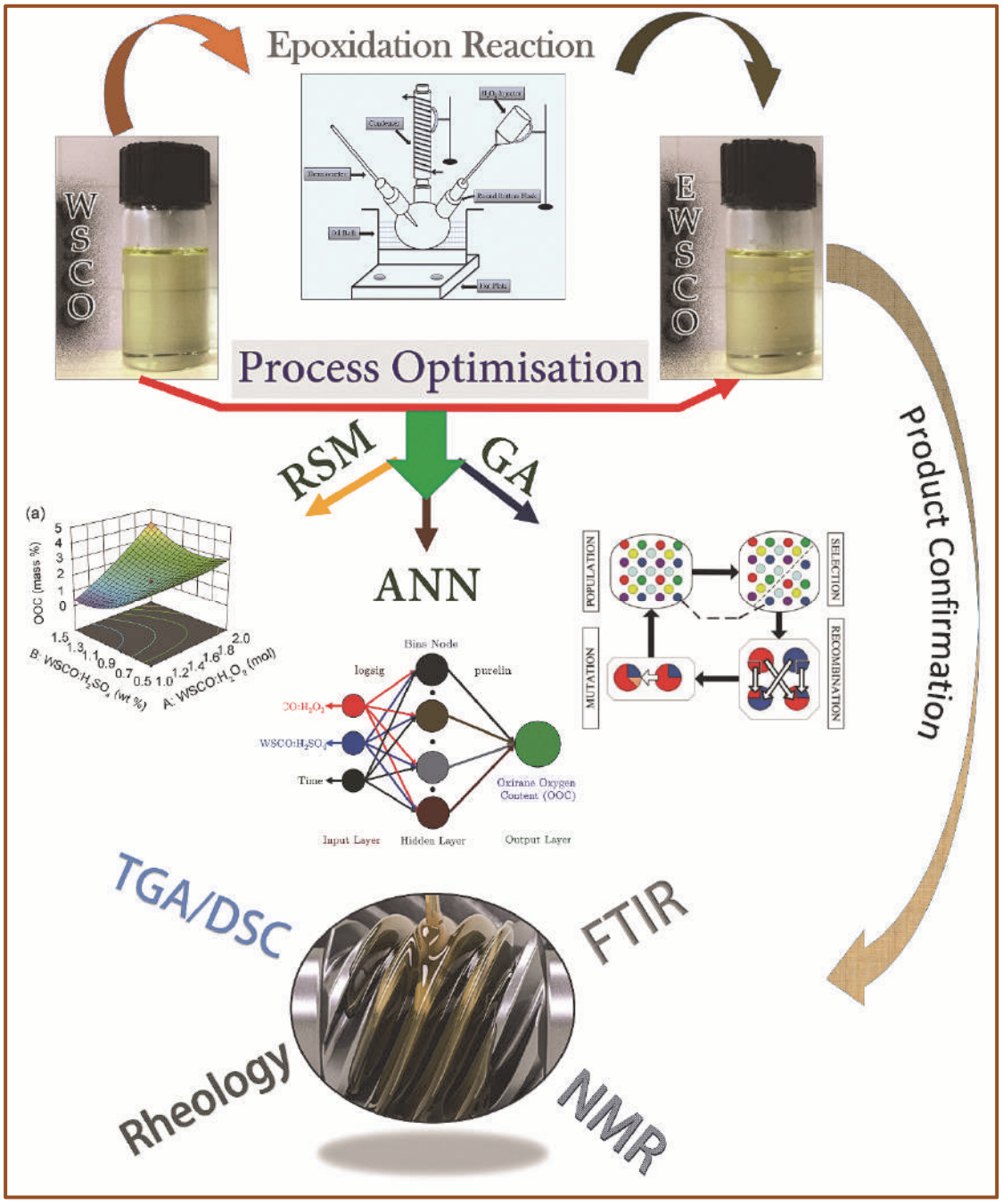

Graphical Abstract of Chapter III

Chapter III

In Situ Epoxidation of Waste Soybean Cooking Oil (WSCO) for Synthesis of Bio-lubricant Base Stocks: Process Parameter Optimisation and Comparison with Response Surface Methodology (RSM), Artificial Neural Network (ANN), and Genetic Algorithm (GA)

In the present investigation, waste soybean cooking oil (WSCO) as bio-lubricant base stocks was prepared via structural modification of unsaturated fatty acids (i.e. in situ epoxidation). Optimisation of the effect of process parameters on maximum oxirane oxygen content (OOC) was studied using RSM. Interaction among the process parameters, such as C=C bonds to H_2O_2 molar ratio, catalyst loading and reaction time were examined by ANOVA using Design Expert software. The main focus of this study was to establish optimum OOC conditions using sulphuric acid (H_2SO_4) as a homogeneous acid catalyst. Optimum OOC of epoxidised waste soybean cooking oil (EWSCO) was found to be 4.69 mass % under the experimental conditions of 60 °C temperature, 6 h of reaction time, 1.5 g of catalyst loading and 1:2 molar ratio of C=C bonds to H_2O_2. The resultant epoxide product was confirmed using Fourier transform infrared spectroscopy (FTIR) (at 844 cm^{-1}) and Nuclear magnetic resonance spectroscopy (NMR) (at δ 2.8 to δ 3.1 ppm) analysis. Apart from that, significant physico-chemical properties of the prepared lubricant base stocks were evaluated at optimum condition using standard methods. The study was also extended to use artificial

neural networks (ANNs) as an alternative tool for modelling and predicting an optimum conversion of the unsaturated fatty acids to epoxide in comparison with the response surface methodology (RSM). Further, ANN modelling and genetic algorithm (GA) optimisation were carried out by using identical data set.

3.1. Effect of Process Parameters

In order to optimise the process, central composite design (CCD) and response surface methodology (RSM) were applied to design the experimental matrix (Table 3.1) to investigate the effect of three process parameters on WSCO epoxidation as the response. The design matrix incorporated three independent variables with three levels. According to the CCD scheme, twenty experimental runs were performed to optimise the effect of process parameters on WSCO epoxidation. Table 3.2a illustrates the chosen three independent process parameters: H_2O_2 molar ratio (A), catalyst loading (B) and reaction time (C). These are analysed to determine the optimal conditions for the maximum epoxide formation. Based on the experimental observations (Table 3.2a), a quadratic model for the response surface was developed in terms of coded variables as shown in Equation 3.1.

$$OOC\ (mass\ \%) = 1.6 + (1.03\times A) - (0.31\times B) - (0.11\times C) + (0.87\times A\times B) - (0.032\times A\times C) - (0.28\times B\times C) + (0.23\times A^2) + (0.75\times B^2) + (0.11\times C^2) \quad (3.1)$$

Since the knowledge about this process is ultimately limited, ANOVA was utilised to understand the interaction among the process variables. The ANOVA of the surface quadratic model was operated as per Equation 3.1, and individual coefficients are compiled and tabulated in Table 3.3. In statistical analysis, a P-value greater than 0.05 (> 0.05) implies that the null hypothesis is strongly

supported and that the null hypothesis is not statistically significant. The null hypothesis is retained, and the alternative hypothesis is rejected as a result of this. It should be noted that the null hypothesis cannot be accepted; we can only reject the null hypothesis or fail to reject the null hypothesis. The impact of process variables during the epoxidation was measured based on the magnitude of obtained F and P values. Greater the F value and smaller the P value ($P < 0.05$), higher would be its effect on the overall response. From the resulted F value (345.31) and P value (<0.0001) of the model, it is evident that the aforementioned quadratic model is highly significant in predicting the measured responses accurately (Table 3.3). Regression coefficient (R^2) value was found to be 0.99 which indicates that the obtained surface model is successful in interpreting the variance of percentage unsaturation conversion in the WSCO by 99 %. Moreover, P values of the process parameters shown in Table 3.3 infer that most of the model terms, i.e. linear (A, B, C), cross (AB, BC) and quadratic terms (A^2, B^2, C^2), are highly significant (since $P < 0.05$). In this model, reaction time with C=C to H_2O_2 molar ratio (AC) has not shown any significant (since $P > 0.05$) effect on WSCO epoxidation. Comparative study on the interaction of process variables revealed that the parameters, time and H_2O_2 molar ratio, are not shown to have any significant effect on the epoxide formation. Whereas, catalyst loading and H_2O_2 molar ratio played an important role to maximise the epoxide formation. Therefore, linear terms, cross terms (except AC), and quadratic terms were highly significant to obtain higher OOC, and the response was purely depended on all these factors. The aforementioned ANOVA results proposed that all these factors are the primary determining factors to form EWSCO with maximum OOC. The 'lack of fit' (F) value for this response showed that it is highly insignificant, i.e. $P < 0.05$ relative to the pure error; this indicates

that the entire model predicted for the responses was adequate. The 'lack of fit' tests compare the residual error to the pure error from replicated design points. Figure 3.1 shows the graphical representation of the predicted and actual values of the response (OOC) which indicate that the developed model was significantly efficient to optimise the process with (Table 3.3) good reproducibility of experimental data for maximum OOC. The sequential model sum of squares is shown in Table 3.4.

Table 3.1. Process parameters and their levels to optimise WSCO epoxidation.

Independent Process Parameters	Symbol	Unit	Process Parameter Coded Levels		
			–1	0	+1
WSCO : H_2O_2	A	mol	1	1.5	2
WSCO : H_2SO_4	B	wt %	0.5	1	1.5
Time	C	h	6	8	10

Table 3.2a. Design matrix (CCD) of experiments for WSCO epoxidation and OOC response

	Input Process Parameters			Experimental Output	RSM Predicted Output	ANN Predicted Output
Run No.	WSCO:H_2O_2 (A)	WSCO: H_2SO_4 (B)	Time (C)		(OOC)	
1	1	0.5	6	2.63±0.25	2.64	2.64
2	2	0.5	6	3.1±0.15	3.03	3.12
3	1	1.5	6	0.75±0.09	0.83	0.76
4	2	1.5	6	4.7±0.24	4.70	4.70
5	1	0.5	10	3.1±0.44	3.04	3.07
6	2	0.5	10	3.45±0.75	3.30	3.44
7	1	1.5	10	0.12±0.05	0.13	0.15
8	2	1.5	10	3.93±0.44	3.86	3.67
9	0.66	1	8	0.58±0.11	0.52	0.68
10	2.34	1	8	3.85±0.08	3.99	3.85
11	1.5	0.16	8	4.12±0.14	4.25	4.12
12	1.5	1.84	8	3.24±0.27	3.20	3.25
13	1.5	1	4.64	2.13±0.12	2.09	2.13

14	1.5	1	11.36	$1.62_{\pm}0.07$	1.73	1.68
15	1.5	1	8	$1.65_{\pm}0.06$	1.60	1.60
16	1.5	1	8	$1.61_{\pm}0.05$	1.60	1.60
17	1.5	1	8	$1.69_{\pm}0.06$	1.60	1.60
18	1.5	1	8	$1.60_{\pm}0.05$	1.60	1.60
19	1.5	1	8	$1.62_{\pm}0.06$	1.60	1.60
20	1.5	1	8	$1.63_{\pm}0.05$	1.60	1.60

Table 3.2b. The calculated value of different error functions.

	Standard Deviation	Mean Square Errors	Root Mean Square Errors	Sum of Squares of Errors	Average Relative Errors	Sum of Absolute Errors	Hybrid Fractional Error Function	Marquart's Percentage Standard Deviation
RSM	0.0467	0.0055	0.0741	0.0415	0.0344	1.1700	0.0030	5.0787
ANN	0.0598	0.0049	0.0698	0.0680	0.0350	0.7662	0.0031	7.8015

Table 3.3. Analysis of variance (ANOVA) for response surface quadratic model.

Source	Sum of Squares	Degrees of Freedom (df)	Mean Square	F–values	P–values
Model	31.16	9	3.46	345.31	< 0.0001
A	14.52	1	14.52	1447.79	< 0.0001
B	1.33	1	1.33	132.54	< 0.0001
C	0.16	1	0.16	15.81	0.0026
AB	6.02	1	6.02	600.50	< 0.0001
AC	0.0084	1	0.0084	0.84	0.3802
BC	0.62	1	0.62	61.45	< 0.0001
A^2	0.79	1	0.79	78.35	< 0.0001
B^2	8.14	1	8.14	811.63	< 0.0001
C^2	0.17	1	0.17	17.31	0.0019
Residual	0.10	10	0.010	—	—
Lack of Fit	0.10	5	0.020	—	—
Pure Error	0.000	5	0.000	—	—
Cor Total	31.26	19	—	—	—
R^2	—	—	—	—	0.9968

— not available or not required

Table 3.4. Sequential model sum of squares.

Source	Sum of Squares	Degrees of Freedom (df)	Mean Square	F–values	P–values	
Mean vs. total	109.98	1	109.98	—	—	
Linear vs. mean	16.00	3	5.33	5.59	0.0081	
2FI vs linear	6.64	3	2.21	3.34	0.0527	
Quadratic vs 2FI	8.51	3	2.84	282.97	< 0.0001	Suggested
Cubic vs quadratic	0.082	4	0.020	6.66	0.0214	Aliased
Residual	0.018	6	0.0031	—	—	
Total	141.24	20	7.06	—	—	

— not available or not required

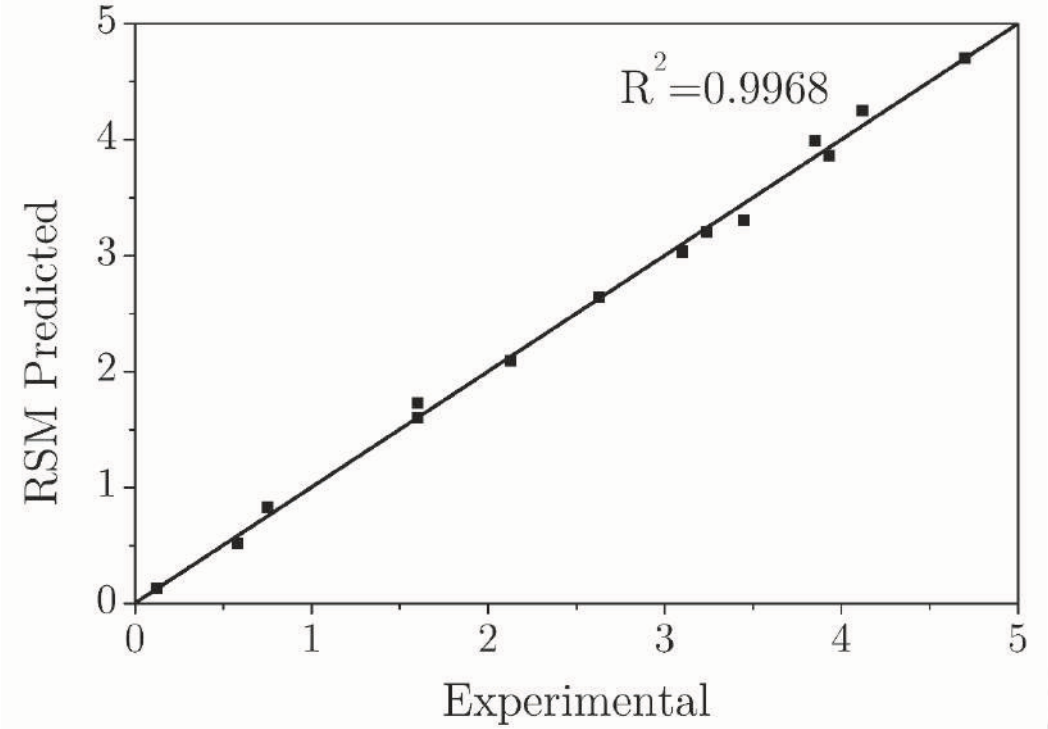

Figure 3.1. Correlation between actual and predicted value of OOC.

To investigate the interactive effects of these process variables on the response, three-dimensional response surface plots and two-dimensional counter-plots are drawn by considering two variables at a time while keeping the other at a central level (0). These plots are a graphical representation of quadratic polynomial (Equation 3.1) from Design Expert software.

Two dimensional response surfaces and contour plots were used to assist a straight forward examination of the influence of experimental variables on the responses as well as to find the local optima for WSCO epoxidation (Figure 3.2). The contour plot as a function of two factors at a time, holding other factors at fixed level, is useful for understanding both the main effects and the interaction effects of these two factors. The effect of H_2O_2 molar ratio and catalyst loading on OOC, while other variable (reaction time) was fixed at central level, showed

that OOC increased linearly with an increase in the H_2O_2 molar ratio and catalyst loading. The other condition of independent variables, reaction time and H_2O_2 molar ratio, showed similar effects (Figure 3.3). Likewise, the contour plot for reaction time and catalyst loading on OOC, where the molar ratio of H_2O_2 was kept at the central level (Figure 3.4), showed increased OOC with catalyst loading, but a decrease in OOC with an increase in the reaction time.

Based on the aforementioned detailed study, it was observed that H_2O_2 molar ratio and catalyst loading were the important factors in determining the success of *in situ* epoxidation. From this study, it was concluded that higher H_2O_2 molar ratio, higher catalyst loading, and shorter reaction time favoured the maximum OOC. All the process variables should be monitored carefully in order to obtain an optimum OOC. From the optimisation study, various sets of experimental conditions were suggested. Among them, the following set of experimental conditions was followed: 2 moles of H_2O_2; 1.5 wt % of catalyst loading and 6 h of reaction time—at this condition, OOC of EWSCO was found to be 4.7 mass %.

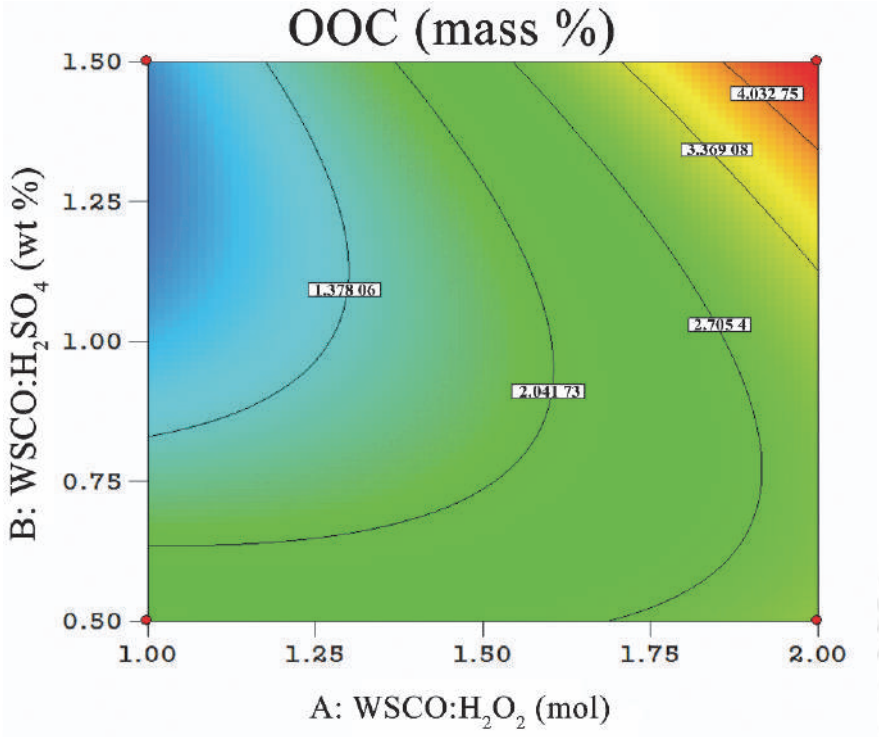

Figure 3.2. Counter plot showing the effect of H_2O_2 molar ratio (A) and H_2SO_4 (B) on OOC when time kept at central level (8 h).

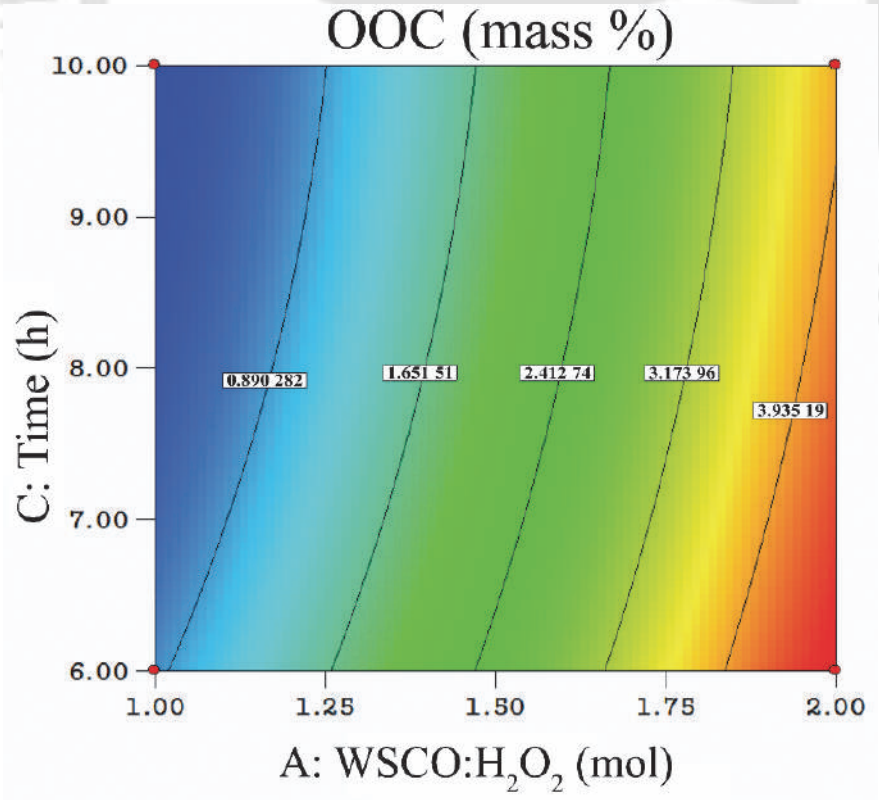

Figure 3.3. Counterplot showing the effect of H_2O_2 molar ratio (A) and time (C) on OOC when catalyst loading kept at central level (1.5 wt %).

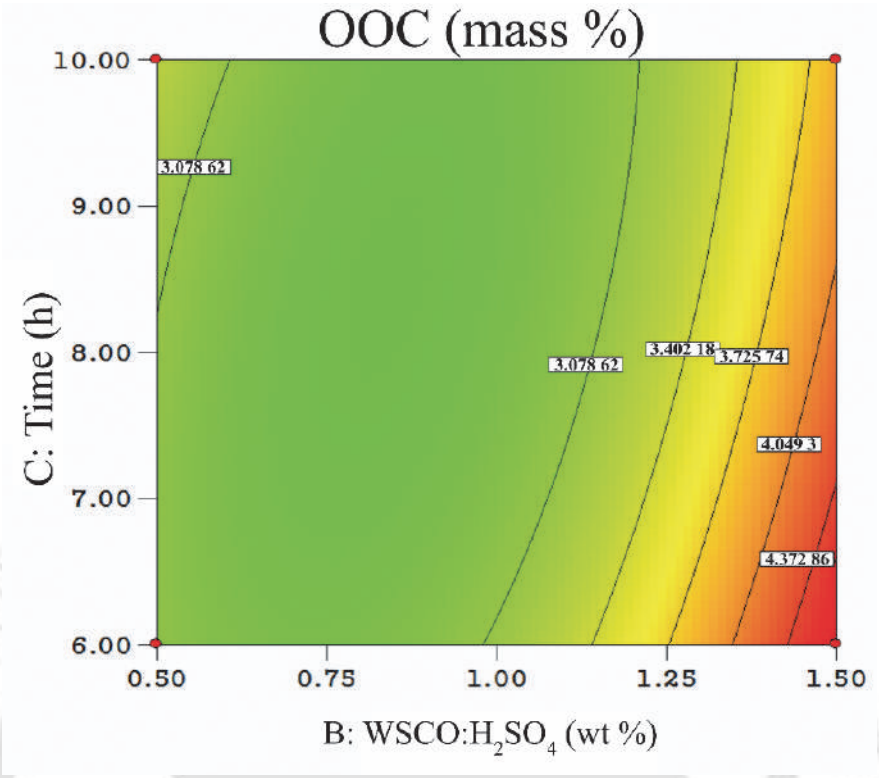

Figure 3.4. Counter plot showing the effect of H_2SO_4 (B) and time (C) on OOC when H_2O_2 molar ratio kept at central level (2 mol).

3.2. Model Validation and Confirmation

In order to verify the predictive capacity of the models, optimum response variables were tested by expermentation at the theoretical condition. At the optimised process condition (4.69 mass %), OOC did not significantly differ from predicted value (4.7 mass %), which suggests that the formulated model was trusted to be precise and reliable. All the experiments (Table 3.2a), including confirmatory experiments, were duplicated at laboratory conditions, and average values were reported. The adequacy of root mean square error (RMSE) (Equation 3.3) value represents the variability proportions amongst the total sample. The RMSE value describes that the model equation can define the system behaviours and can be applied to experimental condition (Maity et al., 2014).

$$R\ Squared = 1 - \frac{\sum (x_{ex,i} - y_{pre,i})^2}{\sum y_{pre,i}^{\ 2} - \frac{\sum y_{pre,i}^{\ 2}}{n}} \tag{3.2}$$

$$RMSE = \sqrt{\frac{1}{n}\sum_{i=1}^{n} (x_{ex,i} - y_{pre,i})^2} \tag{3.3}$$

$x_{ex,i}$= experimental data, $y_{pre,i}$ =predicted data, n= number of experimental data

3.2.1. Error Functions

Average relative error (ARE) indicates a tendency to under or overestimate the experimental data, attempts to minimize the fractional error distribution across the entire dataset. Sum of absolute errors (EABS) approach is similar to the sum square error, with an increase in the errors will provide a better fit. Hybrid fractional error function (HYBRID); to improve the sum of the squares of the errors at lower levels of epoxidation reaction, this error function was developed. In this task, each the sum of the squares of the error values was divided by the experimental OOC value. Marquardt's percent standard deviation (MPSD) follows the geometric mean error which allows for the number of degrees of freedom of the system (Allen et al., 2003; Foo and Hameed, 2010).

$$ARE: \frac{1}{n}\sum_{i=1}^{n} \left| \frac{OOC_{exp} - OOC_{cal}}{OOC_{exp}} \right|_i \tag{3.4}$$

$$EABS: \sum_{i=1}^{n} \left| OOC_{exp} - OOC_{cal} \right|_i \tag{3.5}$$

$$HYBRID: \frac{1}{n-p}\sum_{i=1}^{n} \left[\frac{\left(OOC_{exp} - OOC_{cal}\right)^2}{OOC_{exp}} \right]_i \tag{3.6}$$

$$MPSD : 100\sqrt{\frac{1}{n-p}\sum_{i=1}^{n}\left(\frac{OOC_{exp}-OOC_{cal}}{OOC_{exp}}\right)_i^2} \quad (3.7)$$

Where n is the number of data points, p is the number of parameters within the equation, OOC_{exp} is the experimental value of OOC and OOC_{cal} is the calculated value of OOC by different model.

3.3. Validation through Artificial Neural Network

Response of the artificial neural network was analysed using same process parameters as that used in RSM. Although ANN requires a large dataset to build a network, if the input data points are precisely distributed for the model construction, which is the case with Design Expert, the RSM generated data should be sufficient to build an effective ANN network with a smaller dataset. There are mainly three steps to build an optimum ANN network, a) select a suitable and best back propagation training algorithm, b) use a proper number of neurons, and c) conduct testing and validation of the model.

A neural network is typically composed of individual and interconnected units usually called neurons, nodes, or units. Training a network consists of an iterative process in which network is given the proper inputs along with a correct output for each input. The network architecture was developed with three nodes in the input layer, four nodes in the hidden layer, and one node in the output layer (3–4–1), represented in Figure 3.5. Three inputs (WSCO:H_2O_2, WSCO:H_2SO_4, and Time) were used to develop the ANN model to come up with a single output OOC. The network then tries to alter its weights to attempt and create the correct output (very small error margin). After successful training, it learns the

training set and is prepared to perform on previously unseen data (Lahiri and Ghanta, 2009). The learning weights are slightly adjusted during each iteration through training set (training cycle) until the appropriate weights have been established. It can perform thousands of training cycle depending on the complexity of the task. Once the output is correct (or very close to target), the weights can be used with the same network on unseen data to examine how well it performs.

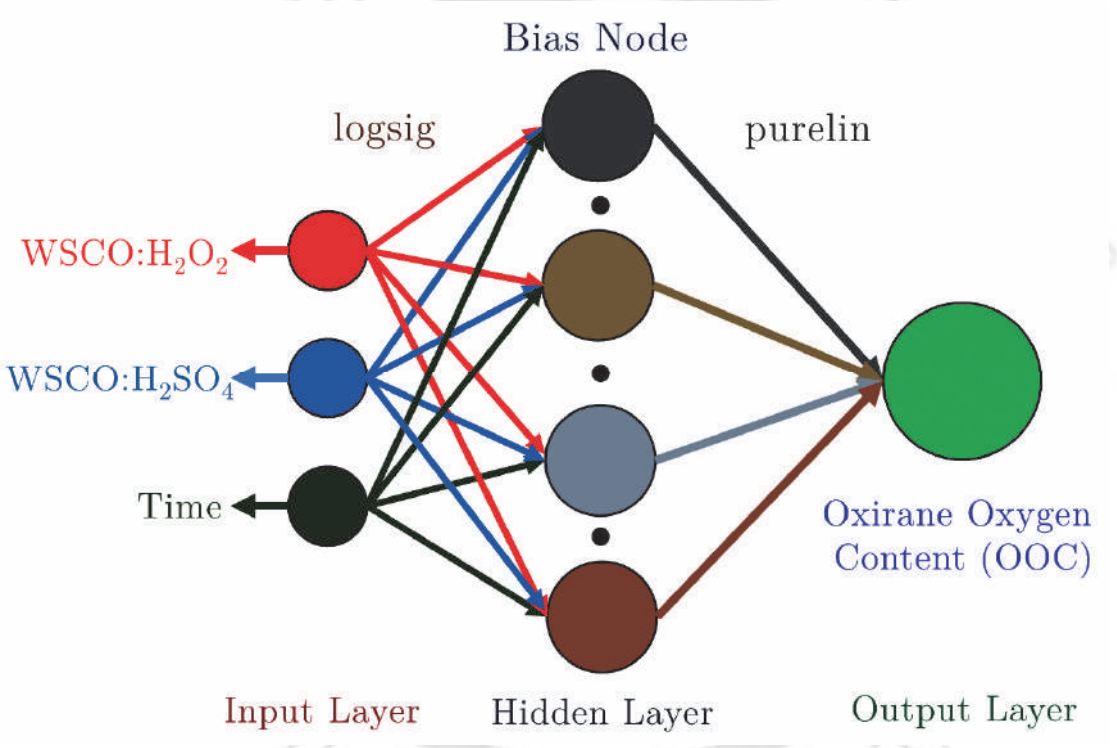

Figure 3.5. Finalised neural network architecture trained via Levenberg–Marquardt (LM) algorithm for Oxirane Oxygen Content (OOC).

The network was constructed and trained via different learning algorithms (BPA and LM). Levenberg–Marquardt (LM) is often regarded as the most efficient, considering speed and accuracy, in finding the optimal point, compared to other algorithms (Figure 3.9) (Kollias and Anastassiou, 1989). Training algorithms are

used to train the network. In this study, thirteen numbers of training methods are used. All these different training methods have different characteristics and performance. Training methods are extremely useful when it comes to certain problems that either cannot be practically written by a programmer or can be done more efficiently by training methods. Adjustment of network parameters is done by adjusting the number of neurons (or nodes) in the hidden layer (logsig) and output layer (purelin).

In ANN, 70 % of data was used to train the model, 15 % was used for validation of the predicted model and 15 % data was used to test the model. The gradient is a value of back propagation algorithm on each iteration in logarithmic scale. The value of the coefficient of determination (0.9988) is shown in Figure 3.6. The overall coefficient of determination was found by the combination of three coefficients of determination obtained from training, testing, and validation plot, which is shown in Figure 3.7. An epoch is a measure of the number of times all of the training vectors are used once to update the weights. For batch training, all of the training samples pass through the learning algorithm simultaneously in one epoch before weights are updated. The best validation preference (2.928×10^{-5} at epoch 9) of the model was determined by a total of 13 epochs (Figure 3.7). The gradient value 7.367×10^{-13} suggests that it reached the bottom of the local minimum of goal function at epoch 13 (Figure 3.8). The model will stop if it fails consecutively for six runs (epochs). Consequent validation failure means more iteration is required to train the model (Beale et al., 2010). Estimation capabilities are shown (Figure 3.10) for both RSM and ANN predicted models, for the experimental values, and they show excellent agreement.

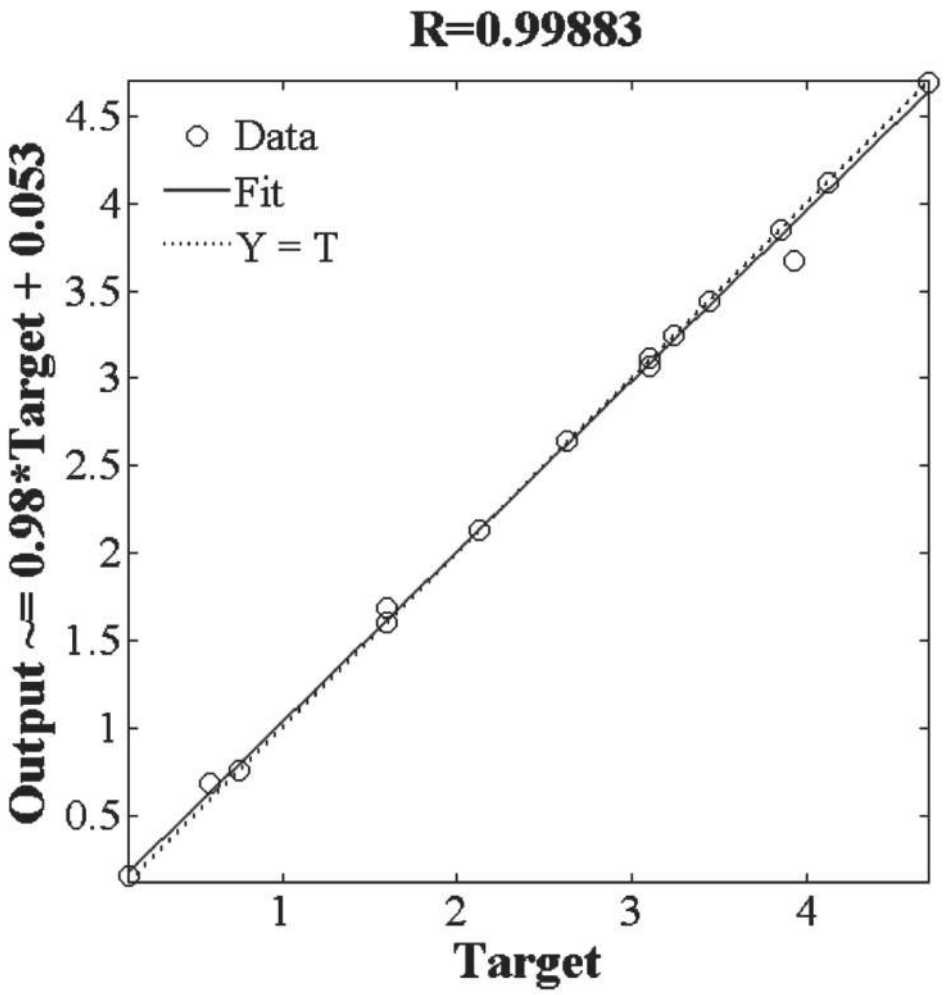

Figure 3.6. Regression analysis of the data for validation in ANN.

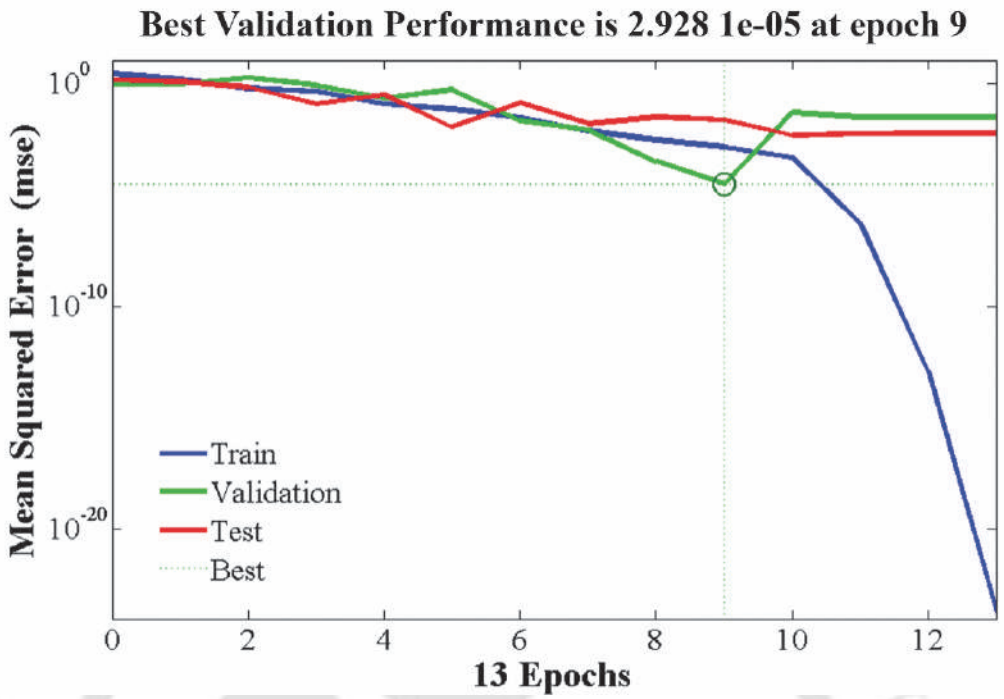

Figure 3.7. Neural network training, validation and test plot for the output response (OOC).

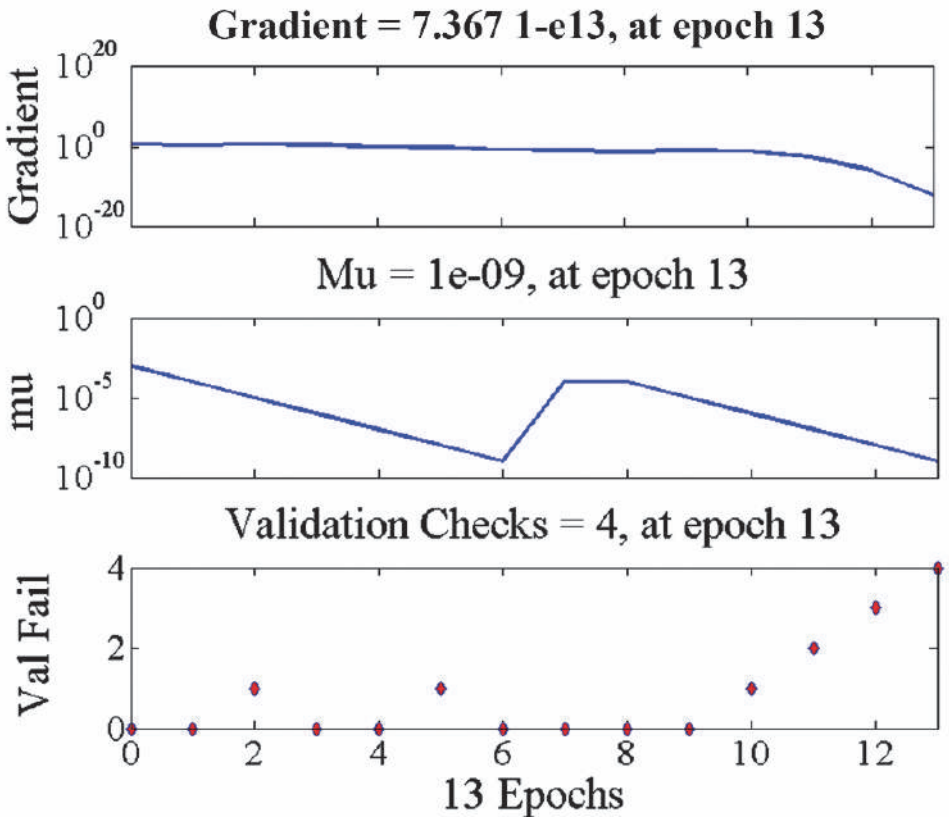

Figure 3.8. ANN training state plot.

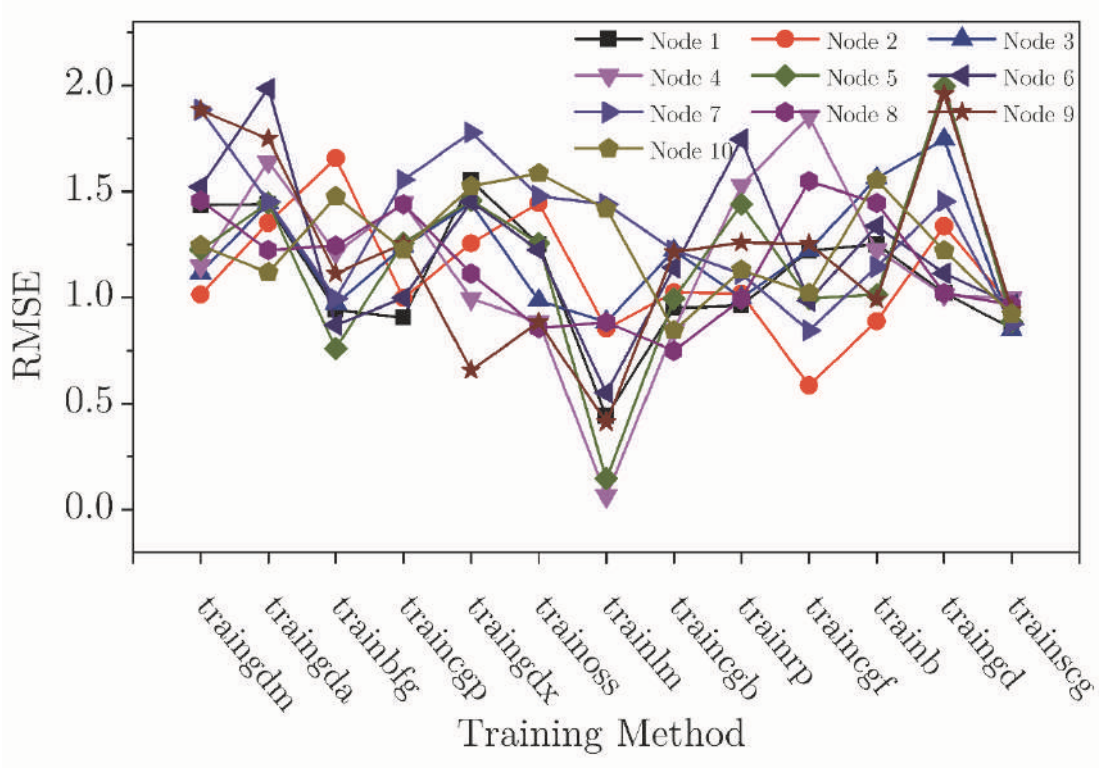

Figure 3.9. Training program of hidden layer transfer functions with RMSE data.

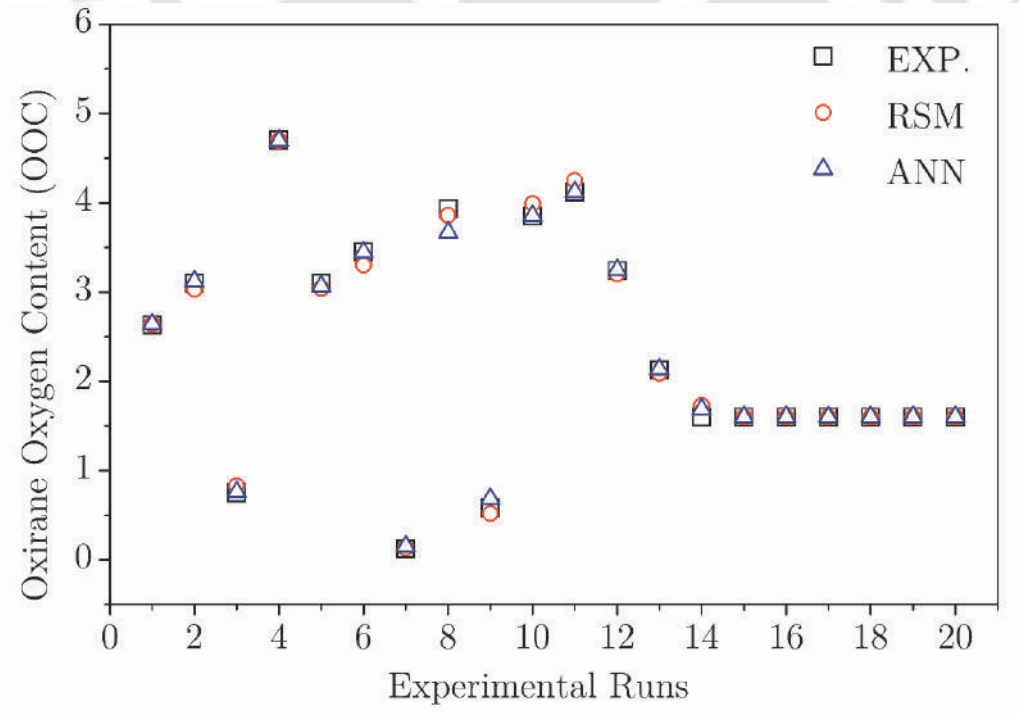

Figure 3.10. Estimation capabilities of both RSM and ANN predicted models to the experimental data.

3.4. Comparison between RSM and ANN Predicted Model

Evaluation based on models' coefficient of determination showed satisfactory convergence between actual and predicted response. Thus, both the models can be considered to perform data fitting, and they offered a stable response. Therefore, from the above study, it can be suggested that both the models should be used in combination, as the RSM prediction for the nonlinear model is not adequate. The observed coefficient of determination obtained from RSM was 0.9968 (Figure 3.1) and from ANN was 0.9988 (Figure 3.6). These values are very close to 1, showing that both the models worked well for this study.

3.5. Sensitivity Analysis by ANN

Sensitivity is defined as the change of output parameter of a trained network with the change of each input. 'Leave one out' approach was employed to achieve the sensitivity analysis of input parameters in order to estimate the effect of each input variable on the model. One input variable is omitted from the model at a time in accordance with the 'leave one out' technique, and the percentage change in the RMSE value with regard to the RMSE value considering all input parameters has been considered as a result (Mohd et al., 2011). If the disappearance of the excluded input parameter results in a higher RMSE value, then the network output is more sensitive to that parameter. The sensitivity analysis of input parameters is shown in Table 3.5. The table shows the percentage change of RMSE due to the exclusion of each input parameter, one at time. The RMSE value considering three parameters (C=C of WSCO to H_2O_2 ratio, WSCO:H_2SO_4, and time) was found to be 0.0661 by ANN. RMSE by considering the elimination of only one parameter, i.e. C=C bonds to H_2O_2, was

found to be 1.5610; that means, RMSE was calculated by eliminating the parameter of C=C bonds to H_2O_2 molar ratio. Similarly, RMSE for parameter WSCO:H_2SO_4 was found to be 2.1242, and for time, it was 0.7284. From Table 3.5, it can be seen that parameter WSCO:H_2SO_4 has the maximum contribution to the network output as the RMSE value increases from 0.0661 to 2.1242 while eliminating WSCO:H_2SO_4 from the other input parameters. Time has the minimum percentage effect (15.71%) on the network output parameter i.e. OOC (mass %).

Table 3.5. Sensitivity analysis of each parameter.

	RMSE	RMSE Difference	Contribution (%)
All Parameters (3)	0.0661	—	—
L–WSCO:H_2O_2	1.5610	1.4949	35.46
L–WSCO:H_2SO_4	2.1242	2.0581	48.83
L–Time	0.7284	0.6623	15.71
Total	—	4.2153	100.00

Note: L: leave one out, — not available or not required

3.6. Genetic Algorithm

Both RSM and ANN are tools which are sufficient to predict the optimum conditions with higher accuracy. But the issue with these models is that they are a generalised model, and the prediction range lies in local convergence. Therefore,

researchers have developed an optimisation tool which is being capable of predicting the optimisation conditions globally (Jena et al., 2010). Genetic Algorithm (GA) works by the Darwinian principle which suggests that only the fittest species (best suitable) will survive during the reproduction (iteration) cycle. Such an extended selection of survival is achieved through various mutations and crossovers (operators). In the present study, it was found that after 50 iterations (reproduction) and crossovers, the best suitable condition was generated with genetic algorithm in a given search space with constraints for C=C:H_2O_2 ratio, WSCO:H_2SO_4 ratio and time with lower (0.66, 0.16, 4.64) and upper bounds (2.34, 1.84, 11.36). Lower and upper bound values obtained from RSM design matrix are tabulated in Table 3.2a, and the same values have been used as input parameter range for GA. Concurrently 50 generations were analysed to find the best-fit individual. The best-optimised condition generated by GA was (2.34, 1.84, and 4.65) which yielded maximum OOC (5.13 mass %) (Figure 3.11). Optimisation parameters predicted from all the three models (RSM, ANN, and GA) for different factors are shown in Table 3.6.

The experimental output (OOC) for the validation experiment is as follows by using optimum data points provided by RSM, ANN, and GA respectively 4.7±0.24 mass %, 4.7±0.24 mass %, and 4.85±0.38 mass %.

Table 3.6. Optimisation table (RSM, ANN, and GA).

	Input Parameters			Output Value
	WSCO: H_2O_2	WSCO: H_2SO_4	Time (h)	OOC (mass %)
RSM	2.00	1.50	6.00	4.69
ANN	2.00	1.50	6.00	4.69
GA	2.34	1.84	4.65	5.13

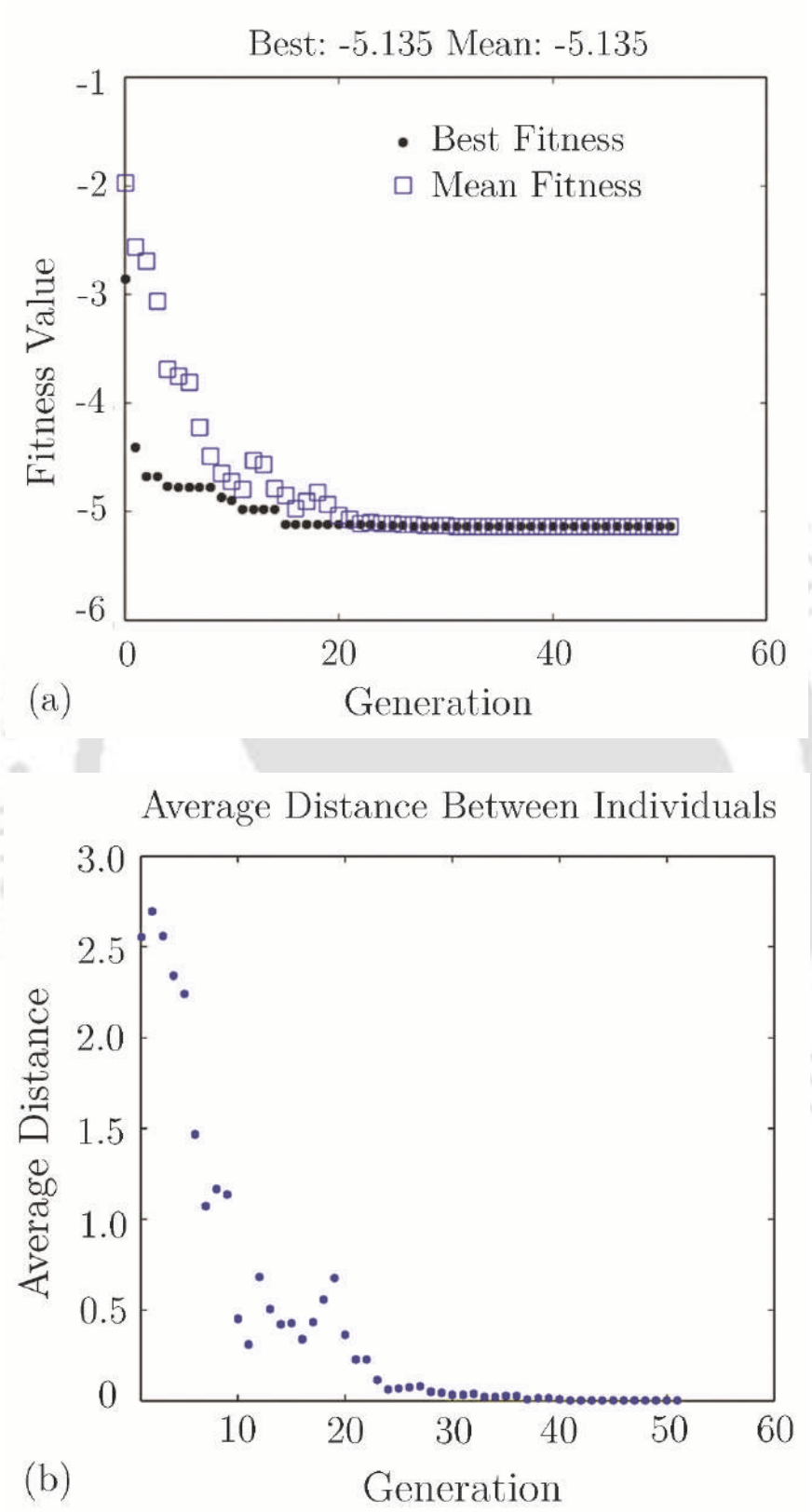

Figure 3.11. A genetic algorithm for prediction of the global optimum condition, a) selection of best-fit individual during mutations and crossovers over several generations, b) average distance between selected individual.

3.7. Physico-chemical Characterisation of Prepared EWSCO

The fatty acid composition of WSCO was determined using Nucon 5765 gas chromatograph using the method discussed in section 2.3.8 and result listed in Table 3.7 below. The fatty acid composition of WSCO mainly consists of 18% saturated, 44% polyunsaturated and 24% mono-unsaturated fatty acids. The fatty acid composition is Oleic acid (24%), Linoleic acid (39%), Linolenic acid (5%), Palmitic acid (14%) and Stearic acid (4%).

Table 3.7. Fatty acid composition of the oil (WSCO).

Fatty Acid	Carbon Number	Fatty Acid Composition (%) of WSCO	Chemical Name of the Fatty Acid	Formula
Oleic	(C18:1)	24.0±1.6	*cis*–9–octadecenoic	$C_{18}H_{34}O_2$
Linoleic	(C18:2)	39.2±1.7	*cis*–9,*cis*–12–octadecadienoic	$C_{18}H_{32}O_2$
Linolenic	(C18:3)	5.2±0.6	*cis*–9,*cis*–12,*cis*–15–octadecadienoic	$C_{18}H_{30}O_2$
Palmitic	(C16:0)	14.2±1.2	Hexadecanoic	$C_{16}H_{32}O_2$
Stearic	(C18:0)	4.1±0.2	Octadecanoic	$C_{18}H_{36}O_2$

3.7.1. Product Confirmation by FTIR

The conversion of unsaturation C=C to OOC (oxirane oxygen) and its subsequent functionalisation were observed under FTIR spectra. The disappearance of double bonds at 3002–3008 cm^{-1} and formation of epoxy groups at 844 cm^{-1} were

confirmed by the transformation of C=C bonds into OOC (oxirane oxygen) via epoxidation reaction. The appearance of an epoxy peak at 820–845 cm^{-1} indicates that epoxidation reaction occurred with sulphuric acid as catalyst. The complete disappearance of C=C bonds in the WSCO epoxide FTIR spectra (Figure 3.12) at 3005 cm^{-1} further supported the almost complete conversion of double bonds to oxirane oxygen. In this study, FTIR spectra also exhibited no trace of –OH absorption peak at approximately 3000–3500 cm^{-1} which represents no oxirane cleavage during WSCO epoxidation.

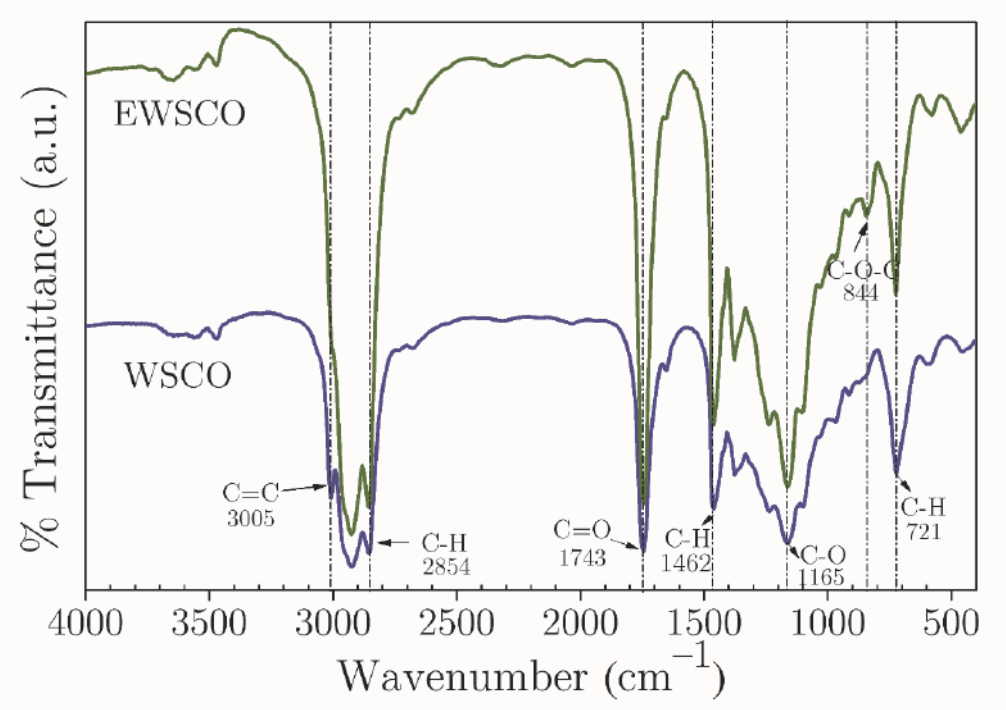

Figure 3.12. FTIR spectra of WSCO and EWSCO.

3.7.2. Product Confirmation by NMR

Proton ^{1}H NMR spectra of WSCO and EWSCO are shown in Figure 3.13. Comparison of crude WSCO and EWSCO spectra shows that the C=C un-saturation present in WSCO at 5.26–5.38 ppm (normally at 5.2 ppm) was replaced with the epoxy group of hydrogen peroxide in EWSCO. The epoxy

protons were observed in the δ 2.8–3.1 ppm region in EWSCO. The methine proton of –CH_2–C**H**–CH_2– back bone is shown at δ 5.26–5.38 ppm, methylene proton of C**H**$_2$–CH– C**H**$_2$ back bone at δ 4.123–4.319 ppm, CH_2 proton adjacent to two epoxy group at δ 2.75–2.78 ppm, –CH– protons of epoxy ring at δ 2.90–3.14 ppm, $\alpha-CH_2$ to >C=O at δ 2.19–2.31 ppm, $\alpha-CH_2$ to epoxy group at 1.59–1.63 ppm, $\beta-CH_2$ to >C=O at δ 1.25–1.30 ppm, $\beta-CH_2$ to epoxy group at δ 1.4–1.55 ppm, saturated methylene groups at δ 1.1–1.4 ppm and terminal –CH_3 groups at δ 0.86–0.90 ppm region.

Further, completion of the epoxidation reaction was confirmed by comparison of iodine values of WSCO and EWSCO. From the reported values (Table 3.8), it was noticed that 98.7% double bonds were converted into epoxides. This three-membered ring of oxirane could form a smooth layer due to a trio-polymerisation which is tribologically effective to reduce friction (Wu et al., 2000).

Table 3.8. Comparison of physico-chemical properties of WSCO and EWSCO.

Physico-chemical Properties	WSCO	EWSCO
Acid Value (mg KOH/g)	0.54± 0.12	0.30 ± 0.07
Density (kg/m^3)	792.0± 4.58	802.1 ± 4.89
Free Fatty Acid (mg KOH/g)	0.27± 0.05	0.15 ± 0.04
Iodine Value (gI_2/100g)	132.9± 2.94	1.74 ± 0.14
Kinematic Viscosity (cSt) at RT*	57.9± 1.7	355.8± 4.32
Kinematic Viscosity (cSt) at 40 °C	33.9± 1.3	267.9± 3.56
Moisture Content (wt %)	0.27± 0.02	0.25 ± 0.02
Pour Point (°C)	–7.8± 0.13	–6.3 ± 0.17
Refractive Index (at 27.6 °C)	1.47± 0.07	1.47 ± 0.1
Oxirane Oxygen Content (Experimental)	—	4.69 ± 0.4
Oxirane Oxygen Content (Theoretical)	—	7.72 ± 0.2

— not available or not required

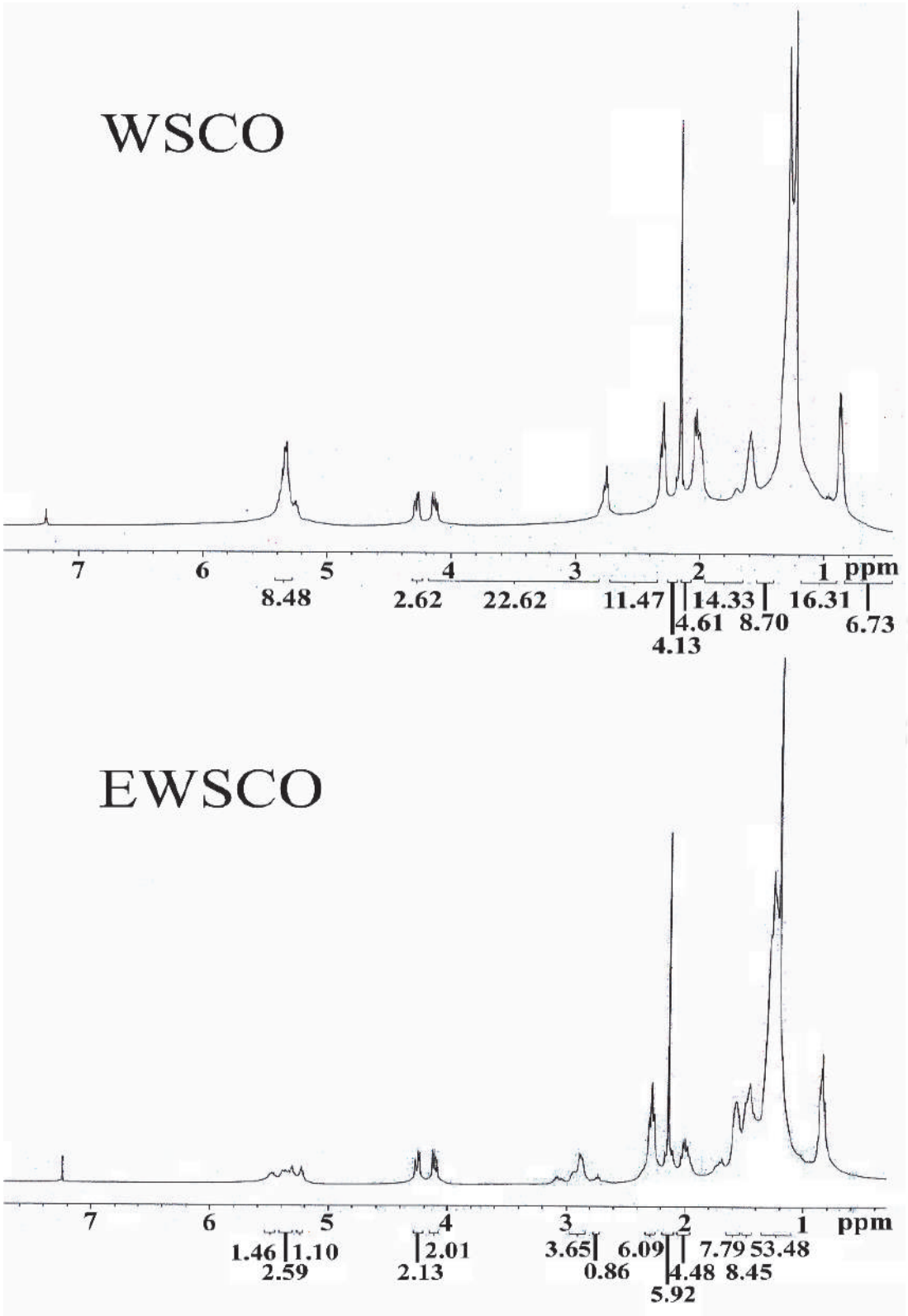

Figure 3.13. ^{1}H NMR spectrum of the WSCO and EWSCO.

3.7.3. Thermo-oxidative Stability

The thermogravimetric analysis (TGA) was performed to evaluate the thermo-oxidative stability of WSCO and EWSCO. Thermo-oxidative stabilities are estimated from thermal and oxidative onset temperatures, respectively (Borugadda and Goud, 2013). Onset temperature corresponds to minimum temperature at which sample decomposition starts; in other words, it corresponds to the maximum temperature up to which the sample can be stable without any weight loss. From the Figure 3.14, it can be observed that WSCO is found to be thermally more stable (degradation initiation temperature, T_i of 365 °C) compared to EWSCO (degradation initiation temperature, T_i of 338 °C). This indicates that WSCO used in this study must be containing high molecular weight polymeric compounds in its composition, as a result it exhibits higher thermal stability compared to EWSCO.

Similarly, to measure the oxidative stability, TG analysis of the sample was performed under air atmosphere. Figure 3.14 shows TG, DTG curve for EWSCO under oxygen environment at 10 °C/min; from the figure, three distinct grooves (for EWSCO) can be observed from room temperature to 600 °C, and degradation of the sample starts nearly at 240 °C. Initially lower boiling point (high volatile) compounds degrade; then between 250–550 °C range, maximum compounds undergo decomposition by breaking higher molecular structure into lower molecular structure. The oxidative degradation initiation temperature of EWSCO was found to be 325 °C (Figure 3.14). Comparison of stability obtained for the present work with that for the other epoxidised oil reveals that EWSCO possesses relatively higher oxidative stability (OS) as compared to propylated canola oil (248 °C) and butylaled canola oil (255 °C), and possesses comparable oxidative stability with jatropha bio-lubricant (trimethylolpropane) which has OS as 325 °C (Borugadda et al., 2017; Resul et al., 2012).

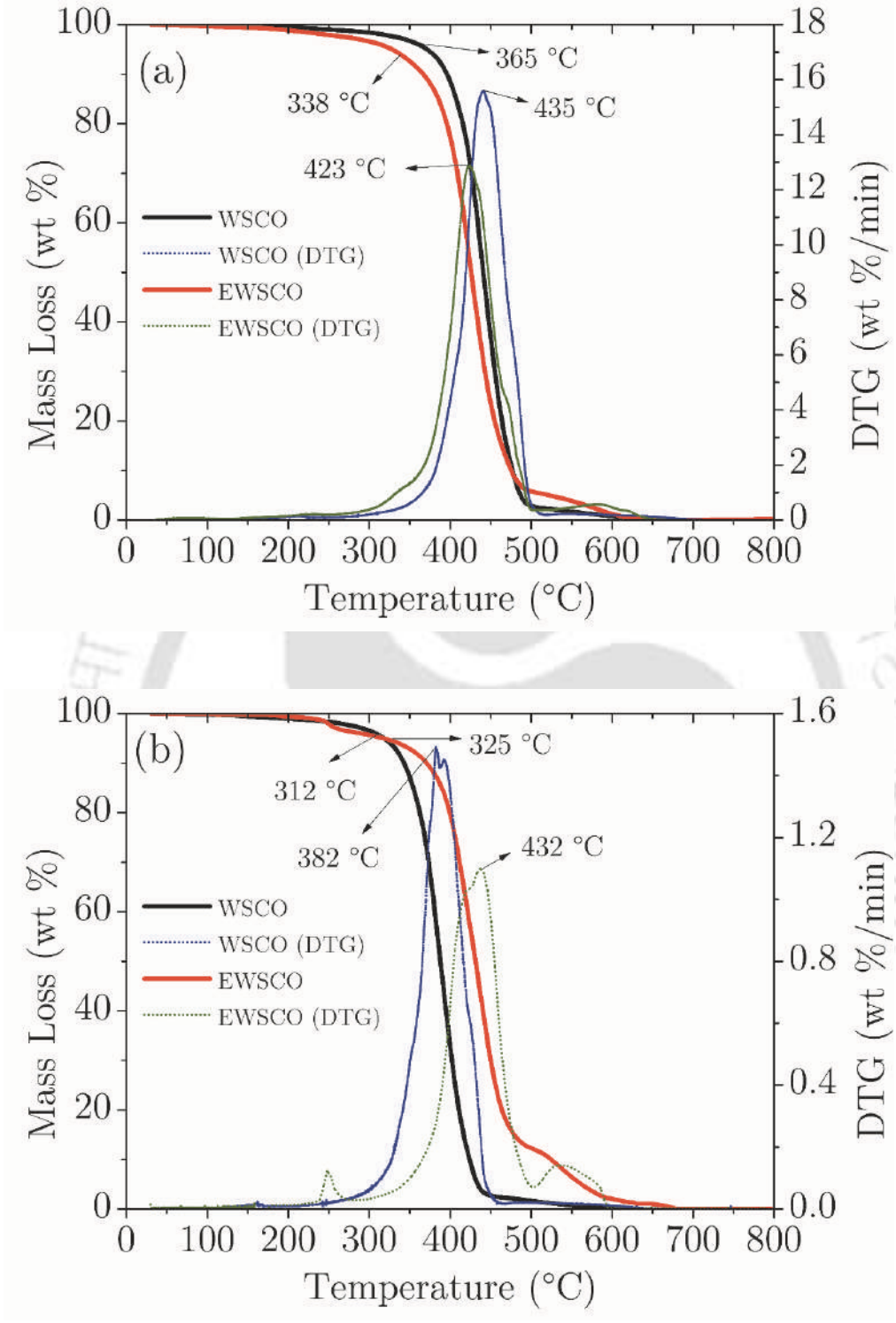

Figure 3.14. TGA stability thermograms for WSCO/EWSCO (a) Thermal stability (b) Oxidative stability.

3.7.4. Cold Flow Properties

The flow characteristic of WSCO and EWSCO was measured under low temperature by using DSC technique following standard method described in our earlier paper (Borugadda and Goud, 2014b). The result showed nearly identical pour points (Table 3.8) (Figure 3.15) for WSCO and EWSCO (Borugadda and Goud, 2013). The literature reported that unsaturation content plays a major role in low temperature properties—more is the unsaturation content, better is the cold flow behaviour (Soriano et al., 2006). The increase in PP of WCO epoxide was due to the removal of unsaturation content. Performing a comparative analysis of the result obtained in the present study with those reported in the literature, it was observed that EWSCO possesses better pour point (-6.3 °C) as compared to epoxidised canola oil (10 °C) (Madankar et al., 2013) and jatropha oil trimethylolpropane esters (-3 °C) (Heikal et al., 2017), and little lower as compared to *Jatropha curcas* bio-lubricant (-12 °C) (Menkiti et al., 2017). Outcomes of the low-temperature properties indicate that the chemical modification can alter the low-temperature properties of WSCO, which is considered as one of the significant problems for vegetable oils to be used as alternative bio-lubricant base stocks. Therefore, structural modification of plant seed oils is an essential step to prepare good quality bio-lubricant base stocks. A study reported that epoxidation did not enhance the cold flow properties considerably, and the same is noticed in the present study as well (Wadumesthrige et al., 2009).

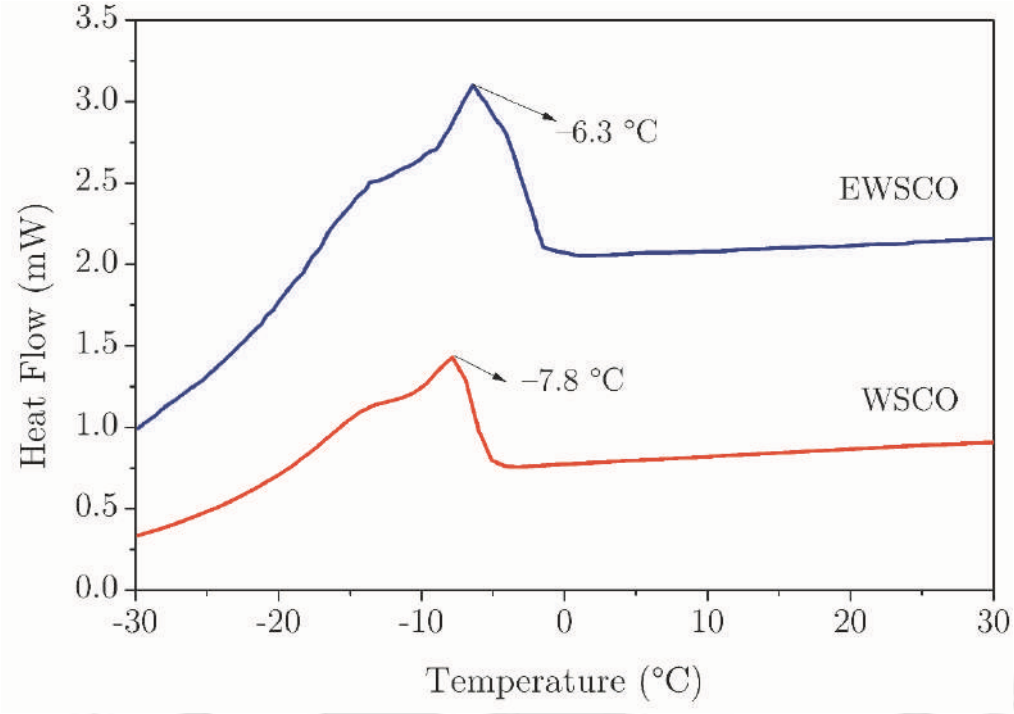

Figure 3.15. DSC thermogram for WSCO and EWSCO.

3.7.5. Rheological Behaviour and Viscosity

Figures 3.16 and 3.17 show the rheological behaviour of EWSCO as a function of temperature (i.e., at room temperature and at 40 °C). The plots of shear stress versus shear rate displayed (Figure 3.16) a straight line passing through the origin, thereby suggesting the Newtonian type of fluid behaviour. From Figure 3.17, it can also be noticed that at room temperature viscosity does not vary with an increased shear rate, while at 40 °C slight deviation was observed at a low shear rate, but the trend was almost similar. From this study, it can be concluded that the viscosity of EWSCO did not change with an increase in the temperature and under applied shear rate, which further confirms the Newtonian fluid nature. The linear and smooth relation between viscosities versus shear rate leads to a smooth performance during usage. Similar results were observed in our earlier findings on epoxidation of WSCO (Borugadda and Goud, 2016b, 2014a).

From the comparative analysis of viscosity values of WSCO and EWSCO, it is evident that viscosity of EWSCO was almost ten times higher than that of WSCO, which implies that EWSCO (after structural modification) serves better lubrication properties compared to WSCO (feedstock). By incorporating the oxygen molecule in the midst of unsaturation, the weight of the epoxide is enhanced thereby improving its viscosity (Table 3.8). Similarly, the acid value of EWSCO obtained in this study was significantly less, i.e. 0.3 mg KOH/g which indicates that epoxides do not create any trouble (i.e. corrosion) during the usage. Free fatty acid (FFA) value is always half of the acid value, which indicates its capacity of soap formation when it is mixed with water; the inferior value of the FFA signifies the smooth performance of the epoxide.

However, the density of EWSCO is found to be higher compared to WSCO—this is due to increase in the molecular weight, polarity, and intermolecular forces during epoxidation. From this study, it was noticed that epoxides had higher molecular weight and polar structure compared to feedstock. A similar trend was observed in the literature (Wu et al., 2000). Further, the moisture content of the sample was determined to evaluate the percentage of moisture present in the EWSCO. The presence of moisture encourages the bacterial growth, which leads to an increased acid value and oxidation (Dörmo et al., 2004). Therefore, lower moisture content is always desirable; from the reported values, prepared epoxides moisture content was found to be 0.25 wt % (Table 3.8). The refractive index of the WSCO and EWSCO was found to be 1.47 (Table 3.8), which shows that very minute amount of heat energy can pass through the WSCO and EWSCO, which is anticipated to protect the chemical and physical integrity of the EWSCO.

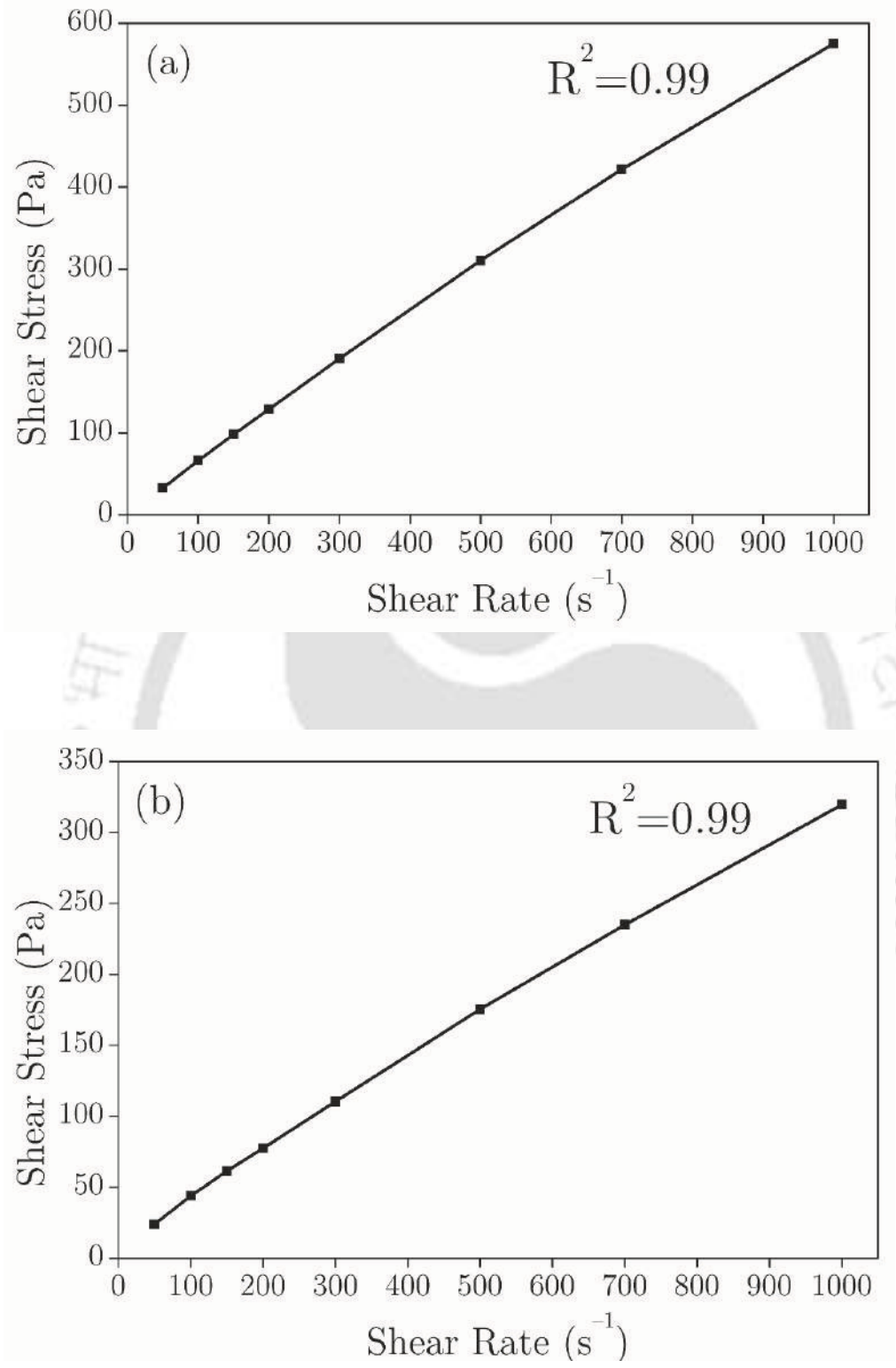

Figure 3.16. Shear stress vs shear rate for EWSCO (a) at room temperature (28 °C) (b) at 40 °C.

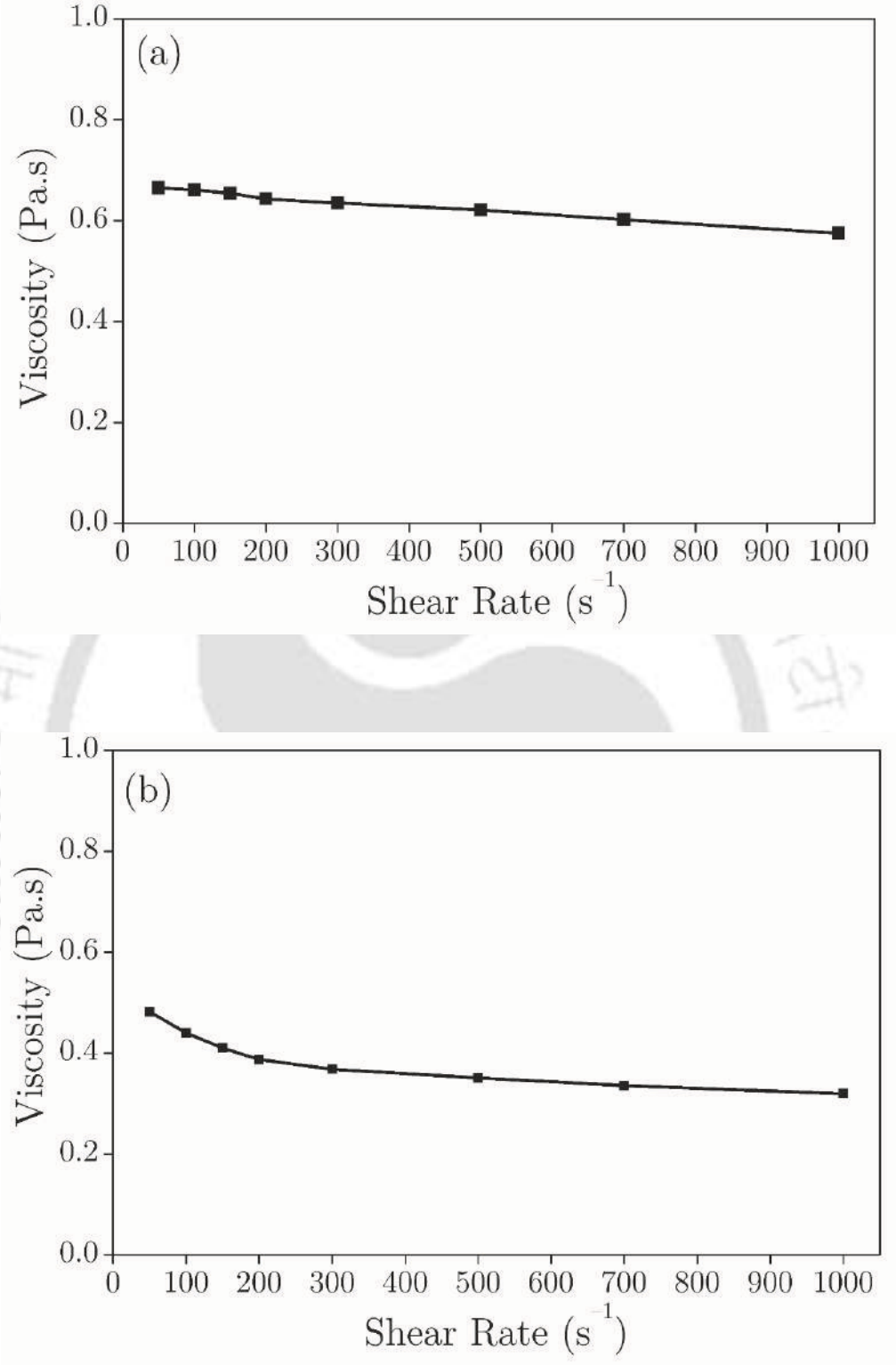

Figure 3.17. Shear rate vs viscosity relation for EWSCO at (a) Room temperature (28 °C) (b) 40 °C

3.8. Summary

This chapter dealt with the epoxidation of WSCO in presence of sulphuric acid as homogeneous acidic catalysts and hydrogen peroxide as an active oxygen donor. Optimisation results revealed that higher catalyst loading and high moles of hydrogen peroxide lead to higher oxirane conversion. Optimum OOC was found at 2 moles of H_2O_2 (C=C bonds to H_2O_2 molar ratio), 1.5 wt % of catalyst loading and 6 h of reaction time. Further, ANN and GA optimisation study were also carried out and compared. At this condition, the OOC of EWSCO was found to be 4.69 mass % by RSM and ANN, and to be 5.13 mass % by GA under the experimental conditions of 60 °C temperature, 4.6 h of reaction time, 1.84 g of catalyst loading and 1:2.34 molar ratio of C=C bonds to H_2O_2. A detailed study on the physico-chemical properties of EWSCO at optimum conditions revealed that the prepared epoxide exhibited satisfactory rheological properties and stability of the product. Finally, from this study, it could be concluded that prepared EWSCO exhibits highly desirable and enhanced physico-chemical properties than the WSCO in all the aspects for environment-friendly bio-lubricants.

CHAPTER IV

Synthesis of Waste Soybean Cooking Oil Methyl Esters and its Epoxidation for the Synthesis of Bio-lubricant Base Stocks via Response Surface Methodology (RSM), Artificial Neural Network (ANN), and Genetic Algorithm (GA)

Effect of Process Parameters on Epoxidation of WSCOME

Optimisation of Epoxidation of WSCOME using RSM, ANN, & GA

Physico-chemical Characterisation of EWSCOME

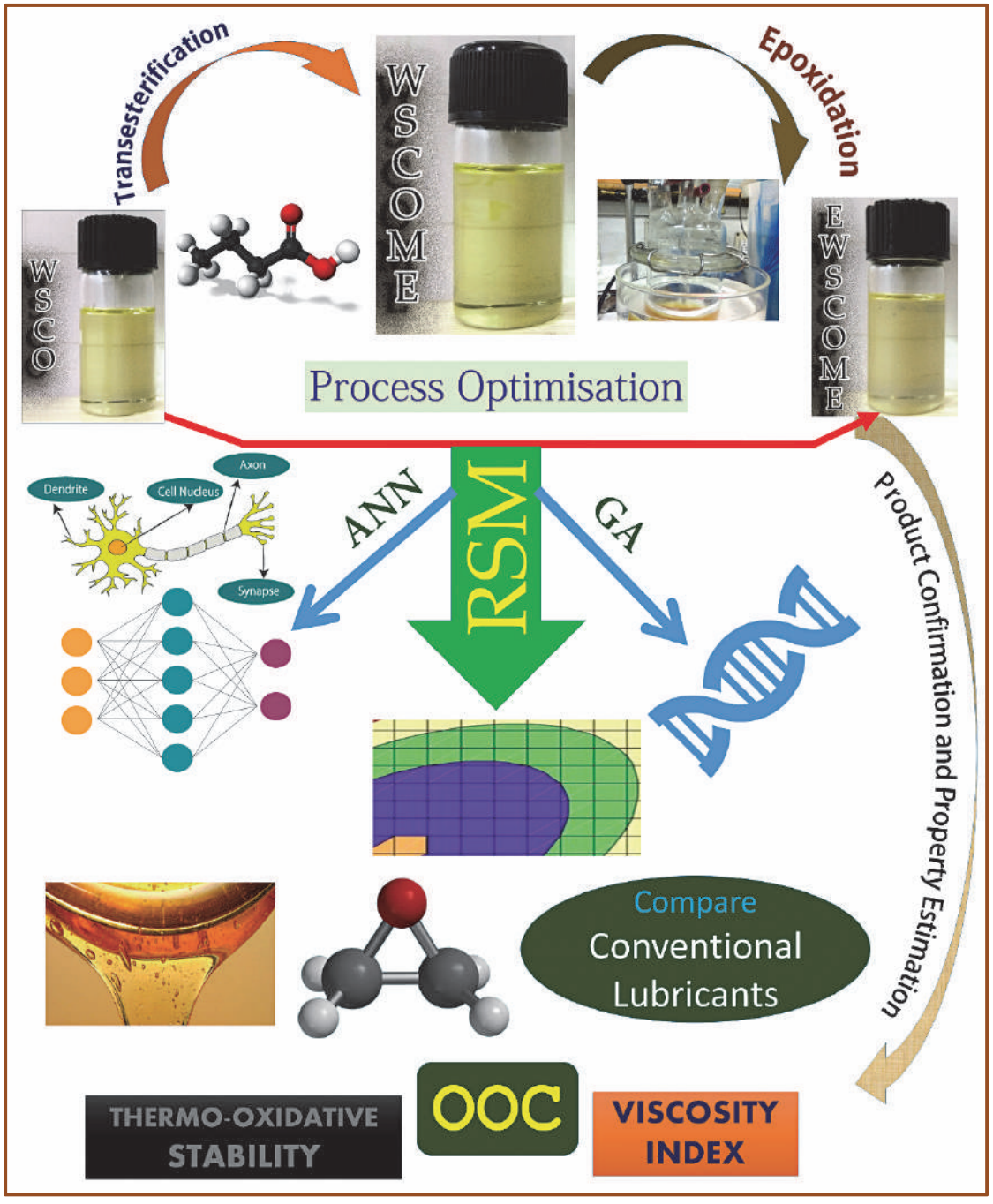

Graphical Abstract of Chapter IV

Chapter IV

Synthesis of Waste Soybean Cooking Oil Methyl Esters and its Epoxidation for the Synthesis of Bio-lubricant Base Stocks via Response Surface Methodology (RSM), Artificial Neural Network (ANN), and Genetic Algorithm (GA)

In this study, artificial neural networks (ANNs) and response surface methodology (RSM) are used to optimise and predict the maximum oxirane oxygen content (OOC) from waste soybean cooking oil methyl esters (WSCOME). WSCOME bio-lubricant base stocks was prepared via in situ epoxidation of unsaturated fatty acid methyl esters. The effect of process parameters to maximise OOC was studied using RSM. Interaction among the process parameters like unsaturation to hydrogen peroxide (H_2O_2) molar ratio, catalyst loading and reaction time was studied by ANOVA using Design Expert software. The optimum OOC of epoxidised waste soybean cooking oil methyl esters (EWSCOME) was found to be 4.92 mass % under the experimental conditions of 60 °C temperature, 4.14 h of reaction time, 1.95 g of catalyst loading and 1:2.21 molar ratio of unsaturation to H_2O_2. The formation of EWSCOME was confirmed by Fourier transform infrared spectroscopy (FTIR) (at 843 cm^{-1}) and Nuclear magnetic resonance spectroscopy (NMR) analysis. Several physico-chemical properties of the prepared bio-lubricant were also measured by standard techniques. After successful optimisation by RSM, ANN and GA optimisation techniques were also applied

to verify the optimum result, and it was found that both the techniques were able to optimise the process parameters.

4.1. RSM Optimisation and ANN Modelling for Oxirane Oxygen Content (OOC)

4.1.1. Experimental Design and Statistical Analysis

A three-level, three factorial CCD was employed to maximise the oxirane oxygen content. Three process variables, i.e. WSCOME:Hydrogen Peroxide (H_2O_2), WSCOME:Sulphuric acid (H_2SO_4), and time, were considered, and their selected range in terms of un-coded parameter is shown in Table 4.1. The accuracy of fit for the model was evaluated by regression coefficient R^2.

Table: 4.1. Independent variable and their levels for response surface design of the WSCOME epoxidation reaction.

			Variable Levels		
Independent Variables	Symbol	Unit	-1	0	+1
WSCOME:Hydrogen Peroxide (H_2O_2)	A	mol	1.5	2.0	2.5
WSCOME:Sulphuric Acid (H_2SO_4)	B	wt %	1.0	1.5	2. 0
Time	C	h	4.0	6.0	8.0

This study shows the application of the proposed RSM framework for the optimisation of WSCOME epoxide using sulphuric acid as homogeneous acid catalyst. Due to the limited knowledge about this process, ANOVA was employed to study the interactions among the selected process variables. The experimental design matrix and the response (OOC) are given in Table 4.4a. In order to develop the response surface model, data were analysed by employing multiple regression techniques.

Table 4.2 and 4.3 depict the quadratic regression coefficients obtained by employing a least-square method to predict model for OOC along with the significance of each process variable. A P-value higher than 0.05 (> 0.05) does not show statistically significant signs of null hypothesis. This indicates that the null assumption is retained and the alternative hypothesis is rejected. The significance is based on high F and low P-value. For OOC of WSCOME epoxide, B^2 was insignificant (since $P > 0.05$). Therefore, linear terms A, B, C, interaction terms AB, AC, BC, and quadratic terms A^2, C^2 were found to be significant for obtaining higher OOC, and the response was purely depended on all these factors. Researchers found that hydrogen peroxide was the most important variable in their study of the epoxidation of linolenic acid (Salimon et al., 2012). When comparing the variables hydrogen peroxide, oleic acid, and formic acid, they discovered that hydrogen peroxide was the most significant of the three. The lack of fit F-value for this response was found to be highly insignificant relative to the pure error. This indicated that all the models predicted for the responses were significant. Regression models for data on response (OOC) were very significant with satisfactory R^2. Nevertheless, R^2 for OOC (0.9930) was almost close to one which made the model very significant. Table 4.2 summarises the ANOVA of all the responses of this study. The equation was generated to predict the OOC content in terms of actual factor (Equation 4.1).

$$OOC\ (mass\ \%) = 3.91 + (0.90 \times A) + (0.53 \times B) - (0.22 \times C) - (0.36 \times A \times B) + (0.095 \times A \times C) + (0.13 \times B \times C) - (0.40 \times A^2) + (0.17 \times C^2) \quad (4.1)$$

One of the most favourable methods to assess the effect of various process variables and its interactive dependency is by RSM. Important fundamental interaction variables (amount of H_2O_2, catalyst loading, and time) in the suited

models were selected as the axis for the response surface plots. The relationship between the selected process variables and resulting response is shown by 3D response surface plots (Figure 4.2). The theoretical oxirane oxygen content and its relative percentage conversion to oxirane was calculated using Equations 4.2 and 4.3.

Theoretical oxirane oxygen content,

$$OO_{th} = \left[\frac{(IV_0 / 2A_i)}{100 + (IV_0 / 2A_i)A_0} \right] A_0 \times 100 \tag{4.2}$$

Where A_i and A_0 are the atomic weights of iodine and oxygen respectively, and IV_0 is the initial iodine value of the WSCOME.

$$\text{Relative percentage conversion to Oxirane} = \left[\frac{OO_{ex}}{OO_{th}} \right] \times 100 \tag{4.3}$$

Where OO_{ex} is the experimentally determined content of oxirane oxygen, and OO_{th} is the theoretically maximum oxirane oxygen content.

Table 4.2. ANOVA for response surface quadratic model.

Source	Sum of Squares	df	Mean Square	F–Value	P–Value Prob > F
Model	19.81	8	2.48	194.65	<0.0001
A-WSCOME:H_2O_2 (mol)	11.17	1	11.17	877.80	<0.0001
B-WSCOME:H_2SO_4 (wt %)	3.78	1	3.78	296.99	<0.0001
C-Time (h)	0.68	1	0.68	53.61	<0.0001
AB	1.05	1	1.05	82.65	<0.0001
AC	0.072	1	0.072	5.68	0.0363
BC	0.13	1	0.13	9.83	0.0095
A^2	2.32	1	2.32	182.59	<0.0001
C^2	0.41	1	0.41	32.29	0.0001
Residual	0.14	11	0.013	—	—
Lack of Fit	0.037	6	0.0062	0.30	0.9103
Pure Error	0.10	5	0.021	—	—
Cor Total	19.95	19	—	—	—
R^2	—	—	—	—	0.9930

— not available or not required

From Figure 4.1, the observed values are found to be very much close to the predicted value. This indicates that the model is extremely accurate without any noise, and results are reproducible. The combined effect of WSCOME:H_2O_2 and WSCOME:Catalyst loading is shown in Figure 4.2a. From the figure, it can be

seen that higher H_2O_2 molar ratio (WSCOME:H_2O_2 ratio) and higher catalyst loading (WSCOME:H_2SO_4) gave satisfactory results for higher OOC (Figure 4.2a). On the other hand, higher catalyst loading and lower reaction time gave satisfactory OOC content (Figure 4.2c). The 3D response surface plot (Figure 4.2b) indicates that extent of OOC content increased with an increase in the H_2O_2 molar ratio and reducing reaction time. Hence, it could be concluded that to achieve maximum OOC content, higher H_2O_2 molar ratio and catalyst and lower reaction time are preferred. All the experiments were monitored carefully in order to recover an optimum percentage of WSCOME epoxide with reasonable OOC content and product yield. The relationship between process variables and response can be better understood by analysing the 3D surface response plots (Figure 4.2) obtained from the predicted model. The variability proportions among the obtained samples were given by R^2 (Equation 4.4) and RMSE (Equation 4.5). The adequacy of RMSE value described that the model equation was able to define system behaviours and could be applied to experimental conditions (Maity et al., 2014).

$$R\ Squared = 1 - \frac{\sum (x_{ex,i} - y_{pre,i})^2}{\sum y_{pre,i}^{\ 2} - \frac{\sum y_{pre,i}^{\ 2}}{n}} \tag{4.4}$$

$$RMSE = \sqrt{\frac{1}{n}\sum_{i=1}^{n} (x_{ex,i} - y_{pre,i})^2} \tag{4.5}$$

$x_{ex,i}$ = experimental data, $y_{pre,i}$ = predicted data, n = number of experimental data

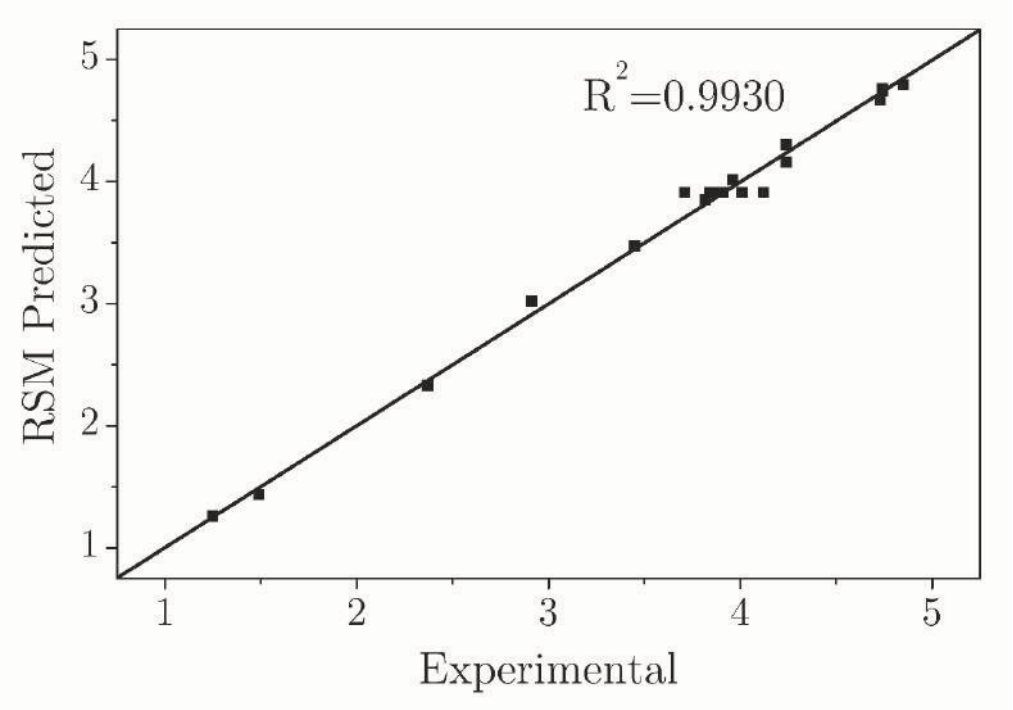

Figure 4.1. Regression analysis by RSM of observed and predicted responses for OOC.

Table 4.3. Sequential model sum of squares.

Source	Sum of Squares	df	Mean Square	F–Value	P–Value Prob > F	
Mean vs. Total	281.03	1	281.03	—	—	
Linear vs. Mean	15.63	3	5.21	19.28	<0.0001	
2FI vs. Linear	1.25	3	0.42	1.76	0.2042	
Quadratic vs. 2FI	2.93	3	0.98	69.92	<0.0001	Suggested
Cubic vs. Quadratic	0.028	4	—	0.37	0.8196	Aliased
Residual	0.11	6	0.019	—	—	
Total	300.97	20	15.05	—	—	

— not available or not required

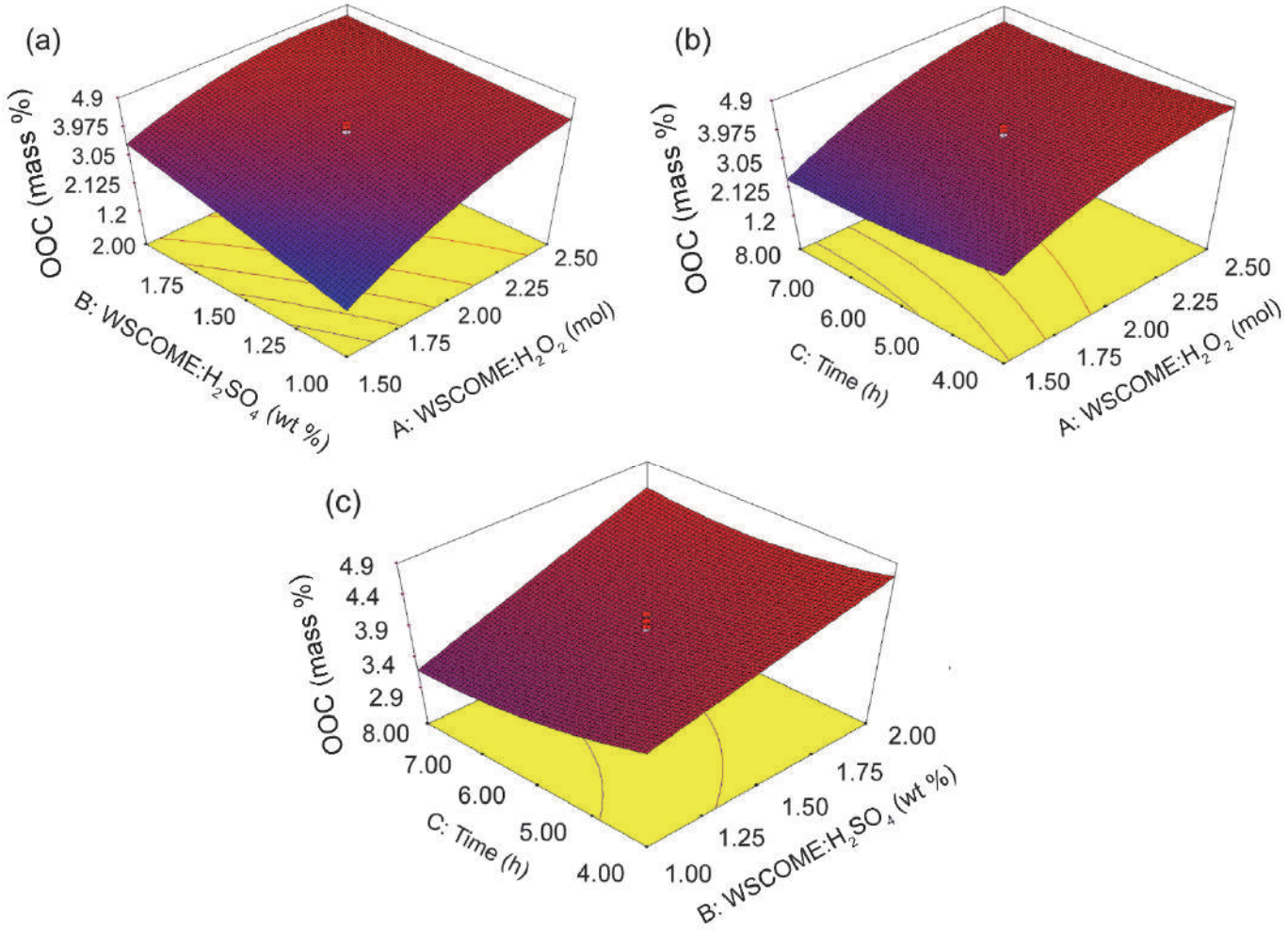

Figure 4.2. Effect of process parameter on Oxirane Oxygen Content (OOC).

Table 4.4a. WSCOME epoxidation experimental design matrix in un-coded form and OOC response.

Input			Experimental Output	RSM Predicted Output	ANN Predicted Output
WSCOME: H_2O_2 (A)	WSCOME: H_2SO_4 (B)	Time (C)	Oxirane Oxygen Content (OOC)		
1.50	1.00	4.00	2.37±0.12	2.33	2.37
2.50	1.00	4.00	4.73±0.22	4.67	4.73
1.50	2.00	4.00	3.82±0.17	3.85	3.82
2.50	2.00	4.00	4.74±0.32	4.75	4.91
1.50	1.00	8.00	1.49±0.10	1.44	1.49
2.50	1.00	8.00	4.24±0.35	4.16	4.24
1.50	2.00	8.00	3.45±0.27	3.47	3.45
2.50	2.00	8.00	4.74±0.24	4.74	4.74
1.16	1.50	6.00	1.25±0.11	1.26	0.79
2.84	1.50	6.00	4.24±0.31	4.30	4.24
2.00	0.66	6.00	2.91±0.21	3.02	2.91
2.00	2.34	6.00	4.85±0.24	4.79	4.85
2.00	1.50	2.64	4.74±0.23	4.76	4.74

2.00	1.50	9.36	3.96±0.15	4.01	3.96
2.00	1.50	6.00	3.85±0.12	3.91	3.94
2.00	1.50	6.00	3.91±0.11	3.91	3.94
2.00	1.50	6.00	3.84±0.13	3.91	3.94
2.00	1.50	6.00	4.12±0.21	3.91	3.94
2.00	1.50	6.00	4.01±0.22	3.91	3.94
2.00	1.50	6.00	3.71±0.19	3.91	3.94
				R^2=0.9930	**R^2=0.9940**

Table 4.4b. The calculated value of different error functions.

	Standard Deviation	Mean Square Errors	Root Mean Square Errors	Sum of Squares of Errors	Average Relative Error	Sum of Absolute Errors	Hybrid Fractional Error Function	Marquart's Percentage Standard Deviation
RSM	0.0578	0.0070	0.0838	0.0635	0.0175	1.2400	0.0022	2.5149
ANN	0.1173	0.0175	0.1322	0.2613	0.0292	1.3300	0.0120	9.2052

4.1.2. Artificial Neural Network

In case of WSCOME epoxidation, the response of artificial neural network was also analysed using the same process parameters as that used in RSM following the procedure explained in Chapter 3. In this case, the network was provided with desired inputs with the related output for those inputs, and the network was run iteratively to train it. The network architecture which mainly consists of three layers, namely three nodes in input layer, eleven nodes in hidden layer and one node in output layer (3–11–1), is shown in Figure 4.3. A single output (OOC) comes from the three parameters (WSCOME:H_2O_2, WSCOME:H_2SO_4 and Time) which are provided as input to the network. After the network is configured, it tries to vary weight to attempt and create desired output with very small error margin. Until the proper weights have been established, the cycle of the network will run, and during each iteration learning weights are slightly adjusted. If the task is complex, then it can perform thousands of training cycles. Once the output is correct (or very near target), the weights can be used with the same network on unseen data to examine its performance.

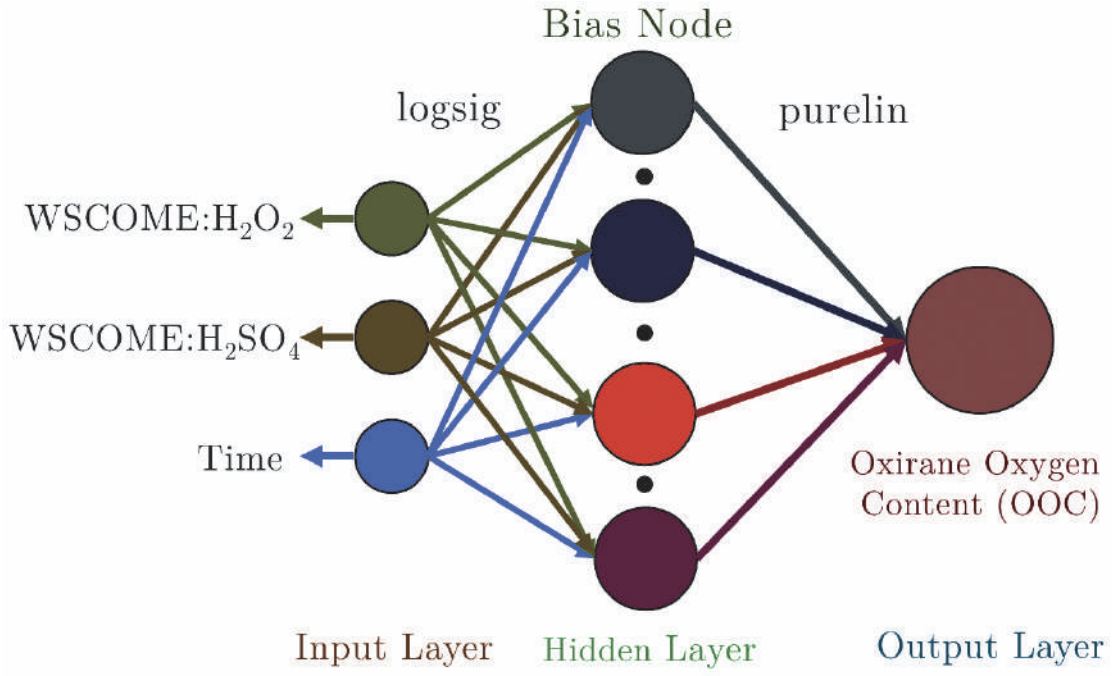

Figure 4.3. Finalised neural network architecture trained via the Levenberg-Marquardt (LM) algorithm for Oxirane Oxygen Content (OOC).

As discussed in the previous chapter, compared to other algorithms, Levenberg-Marquardt (LM) is often regarded as the most efficient algorithm in terms of speed and accuracy in finding the optimal point (Kollias and Anastassiou, 1988).

The results of our previous studies reveal that LM shows the best result compared to other algorithms (Paul et al., 2018). That is the reason for which, in this study, only LM was used to predict the output. The numbers of neurons or nodes were varied to find the optimal solution. In this study, logsig is used as a hidden layer transfer function and purelin as an output layer transfer function.

To train the model 70% data was used in ANN, for validation of the predicted model 15% data was used, and for testing the model 15% data was used. In a logarithmic scale, a value called gradient was calculated in back propagation

algorithm on each iteration. The value of regression coefficient as 0.994 is shown in Figure 4.5. At epoch 4, the gradient value of 1.9589×10^{-9} suggests that it reached the bottom of the local maximum of the goal function (Figure 4.6). The model finds the best validation performance of 0.073897 at epoch 3 from a total of 4 epochs (Figure 4.5). The model will stop if there is consecutive failure of six runs. If it shows consequent validation failure, it means that model required more iteration to train the model (Beale et al., 2010). Estimation capabilities (Figure 4.7) of both RSM and ANN models are indicated by a good agreement shown by experimental values and predicted values.

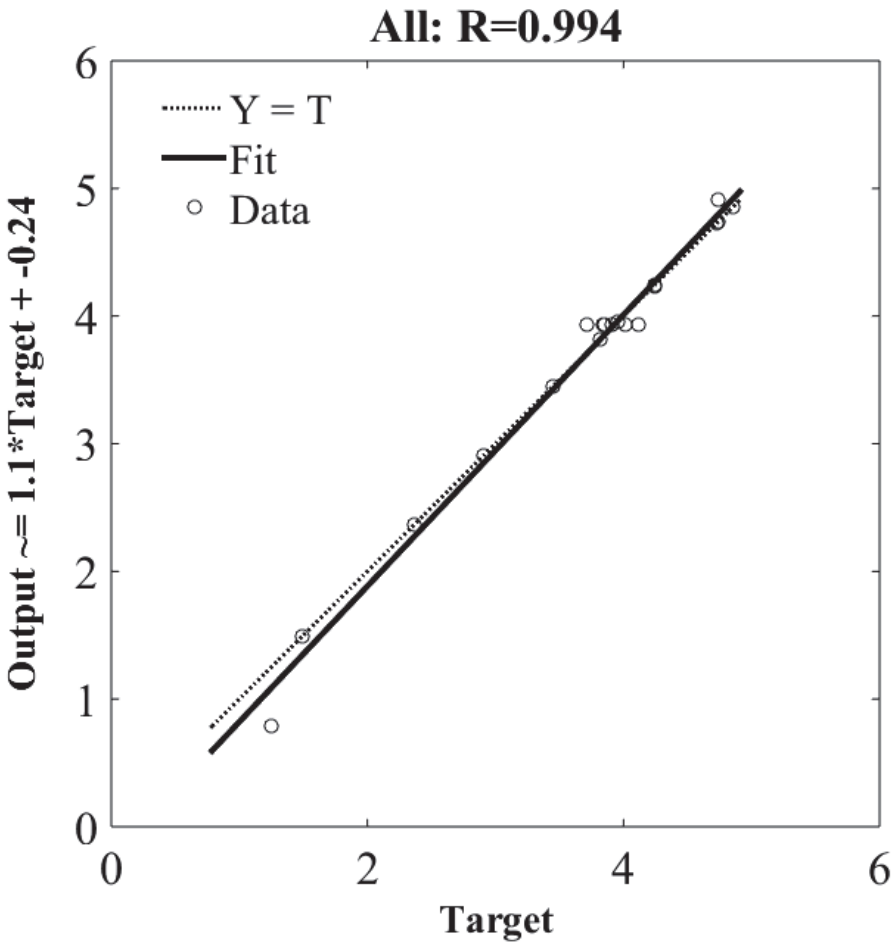

Figure 4.4. Regression analysis by ANN of the data for validation.

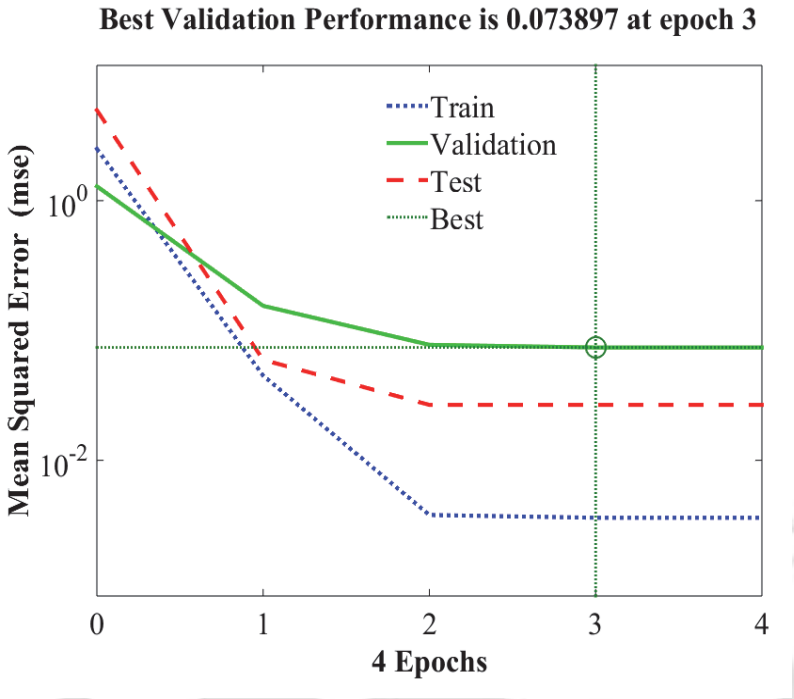

Figure 4.5. Neural network training, validation and test plot for the output response of OOC.

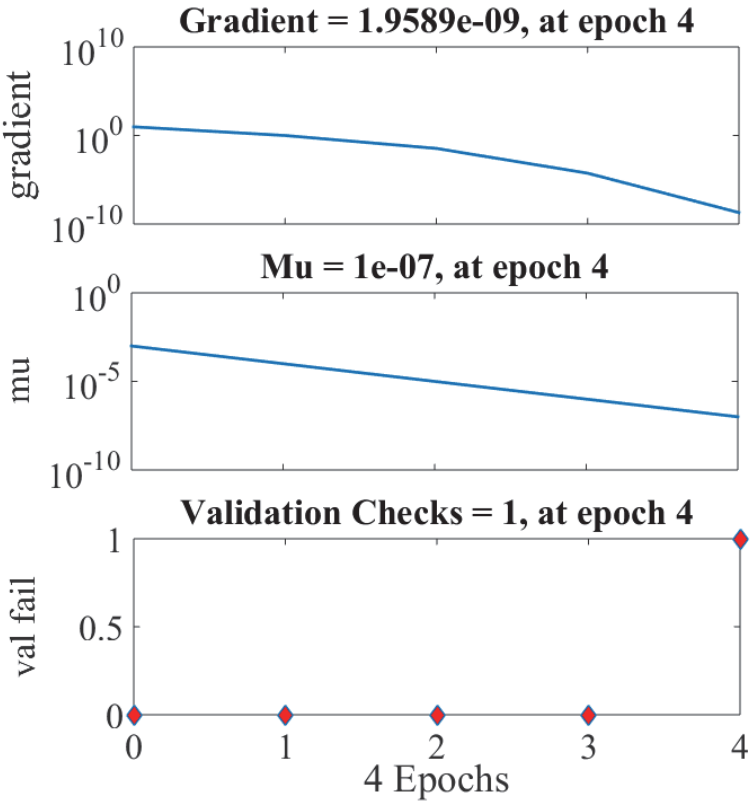

Figure 4.6. ANN training state plot.

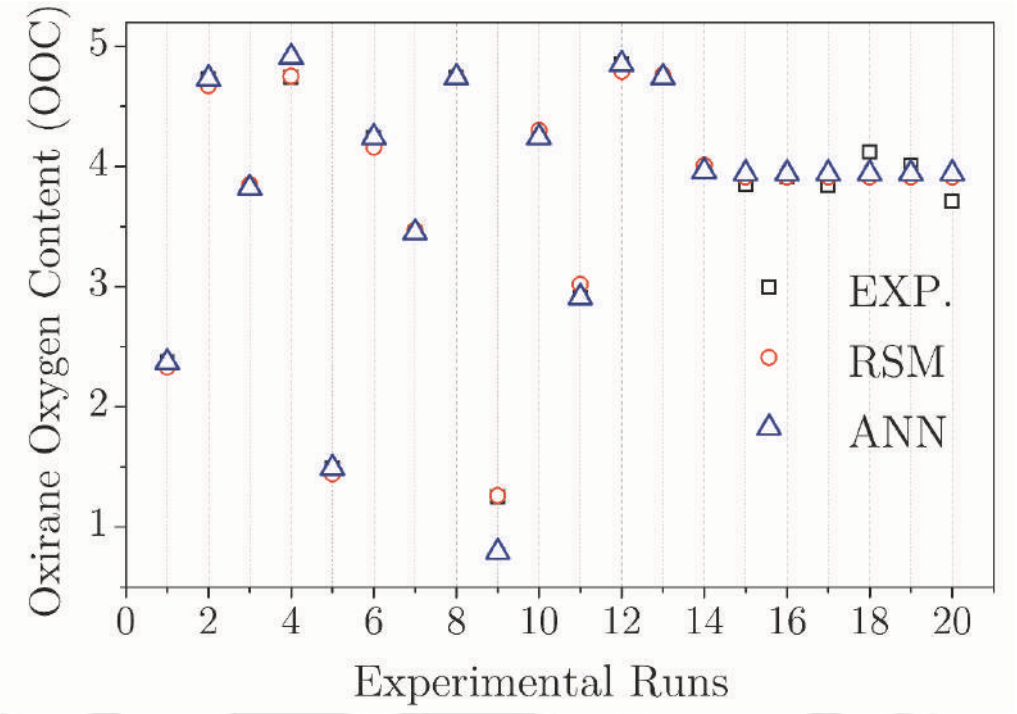

Figure 4.7. Estimation capabilities of both RSM and ANN predicted models with respect to the experimental data.

4.1.2.1. Levenberg–Marquardt (LM) Algorithm

Levenberg-Marquardt (LM) is the most widely used optimisation algorithm among the various existing transfer algorithms. The details about the same have been described in the previous chapter; however, we reproduce it here for the reader's convenience. For different problems, it outcompetes the simple and conjugate gradient methods. It is basically a combination of vanilla gradient descent and Gauss-Newton iteration. It is also considered as a trust-region method. The solution provided by the LM algorithm is known as Nonlinear Least Squares Minimisation, and the function to be minimised is governed by the following Equation 4.6.

$$f(x) = \frac{1}{2}\sum_{j=1}^{m} rj^2(x) \tag{4.6}$$

Where $x = (x_1, x_2, \ldots\ldots, x_n)$ is a vector, and each r_j is a function from R^n to R .

The r_j are referred to as residual, and it is assumed that $m \geq n$.

4.1.2.2. Comparison Between RSM and ANN Predicted Model

The responses obtained by RSM and ANN are tabulated in Table 4.4a. The adequate convergence between the actual and predicted responses was determined by evaluating the model's coefficient. The RSM predicted non-linear model is not sufficient enough for understanding the response behaviour, (Srivastava et al., 2018) and therefore, both RSM and ANN are considered for the present study. The observed regression coefficients for RSM and ANN were found to be 0.993 (Figure 4.1) and 0.994 (Figure 4.4), respectively, which confirmed that both the methods performed well for the present study.

4.1.2.3. Sensitivity Analysis by ANN

To carry out the sensitivity analysis of the input parameter, leave one parameter out approach was used in the present study. In this method, initially the RMSE value was evaluated considering all the three parameters. Then, each time one input parameter was left out at a time in turn and RMSE was evaluated based on remaining other two parameters (Mohd et al., 2011). The results of sensitivity analysis shown in Table 4.5 indicate that higher is the RMSE value, higher is the contribution of that parameter. For example, when the parameter WSCOME:H_2O_2 molar ratio was not considered for RMSE evaluation, the value increased from 0.1327 to 1.1492. Similarly, the RMSE value increased to 0.5125 and to 0.6521 when WSCOME:H_2SO_4 and time was not considered for evaluation, respectively. These results essentially indicate WSCOME:H_2O_2 molar ratio as the significant parameter to maximise the OOC content.

Table 4.5. Sensitivity analysis of each parameter.

	RMSE	RMSE Difference	Contribution (%)
All Parameters (3)	0.1327	—	—
L–WSCOME: H_2O_2	1.1492	1.0165	53.06
L–WSCOME: H_2SO_4	0.5125	0.3798	19.83
L–Time	0.6521	0.5194	27.11
Total	—	1.9157	100

Note: L: leave one out, — not available or not required

Table 4.6. Optimisation table (RSM, ANN, and GA).

	Input Parameters			Output Value
	WSCOME: H_2O_2	WSCOME: H_2SO_4	Time (h)	OCC (mass %)
RSM	2.28	2.00	4.00	4.82
ANN	2.28	2.00	4.00	4.84
GA	2.21	1.95	4.14	4.92

4.1.3. Genetic Algorithm

The RSM and ANN models are adequate to predict the optimisation conditions within the selected process variable range, i.e. local convergence. Therefore, researchers have developed an optimisation tool which is capable of predicting the optimisation conditions globally, i.e. Genetic Algorithm (GA). It works on the Darwinian principle which suggests that only the fittest species (best suitable) will survive during the reproduction (iteration) cycle after such an extended selection of survival achieved through various mutations and crossovers (operators). In this present study, it was found that after 77 iterations (reproduction) and crossovers, the best suitable condition was generated with genetic algorithm in a given search space with constraints for WSCOME:H_2O_2 ratio, WSCOME:H_2SO_4 ratio and time with lower (1.16, 0.66, 2.64) and upper (2.84, 2.34, 9.36) bounds. Concurrently 77 generations were analysed to find the best-fit individual. The best-optimised condition generated for GA was (2.21, 1.95 and 4.14) which gave the maximum OOC (4.92 mass %). Optimisation parameters predicted from all three models (RSM, ANN, and GA) for different factors are shown in Table 4.6.

The experimental output (OOC) for the validation experiment is as follows by using optimum data points provided by RSM, ANN, and GA respectively 4.8±0.32 mass %, 4.8±0.32 mass %, and 4.9±0.24 mass %.

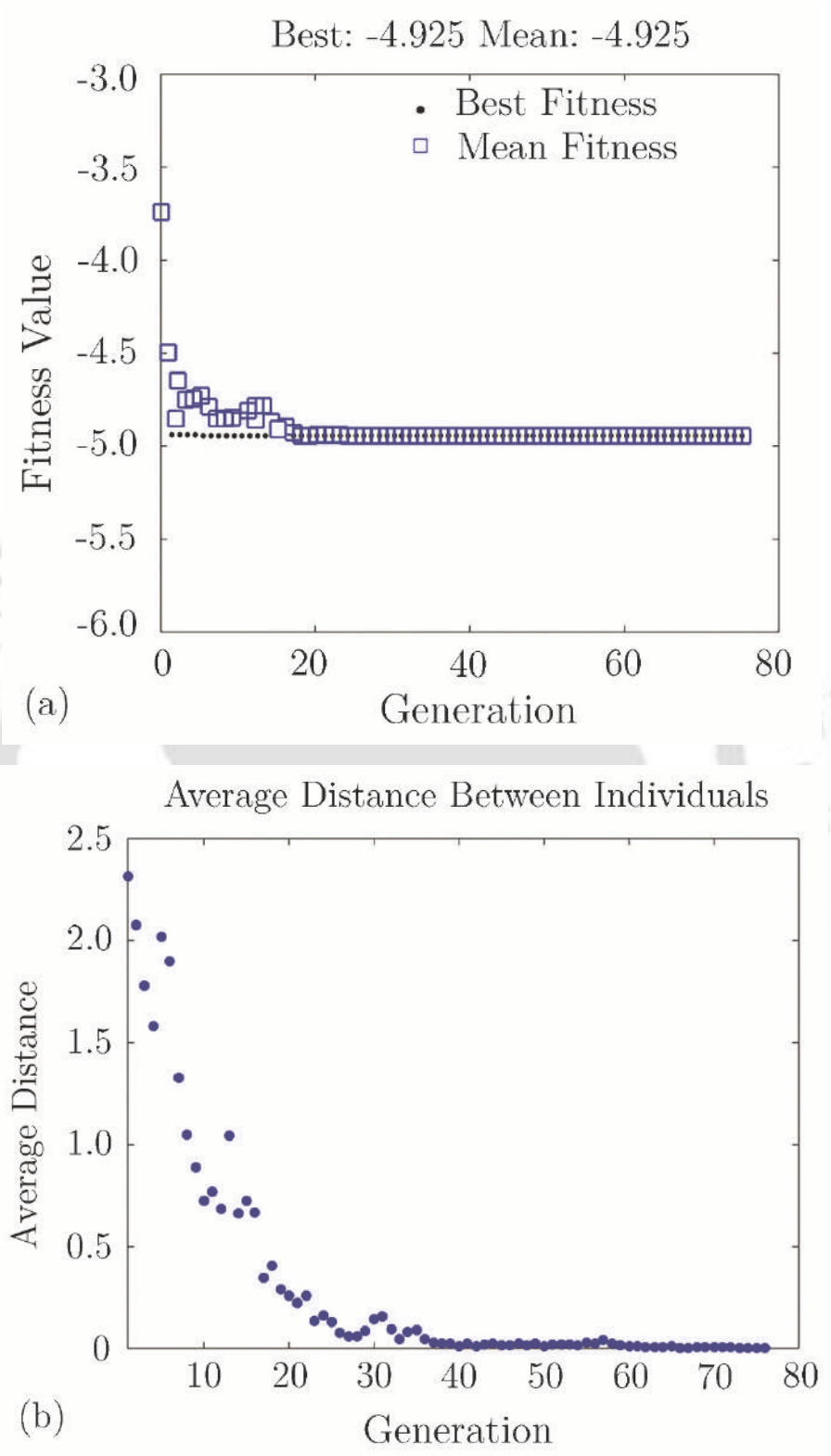

Figure 4.8. A genetic algorithm for prediction of the global optimum condition; (a) selection of best-fit individual during mutations and crossovers over several generations, (b) the average distance between selected individuals.

4.2. Physico-chemical Characterisation of Prepared EWSCOME

4.2.1. Product Confirmation by FTIR

The FTIR spectra of EWSCOME and WSCOME are compared and shown in Figure 4.9. As the hydrocarbon chain undergoes a structural change with the removal of glycerine and subsequent substitution of methanol, the FTIR spectra of methyl esters and triglyceride do not differ much; however, a noteworthy dissimilarity in the spectra was observed from 500–1500 cm^{-1}. FTIR spectra could also detect the conversion of unsaturation C=C to OOC (oxirane oxygen) and its subsequent functionalisation. Transformation of C=C bonds to three-membered oxirane ring following the epoxidation reaction, as shown in Figure 4.9, was confirmed by the appearance of epoxy groups at 843 cm^{-1} and disappearance of double bonds at 3004 cm^{-1}. Catalytic role of sulphuric acid in the epoxidation reaction was proposed due to the appearance of OOC peak at 843 cm^{-1}.

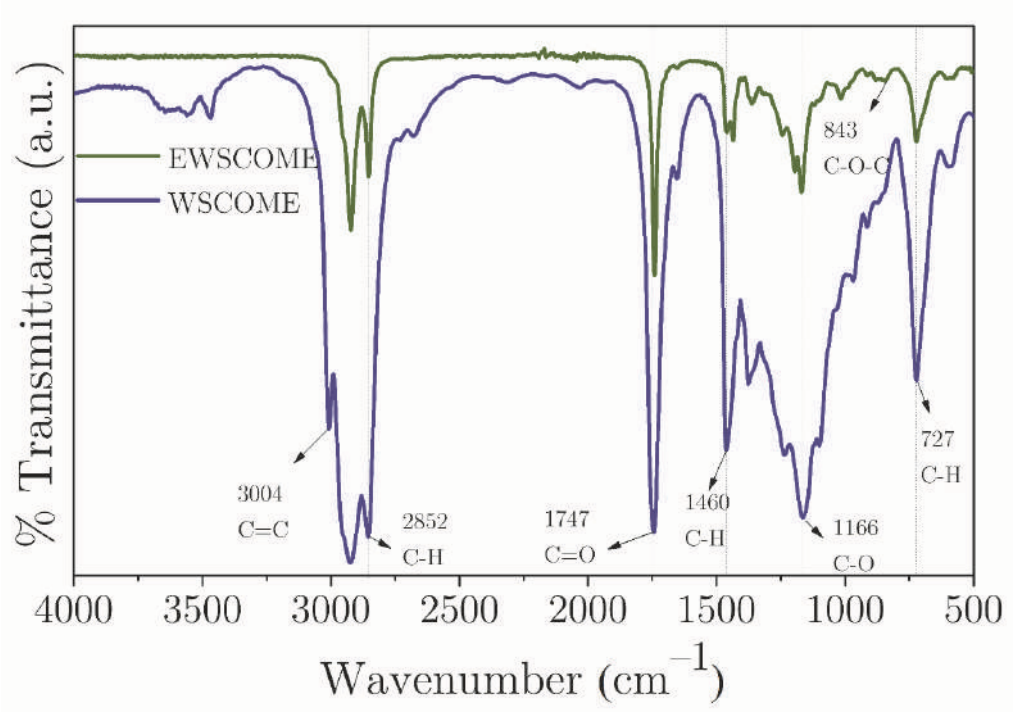

Figure 4.9. FTIR spectra of WSCOME and EWSCOME.

4.2.2. Cold Flow Properties

The ability of epoxide to continue in a liquid state at lower temperature is a highly significant property for many of the industrial materials, such as lubricants, surfactants, and fuels. Cold flow property reveals the lowest temperature at which epoxides can be used in various applications. Heat flow versus temperature profiles of WSCOME and its epoxides (cooling thermograms) obtained using DSC thermal analysis are shown in Figure 4.10. The structurally modified EWSCOME showed pour point (PP) as 2.6 °C, while for WSCOME, it was around -1.3 °C, which indicated a significant increase in PP after structural modification which might be due to the conversion of unsaturation into epoxides. Other researchers have noticed similar trends with respect to the unsaturated fatty acid composition of oils and esters (Borugadda and Goud, 2014b, 2014a; Farias et al., 2010).

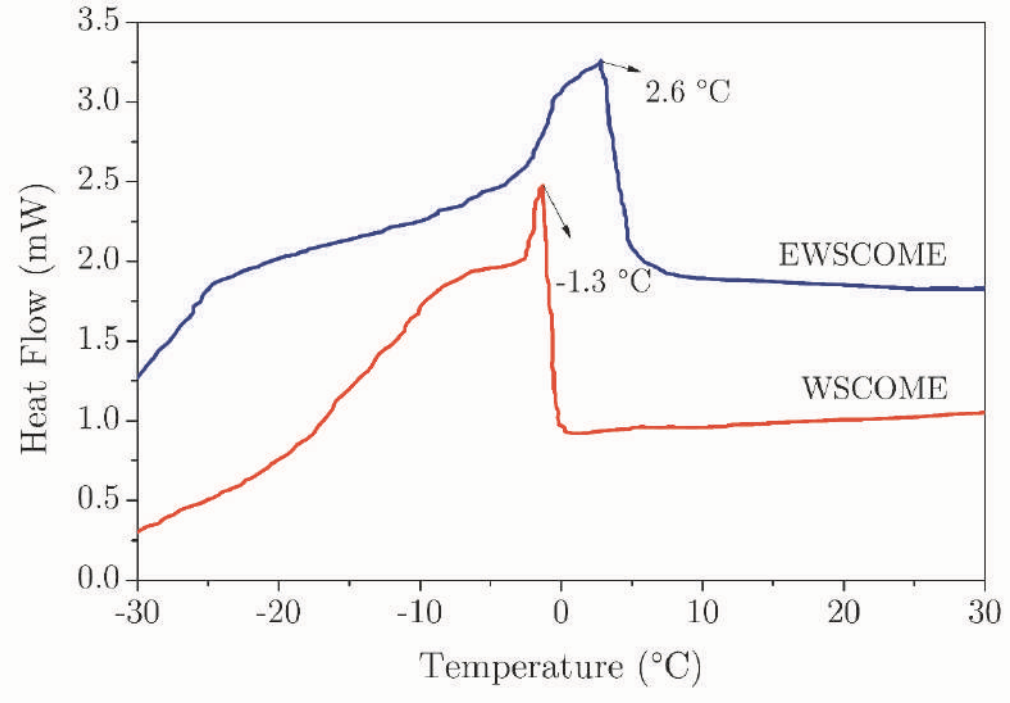

Figure 4.10. DSC thermogram for WSCOME and EWSCOME.

4.2.3. Product Confirmation by NMR

Nuclear magnetic resonance (NMR) spectroscopy was recorded to observe the structural changes in crude WSCOME and EWSCOME; completion of reaction was confirmed by proton ^{1}H NMR peaks. The advantage of using ^{1}H NMR is that it requires a very small amount of sample and gives quantitative information about the chemical species present in the sample. The change in ^{1}H NMR spectrum with WSCOME and EWSCOME is shown in Figure 4.11. The peak between δ 5.3 ppm and δ 5.4 ppm indicates the presence of unsaturated protons (bis-allylic hydrogens). The ^{1}H NMR of EWSCOME confirmed the formation of epoxides as new chemical shifts at δ 2.8 ppm to δ 3.1 ppm were observed, which corresponds to epoxy protons (Figure 4.11). The characteristic peak of oxirane at δ 2.8 ppm to δ 3.1 ppm is attributed to epoxide formation, which was absent in the methyl esters. Thus, the NMR spectrum confirmed the successful conversion of WSCOME and EWSCOME.

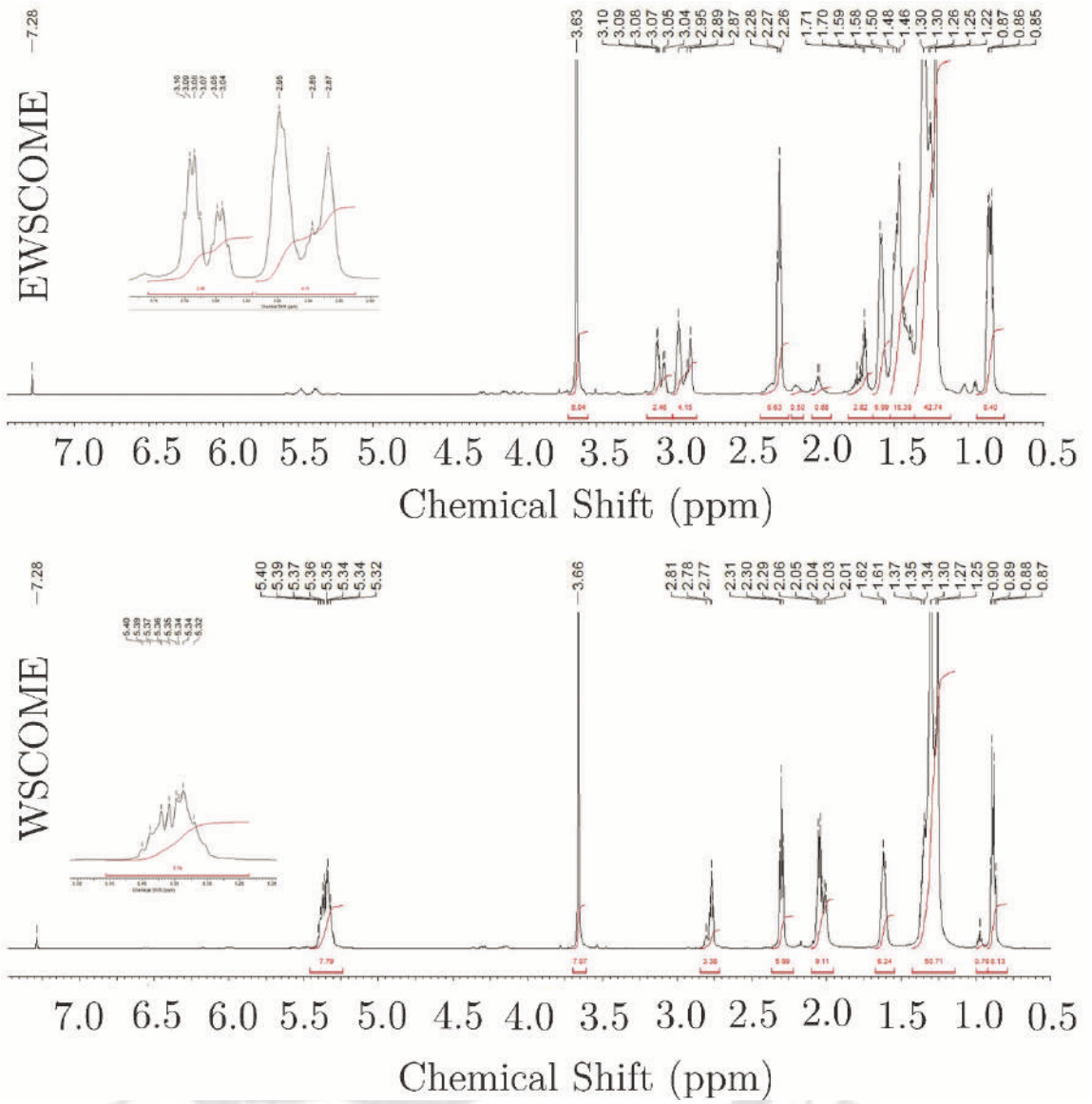

Figure 4.11. ^{1}H NMR spectrum of the WSCOME and EWSCOME.

4.2.3. Thermal and Oxidative Stability

Thermogravimetric analysis (TGA) of the sample (EWSCOME and WSCOME) was performed at N_2 atmosphere to check the thermal stability and degradation profile of the samples. Thermal stability of the sample was determined from the onset temperature of thermal decomposition under inert atmosphere. Comparison

of TGA profile of WSCOME and EWSCOME samples at 10 °C/min under nitrogen atmosphere is shown in Figure 4.12a. The curve shows two consecutive stages of thermal decomposition for the samples. As shown in the figures, the degradation initiation temperatures (T_i) of EWSCOME and WSCOME were 204 °C and 183 °C relatively in an inert atmosphere. Similarly, maximum decomposition temperature corresponds to the temperature at which the maximum weight loss occurred, i.e. at 317 °C and 279 °C for EWSCOME and WSCOME, respectively. The results of the study revealed that EWSCOME exhibits more thermal stability compared to WSCOME. Higher thermal stability of EWSCOME was attributed to the disappearance of unsaturation, which eventually helps to improve thermal stability of epoxides.

Similarly, to measure the oxidative stability, TGA analysis of the sample was performed in oxygen atmosphere. Oxidation process is a principally exothermic reaction which occurs between the sample and oxygen (Borugadda and Goud, 2014b). Oxidative stability is the quality indicative parameter for the epoxides in real-life applications. It is defined as the resistance of oil sample against oxidation. Oxidation of epoxides results in decreasing shelf life along with increase in viscosity and acid value simultaneously (Romero et al., 1998). Figure 4.12b shows TG, DTG curve for EWSCOME and WSCOME under oxygen environment at heating rate of 10 °C/min. It was shown that (Figure 4.12b) WSCOME was stable up to 198 °C and EWSCOME up to 215 °C in oxygen atmosphere. Because unsaturated compounds are more sensitive to oxidation than saturated compounds with the same length of hydrocarbon chain, unsaturated compounds are more reactive than saturated ones (Sharma et al., 2019). The oxidative stability of vegetable oils is determined by the presence of the most prominent fatty acids in the triglyceride structure (Rudnick, 2020). The oxidative stability

of oils decreases as the amount of unsaturation in the oil increases. Unsaturated carbon-carbon bonds serve as active sites for a variety of undesired reactions, including oxidation events, due to their high reactivity (Fox and Stachowiak, 2007). The polymerisation of vegetable oils raises the viscosity of the lubricant, reducing its ability to perform its intended purpose (Asadauskas et al., 1996). A high percentage of unsaturated fatty acids in vegetable oils will lead to a reduction in the pour point (Jayadas and Nair, 2006). Vegetable oils are effective as boundary lubricants and can be used in this capacity (Adhvaryu et al., 2005). Increased polarity of the oils will result from the ester functionality of these oils, which will aid in the production of an excellent tribo-film, which will result in improved tribological characteristics. Poly-unsaturated compounds, on the other hand, are more reactive than mono-unsaturated molecules, for several reasons (Luna et al., 2011; Zhang et al., 2020). As a result of the current investigation into the oxidative stability of WSCOME and its epoxide, it was discovered that epoxidation of WSCOME reduces the unsaturation content of the compound, thereby increasing its oxidative stability.

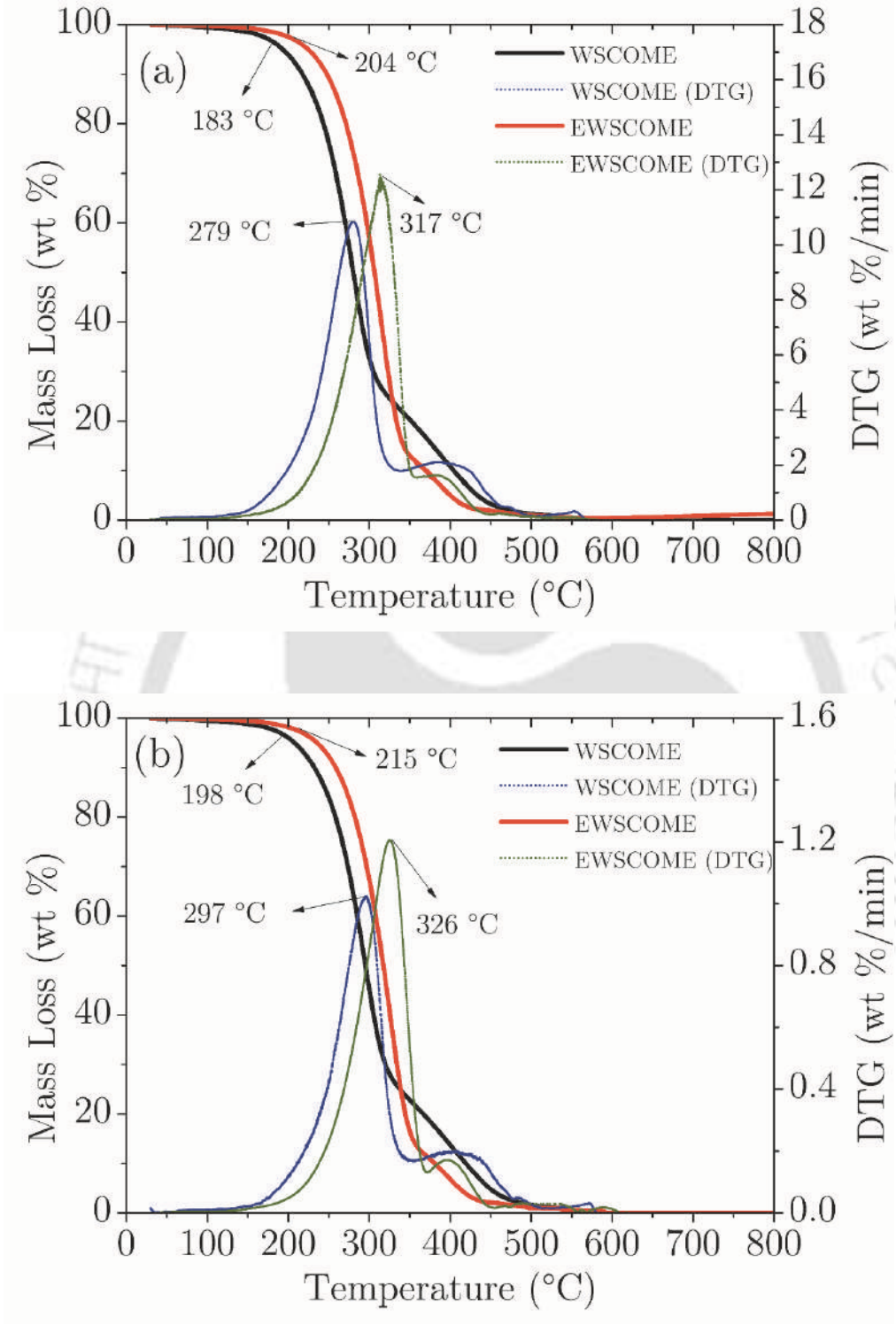

Figure 4.12. TGA stability thermograms for (a) WSCOME and EWSCOME (thermal stability) and (b) WSCOME and EWSCOME (oxidative stability).

Table 4.7. Comparison of physico-chemical properties of WSCOME and EWSCOME

Properties	Unit	WSCOME	EWSCOME
Specific Gravity	—	0.75	0.77
Kinematic Viscosity[a]	cSt	4.51± 0.1	12.15 ± 0.87
Density	kg/m^3	755.4± 3.24	773.8 ± 3.71
Iodine Value	g I_2/100g	132.9± 3.14	2.41±0.17
Acid Value	mg KOH/g	0.30±0.07	0.20±0.04
Refractive Index @ 24 °C	—	1.47±0.1	1.48±0.08
Pour Point[b]	°C	–1.3±0.1	2.6±0.01
Moisture Content	wt %	0.21±0.02	0.18±0.03
Oxirane Content (Experimental)	—	—	4.81±0.5
Oxirane Content (Theoretical)	—	—	7.94±0.3
Relative Percentage Conversion of Oxirane	%	—	60.57±3.84
Glycol Content (Theoretical)	—	—	0.44±0.01
Glycol Content (Experimental)	—	—	0.14±0.01
Relative Percentage Conversion α-glycol	mol/100 g	—	31.81±2.8

[a]measured at 40 °C, [b]DSC method, — not available or not required

4.2.4. Rheological Behaviour and Viscosity

Rheological (flow behaviour) behaviour of WSCOME and EWSCOME was studied using Anton-Paar Rheometer to examine the correlations between shear stress (Pa) vs shear rate (s^{-1}) and dynamic viscosity (Pa.s) vs shear rate (s^{-1}). The experiments were performed at different shear rate ranges of 50, 100, 150, 300, and 500 s^{-1}. The rheological behaviour of WSCOME and EWSCOME as a function of temperature (i.e. at room temperature and at 40 °C) is shown in

Figure 4.13 and 4.14. The plots between shear stress and shear rate (Figure 4.13) indicate the Newtonian type of fluid behaviour. As can be seen from Figure 4.14, viscosity at room temperature as well as at 40 °C did not vary much with the increased shear rate. Similar trend was noticed in our earlier findings on epoxidation of waste oils (Borugadda and Goud, 2014a). The comparative analysis of viscosities of WSCOME and EWSCOME revealed that EWSCOME (9.4 mPa.s at 40 °C) viscosity was almost five times higher than WSCOME (2.5 mPa.s at 40 °C), which implied that EWSCOME (after structural modification) has better lubrication properties compared to WSCOME. The weight of epoxide was enhanced by incorporating the oxygen molecule in the midst of the unsaturation, which also improved its viscosity (Table 4.7).

Apart from that, the acid value of EWSCOME was found to be as low as 0.2 mg KOH/g, which confirms that epoxides do not create any trouble (i.e. corrosion) during the usage. Further, the density of EWSCOME was measured and found to be higher compared to WSCOME—this is due to increase in the molecular weight, polarity, and intermolecular forces during epoxidation (Wu et al., 2000). To find the percentage of moisture present in EWSCOME, moisture content was determined. The presence of moisture in samples encourages bacterial growth, which leads to an increased acid value and increased oxidation (Dörmo et al., 2004). The moisture content of crude epoxides sample was found to be 0.18%, which was within acceptable limits (Table 4.7). The refractive index of WSCOME and EWSCOME was found to be 1.47 and 1.48 (Table 4.7), respectively, which shows that very minute amount of heat energy can pass through the WSCOME and EWSCOME, which is desired to protect the chemical and physical integrity of the EWSCOME.

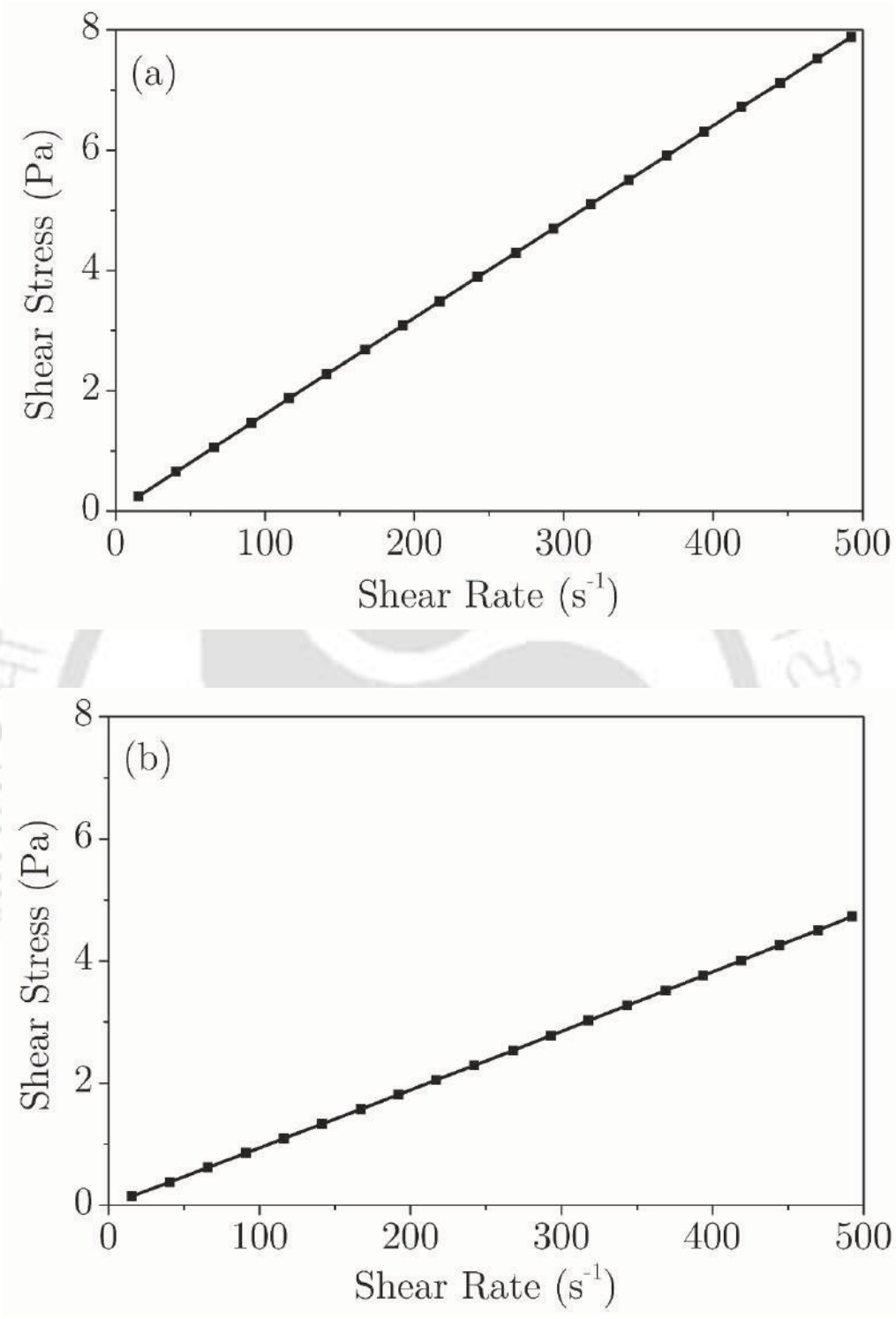

Figure 4.13. Shear stress vs shear rate for EWSCOME at (a) room temperature (25 °C), (b) 40 °C.

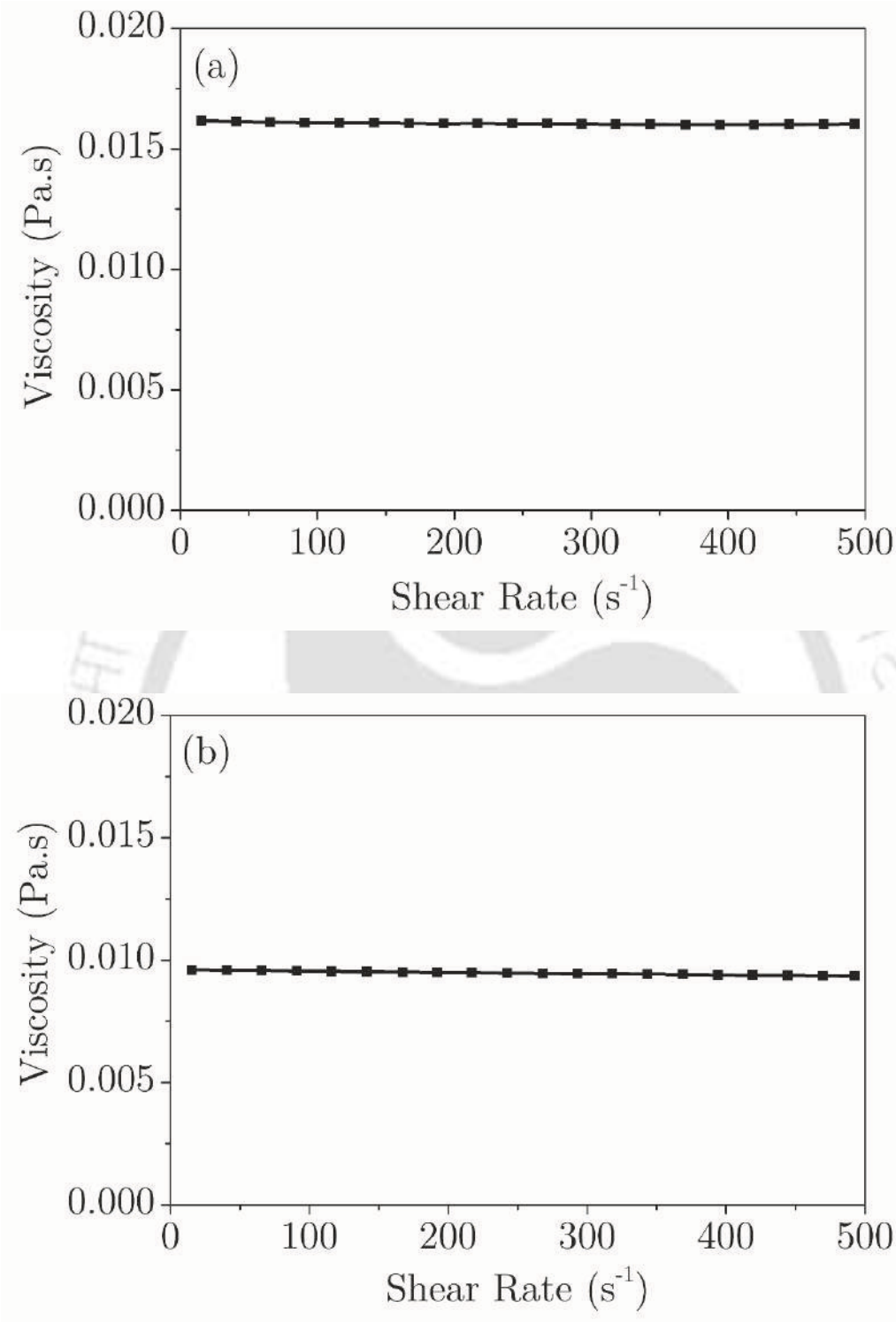

Figure 4.14. Shear rate versus viscosity relation for EWSCOME at (a) room temperature (25 °C), (b) 40 °C.

Similarly, practical applications of the prepared epoxidised waste soybean cooking oil methyl esters were identified by a relative comparison of viscosity index with the ISO vegetable grade lubricants and other agricultural grade lubricants that are reported in Table 4.8. The viscosity index is one of the critical parameters to measure the change in viscosity with varying temperatures. From Table 4.8, the epoxidised waste soybean cooking oil methyl esters viscosity index was observed to be higher than the ISO VG 32, ISO VG 46, SAE 20W40, AG 100, Paraffin VG 95, and Paraffin VG 460. All the estimated physico-chemical properties showed that the prepared epoxide could act as a potential supplement to these standard bio-lubricants in the market.

Table 4.8. Relative comparison of viscosity index for Epoxidised waste soybean cooking oil methyl esters with ISO and other renewable lubricants (McNutt and He, 2016).

Name of the Sample	Viscosity Index
Epoxidised Waste Soybean Cooking Oil Methyl Esters (EWSCOME)	151.97 (current study)
ISO VG 32	>90
ISO VG 46	>90
ISO VG 68	>198
ISO VG 100	>216
SAE 20W40	132
AG 100	103
Paraffin VG 95	102
Paraffin VG 460	97

4.3. Summary

The current work has demonstrated the synthesis of bio-lubricant base stocks from WSCOME via epoxidation. The optimisation study revealed that 2.21 moles of H_2O_2 (WSCOME:H_2O_2 molar ratio), 1.95 wt % of catalyst loading, and 4.14 h of reaction time lead to optimum OOC conversion of 4.81 mass %. Besides RSM optimisation analysis, ANN and GA were also performed and compared. The OOC of EWSCOME was found to be 4.82, 4.84, and 4.92 mass % under the experimental conditions by RSM, ANN, and GA, respectively. Further, the study revealed that the prepared EWSCOME exhibits more desired physico-chemical properties than WSCOME in all the aspects for environment-friendly bio-lubricants. Interesting findings of the prepared bio-lubricant base stocks indicate that they could be a potential complement to ISO VG 32, ISO VG 46, SAE 20W40, AG 100, Paraffin VG 95, and Paraffin VG 460 grade bio-lubricants available in the market.

CHAPTER V

Studies on the Rheological Properties of Epoxides of Waste Soybean Cooking Oil (EWSCO) and Waste Soybean Cooking Oil Methyl Esters Epoxides (EWSCOME)

Physico-chemical Properties of WSCO, WSCOME, and their Epoxides

Rheological Behaviours

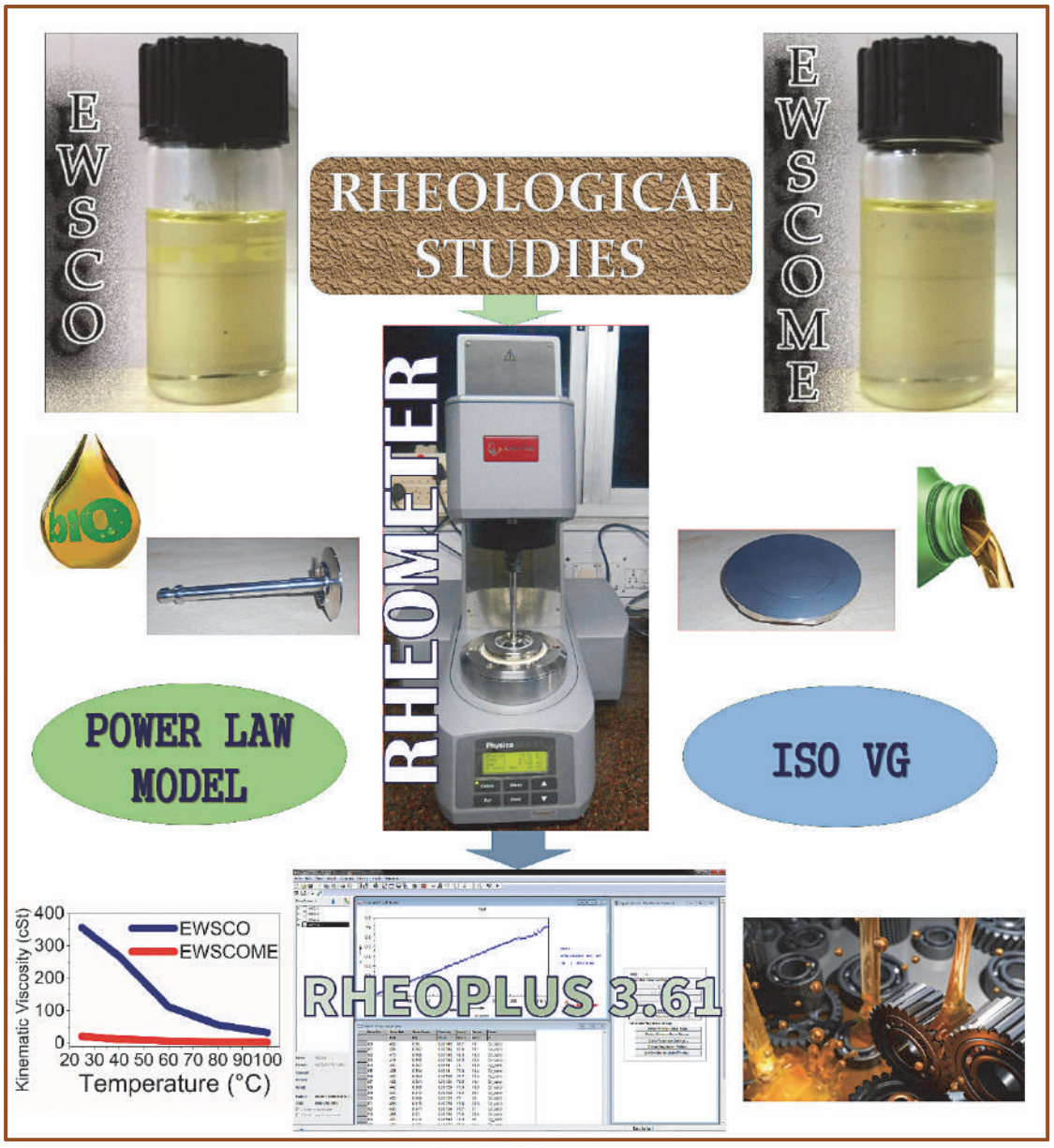

Graphical Abstract of Chapter V

Chapter V

Studies on the Rheological Properties of Epoxides of Waste Soybean Cooking Oil (EWSCO) and Waste Soybean Cooking Oil Methyl Esters Epoxides (EWSCOME)

In this chapter, rheological behaviour of epoxides of waste soybean cooking oil and waste soybean cooking oil methyl esters epoxides was analysed for bio-lubricant applications. Rheological properties of the prepared epoxides were measured at the temperature and shear rate ranging from 25–100 °C and 5–300 s^{-1}, respectively. As viscosity is one of the critical parameters for potential bio-lubricant applications, in the present study, the power law model was used to investigate the flow behaviour of epoxides and indicated Newtonian type of fluid behaviour in the studied temperature range. Different shear rates (5-100 s^{-1}, 5-300 s^{-1}, 100-300 s^{-1}) were studied to understand the shear rate dependency of epoxides of waste cooking oil and its methyl esters at different temperatures. The average viscosity values indicated that the epoxides had identical results at all shear rates. The dynamic viscosities of epoxides of waste cooking oil and its methyl esters were found to be dependent on fatty acids chain length, unsaturation, and temperature. Based on the viscosity of EWSCO (278 cSt) and EWSCOME (12 cSt), and viscosity index of EWSCO (164) and EWSCOME (151), and other physico-chemical properties, it appears that the prepared epoxides could act as a potential candidate for suitable bio-lubricant applications.

5.1. Physico-chemical Properties of WSCO, WSCOME and their Epoxides

Physico-chemical properties of all the sample were determined and tabulated in Table 5.1. The lower acid value of EWSCO (0.3) and EWSCOME (0.2) signifies that they do not create any trouble or damage (due to corrosion) to the machinery during its usage. Free fatty acid (FFA) content is always half of the AV, which indicates the formation of soap when it is mixed with water; the estimated FFA value was very less (0.15 mg KOH/g and 0.10 mg KOH/g for EWSCO and EWSCOME, respectively). Similarly, the density of WSCO and WSCOME was found to be 792 and 755 kg/m^3, respectively; after chemical modification (EWSCO and EWSCOME), it increased to 802 and 773 kg/m^3, respectively. An increase in the viscosity is owing to the increased molecular weight which was attributed to the addition of oxygen molecule at unsaturation sites, polarity, and intermolecular forces in the epoxides after reaction (Scala and Wool, 2005).

The evaluation of IV (i.e. unsaturation sites) after epoxidation is one of the ways to confirm the oxirane formation. Initial IV of WSCO was found to be 132 (g I_2/100 g of oil), whereas after the reaction it decreased to 1.74 (g I_2/100 g of epoxide). From IV, it was confirmed that 98.66% double bonds were transformed into oxirane ring via epoxidation as shown in the Figure 5.1, and the conversion was calculated based on initial and final IVs. These three-membered rings of oxirane could form a smooth layer due to tribopolymerisation which is tribologically effective to reduce friction during usage (Wu et al., 2000). Similarly, relative percentage conversion to oxirane was found to be 60.75% (based on Equation 2.4). One of the considerable properties of epoxides is moisture content, which indicates the presence of water in the epoxide. In general, the presence of

moisture encourages bacteria to grow; this leads to an increased AV and viscosity, and forms free radical compounds via oxidation (Sharma et al., 2008). In this study, epoxides moisture content was found to be 0.25 and 0.18 wt % respectively for EWSCO and EWSCOME, (Table 5.1), which again favours the usage of EWSCO and EWSCOME without any trouble. The refractive index of EWSCO was found to be 1.47 (Table 5.1), which shows that very less amount of heat energy can pass through the epoxide, which is the desired property for lubricants to maintain their structural integrity. Lower refractive index lubricants are preferred to avoid thermal variations from the application point of view during usage. Lower specific gravity (0.7) of the EWSCOME indicated the completion of the reaction and removal of heavy glycerine from EWSCOME.

The structure of the epoxides derived from natural triglycerides is located along a hydrocarbon chain so that each carbon of the cyclic ether bears an alkyl substituent. To make use of epoxides for a specific application, they should maintain their physical, chemical, and structural integrity at all storage conditions. The epoxidised derivatives can be used as lubricant base fluids due to their good lubricity and higher thermo-oxidative stability compared to their structurally unmodified feedstock (Adhvaryu et al., 2005).

Further, fatty acid composition of WSCO was estimated using GC (gas chromatography). The saturated fatty acid (FA) content of WSCOME was 18%. No significant changes were noticed in the fatty acid alkyl chain methyl esters and epoxide samples compared to original oil. Linoleic acid (39%) was abundant in WSCO/WSCOME, followed by oleic (24%), linolenic (5%), and Stearic acid (4%). Fatty acid composition of oil is shown in Table 5.2.

Table 5.1. Comparison of physico-chemical properties of WSCO, WSCOME, and epoxides.

Properties	Unit	WSCO	WSCOME	EWSCO	EWSCOME	Epoxidised Waste Cooking Oil Fatty Acid Methyl Esters (McNutt and He, 2016)	Methyl Esters of 9,10-Palmitoyloxy-acetoxy Stearic Acid (MEPASA) (Kleinová et al., 2008)	Epoxidised Soybean Oil (ESBO) (Adhvaryu and Erhan, 2002)	ISOVG 32 (McNutt and He, 2016)
Specific Gravity	—	0.79	0.75	0.80	0.77	—	—	—	—
Kinematic Viscosity[a]	cSt	33.94± 1.39	4.51± 0.1	267.9 ± 3.56	12.15 ± 0.87	15.9	44.6	170.8	28.8
Density	kg/m^3	792.0± 4.58	755.4± 3.24	802.1 ± 4.89	773.8 ± 3.71	—	942	—	—
Iodine Value	g I_2/100 g	132.9± 2.94	132.9± 3.14	1.74 ± 0.14	2.41 ± 0.17	—	5.05	9.11	—
Acid Value	mg KOH/g	0.54± 0.12	0.30± 0.07	0.30 ± 0.07	0.20 ± 0.04	—	—	0.09	—

Free Fatty Acid	mg KOH/g	0.27± 0.05	0.15± 0.03	0.15 ± 0.04	0.10 ± 0.02	—	—	0.045	—
Refractive Index at 24 ℃	—	1.47± 0.07	1.47± 0.1	1.47 ± 0.1	1.48 ± 0.08	—	—	—	—
Pour Point	°C	-7.8± 0.13	-1.3± 0.1	-6.3 ± 0.17	2.60 ± 0.03	-15	-20	—	-6
Moisture Content	wt %	0.27± 0.02	0.21± 0.02	0.25 ± 0.02	0.18 ±0.03	—	—	—	—
Oxirane Content (Experimental)	—	—		4.69 ± 0.4	4.81 ± 0.5	—	—	—	—
Oxirane Content (Theoretical)	—	—		7.72 ± 0.2	7.94 ± 0.3	—	—	—	—
Relative percentage Conversion of Oxirane (%)	—	—		60.75±3.85	60.57±3.84	—	—	—	—

[a] measured at 40 ℃, — not available or not required

Table 5.2. Fatty acid composition of the oil (WSCO/WSCOME).

Fatty Acid	Carbon Number	Fatty Acid Composition (%) of WSCO/WSCOME	Chemical Name of the Fatty Acid	Formula
Oleic	(C18:1)	24.0±1.6	*cis*–9–octadecenoic	$C_{18}H_{34}O_2$
Linoleic	(C18:2)	39.2±1.7	*cis*–9,*cis*–12–octadecadienoic	$C_{18}H_{32}O_2$
Linolenic	(C18:3)	5.2±0.6	*cis*–9,*cis*–12,*cis*–15–octadecadienoic	$C_{18}H_{30}O_2$
Palmitic	(C16:0)	14.2±1.2	Hexadecanoic	$C_{16}H_{32}O_2$
Stearic	(C18:0)	4.1±0.2	Octadecanoic	$C_{18}H_{36}O2$

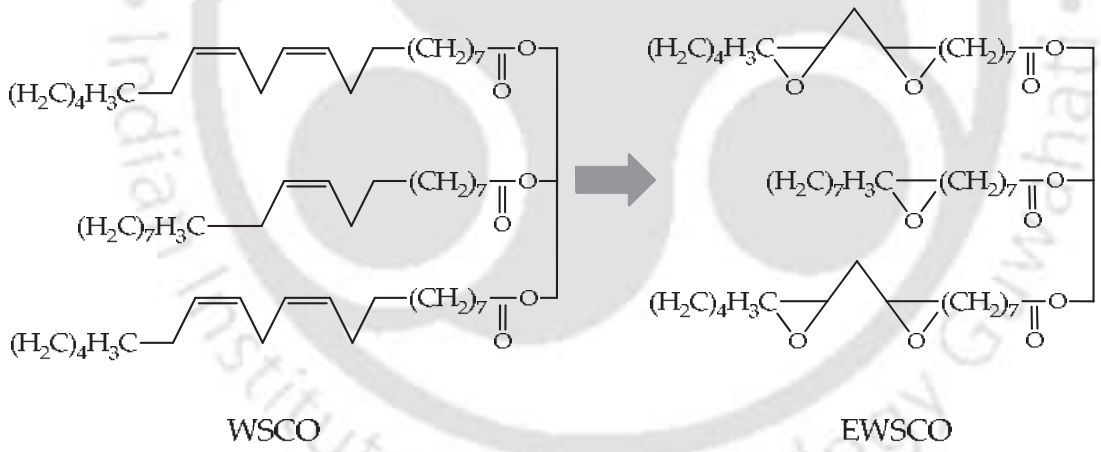

Figure 5.1. Chemical structure of the fatty acids presents in WSCO and EWSCO.

5.1.1. Rheological Properties

Internal flow property is an important property of fuel that depends on the fatty acid composition of oil. It is one of the important properties that should be the limit of standard value. The viscous property of oil, methyl esters and epoxidised

oil exerts great influence on fluid dynamic properties of fuel, such as fuel circulation and fuel injection during engine operation. There are three different regions of shear rate, i.e. 5–100 s^{-1}, 100–300 s^{-1}, and 5–300 s^{-1}. Shear rate was divided into three regions because it was observed that different shear rates show different flow properties. Experiment was done for 5–300 s^{-1} shear rate region, and among the observations, three regions were selected. The plot of shear stress vs shear rate at 40 °C showed a linear relationship with R^2 greater than 0.99 (Figure 5.2 and 5.3). Furthermore, the flow behaviour of samples was analysed using power law model (Equation 5.1).

$$\tau = k\gamma^n \tag{5.1}$$

Where, τ is a shear stress (Pa), γ is the shear rate (s^{-1}), n and k are the power law coefficients and can represent resistance of the fluid to flow. k is a flow consistency index (Pa. s^n) and n is called as non-Newtonian flow behaviour index (dimensionless). n and k values were estimated from the linearisation of power law equation. Plot of $\ln\gamma$ vs $\ln\tau$ should be a straight line with slope n and intercept $\ln k$ (Equation 5.2).

$$\ln\tau = \ln k + n\ln\gamma \tag{5.2}$$

According to Equation 5.2, plot between $\ln\tau$ and $\ln\gamma$ is expected to show a straight line relationship (Figure 5.4, 5.5) with slope n and intercept $\ln k$. The $\ln\tau$ dependence of $\ln\gamma$ for EWSCO and EWSCOME at various temperatures, ranging from ambient to 100 °C, is shown in Figure 5.4 and 5.5 indicating that at various temperatures a linear relationship exists between $\ln\tau$ and $\ln\gamma$. From this dependency, k and n values were evaluated by linear regression analysis, and the results are reported in Table 5.3. Increase in the epoxides molecular weight can be attributed to the addition of oxygen molecule at unsaturation sites.

Table 5.3. Rheological parameter values of epoxides at 40 °C.

	EWSCO			EWSCOME			Diesel
Shear rate (s^{-1})	5–100[a]	100–300[b]	5-300[c]	5–100[a]	100–300[b]	5-300[c]	5–300[c]
k (mPa.s^n)	213.30	221.68	212	9.25	9.29	9.30	1.72
k_{exp} (mPa.s)	222.97	239.88	224.9	9.07	9.18	9.19	1.95
n (–)	0.99	0.98	0.98	1.00	1.00	1.00	1.00

k: flow consistency index obtained from power law model, k_{exp} : average dynamic viscosity obtained from experiment, n: non-Newtonian flow behaviour index, [a] lower shear rate (LSR), [b] higher shear rate (HSR), [c] Full shear rate

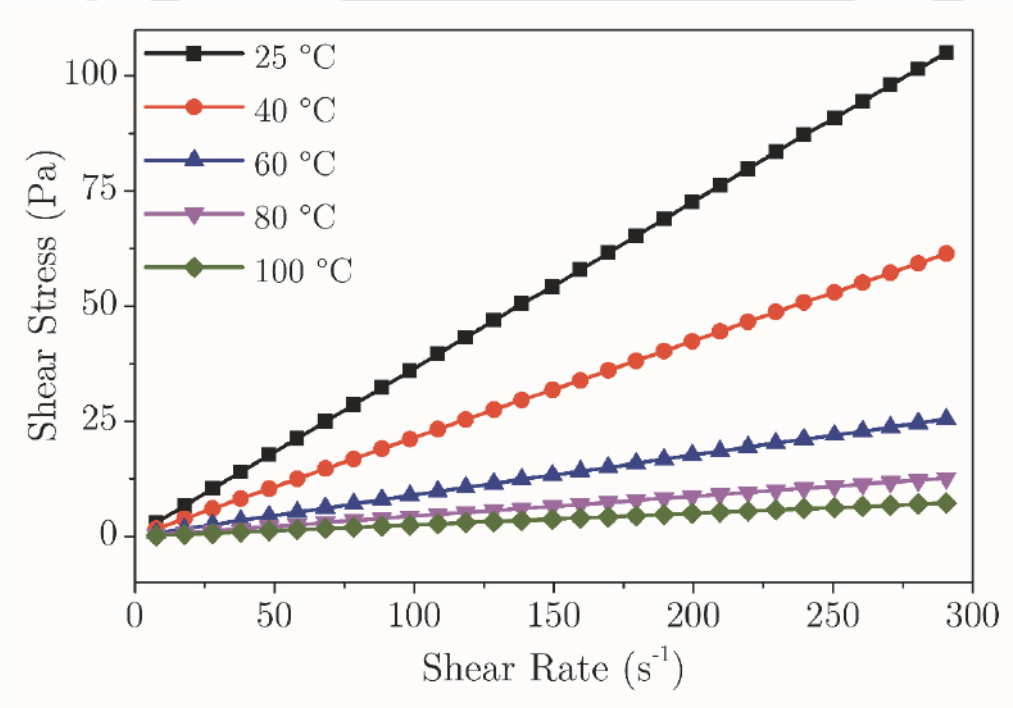

Figure 5.2. Shear stress vs shear rate plot for EWSCO.

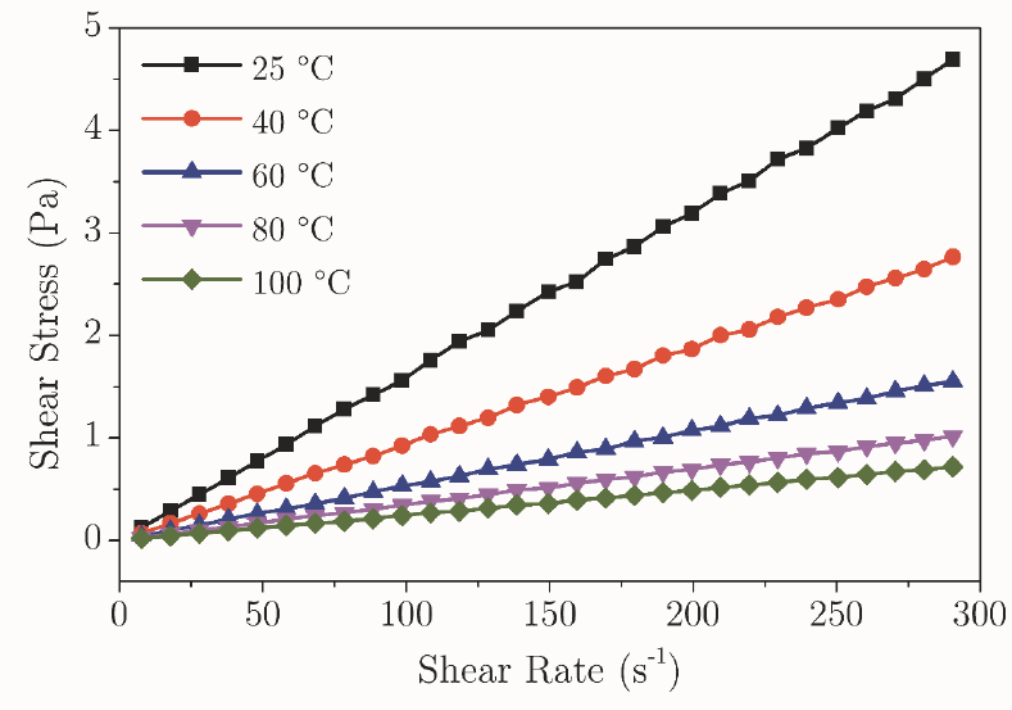

Figure 5.3. Shear stress vs shear rate plot for EWSCOME.

5.1.1.1. Viscosity Behaviour of Epoxides

The rheological experiments of the epoxides samples were carried out using the procedure described in the materials and methods (Chapter 2) section. The rheological behaviour of WSCO epoxides at various temperatures was studied and shown in Figure 5.2, 5.4 and 5.6–5.11. Figure 5.2 and 5.3 show increased shear rate with respective to shear stress, in spite of temperature variation. This linear relation between shear stress versus shear rate suggests Newtonian type fluid behaviour for EWSCO. Epoxidation of the unsaturated bonds that occur along the fatty acid chains of the oil produces more reactive oxirane groups. This three-member ring provides a more energetically favourable site for reaction and represents a chemical intermediate for the preparation of derivatives that would be difficult to obtain directly from the unsaturated bond (Xu and Qu, 2009). From Figure 5.2 and 5.4, it can also be noticed that, with an increase in the

temperature, shear stress decreased gradually. In the present study, rheological behaviour of WSCO epoxides was estimated using power law model. From this dependency, k and n values were evaluated by linear regression analysis, and the results are reported in Table 5.3 and shown in Figure 5.6 to 5.11, which express that flow behaviour index decreases with temperature, and consistency coefficient always remains constant and close to 1, irrespective of temperature variation.

A similar kind of results was reported by Yen and Yang (Yen and Yang, 2003) in their study on rheological behaviour of polyacrylamide solution. This behaviour of epoxides signifies that WSCO epoxides adopt the Newtonian fluid behaviour (Gorla et al., 2013). Therefore, based on the aforementioned rheological characterisation, it could be predicted that WSCO epoxides provide a smooth performance during its usage without any operational difficulties. Non-Newtonian flow behaviour index (n) versus temperature (°C) plot is shown in Figure 5.9 to 5.11, and from the figures, it was observed that n value varied from 0.9 to 1. It was also confirmed that samples show Newtonian behaviour throughout the temperature variation. The viscosity of epoxidised oil increased slightly with the extent of epoxidation. The viscosity increased monotonically from approximately 45 mPa.s for WSCO to as high as 365 mPa.s for EWSCO with 4.69 epoxide groups per triglyceride at room temperature. At 40 °C, the viscosity of EWSCO decreased to 213 mPa.s. Kinematic viscosity of EWSCO and EWSCOME obtained at different temperatures is shown in Figure 5.12.

5.1.1.2. Viscosity Behaviour of Methyl Esters Epoxides

The rheological behaviour of EWSCOME samples studied at various

temperatures is shown in Figure 5.3 and Figure 5.5 to 5.11. An important observation to note is that rheological behaviour is almost similar for EWSCOME and EWSCO. Shear stress versus shear rate plot of EWSCOME is shown in Figure 5.3 for all the temperature ranges and indicates that shear stress gradually decreased with an increase in temperature. Similar to EWSCO, for this sample (EWSCOME) also, the viscosity increased monotonically from approximately 3.6 mPa.s for WSCOME to as high as 16.0 mPa.s for EWSCOME with 4.8 epoxide groups per triglyceride at room temperature. At 40 °C, the viscosity of EWSCOME decreased to 9.4 mPa.s. All the flow properties like k, k_{exp} and n are also evaluated for mineral diesel fuel and reported in Table 5.3 which indicates that EWSCO had higher viscosity than EWSCOME and showed significant deviation from the mineral diesel.

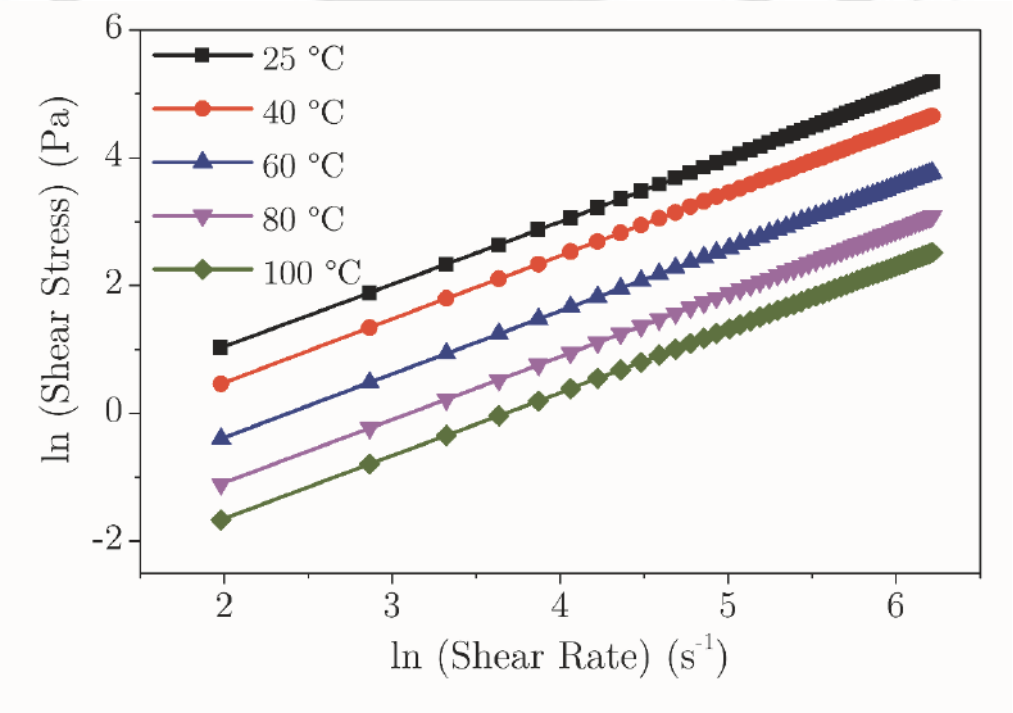

Figure 5.4. Logarithmic plot of shear stress vs shear rate for EWSCO.

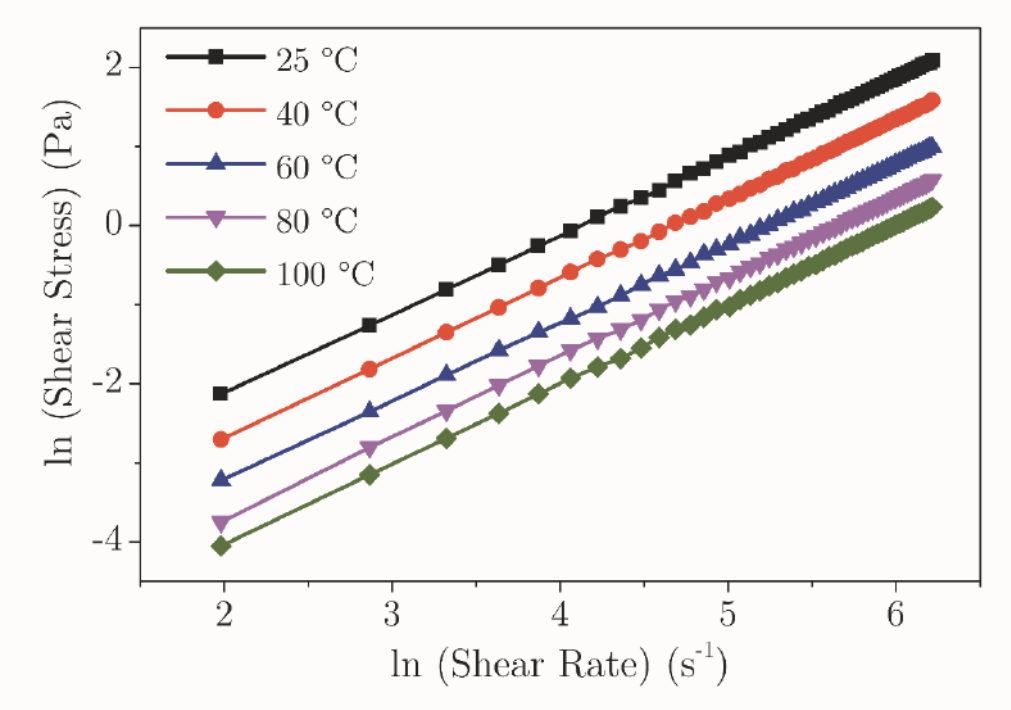

Figure 5.5. Logarithmic plot of shear stress vs shear rate for EWSCOME.

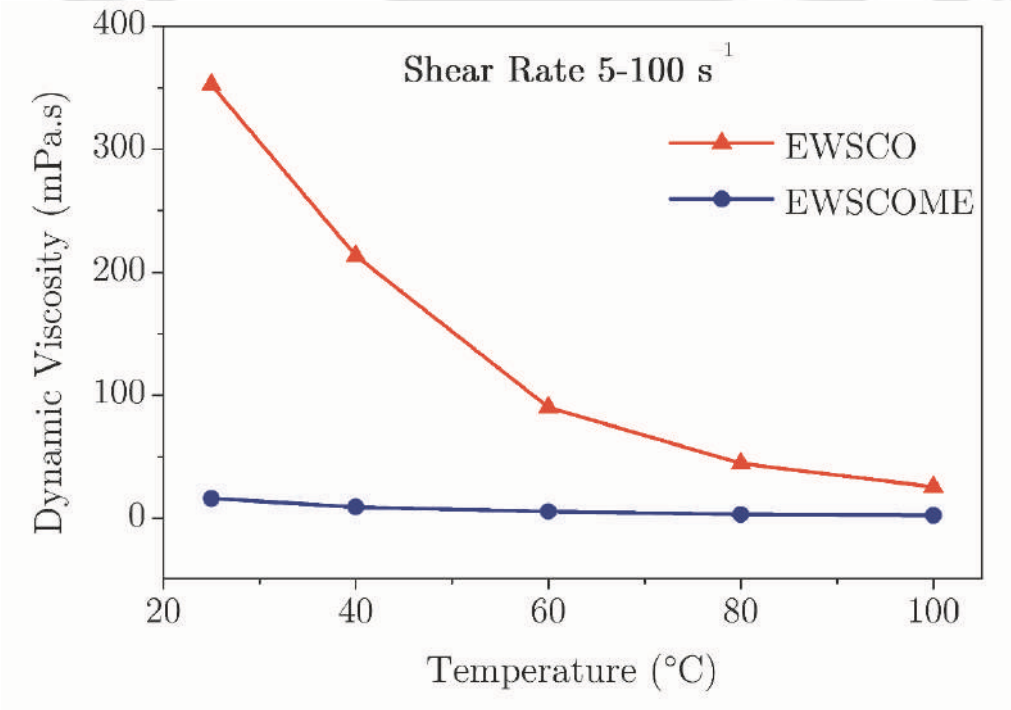

Figure 5.6. Viscosity vs Temperature plot for EWSCO and EWSCOME (Shear rate range 5–100 s^{-1}).

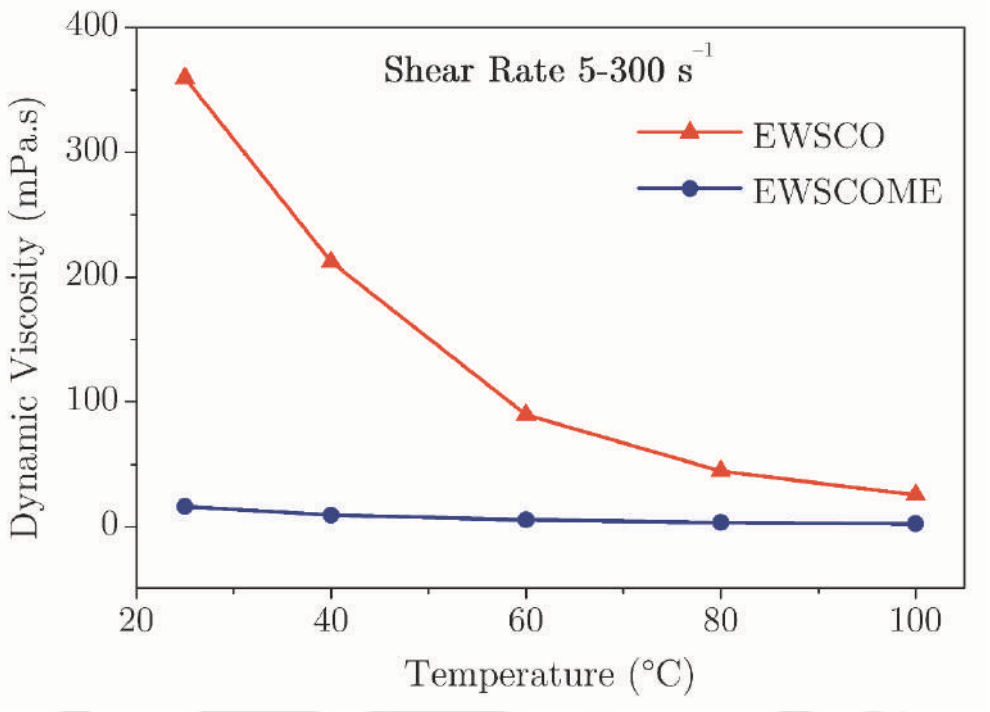

Figure 5.7. Viscosity vs temperature plot for EWSCO and EWSCOME (Shear rate range 5–300 s^{-1}).

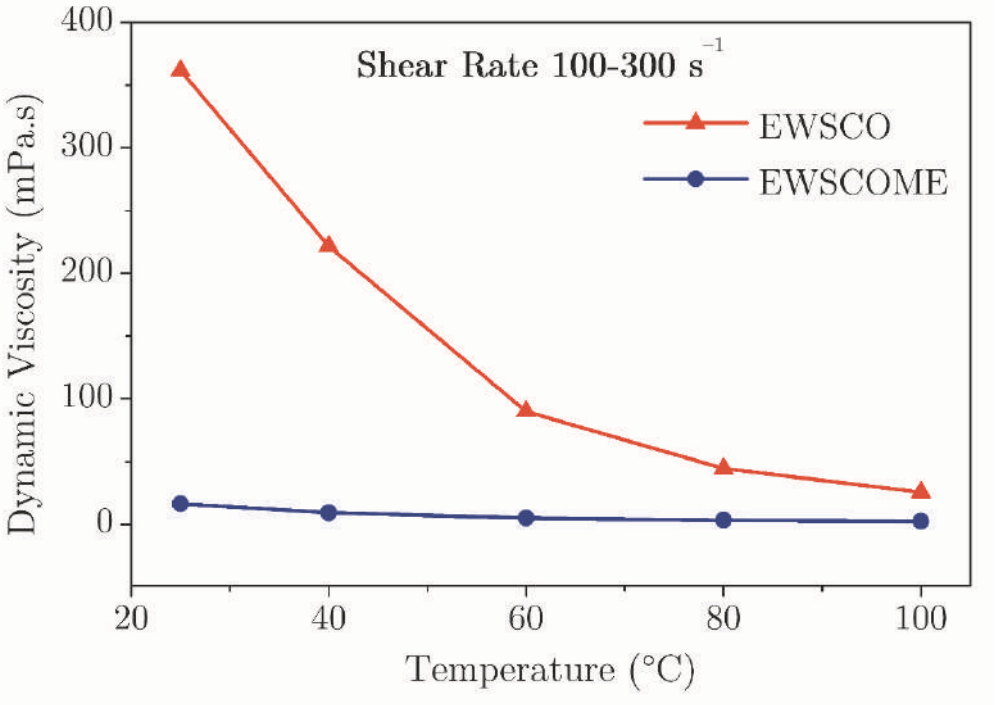

Figure 5.8. Viscosity vs temperature plot for EWSCO and EWSCOME (Shear rate range 100–300 s^{-1}).

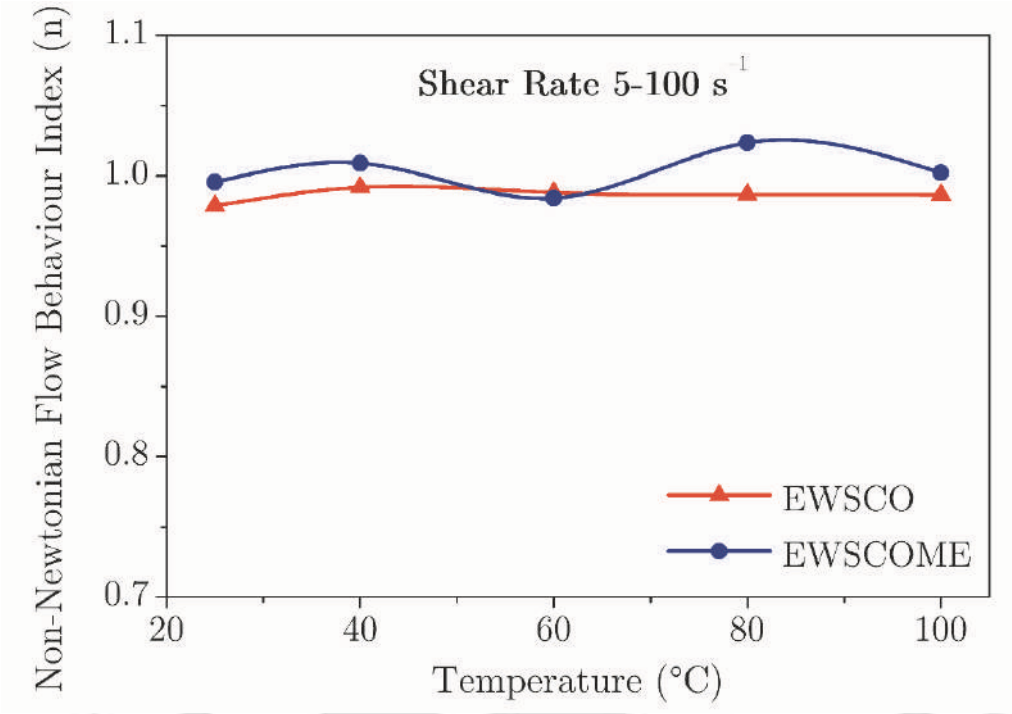

Figure 5.9. Non-Newtonian flow behaviour index plot for epoxides samples (Shear rate range 5–100 s^{-1}).

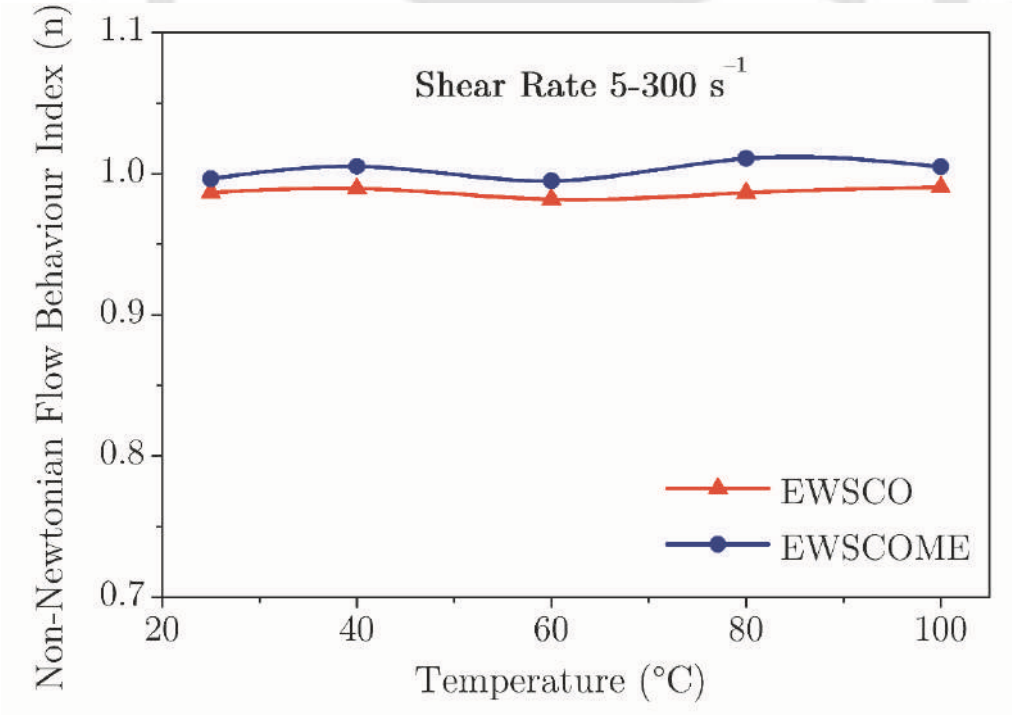

Figure 5.10. Non-Newtonian flow behaviour index plot for epoxides samples (Shear rate range 5–300 s^{-1}).

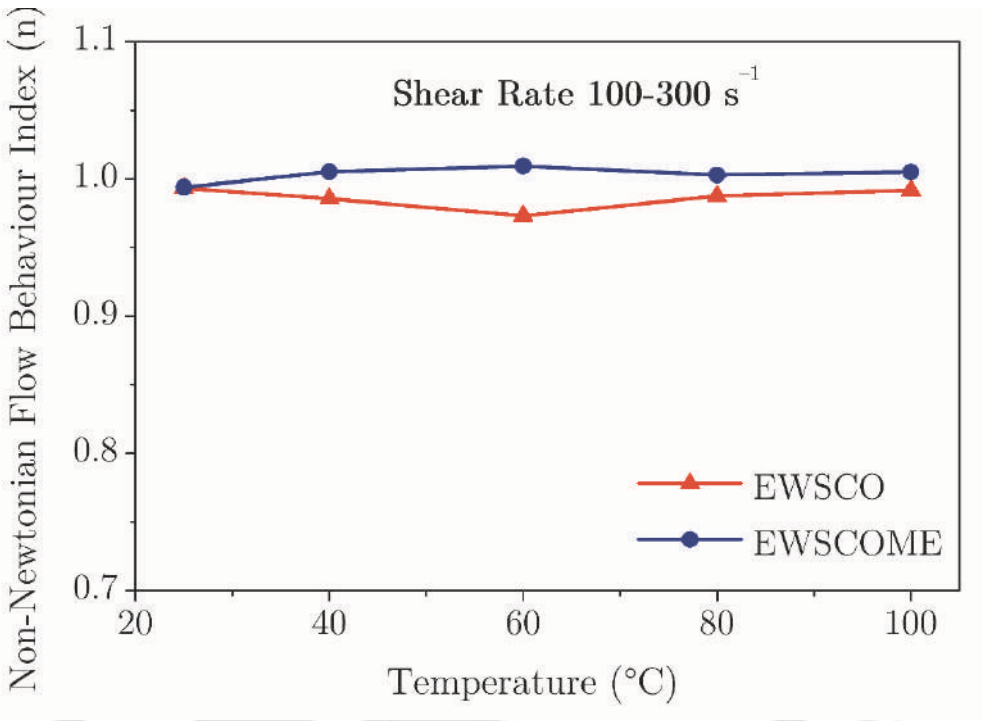

Figure 5.11. Non-Newtonian flow behaviour index plot for epoxide samples (Shear rate range 100–300 s^{-1}).

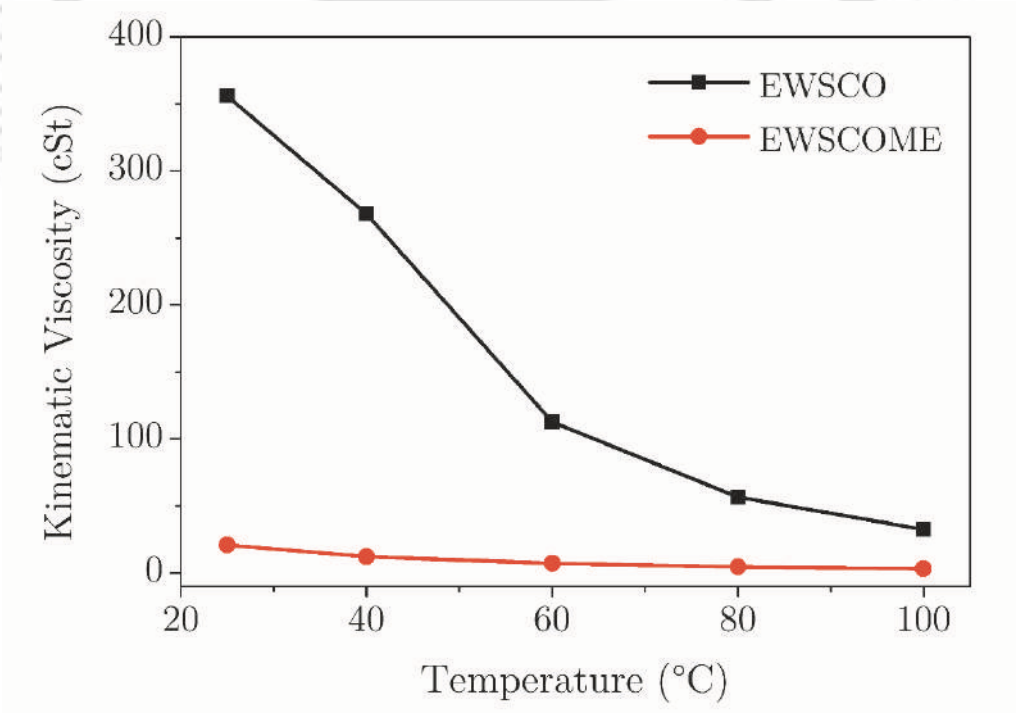

Figure 5.12. Temperature vs kinematic viscosity plot of EWSCO and EWSCOME.

5.1.2. Applications of EWSCO and EWSCOME

Practical applications of the prepared epoxidised waste soybean cooking oil and epoxidised waste soybean cooking oil methyl esters were identified by relative comparison of the viscosity index with the ISO vegetable grade (VG) lubricants. The viscosity index is one of the critical parameters to measure the change in viscosity with varying temperatures. From Table 5.4, it can be observed that the epoxidised waste cooking oil and epoxidised waste cooking oil methyl esters could complement up to ISO VG 220 and ISO VG 10 standards based on the mid-range of the viscosity values relative to the ISO VG standards. Viscosity index (VI) for EWSCO and EWSCOME was found to be 164 and 151, respectively, which were in the range of standard lubricant requirements (McNutt and He, 2016). Hernández-Sierra et al. (2019) studied friction and wear for natural oil with synthetic esters; these lubricants showed lowest friction with moderate viscosity index. Further, it was also observed that the high viscosity and high pressure-viscosity coefficient exhibited the thickest lubricating film. Bio-lubricants derived from vegetable oils have better lubrication and anti-wear capacities relative to other hybrid lubricants (metal-ceramic) in mechanical systems. Those characteristics indicate that the prepared lubricants do not have any technical deficiencies for engineering applications, and that makes vegetable oil derived lubricants a good choice for the manufacture of green lubricants. If high-viscosity lubricating oils are desired, the prepared lubricants can be tailored by blending with additives to boost viscosity for engine, automotive and industrial gear applications (García-Zapateiro et al., 2013). From the comparative analysis of VI, it appears that these values are in accordance with other plant/vegetable oil derived bio-lubricants, like epoxidised fatty acid waste cooking oil methyl esters (157) (McNutt and He, 2016), ring opened epoxidised soybean oil (137–149) (Hwang and Erhan, 2006), methyl ester of 9,10-palmitoyloxy-acetoxy stearic acid (171), methyl esters of 9,10-lauroyloxy-capronoyloxy stearic acid (137) (Kleinová et al., 2008), etc.

Table 5.4. Relative comparison of the viscosity for the prepared bio-lubricants with ISO VG lubricants ("The DIN 51519 Table," n.d.).

ISO Viscosity	Viscosity at 40 °C (cSt)	Viscosity limits (cSt)		Viscosity Index (McNutt and He, 2016)
	Mid-range	Minimum	Maximum	
Epoxidised Waste Soybean Cooking Oil (Present Study)	267.9	248.6	281.4	164.9
Epoxidised Waste Soybean Cooking Oil Methyl Esters (Present Study)	12.1	10.4	13.8	151.9
ISO VG 2	2.2	1.98	2.42	—
ISO VG 3	3.2	2.88	3.52	—
ISO VG 5	4.6	4.14	4.06	—
ISO VG 7	6.8	6.12	7.48	—
ISO VG 10	10	9.00	11	—
ISO VG 15	15	13.5	16.5	—
ISO VG 22	22	19.8	24.2	—
ISO VG 32	32	28.8	35.2	>90
ISO VG 46	46	41.4	50.6	>90
ISO VG 68	68	61.2	74.8	>198
ISO VG 100	100	90	110	>216
ISO VG 150	150	135	165	—
ISO VG 220	220	198	242	—
ISO VG 320	320	288	352	—
ISO VG 460	460	414	506	—
ISO VG 680	680	612	748	—
ISO VG 1000	1000	900	1100	—
ISO VG 2200	2200	1980	2420	—
ISO VG 3200	3200	2880	3520	—
2T engine oil#	45	—	—	105.4

#(Agrawal et al., 2017), — not available or not required

5.2. Comparison of Conventional and Bio-lubricant Base Stocks

Table 5.5 gives a comparative assessment of the thermo-oxidative stability of the collected conventional lubricants (Borugadda, 2015) with that of biodegradable lubricant base stocks. The thermo-oxidative stability of WSCO derivatives is substantially within the acceptable range of traditional hydraulic and transmission lubricants, according to a comparison of the thermos-oxidative stability of conventional lubricants with that of the produced bio-lubricant base stocks. This suggests that the produced bio-lubricant base stocks might be utilised as a possible replacement for traditional transmission and hydraulic lubricants.

Table 5.5. Comparison of thermo-oxidative stabilities of conventional and bio-lubricant base stocks.

Property	Conventional Lubricants (Borugadda, 2015)	Bio-lubricant Base Stocks (Current Study)
Thermal Stability (°C)	188 to 314	183 to 365
Oxidative Stability (°C)	180 to 320	198 to 325
Pour Point (°C)	(-24) to (-1)	(-7.8) to (2.6)

5.3. Summary

This chapter highlights the physico-chemical properties and rheological behaviour of EWSCO and EWSCOME. The study reveals that the viscosity of epoxides increased as a result of the chemical modifications due to increased intermolecular interactions among the molecules. The epoxides are considerably more polar and, as a result, had a significantly higher viscosity. Temperature is found to have moderate effect on the viscosities of EWSCO and EWSCOME. The power law model has been applied to model the rheological behaviour, and shows that both the epoxides lie in the Newtonian region, as values of n are nearly equal to 1. EWSCO and EWSCOME showed a favourable viscosity index (164 and 151, respectively) for lubricant requirements, and they could complement ISO VG 10 (for EWSCOME) and ISO VG 220 (for EWSCO) lubricant standards.

CHAPTER VI

Studies on Degradation Kinetics of Waste Soybean Cooking Oil Epoxides (EWSCO) and Waste Soybean Cooking Oil Methyl Esters Epoxides (EWSCOME)

Kinetics Analysis for WSCO and WSCOME

Kinetics Analysis for EWSCO and EWSCOME

Kinetics Model

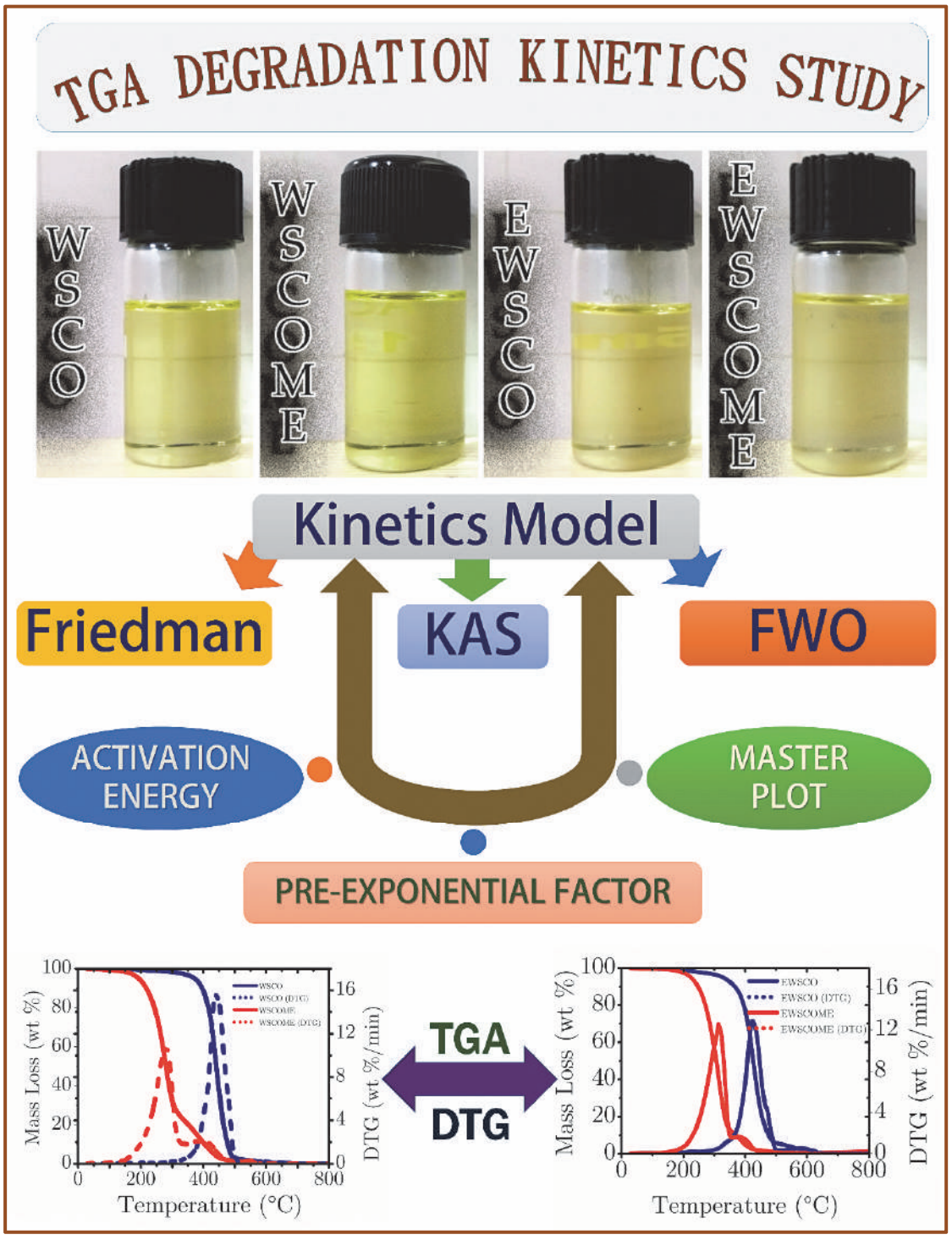

Graphical Abstract of Chapter VI

Chapter VI

Studies on Degradation Kinetics of Waste Soybean Cooking Oil Epoxides (EWSCO) and Waste Soybean Cooking Oil Methyl Esters Epoxides (EWSCOME)

In the present research, thermal characteristics and kinetics parameters of waste soybean cooking oil (WSCO), waste soybean cooking oil methyl esters (WSCOME), epoxides of waste soybean cooking oil (EWSCO), and epoxides of waste soybean cooking oil methyl esters (EWSCOME) were determined by thermogravimetry under non-isothermal heating conditions. A series of experiments was performed by increasing the temperature up to 800 °C at different heating rates of 10, 20, 30 and 50 °C/min, in an inert atmosphere of nitrogen. The mass loss curves showed that the degradation of the prepared bio-lubricant samples occurred mainly in the range of 200–500 °C, due to the breakage of the weak chemical bonds, leading to the formation of smaller molecules of volatile organic compounds and gaseous products. WSCO was found to be thermally stable up to 200 °C whereas biodiesel prepared from WSCO (i.e. WSCOME) was thermally stable up to 100 °C. This clearly indicated that WSCO was more stable compared to its methyl esters (WSCOME), while WSCOME was more stable as compared to petroleum diesel (T_o = 78 °C). It was also noticed that an increase in the heating rate caused a shift in the maximum rate loss to a higher temperature in all the samples. Three separate techniques, namely Friedman, Kissinger-Akahira-Sunose (KAS), and Flynn-Wall-Ozawa (FWO) methods, were used to determine the apparent activation energy (E) of

degradation of the prepared materials. Activation energy of WSCO, WSCOME, EWSCO, and EWSCOME as determined by the above mentioned methods were found to be 171, 51, 140, and 86 kJ/mol, respectively. The analyses of the process mechanism by the methods of Criado and Coats-Redfern showed that the most probable model for the degradation of EWSCO agrees with the phase boundary controlled (contracting volume) (R3) model, and the thermal degradation process of EWSCOME responds to a mechanism involving phase boundary controlled (contracting area) (R2) model. In addition, the results also indicated that structural modification of WSCO affected the kinetics and mechanism of bio-lubricant synthesis as well.

6.1. Physico-chemical Properties of WSCO, WSCOME and its Epoxides

Fatty acid composition of WSCO methyl esters was analysed—the saturated fatty acid (FA) content was found to be 18.27 wt %. The rest of the fatty acids were unsaturated which is responsible for lower thermal stability. Detailed discussion on physico-chemical properties is given in Chapter 3 and 4.

6.2. Thermogravimetric and Kinetics Analysis for Thermal Degradation of WSCO and WSCOME

Thermal stability of WSCO and WSCOME was determined at different heating rates under nitrogen atmosphere using thermogravimetric analysis as shown in Figure 6.1. Thermogravimetry (TG) and derivative thermogravimetric (DTG) curves of WSCO and WSCOME show a distinct thermal degradation pattern. In the thermal degradation of WSCO, only one degradation step was observed in

the range of 360–660 °C at heating rates of 10 to 50 °C/min (Figure 6.2). Similar observations were made through literature for the degradation of oil and biodiesel from other sources such as corn, rapeseed, jatropha, peanut, and coffee (Dantas et al., 2007b; Li et al., 2015; Todaka et al., 2013). On heating the samples in nitrogen environment, the weak chemical bonds gradually break to form smaller molecules of volatile organic compounds and gaseous products. As shown in Table 6.1, T_o is the onset temperature of thermal degradation at which a deflection from the baseline of the first derivative of the thermogravimetric (DTG) curve is first observed (it was calculated as per the guidelines from ASTM standard test method E2550–17). WSCO was thermally stable up to 200 °C whereas biodiesel prepared from WSCO (i.e. WSCOME) was stable up to 100 °C. This indicates that WSCO was thermally more stable as compared to its methyl ester WSCOME, and WSCOME was more stable as compared to petroleum diesel (T_o = 78 °C). This behaviour can be explained due to the fact that WSCO contains fatty acid and triglyceride compounds of more thermal stability, higher boiling point, and higher molecular mass, whereas WSCOME consists of smaller molecules of fatty acid methyl esters which have lower boiling point. Thermal stability of WSCOME was found to be higher compared to petroleum diesel fuel (T_o = 78 °C) due to the higher viscosity and intermolecular forces in WSCOME (Shancita et al., 2016). Also, it was evident from the bond dissociation energies (BDEs) derived from a multi reference (MR) method that C(O)−O bond of ester group was the strongest bond in WSCOME and C=C double bonds in its alkyl chains provide more strength to the bonds adjacent to double bond by restricting the rotation of hydrogen bonds (Oyeyemi et al., 2014). T_i was the temperature at the initiation of mass change peak, which has been considered for the calculation of TGA kinetics data of thermal degradation step (it was calculated

as per the guidelines from ASTM standard test method E1641–18). The initiation temperature of the degradation for WSCO and WSCOME was 365 °C and 179 °C, respectively, at which 4.4 % and 3.2 % mass were degraded at the degradation rate of 1 wt %/min. For WSCO sample, a single mass loss peak was observed with DTG on heating from temperature 365 °C to 662 °C at 10 °C/min of heating rate. This peak revealed about 96% of mass loss with maximum degradation rate of 16 wt %/min at a peak temperature of 435 °C. The initial degradation temperature of diesel fuel determined by Shancita et al. (Shancita et al., 2016) was 129 °C which was lower than WSCOME degradation temperature.

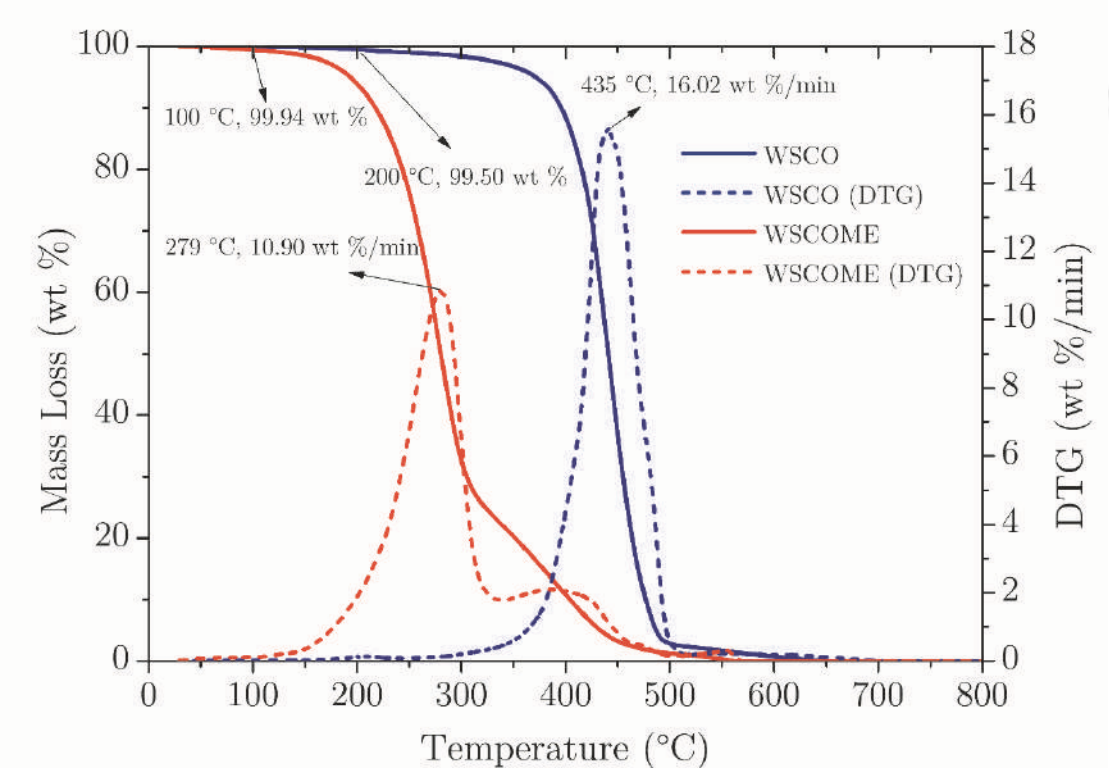

Figure 6.1. TG and DTG plots of WSCO and WSCOME at heating rate of 10 °C/min.

The change in heating rate affects the lateral shift of TG curves and the position of peaks of DTG curves, as shown in Figure 6.2. For WSCO sample, by increasing

the heating rate from 10–50 °C/min, peak temperature shifts from 436–486 °C, and the rate of degradation increases from 16–50 wt %/min. Similar thermal behaviours were observed for WSCOME sample. With increasing heating rate, the sample experiences shorter heating time than the particle conversion time. Due to these heat transfer limitations, the degradation curves and peaks show a lateral shift towards higher temperature. This behaviour is in consistence with the observations made by authors (Di Blasi, 1996; Kim et al., 2010). The extent of degradation (% weight loss) increased with an increase in the heating rate, as at higher heating rate more amount of thermal energy is available for the conversion. Subsequently, the rate of degradation also increases with an increased heating rate (Kim et al., 2010). The effect of change of heating rates was significantly lower for WSCO sample as compared to WSCOME, depicting more stability of WSCO sample in the range of 350–550 °C. It should be noted that more amount of energy is required for the degradation of stable compounds.

The chemical kinetics analysis of degradation process was carried out using the results obtained from TGA to determine the kinetics parameters, i.e. activation energy (E), pre-exponential factor (A), and degradation mechanism $(f(\alpha))$. Apparent activation energy which is required to initiate the thermochemical conversion of the sample signifies that the conversion is faster if activation energy is lower for a given value of pre-exponential factor. As activation energy is highly dependent on the conversion, the distribution of E versus α is calculated at 10 data points using isoconversional methods at heating rates 10–50 °C/min, and represented in Table 6.4a / Figure 6.5. For WSCO sample, the values of E calculated using both the isoconversional methods were distributed in the range 145 to 195 kJ/mol representing similar pattern and stability with conversion. Values of E are smaller and lie in the range 145–158 kJ/mol at $\alpha = 0 - 0.5$, and

beyond $\alpha = 0.6$, increase substantially as 165–195 kJ/mol. At lower conversion rates, the activation energies have a lower value. This demonstrates that the WSCO sample transforms more easily when the conversion rate is low. Energy required for degradation increased at higher values of conversion, which can be attributed to the formation of thermally more stable chemical composition or to refractory residual material at higher α demanding supply of more energy for further degradation (Vyazovkin et al., 2011).

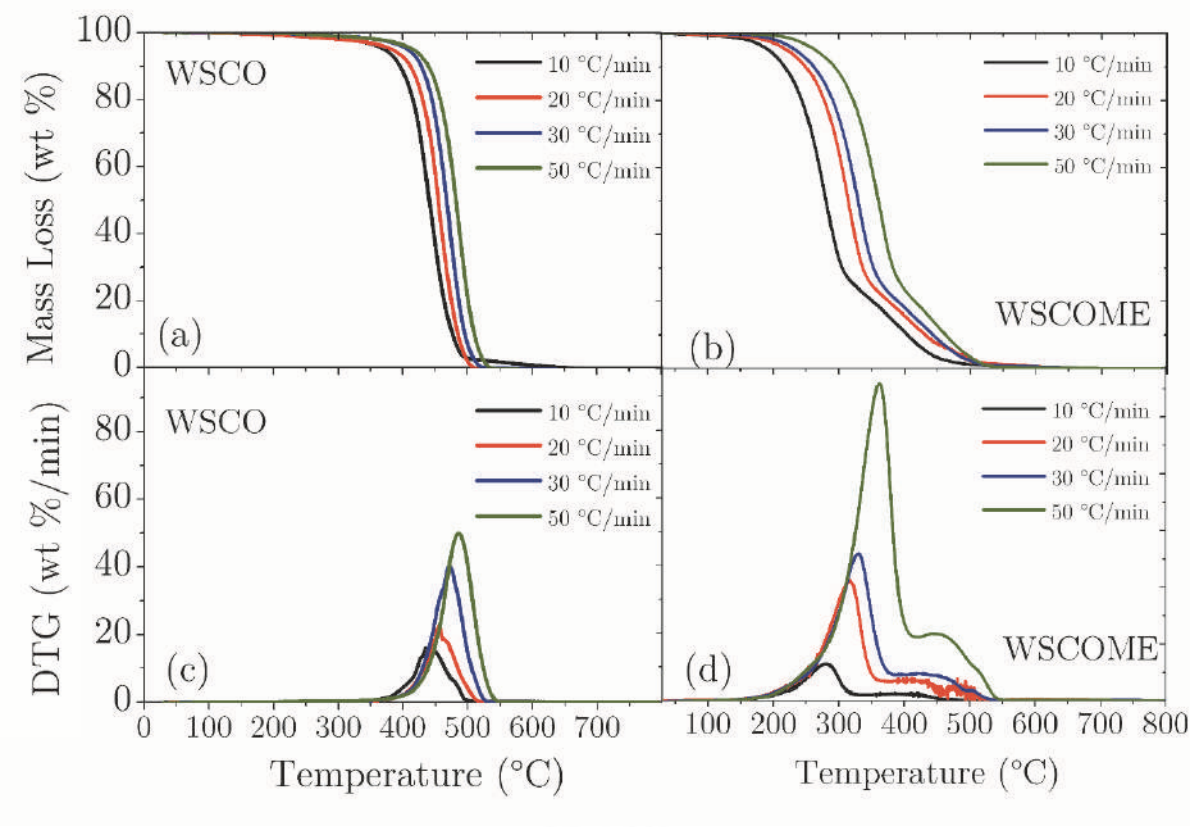

Figure 6.2. TG and DTG plot at different heating rates: (a) WSCO, (b) WSCOME.

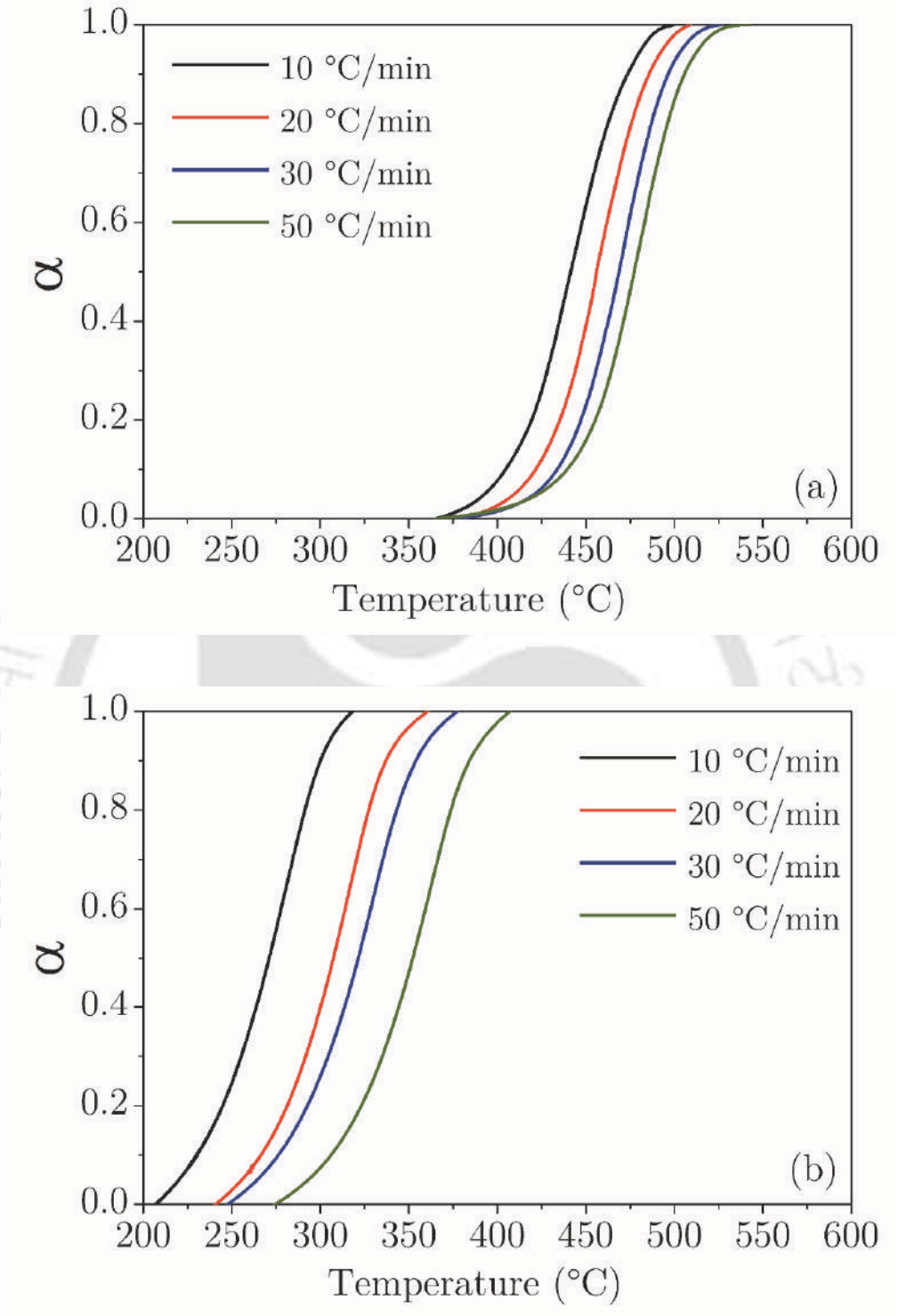

Figure 6.3. α vs T curves for the thermal decomposition of (a) WSCO, (b) WSCOME.

Table 6.1. Thermal degradation analysis of WSCO and WSCOME samples.

Sample	Heating Rate (°C/min)	Onset Temperature T_o (°C)	Degradation Initiation Temperature T_i (°C)	Degradation Offset Temperature T_f (°C)	Maximum Degradation Temperature T_p (°C)	Mass Loss (wt %)	Rate of Mass Loss $(dw/dt)_{max}$ (wt %/min)
WSCO	10	200.78	365.00	661.85	435.45	95.65	16.02
	20	210.12	379.11	636.89	455.20	95.37	22.40
	30	228.65	382.07	564.49	470.92	97.36	40.11
	50	240.88	395.92	551.70	485.65	97.55	49.91
WSCOME	10	100.35	183.45	458.24	279.27	94.01	10.90
	20	115.93	206.47	527.14	317.22	97.07	35.26
	30	129.86	218.35	529.68	329.21	98.32	42.85
	50	155.74	240.59	546.98	361.65	99.30	93.88

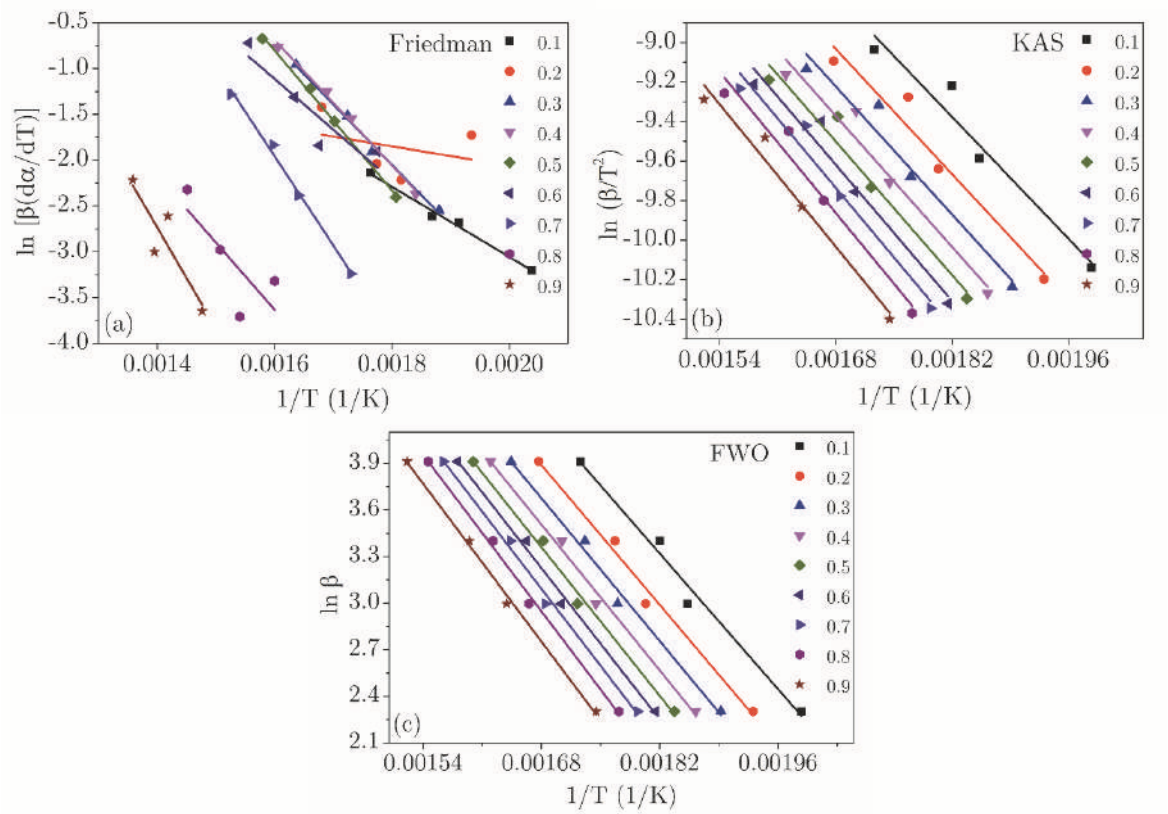

Figure 6.4. R-squared correlation for determination of activation energy by (a) Friedman, (b) KAS, and (c) FWO methods for WSCOME.

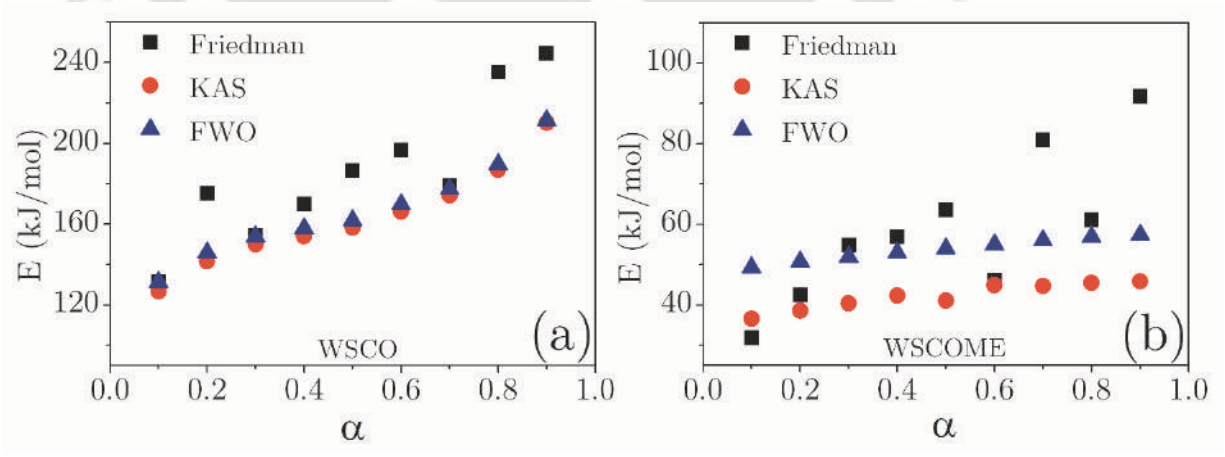

Figure 6.5. Values of the activation energy determined using Friedman, KAS and FWO methods for the thermal decomposition of (a) WSCO and (b) WSCOME.

Further, to comprehend the information of thermal degradation mechanism of the samples, it is required to determine the mathematical model to fit the experimental data. Criado master plot method was followed for the determination of mathematical model of degradation. From Figure 6.6, it can be seen that sigmoidal models are applicable for this data (Vyazovkin et al., 2011). Vyazovkin et al. (Vyazovkin et al., 2001) illustrated that the thermal degradation of liquid compounds can be demonstrated using reaction models such as first-order reaction model (F1), autocatalytic models (A1, A2, A3), and contracting geometry models (R2, R3). Experimental master plot curve was constructed using activation energy calculated from isoconversional methods as presented in Figure 6.6, and was compared with graphs of theoretical master plots (Table 6.3). The master plot revealed that first-order reaction model (F1) and Avrami-Erofeyev model showed a best agreement to experimental data. Avrami-Erofeyev model represents a nucleation and nuclei growth mechanism through the ingestion or coalescence of product nuclei (Khawam and Flanagan, 2006). This mechanism of nucleation and nuclei growth is not consistent with the degradation of WSCO as the compound is being completely vanished after the degradation cycle, whereas first-order reaction model (F1) is more promising as its applicability is evident in the homogeneous liquid-phase kinetics, which represents thermal decomposition of the liquid reactant to form volatiles or gaseous products $A_l \rightarrow C_g$. Therefore, the thermal degradation of WSCO can be corroborated using F1 kinetics model. The pre-exponential factor determined from the knowledge of activation energies and the thermal degradation model are represented in Figure 6.7.

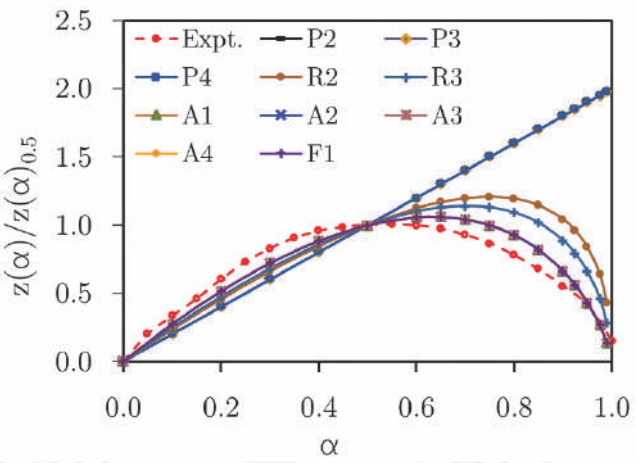

Figure 6.6. Estimating thermal decomposition mechanism of WSCO using Criado master plot method (representative plot).

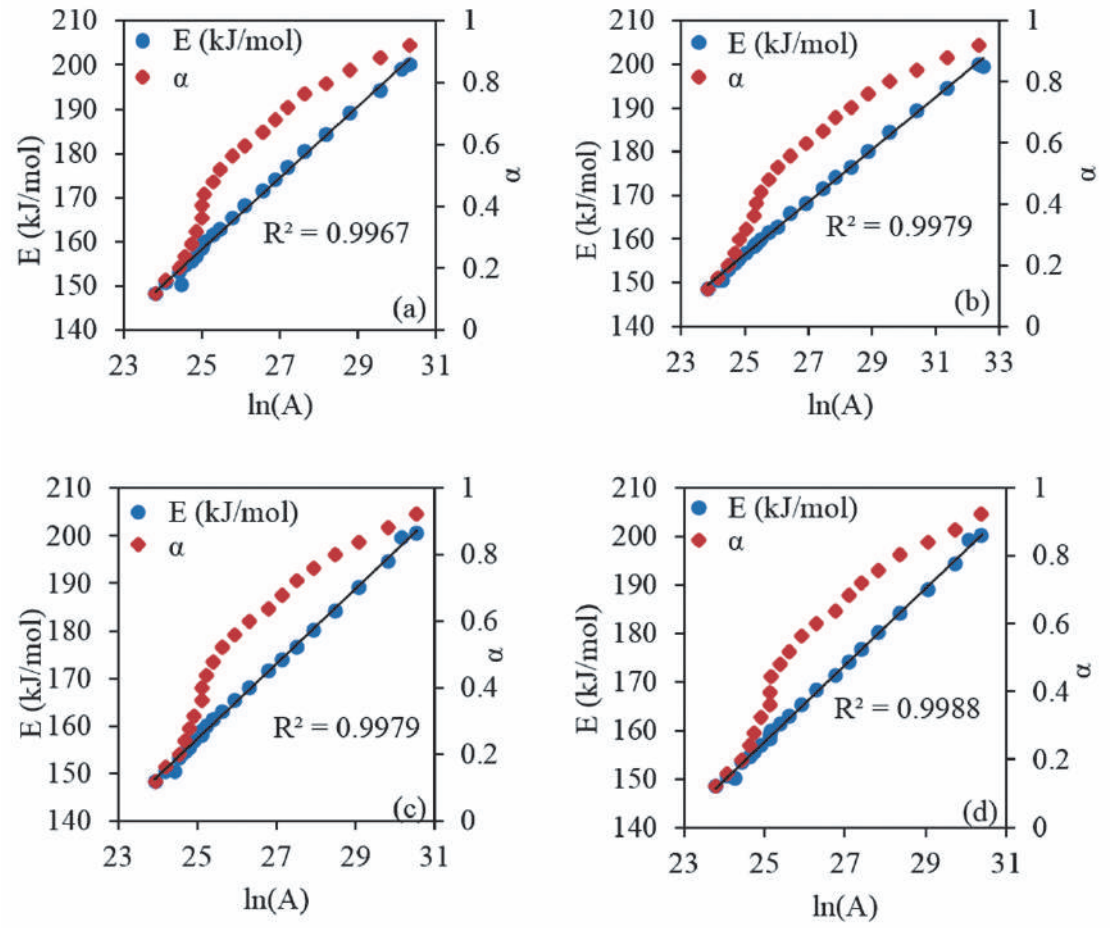

Figure 6.7. Pre-exponential factor as a function of activation energy and conversion for the thermal decomposition of WSCO determined using FWO at heating rates (a) 10 °C/min, (b) 20 °C/min, (c) 30 °C/min and (d) 50 °C/min (representative plot).

6.3. Thermogravimetric and Kinetics Analysis of Thermal Degradation of EWSCO and EWSCOME

Thermogravimetric analysis (TGA) was used to study the thermal stability and degradation mechanism of the prepared epoxides (EWSCO and EWSCOME). Thermal stability of epoxide was determined by thermogravimetric analysis (TGA) technique in an inert (N_2) atmosphere. As observed in Figure 6.8 (TGA and DTG) and Table 6.2, with an increased heating rate, the maximum degradation temperature (T_p) of all the samples shifts towards a higher temperature. This behaviour can be attributed to the heat and mass transfer limit in the sample, which lead to a difference in temperature between the sample and the reference (causing the actual temperature of the sample to become lower than the reference (i.e., furnace) temperature upon a higher heating rate) (Ferdosian et al., 2016).

The thermal decomposition of EWSCO sample (Figure 6.8) exhibited a single decomposition step in the range of 326–500 °C with the maximum rate of decomposition at around 423 °C depending on the heating rate of 10 °C/min, and observed a small shoulder at a higher temperature. With increased heating rates, the T_p increased in the range of 423–479 °C. The decomposition trend of epoxide was in a good agreement with that reported in literature (Ferdosian et al., 2016). The thermal decomposition of EWSCOME sample (Figure 6.8) exhibited a single step decomposition in the range of 170–410 °C with the maximum rate of decomposition at around 317 °C depending on the heating rate of 10 °C/min, and observed a small shoulder at a higher temperature. With increased heating rates, the T_p increased in the range of 317–364 °C.

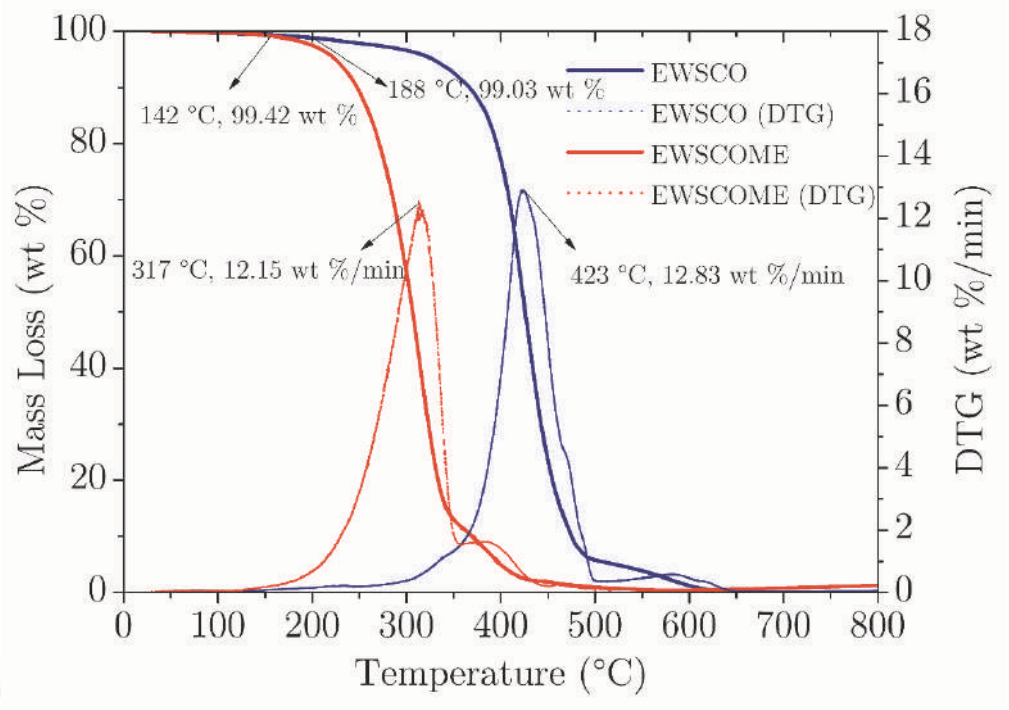

Figure 6.8. TG and DTG plots of EWSCO and EWSCOME at heating rate of 10 °C/min.

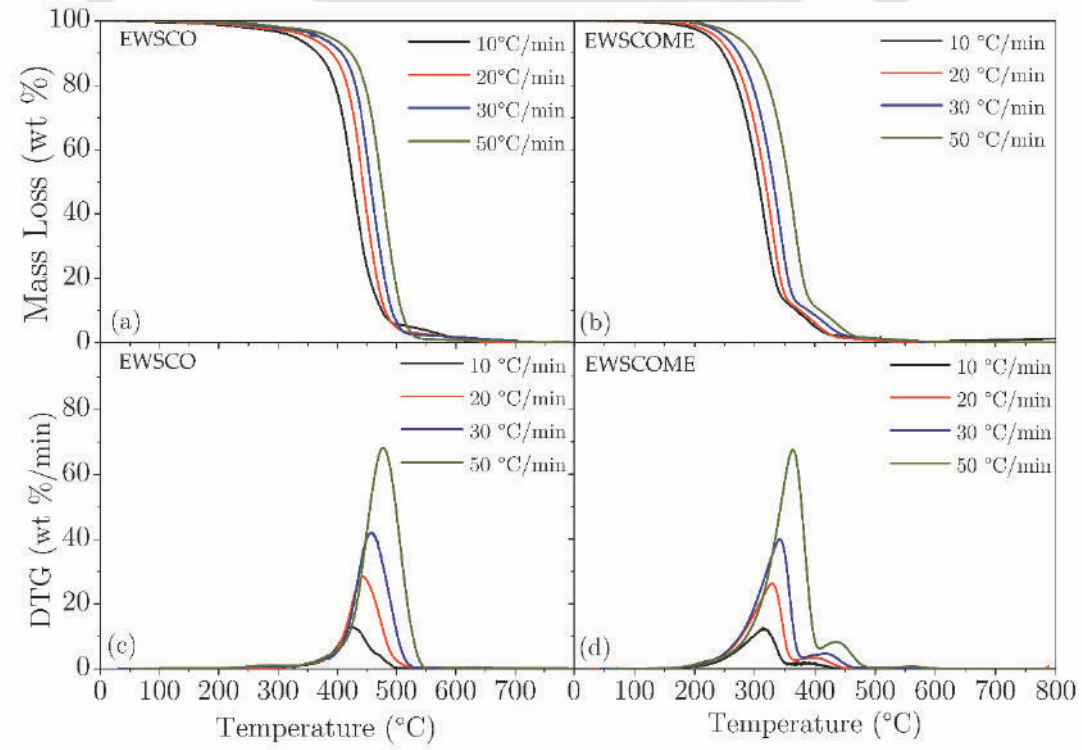

Figure 6.9. TG and DTG plots of (a) EWSCO and (b) EWSCOME; and DTG Plot of (c) EWSCO and (d) EWSCOME.

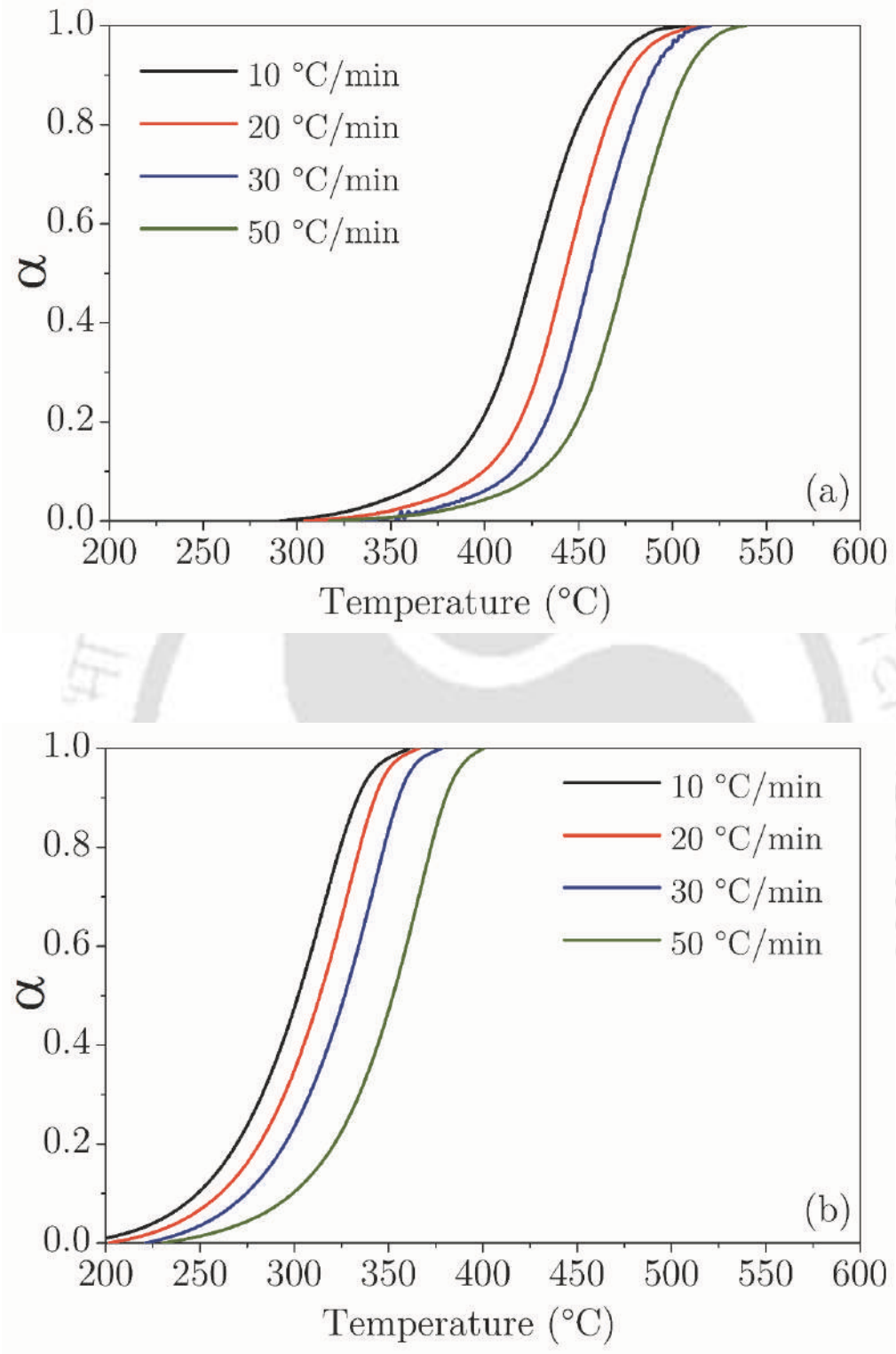

Figure 6.10. *α vs T* curves for the thermal decomposition of (a) EWSCO, (b) EWSCOME.

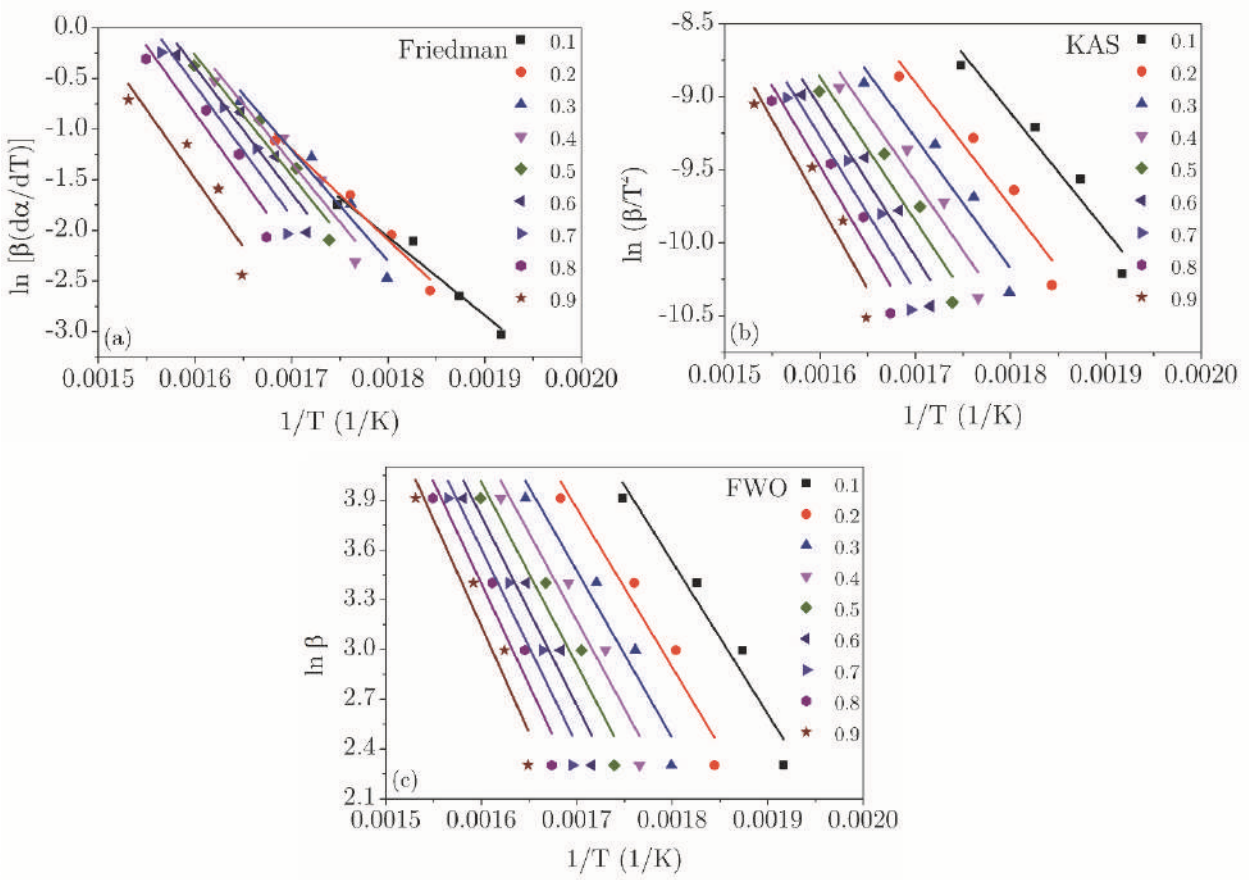

Figure 6.11. R-squared correlation for determination of activation energy by (a) Friedman, (b) KAS and (c) FWO methods for EWSCOME.

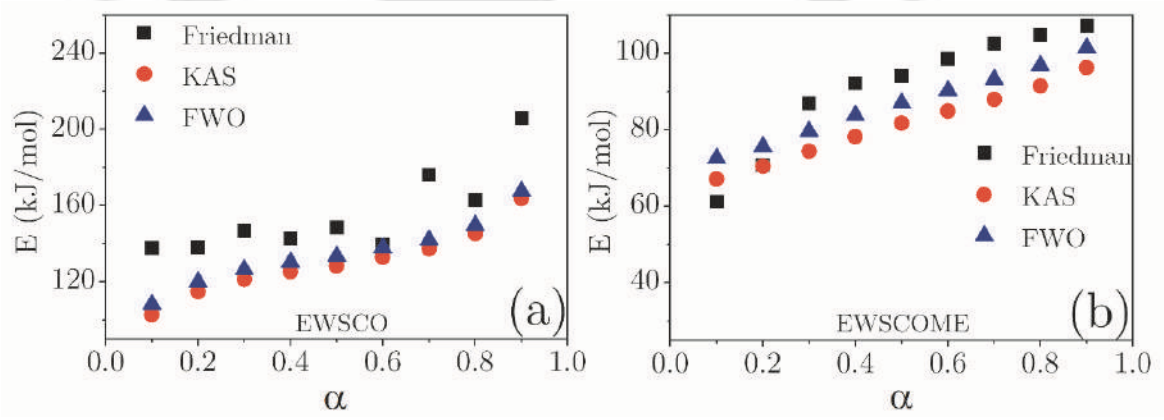

Figure 6.12. Values of the activation energy determined using Friedman, KAS and FWO methods for the thermal decomposition of (a) EWSCO and (b) EWSCOME

Table 6.2. TGA and DTG analysis of (a) EWSCO, (b) EWSCOME.

Sample	Heating Rate (°C/min)	Onset Temperature T_o (°C)	Degradation Initiation Temperature T_i (°C)	Degradation Offset Temperature T_f (°C)	Maximum Degradation Temperature T_p (°C)	Mass Loss (wt %)	Rate of Mass Loss $(dw/dt)_{max}$ (wt %/min)
EWSCO	10	188.75	338.45	498.52	423.43	89.30	12.83
	20	206.44	349.19	523.45	440.37	93.40	28.60
	30	238.41	378.94	530.17	459.49	94.83	41.82
	50	251.84	398.47	556.59	478.98	96.64	68.17
EWSCOME	10	142.49	204.65	355.64	317.91	87.12	12.15
	20	153.41	228.18	367.18	331.34	87.03	25.96
	30	158.95	239.74	379.53	343.21	87.04	39.80
	50	169.47	250.85	408.17	363.19	87.08	67.56

Activation energy (E) of the thermal decomposition process can be used as a criterion for comparing the thermal stability of prepared epoxides (Ferdosian et al., 2016). In order to investigate the thermal stability of EWSCO and EWSCOME, the activation energy was determined on the basis of three different model free kinetics, namely Friedman, KAS, and FWO methods (Table 6.3b).

Several authors (Borugadda and Goud, 2014a) reported that plant oil esters with saturated fatty acids and mono un-saturation content have a positive influence and are thermally and oxidatively more stable than the esters with poly-unsaturation content. It was observed that EWSCO had higher activation energy than EWSCOME. The highest activation energy (155 kJ/mol) was obtained for EWSCO. Thus, based on the overall activation energy, EWSCO was found to be thermally more stable. Zaher et al. (Zaher et al., 1989) reported activation energy (E) for commercial epoxidised soybean oil as 66 kJ/mol and 76 kJ/mol. However, the decomposition of both epoxides samples is a very complex process with multiple reactions taking place simultaneously. Therefore, a single activation energy is unable to explain the entire process, and it would be better to use isoconversional methods to calculate the activation energy as a function of conversion.

Generally, an Arrhenius plot with a steeper slope yielded high activation energy of the transesterification/epoxidation reaction whereas a flat slope implied a low E. It is also understood that over the same temperature range, such reactions with higher E change more rapidly and are highly dependent on temperature as they are more sensitive to change of temperature (Pauline et al., 2021). On the other hand, reaction with a low E and a flat slope revealed that the rate of reaction remains unaffected over the range of temperature. However, because the

Arrhenius equation is typically relevant to gas phase systems, all of the numbers found and the discussion that followed should be examined with caution (Salmasi et al., 2020). R-squared correlation for determination of activation energy plots by KAS and FWO for the EWSCOME are shown in Figure 6.11. Parallel straight lines are observed at different conversions for the sample. The parallel lines observed in each conversion ranging from $\alpha = 0.1$ to 0.9 for every sample indicate the suitability of the FWO model to the present system. The calculated activation energy (E) values are tabulated in Table 6.3b. The activation energy was increasing gradually with increasing α, which indicates the less energy requirement to break bond at initial level of conversions. Also, similar activation energy indicates the breakage of similar type of bonds. With the increase in the conversion rate, the mass fraction and the activity of reactants decreased while the apparent activation energy increased, and the apparent activation energy curve tend to be stable (Liu et al., 2020).

The apparent activation energy calculated by the FWO method was slightly higher than that calculated by the KAS method. The apparent activation energy was affected by the slope of linear fitting (x, y). The values of x and y went up with increased heating rates. At the same conversion rates, $x\,(-1/T)$ for KAS and FWO and the values of Δx are the same. When Δx is the same, the slope of linear fitting is decided by Δy. $y\,[\ln(\beta/T^2)]$ for KAS and $y\,(\ln\beta)$ for FWO are different. T is much larger than β, so the value of β/T^2 and the value of $\Delta\beta/T^2$ are small. The value of Δy for KAS was smaller than that for FWO, which causes the slope of KAS to be smaller than that of FWO and further affects the apparent activation energy for KAS and FWO.

The average apparent activation energies of EWSCO and EWSCOME calculated by the FWO method were 135 kJ/mol and 86 kJ/mol, while those calculated by the KAS method were 130 kJ/mol and 81 kJ/mol, respectively. After $\alpha \geq 0.5$, an increase in activation energy was observed in EWSCO and EWSCOME. This indicated that the thermal decomposition of the prepared bio-lubricants follows a complex mechanism which may include random scission, depolymerisation, diffusion, inter- and intramolecular esterification, etc. (Fedunik-Hofman et al., 2019; Pauline et al., 2021; Pugazhendhi et al., 2020). A comparable investigation was conducted previously for transesterification reaction (Birla et al., 2012; Pugazhendhi et al., 2020; Salmasi et al., 2020).

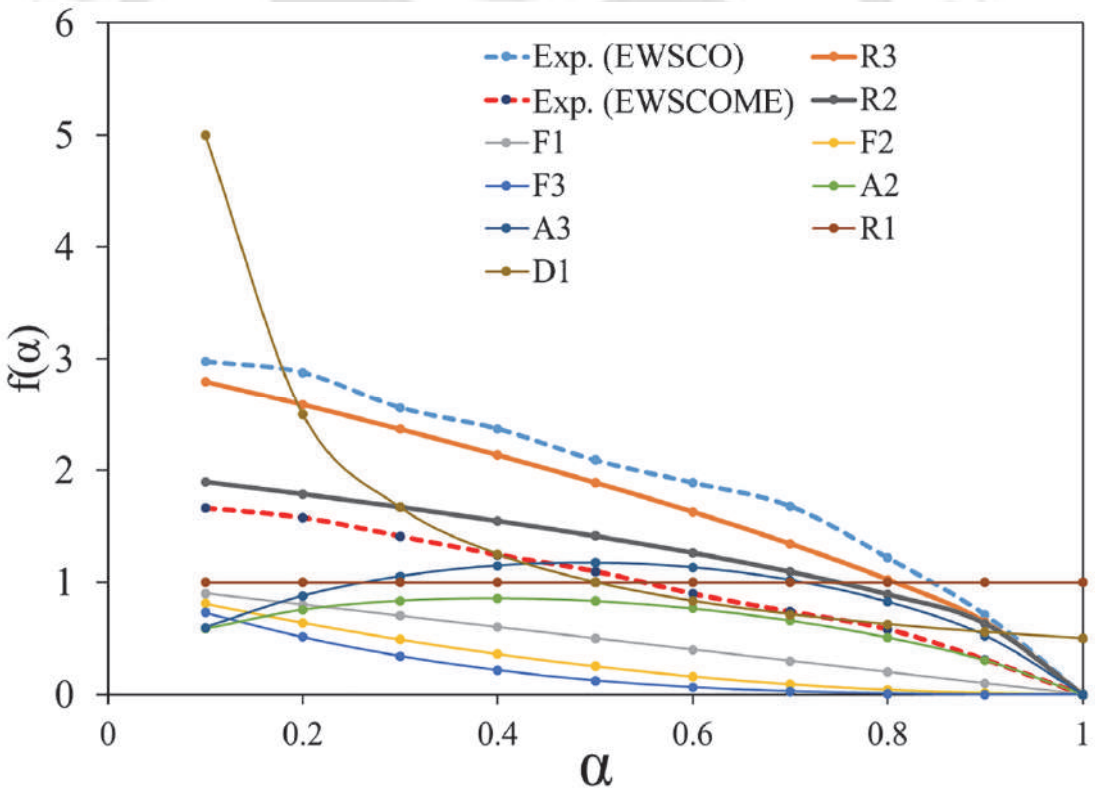

Figure 6.13. Master plot of model free methods.

Table 6.3a. Kinetics parameters determined from different models for samples (a) WSCO and (b) WSCOME.

Conversion	WSCO						WSCOME					
	Friedman		KAS		FWO		Friedman		KAS		FWO	
	E (kJ/mol)	R^2	*E* (kJ/mol)	R^2	*E* (kJ/mol)	R^2	*E* (kJ/mol)	R^2	*E* (kJ/mol)	R^2	*E* (kJ/mol)	R^2
0.1	131.33	0.9736	126.63	0.9833	131.29	0.9860	31.85	0.9896	36.53	0.9266	49.31	0.9771
0.2	175.37	0.9825	141.67	0.9932	145.88	0.9942	42.49	0.9954	38.60	0.9330	50.79	0.983
0.3	154.23	0.9866	149.98	0.9943	153.95	0.9951	54.86	0.9901	40.43	0.9389	51.89	0.9869
0.4	169.95	0.9778	154.02	0.9942	157.91	0.9950	56.90	0.9941	42.33	0.9433	52.99	0.9893
0.5	186.62	0.9835	158.22	0.9907	161.99	0.9921	63.55	0.9937	41.10	0.9445	54.00	0.9905
0.6	196.65	0.9799	166.26	0.9882	169.75	0.9898	46.06	0.8397	44.90	0.9454	54.99	0.9917
0.7	179.05	0.9990	174.27	0.9839	177.47	0.9860	80.96	0.9933	44.72	0.9463	56.00	0.9926
0.8	235.25	0.9744	186.82	0.9832	189.52	0.9801	61.08	0.8475	45.42	0.9517	56.88	0.9943
0.9	244.37	0.9641	210.22	0.9854	211.39	0.9708	91.70	0.8741	45.83	0.9596	57.38	0.9954
Average	185.87	0.9802	163.12	0.9885	166.57	0.9877	58.83	0.9464	42.21	0.9432	53.80	0.989

Table 6.3b. Kinetics parameters determined from different models for samples (a) EWSCO and (b) EWSCOME.

Conversion	EWSCO						EWSCOME					
	Friedman		KAS		FWO		Friedman		KAS		FWO	
	E (kJ/mol)	R^2	*E* (kJ/mol)	R^2	*E* (kJ/mol)	R^2	*E* (kJ/mol)	R^2	*E* (kJ/mol)	R^2	*E* (kJ/mol)	R^2
0.1	137.76	0.9903	102.66	0.9913	108.13	0.9933	61.14	0.9845	67.14	0.9046	72.54	0.9296
0.2	138.12	0.9852	114.83	0.9992	120.11	0.9996	70.82	0.9475	70.45	0.9254	75.65	0.9343
0.3	146.74	0.9695	121.35	0.9975	126.52	0.9989	86.85	0.9568	74.38	0.8901	79.68	0.9145
0.4	142.91	0.9768	125.24	0.9948	130.35	0.9958	92.19	0.9256	78.19	0.8925	83.79	0.9254
0.5	148.62	0.9751	128.31	0.9924	133.49	0.9935	94.08	0.9023	81.67	0.8875	86.98	0.9142
0.6	139.59	0.9935	132.88	0.9897	137.75	0.9914	98.42	0.9165	84.84	0.9214	90.24	0.9288
0.7	176.13	0.9536	137.39	0.9878	142.12	0.9895	102.41	0.8792	87.95	0.9115	93.22	0.9345
0.8	162.84	0.9809	145.26	0.9819	149.81	0.9848	104.77	0.9124	91.42	0.8962	96.85	0.9147
0.9	205.91	0.9424	163.61	0.9616	167.54	0.9579	107.08	0.8978	96.24	0.9247	101.44	0.9241
Average	155.40	0.9741	130.17	0.9885	135.09	0.9894	90.86	0.9247	81.36	0.9060	86.71	0.9245

As discussed by Fedunik-Hofman et al. (2019), the geometric contraction (R2–R3) model assumes that nucleation occurs rapidly on the solid surface (Fedunik-Hofman et al., 2019). The reaction is regulated by the reaction interface that forms as the reaction progresses towards the centre. If the solid particle is considered to be cylindrical, the contracting area (R2) model is used; if the solid particle is assumed to be spherical or cubical, the contracting volume (R3) model is used. The kinetics parameters of EWSCO and EWSCOME are given in Table 6.4b. For EWSCO, three dimensional surface reaction model (R3) showed best fit with experimental data. R3 is geometrical contraction models, and assumes that the rate of degradation reaction starts at the surface and the rate is controlled by the resulting interface reaction (Khawam and Flanagan, 2006). On the other hand, for EWSCOME, phase boundary controlled (contracting area) model (R2) showed best fit.

6.4. Error Analysis

Different statistical error functions are analysed and tableted in Table 6.4a and 6.4b. Calculation method and procedure was discussed earlier in Section 3.2.1.

Recommendations

Applicability and accuracy of the kinetics data determined in this study are limited for samples in liquid phase within the temperature range 25–800 °C in which the predictions are made. Most of the models developed to determine the thermal degradation mechanism are applicable for solid–solid degradation kinetics, whereas very few models are available to demonstrate the thermal degradation of liquids

Table 6.4a. The calculated value of different error functions (a) WSCO and (b) WSCOME.

	Conversion	Standard Deviation	Mean Square Errors	Root Mean Square Errors	Sum of Squares of Errors	Average Relative Error	Sum of Absolute Errors	Hybrid Fractional Error Function	Marquart's Percentage Standard Deviation
WSCO	0.1	2.70	4.87	2.21	14.60	0.02	6.24	0.06	2.11
	0.2	18.36	224.79	14.99	674.36	0.09	42.13	2.07	11.34
	0.3	2.38	3.77	1.94	11.30	0.01	5.48	0.04	1.57
	0.4	8.31	45.98	6.78	137.95	0.04	18.65	0.42	5.07
	0.5	15.42	158.60	12.59	475.80	0.07	35.35	1.35	8.78
	0.6	16.63	184.37	13.58	553.11	0.07	38.19	1.49	8.99
	0.7	2.44	3.95	1.99	11.86	0.01	5.32	0.03	1.38
	0.8	27.22	493.78	22.22	1481.33	0.10	62.77	3.41	12.62
	0.9	19.39	250.59	15.83	751.76	0.07	44.75	1.62	8.38
WSCOME	0.1	9.04	54.45	7.38	163.36	0.17	20.16	1.99	22.47
	0.2	6.23	25.85	5.08	77.54	0.10	13.66	0.86	13.89
	0.3	7.62	38.71	6.22	116.13	0.12	17.26	1.30	17.28
	0.4	7.54	37.91	6.16	113.74	0.12	16.82	1.22	16.28
	0.5	11.27	84.62	9.20	253.87	0.16	23.57	2.60	23.54
	0.6	5.52	20.32	4.51	60.97	0.09	12.68	0.59	10.82
	0.7	18.55	229.29	15.14	687.86	0.23	40.80	5.56	31.27
	0.8	8.11	43.80	6.62	131.40	0.12	18.08	1.31	16.30
	0.9	23.86	379.48	19.48	1138.44	0.28	53.46	8.39	37.21

Table 6.4b. The calculated value of different error functions (a) EWSCO and (b) EWSCOME.

	Conversion	Standard Deviation	Mean Square Errors	Root Mean Square Errors	Sum of Squares of Errors	Average Relative Error	Sum of Absolute Errors	Hybrid Fractional Error Function	Marquart's Percentage Standard Deviation
EWSCO	0.1	18.89	237.76	15.42	713.29	0.12	43.15	2.88	15.40
	0.2	12.21	99.41	9.97	298.22	0.07	27.53	1.16	9.50
	0.3	13.42	120.03	10.96	360.08	0.08	30.41	1.31	9.84
	0.4	9.09	55.12	7.42	165.36	0.05	20.15	0.61	6.71
	0.5	10.55	74.25	8.62	222.75	0.06	23.63	0.79	7.52
	0.6	3.47	8.01	2.83	24.04	0.02	7.72	0.09	2.56
	0.7	21.13	297.76	17.26	893.28	0.10	48.50	2.77	13.19
	0.8	9.12	55.50	7.45	166.51	0.04	20.41	0.53	5.86
	0.9	23.37	364.11	19.08	1092.33	0.10	53.78	2.87	12.37
EWSCOME	0.1	5.70	21.68	4.66	65.04	0.06	11.60	0.49	8.65
	0.2	2.90	5.61	2.37	16.84	0.03	6.69	0.11	3.93
	0.3	6.26	26.11	5.11	78.33	0.05	13.09	0.49	7.77
	0.4	7.05	33.10	5.75	99.31	0.06	14.93	0.58	8.27
	0.5	6.23	25.85	5.08	77.54	0.05	13.01	0.44	7.09
	0.6	6.84	31.17	5.58	93.50	0.05	14.51	0.51	7.45
	0.7	7.32	35.70	5.98	107.11	0.06	15.77	0.56	7.65
	0.8	6.71	30.05	5.48	90.14	0.05	14.18	0.46	6.83
	0.9	5.42	19.60	4.43	58.79	0.04	10.99	0.29	5.35

6.4. Summary

In this study, thermal characteristics and kinetics parameters of WSCO, EWSCO, WSCOME, and EWSCOME were determined by thermogravimetry under non-isothermal heating conditions. In an inert nitrogen atmosphere, a series of experiments was carried out up to 800 °C at varying heating rates of 10, 20, 30, and 50 °C/min. The mass loss curves revealed that the degradation of the manufactured bio-lubricant samples occurred mostly between 200 and 500 °C, owing to the breakdown of weak chemical bonds, which resulted in the creation of smaller molecules of volatile organic compounds and gaseous products. From the study, WSCO was found to be thermally stable up to 200 °C, while biodiesel made from WSCO (i.e. WSCOME) was found to be thermally stable up to 100 °C. This clearly indicated that WSCO was more stable in comparison to its methyl esters (WSCOME), and WSCOME was more stable as compared to petroleum diesel (T_0 = 78 °C). Thermal stability of EWSCO and EWSCOME was found to be 189 °C and 142 °C, respectively. In all of the samples, increasing the heating rate resulted in a shift in the maximum rate loss to a higher temperature. Three models, namely Friedman, Kissinger-Akahira-Sunnose (KAS), and Flynn-Wall-Ozawa (FWO) models, were used to determine the apparent activation energy (E) of degradation of the prepared materials. According to the aforementioned methodologies, E of WSCO, WSCOME, EWSCO, and EWSOME was found to be 171, 51, 140, and 86 kJ/mol, respectively. The higher activation energy of EWSCO indicated that the sample was thermally more stable than EWSCOME. The loss of intrinsic moisture results in lower activation energies at the beginning of degradation. The subsequent increase in the activation energy corresponds to the degradation of heavier

molecules. The reaction kinetics of EWSCO followed phase boundary controlled (contracting volume) (R3) model and EWSCOME followed phase boundary controlled (contracting area) (R2) model. The complex structure of epoxides is reflected in the change in activation energy with respect to conversion and in the changes in reaction mechanism during degradation. The probable break in the molecular bonds of unsaturated fatty acids caused an increase in the activation energy in relation to the steps (setting of different heating rates in increasing order) in thermal degradation of samples. Furthermore, the results showed that structural modifications to WSCO had an influence on bio-lubricant production kinetics and mechanism.

CHAPTER VII

Overall Conclusions and Scope for Future Works

Significance of the Study and Conclusions

Scope for Future Works

Chapter VII

Overall Conclusions and Scope for Future Works

This chapter summarises the appropriate conclusions of the work presented in this thesis, based on all the characterisations and investigations. This chapter also provides some useful recommendations for future research in the relevant field.

7.1. Significance and Salient Features of the Study

The work presented in this thesis dealt with the preparation, characterisation and applications of the bio-lubricant base stocks derived from waste soybean cooking oil and its methyl esters via chemical modification (i.e. epoxidation). The performance limitation properties (thermal stability and cold flow properties) and the physico-chemical characterisations (mainly the rheological study for the lubricant properties) of the prepared epoxides indicated that the prepared base stocks possessed desirable properties to develop them as bio-lubricant base stocks. The prepared bio-lubricants are capable of replacing the conventional lubricants for hydraulic and transmission applications in various fields. From the perspective of thesis novelty, the major conclusions obtained from this study are summarised below.

7.2. Overall Conclusions

- Epoxidation of waste soybean cooking oil (WSCO) was successfully achieved by using sulphuric acid as the homogeneous acid catalyst. Optimisation results revealed that higher catalyst loading and high moles of hydrogen peroxide led to higher conversion of unsaturation into oxirane oxygen (epoxide) formation.
- The optimisation techniques, namely response surface methodology (RSM), artificial neural network (ANN), and genetic algorithm (GA), were applied to optimise the process parameters to maximise the oxirane oxygen content. ANN study was done by using Levenberg–Marquardt (LM) algorithm as training algorithm with an architecture of 3–4–1 (three nodes in the input layer, four nodes in the hidden layer, and one node in the output layer), logsig as the hidden layer transfer function, and purelin as the output layer transfer function. Fifty (50) iterations (reproductions) were taken by GA to predict the optimum results.

- The epoxidation conditions for WSCO were optimised as 2 mol of H_2O_2 (WSCO: H_2O_2 ratio), 1.5 g of catalyst (WSCO: H_2SO_4) and 6 h of reaction time. At these conditions, the maximum oxirane oxygen content (OOC) of WSCO epoxide was found to be 4.69 mass %. Apart from this, ANN modelling was also employed to predict the most correct result (2 mol of H_2O_2, 1.5 g of catalyst, 6 h of reaction time; 4.69 mass % OOC). Under the experimental conditions of 60 °C temperature, 4.6 h of reaction time, 1.84 g of catalyst loading and 1:2.34 molar ratio of C=C bonds to H_2O_2, GA predicted the OOC as 5.13 mass %. Double bond conversion in the range of 96–98.6 % was achieved during the epoxidation process.

- After successful preparation of the epoxides of waste soybean cooking oil (EWSCO), epoxidation of waste soybean cooking oil methyl esters (EWSCOME) was successfully achieved by using sulphuric acid as the homogeneous acid catalyst. In case of EWSCOME, similar optimisation tools (RSM, ANN, and GA) were used to predict the optimum conversion of unsaturated fatty acids to oxirane oxygen content (OOC). The ANN network consisted of three layers—three nodes in the input layer, eleven nodes in the hidden layer, and one node in the output layer—and the architecture was shown as 3–11–1 using the Levenberg–Marquardt (LM) algorithm as the training algorithm, with logsig as the hidden layer transfer function, and purelin as the output layer transfer function. GA used seventy-seven (77) iterations (reproductions) to predict the optimum results.

- The epoxidation conditions of WSCOME were optimised as 2.28 mol of H_2O_2 (WSCOME: H_2O_2 ratio), 2 wt % of catalyst loading and 4 h of reaction time, and the OOC was found to be 4.82 mass %. The optimised conditions predicted by ANN were 2.28 mol of H_2O_2, 2 wt % of catalyst loading, 4 h of reaction time, with OOC as 4.84 mass %, and by GA were 2.21 mol of H_2O_2, 1.95 wt % of catalyst loading, 4.14 h of reaction time, with OOC as 4.92 mass %. Double bond conversion in the range of 96–98.1 % was achieved during the epoxidation process.

- Three different ranges of shear rate (5–100, 5–300 and 100–300 s^{-1}) were tested for each sample at varying temperatures from 25 °C to 100 °C, and it was found that dynamic viscosity (k) and non-Newtonian flow behaviour index (n) changed with different shear rate region. From the average

viscosity values, it was found that the epoxides showed identical results at all shear rates. The dynamic viscosities of the epoxidised waste cooking oil and its methyl esters epoxides were found to be dependent on fatty acid chain length, unsaturation, and temperature. All samples showed gradual decrease in viscosity with increasing temperature because of decreased intermolecular interaction. All the samples displayed Newtonian behaviour irrespective of shear rate range and temperature effect. As viscosity is one of the critical parameters for potential bio-lubricant application, the power law model was used, in the present study, to investigate the flow behaviour of the epoxides. Kinematic viscosity of all the samples at 40 °C was listed as 33 cSt (WSCO), 4.5 cSt (WSCOME), 267 cSt (EWSCO), and 12 cSt (EWSCOME).

- Thermal degradation kinetics of WSCO, WSCOME, EWSCO, and EWSOME, investigated using different techniques, resulted in the average activation energy (E) of 171, 51, 140, and 86 kJ/mol, for the aforementioned samples, respectively. Mainly the higher activation energy contributed to higher thermal stability. The analyses of the process mechanism by the methods of Criado and Coats–Redfern showed that the most probable model for the degradation of EWSCO followed phase boundary controlled (contracting volume) (R3) model, and that of EWSCOME followed phase boundary controlled (contracting area) (R2) model. Activation energies at the beginning of degradation is low due to the loss of inherent moisture. The subsequent increase in activation energy corresponds to the degradation of the heavier molecules. The change of activation energy with respect to conversion, and the shift of reaction

mechanism during degradation reflected the complex nature of the epoxides.

- The TGA thermogram showed that the thermal stability of the samples was in good agreement with that of bio-lubricant standard. Thermal stability of the prepared samples was calculated to be 365 °C (T_o=200 °C) (WSCO), 183 °C (T_o=100 °C) (WSCOME), 338 °C (T_o=188 °C) (EWSCO), and 204 °C (T_o=142 °C) (EWSCOME), at 10 °C/min heating rate in nitrogen atmosphere. Oxidative degradation initiation temperatures were found to be as 312 °C (T_o=162 °C) (WSCO), 198 °C (T_o=140 °C) (WSCOME), 325 °C (T_o=181 °C) (EWSCO), and 215 °C (T_o=155 °C) (EWSCOME), at 10 °C/min heating rate in oxygen atmosphere.
- Further, it was found that the performance properties of the prepared base stocks were very much close to that of ISO grade 32, 46, 68, 100, SAE20W40 lubricants. Also, the viscosity index of WSCO, WSCOME, EWSCO, and EWSCOME were calculated to be 403, 372, 164, and 151, respectively.

In summary, the thesis outlines the efficacy of the bio-lubricant base stocks—synthesised from waste oil, a low cost feedstock—as a substitute to conventional lubricants. The obtained data anticipates to serve as the reference data for further research in the field of low cost bio-lubricant base stocks synthesis, characterisation and applications.

7.3. Scope for Future Works

Research findings of this work provided a good number of insights with respect to preparation, characterisation and applications of bio-lubricant base stocks synthesised from waste and renewable feedstocks via chemical modification techniques. There are certainly several areas which merit further research attention in future to take this promising research domain to newer heights. A few research areas for future work are proposed as follows:

- Epoxidation, hydroxylation, and hexanoylation of various feedstocks using sulphuric acid as the homogeneous strong acid catalyst can be done. Other catalysts such as enzymatic catalysts can also be used for the study. Additionally, employing the same catalyst for all the reactions could make an innovative study.
- There are many more kinetics models available. Exploration of all the suitable kinetics models is highly recommended.
- Studies on the use of different additives to improve the performance properties of the prepared epoxides products can be carried out.
- Real field applications of the prepared bio-lubricants need to be studied.
- Biodegradability study of the prepared bio-lubricants is an important task to be done.
- Detailed cost analysis of the prepared bio-lubricants is required.

References

References

Abdullah, B.M., Salih, N., Salimon, J., 2014. Optimization of the chemoenzymatic mono-epoxidation of linoleic acid using D-optimal design. J. Saudi Chem. Soc. 18, 276–287. https://doi.org/10.1016/j.jscs.2011.07.012

Aboulkas, A., Harfi, K. El, 2008. Study of the kinetics and mechanisms of thermal decomposition of Moroccan Tarfaya oil shale and its kerogen. Oil Shale 25, 426–443. https://doi.org/10.3176/oil.2008.4.04

Adhvaryu, A., Erhan, S.Z., 2002. Epoxidized soybean oil as a potential source of high-temperature lubricants. Ind. Crops Prod. 15, 247–254. https://doi.org/10.1016/S0926-6690(01)00120-0

Adhvaryu, A., Liu, Z., Erhan, S.Z., 2005. Synthesis of novel alkoxylated triacylglycerols and their lubricant base oil properties. Ind. Crops Prod. 21, 113–119. https://doi.org/10.1016/j.indcrop.2004.02.001

Afifah, A.N., Syahrullail, S., Wan Azlee, N.I., Rohah, A.M., 2021. Synthesis and tribological studies of epoxidized palm stearin methyl ester as a green lubricant. J. Clean. Prod. 280, 124320. https://doi.org/10.1016/j.jclepro.2020.124320

Aghbashlo, M., Peng, W., Tabatabaei, M., Kalogirou, S.A., Soltanian, S., Hosseinzadeh-Bandbafha, H., Mahian, O., Lam, S.S., 2021. Machine learning technology in biodiesel research: A review. Prog. Energy Combust. Sci. 85. https://doi.org/10.1016/j.pecs.2021.100904

Agrawal, A.J., Karadbhajne, V.Y., Agrawal, P.S., Arekar, P.S., Chakole, N.P., 2017. Synthesis of Biolubricants from Non Edible Oils. Int. Res. J. Eng. Technol. 4, 1753–1757.

Allen, S.J., Gan, Q., Matthews, R., Johnson, P.A., 2003. Comparison of optimised isotherm models for basic dye adsorption by kudzu. Bioresour. Technol. 88, 143–152. https://doi.org/10.1016/S0960-8524(02)00281-X

Anand, O.N., Chhibber, V.K., 2006. Vegetable oil derivatives: Environment-friendly lubricants and fuels. J. Synth. Lubr. 23, 91–107. https://doi.org/10.1002/jsl.14

Antony, J., 2014. Full Factorial Designs, in: Design of Experiments for Engineers and Scientists. Elsevier, pp. 63–85. https://doi.org/10.1016/B978-0-08-099417-8.00006-7

Asadauskas, S., Perez, J.M., Duda, J.L., 1996. Oxidative stability and antiwear properties of high oleic vegetable oils©. Lubr. Eng. 52, 877–882.

Attia, N.K., El-Mekkawi, S.A., Elardy, O.A., Abdelkader, E.A., 2020. Chemical

and rheological assessment of produced biolubricants from different vegetable oils. Fuel 271. https://doi.org/10.1016/j.fuel.2020.117578

Azaman, S.N.A., Ramakrishnan, N.R., Tan, J.S., Rahim, R.A., Abdullah, M.P., Ariff, A.B., 2010. Optimization of an induction strategy for improving interferon-α2b production in the periplasm of Escherichia coli using response surface methodology . Biotechnol. Appl. Biochem. https://doi.org/10.1042/ba20100104

Banerjee, A., Varshney, D., Kumar, S., Chaudhary, P., Gupta, V.K., 2017. Biodiesel production from castor oil: ANN modeling and kinetic parameter estimation. Int. J. Ind. Chem. 8, 253–262. https://doi.org/10.1007/s40090-017-0122-3

Bart, J.C.J., Gucciardi, E., Cavallaro, S., 2013. Biolubricants: Science and Technology. Woodhead Publishing Limited. https://doi.org/10.1533/9780857096326

Basheer, I.A., Hajmeer, M., 2000. Artificial neural networks: fundamentals, computing, design, and application. J. Microbiol. Methods 11, 3–31. https://doi.org/10.1016/S0167-7012(00)00201-3

Battersby, N.S., 2000. The biodegradability and microbial toxicity testing of lubricants - Some recommendations. Chemosphere 41, 1011–1027. https://doi.org/10.1016/S0045-6535(99)00517-2

Beale, M., Hagan, M., Demuth, H., 2010. Neural network toolbox 7. User's Guide. MathWorks.

Bepari, R.A., Bharali, P., Das, B.K., 2017. Controlled synthesis of α- and γ-Fe2O3 nanoparticles via thermolysis of PVA gels and studies on α-Fe2O3 catalyzed styrene epoxidation. J. Saudi Chem. Soc. 21, S170–S178. https://doi.org/10.1016/j.jscs.2013.12.010

Berry, G.C., Fox, T.., 2006. The viscosity of polymers and their concentrated solutions. Fortschritte der Hochpolym. 261–357. https://doi.org/10.1007/bfb0050985

Bezerra, M.A., Santelli, R.E., Oliveira, E.P., Villar, L.S., Escaleira, L.A., 2008. Response surface methodology (RSM) as a tool for optimization in analytical chemistry. Talanta. https://doi.org/10.1016/j.talanta.2008.05.019

Bhatti, M.S., Kapoor, D., Kalia, R.K., Reddy, A.S., Thukral, A.K., 2011. RSM and ANN modeling for electrocoagulation of copper from simulated wastewater: Multi objective optimization using genetic algorithm approach. Desalination 274, 74–80. https://doi.org/10.1016/j.desal.2011.01.083

Bio-lubricants market [WWW Document], 2020. . Mark. Mark. URL https://www.marketsandmarkets.com/Market-Reports/biolubricants-

market-17431466.html (accessed 6.22.21).

Birla, A., Singh, B., Upadhyay, S.N., Sharma, Y.C., 2012. Kinetics studies of synthesis of biodiesel from waste frying oil using a heterogeneous catalyst derived from snail shell. Bioresour. Technol. 106, 95–100. https://doi.org/10.1016/j.biortech.2011.11.065

Bolina, I.C.A., Gomes, R.A.B., Mendes, A.A., 2021. Biolubricant production from several oleaginous feedstocks using lipases as catalysts: current scenario and future perspectives. BioEnergy Res. https://doi.org/10.1007/s12155-020-10242-4

Borugadda, V.B., 2015. Synthesis of Bio-lubricant Basestocks: Substitute to Conventional Lubricants.

Borugadda, V.B., Dalai, A.K., 2018. In-situ synthesis and characterization of biodegradable estolides via epoxidation from canola biodiesel. Lubricants 6. https://doi.org/10.3390/lubricants6040094

Borugadda, V.B., Goud, V. V., 2019. Hydroxylation and hexanoylation of epoxidized waste cooking oil and epoxidized waste cooking oil methyl esters: Process optimization and physico-chemical characterization. Ind. Crops Prod. 133, 151–159. https://doi.org/10.1016/j.indcrop.2019.01.069

Borugadda, V.B., Goud, V. V., 2016a. Improved thermo-oxidative stability of structurally modified waste cooking oil methyl esters for bio-lubricant application. J. Clean. Prod. 112, 4515–4524. https://doi.org/10.1016/j.jclepro.2015.06.046

Borugadda, V.B., Goud, V. V., 2016b. Physicochemical and rheological characterization of waste cooking oil epoxide and their blends. Waste and Biomass Valorization 7, 23–30. https://doi.org/10.1007/s12649-015-9434-8

Borugadda, V.B., Goud, V. V., 2014a. Synthesis of Waste Cooking Oil Epoxide as a Bio-Lubricant Base Stock: Characterization and Optimization Study. J. Bioprocess Eng. Biorefinery 3, 57–72. https://doi.org/10.1166/jbeb.2014.1077

Borugadda, V.B., Goud, V. V., 2014b. Thermal, oxidative and low temperature properties of methyl esters prepared from oils of different fatty acids composition: A comparative study. Thermochim. Acta 577, 33–40. https://doi.org/10.1016/j.tca.2013.12.008

Borugadda, V.B., Goud, V. V., 2013. Comparative studies of thermal, oxidative and low temperature properties of waste cooking oil and castor oil. J. Renew. Sustain. Energy 5. https://doi.org/10.1063/1.4830257

Borugadda, V.B., Goud, V. V, 2018. Long-Term Storage Stability of Epoxides Derived from Vegetable Oils and Their Methyl Esters. Energy and Fuels 32,

3428–3435. https://doi.org/10.1021/acs.energyfuels.7b02351

Borugadda, V.B., Somidi, A.K.R., Dalai, A.K., 2017. Chemical/structural modification of canola oil and canola biodiesel: Kinetic studies and biodegradability of the alkoxides. Lubricants 5. https://doi.org/10.3390/lubricants5020011

Boyde, S., 2002. Green lubricants. Environmental benefits and impacts of lubrication. Green Chem. 4, 293–307. https://doi.org/10.1039/b202272a

Campanella, A., Fontanini, C., Baltanás, M.A., 2008. High yield epoxidation of fatty acid methyl esters with performic acid generated in situ. Chem. Eng. J. 144, 466–475. https://doi.org/10.1016/j.cej.2008.07.016

Campanella, A., Rustoy, E., Baldessari, A., Baltanás, M.A., 2010. Lubricants from chemically modified vegetable oils. Bioresour. Technol. 101, 245–254. https://doi.org/10.1016/j.biortech.2009.08.035

Carnes, K., 2004. Offroad hydraulic fluids: Beyond biodgradability. Tribol. Lubr. Technol. 60, 32–40.

Chi, G., Hu, S., Yang, Y., Chen, T., 2012. Response surface methodology with prediction uncertainty: A multi-objective optimisation approach. Chem. Eng. Res. Des. https://doi.org/10.1016/j.cherd.2011.12.012

Chua, S.C., Xu, X., Guo, Z., 2012. Emerging sustainable technology for epoxidation directed toward plant oil-based plasticizers. Process Biochem. https://doi.org/10.1016/j.procbio.2012.05.025

Ciannamea, E.M., Ruseckaite, R.A., 2018. Pressure Sensitive Adhesives Based on Epoxidized Soybean Oil: Correlation Between Curing Conditions and Rheological Properties. JAOCS, J. Am. Oil Chem. Soc. 95, 525–532. https://doi.org/10.1002/aocs.12046

Conceição, M.M., Candeia, R.A., Dantas, H.J., Soledade, L.E.B., Fernandes, V.J., Souza, A.G., 2005. Rheological behavior of castor oil biodiesel. Energy and Fuels 19, 2185–2188. https://doi.org/10.1021/ef050016g

Cornish-Bowden, A., 2001. Detection of errors of interpretation in experiments in enzyme kinetics. Methods 24, 181–190. https://doi.org/10.1006/meth.2001.1179

Cortés-Triviño, E., Valencia, C., Delgado, M.A., Franco, J.M., 2019. Thermo-rheological and tribological properties of novel bio-lubricating greases thickened with epoxidized lignocellulosic materials. J. Ind. Eng. Chem. 80, 626–632. https://doi.org/10.1016/j.jiec.2019.08.052

Criado, J.M., 1978. Kinetic analysis of DTG data from master curves. Thermochim. Acta 24, 186–189. https://doi.org/10.1016/0040-6031(78)85151-X

Czerwik-Marcinkowska, J., Gałczyńska, K., Oszczudłowski, J., Massalski, A., Semaniak, J., Arabski, M., 2020. Fatty Acid Methyl Esters of the Aerophytic Cave Alga Coccomyxa subglobosa as a Source for Biodiesel Production. Energies 13, 6494. https://doi.org/10.3390/en13246494

Da Silva, J.A.C., Habert, A.C., Freire, D.M.G., 2013. A potential biodegradable lubricant from castor biodiesel esters. Lubr. Sci. 25, 53–61. https://doi.org/10.1002/ls.1205

Daniel, Purba, J.M.E., Saleh, C., Magdaleni, A.R., 2019. Synthesis of polyol from Bintaro seed oil (Cerbera manghas L.) as lubricant base by epoxidation reaction and insitu opening oxirane. J. Phys. Conf. Ser. 1277, 012016. https://doi.org/10.1088/1742-6596/1277/1/012016

Dantas, M.B., Almeida, A.A.F., Conceição, M.M., Fernandes, V.J., Santos, I.M.G., Silva, F.C., Soledade, L.E.B., Souza, A.G., 2007a. Characterization and kinetic compensation effect of corn biodiesel. J. Therm. Anal. Calorim. 87, 847–851. https://doi.org/10.1007/s10973-006-7786-9

Dantas, M.B., Conceição, M.M., Fernandes, V.J., Santos, N.A., Rosenhaim, R., Marques, A.L.B., Santos, I.M.G., Souza, A.G., 2007b. Thermal and kinetic study of corn biodiesel obtained by the methanol and ethanol routes. J. Therm. Anal. Calorim. 87, 835–839. https://doi.org/10.1007/s10973-006-7780-2

Dasari, V.R.R.K., Donthireddy, S.R.R., Nikku, M.Y., Garapati, H.R., 2009. Optimization of medium constituents for Cephalosporin C production using response surface methodology and artificial neural networks. J. Biochem. Technol. 1, 69–74.

Dave, V.J., Patel, H.S., 2017. Synthesis and characterization of interpenetrating polymer networks from transesterified castor oil based polyurethane and polystyrene. J. Saudi Chem. Soc. https://doi.org/10.1016/j.jscs.2013.08.001

De Souza, A.G., Oliveira Santos, J.C., Conceição, M.M., Dantas Silva, M.C., Prasad, S., 2004. A thermoanalytic and kinetic study of sunflower oil. Brazilian J. Chem. Eng. 21, 265–273. https://doi.org/10.1590/s0104-66322004000200017

Deb, K., 2011. Multi-objective Optimisation Using Evolutionary Algorithms: An Introduction. Multi-objective Evol. Optim. Prod. Des. Manuf. 3–34. https://doi.org/10.1007/978-0-85729-652-8_1

Di Blasi, C., 1996. Kinetic and Heat Transfer Control in the Slow and Flash Pyrolysis of Solids. Ind. Eng. Chem. Res. 35, 37–46. https://doi.org/10.1021/ie950243d

Dörmo, N., Bélafi-Bakó, K., Bartha, L., Ehrenstein, U., Gubicza, L., 2004.

Manufacture of an environmental-safe biolubricant from fusel oil by enzymatic esterification in solvent-free system. Biochem. Eng. J. 21, 229–234. https://doi.org/10.1016/j.bej.2004.06.011

Ebrahimpour, A., Rahman, R.N.Z.R.A., Ean Ch'ng, D.H., Basri, M., Salleh, A.B., 2008. A modeling study by response surface methodology and artificial neural network on culture parameters optimization for thermostable lipase production from a newly isolated thermophilic Geobacillus sp. strain ARM. BMC Biotechnol. 8, 1–15. https://doi.org/10.1186/1472-6750-8-96

Elmelawy, M.S., El-Meligy, A., Mawgoud, H.A., Morshedy, A.S., Hanafy, S.A., El-sayed, I.E. tantawy, 2021. Synthesis and kinetics study of trimethylolpropane fatty acid triester from oleic acid methyl ester as potential biolubricant. Biomass Convers. Biorefinery. https://doi.org/10.1007/s13399-020-01220-z

Elsheikh, A.H., Sharshir, S.W., Abd Elaziz, M., Kabeel, A.E., Guilan, W., Haiou, Z., 2019. Modeling of solar energy systems using artificial neural network: A comprehensive review. Sol. Energy 180, 622–639. https://doi.org/10.1016/j.solener.2019.01.037

Enweremadu, C.C., Mbarawa, M.M., 2009. Technical aspects of production and analysis of biodiesel from used cooking oil-A review. Renew. Sustain. Energy Rev. 13, 2205–2224. https://doi.org/10.1016/j.rser.2009.06.007

Erhan, S.Z., Perez, J.M., 2002. Biobased Industrial Fluids and Lubricants. Biobased Ind. Fluids Lubr. https://doi.org/10.4324/9781003040477

Erhan, S.Z., Sharma, B.K., Liu, Z., Adhvaryu, A., 2008. Lubricant base stock potential of chemically modified vegetable oils. J. Agric. Food Chem. 56, 8919–8925. https://doi.org/10.1021/jf801463d

Farias, M., Martinelli, M., Bottega, D.P., 2010. Epoxidation of soybean oil using a homogeneous catalytic system based on a molybdenum (VI) complex. Appl. Catal. A Gen. 384, 213–219. https://doi.org/10.1016/j.apcata.2010.06.038

Fedunik-Hofman, L., Bayon, A., Donne, S.W., 2019. Kinetics of solid-gas reactions and their application to carbonate looping systems. Energies 12. https://doi.org/10.3390/en12152981

Ferdosian, F., Zhang, Y., Yuan, Z., Anderson, M., Xu, C. (Charles), 2016. Curing kinetics and mechanical properties of bio-based epoxy composites comprising lignin-based epoxy resins. Eur. Polym. J. 82, 153–165. https://doi.org/10.1016/j.eurpolymj.2016.07.014

Flynn, J.H., Wall, L.A., 1966. A quick, direct method for the determination of activation energy from thermogravimetric data. J. Polym. Sci. Part B Polym.

Lett. 4, 323–328. https://doi.org/10.1002/pol.1966.110040504

Foo, K.Y., Hameed, B.H., 2010. Insights into the modeling of adsorption isotherm systems. Chem. Eng. J. 156, 2–10. https://doi.org/10.1016/j.cej.2009.09.013

Fox, N.J., Stachowiak, G.W., 2007. Vegetable oil-based lubricants-A review of oxidation. Tribol. Int. 40, 1035–1046. https://doi.org/10.1016/j.triboint.2006.10.001

Frenkel, J., 1930. The Viscosity of Liquids. Nature 125, 581–582. https://doi.org/10.1038/125581b0

Friedman, H.L., 1964. Kinetics of thermal degradation of char-forming plastics from thermogravimetry. Application to a phenolic plastic. J. Polym. Sci. Part C Polym. Symp. 6, 183–195. https://doi.org/10.1002/polc.5070060121

Gapinski, R.E., Joseph, I.E., Layzell, B.D., 1994. A vegetable oil based tractor lubricant. SAE Tech. Pap. https://doi.org/10.4271/941758

García-Zapateiro, L.A., Franco, J.M., Valencia, C., Delgado, M.A., Gallegos, C., 2013. Viscous, thermal and tribological characterization of oleic and ricinoleic acids-derived estolides and their blends with vegetable oils. J. Ind. Eng. Chem. 19, 1289–1298. https://doi.org/10.1016/j.jiec.2012.12.030

Garciaa-Gimeno, R.M., Hervas-Martianez, C., Barco-Alcala, E., Zurera-Cosano, G., Sanz-Tapia, E., 2003. An Artificial Neural Network Approach to Escherichia Coli O157:H7 Growth Estimation. J. Food Sci. 68, 639–645. https://doi.org/10.1111/j.1365-2621.2003.tb05723.x

Ghaffari, A., Abdollahi, H., Khoshayand, M.R., Bozchalooi, I.S., Dadgar, A., Rafiee-Tehrani, M., 2006. Performance comparison of neural network training algorithms in modeling of bimodal drug delivery. Int. J. Pharm. 327, 126–138. https://doi.org/10.1016/j.ijpharm.2006.07.056

Gorla, G., Kour, S.M., Padmaja, K. V., Karuna, M.S.L., Prasad, R.B.N., 2013. Preparation and properties of lubricant base stocks from epoxidized karanja oil and its alkyl esters. Ind. Eng. Chem. Res. 52, 16598–16605. https://doi.org/10.1021/ie4024325

Gryglewicz, S., Muszyński, M., Nowicki, J., 2013. Enzymatic synthesis of rapeseed oil-based lubricants. Ind. Crops Prod. 45, 25–29. https://doi.org/10.1016/j.indcrop.2012.11.038

Gul, M., Masjuki, H.H., Kalam, M.A., Zulkifli, N.W.M., Mujtaba, M.A., 2020. A Review: Role of Fatty Acids Composition in Characterizing Potential Feedstock for Sustainable Green Lubricants by Advance Transesterification Process and its Global as Well as Pakistani Prospective. Bioenergy Res. 13. https://doi.org/10.1007/s12155-019-10040-7

Gul, M., Zulkifli, N.W.M., Kalam, M.A., Masjuki, H.H., Mujtaba, M.A., Yousuf,

S., Bashir, M.N., Ahmed, W., Yusoff, M.N.A.M., Noor, S., Ahmad, R., 2021. RSM and Artificial Neural Networking based production optimization of sustainable Cotton bio-lubricant and evaluation of its lubricity & tribological properties. Energy Reports 7, 830–839. https://doi.org/10.1016/j.egyr.2021.01.033

Guo, A., Demydov, D., Zhang, W., Petrović, Z.S., 2002. Structure and Properties of Halogenated and Non-halogenated Soy-Based Polyols. J. Polym. Environ. 10, 49–52.

Haider, M.A., Pakshirajan, K., Singh, A., Chaudhry, S., 2008. Artificial neural network-genetic algorithm approach to optimize media constituents for enhancing lipase production by a soil microorganism. Appl. Biochem. Biotechnol. https://doi.org/10.1007/s12010-007-8017-y

Hajar, M., Vahabzadeh, F., 2014. Artificial neural network modeling of biolubricant production using Novozym 435 and castor oil substrate. Ind. Crops Prod. 52, 430–438. https://doi.org/10.1016/j.indcrop.2013.11.020

Hazwan, M.H.M., Shayfull, Z., Sharif, S., Nasir, S.M., Rashidi, M.M., 2017. Warpage Optimisation on the Moulded Part using Response Surface Methodology (RSM) and Glowworm Swarm Optimisation (GSO). MATEC Web Conf. 97. https://doi.org/10.1051/matecconf/20179701105

Heikal, E.K., Elmelawy, M.S., Khalil, S.A., Elbasuny, N.M., 2017. Manufacturing of environment friendly biolubricants from vegetable oils. Egypt. J. Pet. 26, 53–59. https://doi.org/10.1016/j.ejpe.2016.03.003

Hernández-Sierra, M.T., Bravo-Sánchez, M.G., Báez, J.E., Aguilera-Camacho, L.D., García-Miranda, J.S., Moreno, K.J., 2019. Improvement effect of green lubricants on the tribological and mechanical performance of 4140 steel. Appl. Sci. 9. https://doi.org/10.3390/app9224896

Honary, L.A.T., Richter, E., 2011. Biobased Lubricants and Greases: Technology and Products. Biobased Lubr. Greases Technol. Prod. https://doi.org/10.1002/9780470971956

Huang, J., Wang, Y., Hao, Z., Peng, X., 2017. A recyclable Fe3O4-supported cobalt nanocatalyst for the epoxidation of olefins using aqueous hydrogen peroxide. J. Saudi Chem. Soc. 21, 811–816. https://doi.org/10.1016/j.jscs.2015.12.005

Hwang, H.S., Erhan, S.Z., 2006. Synthetic lubricant basestocks from epoxidized soybean oil and Guerbet alcohols. Ind. Crops Prod. 23, 311–317. https://doi.org/10.1016/j.indcrop.2005.09.002

Jain, A., Suhane, A., 2012. Research Approach & Prospects of Non edible vegetable oil as a potential resource for biolubricant-A review. Adv. Eng.

Appl. Sci. Int. J. 1, 23–32.

Jayadas, N.H., Nair, K.P., 2006. Coconut oil as base oil for industrial lubricants-evaluation and modification of thermal, oxidative and low temperature properties. Tribol. Int. 39, 873–878. https://doi.org/10.1016/j.triboint.2005.06.006

Jena, P.C., Raheman, H., Prasanna Kumar, G. V., Machavaram, R., 2010. Biodiesel production from mixture of mahua and simarouba oils with high free fatty acids. Biomass and Bioenergy 34, 1108–1116. https://doi.org/10.1016/j.biombioe.2010.02.019

Kamalakar, K., Rajak, A.K., Prasad, R.B.N., Karuna, M.S.L., 2013. Rubber seed oil-based biolubricant base stocks: A potential source for hydraulic oils. Ind. Crops Prod. 51, 249–257. https://doi.org/10.1016/j.indcrop.2013.08.058

Kamalakar, K., Sai Manoj, G.N.V.T., Prasad, R.B.N., Karuna, M.S.L., 2015. Thumba (Citrullus colocynthis L.) seed oil: a potential bio-lubricant base-stock. Grasas y Aceites 66, e055. https://doi.org/10.3989/gya.0576141

Kana, E.B.G., Oloke, J.K., Lateef, A., Adesiyan, M.O., 2012. Modeling and optimization of biogas production on saw dust and other co-substrates using Artificial Neural network and Genetic Algorithm. Renew. Energy 46, 276–281. https://doi.org/10.1016/j.renene.2012.03.027

Karadeniz, K., Aki, H., Sen, M.Y., Çaliko¬lu, Y., 2015. Ring opening of epoxidized soybean oil with compounds containing two different functional groups. JAOCS, J. Am. Oil Chem. Soc. 92, 725–731. https://doi.org/10.1007/s11746-015-2638-z

Karimmaslak, H., Najafi, B., Band, S.S., Ardabili, S., Haghighat-Shoar, F., Mosavi, A., 2021. Optimization of performance and emission of compression ignition engine fueled with propylene glycol and biodiesel–diesel blends using artificial intelligence method of ANN-GA-RSM. Eng. Appl. Comput. Fluid Mech. 15, 413–425. https://doi.org/10.1080/19942060.2021.1880970

Karmakar, B., Mishra, J.R., Datta, A., Muthangi, K.R., Tiwari, O.N., Halder, G., 2021. Transesterifying Madhuca indica and waste cooking oil blends with C1–C3 alcohol mixtures: two-step catalysis using Delonix regia and Mesua ferrea linn supports. Biomass Convers. Biorefinery. https://doi.org/10.1007/s13399-021-01640-5

Karthic, P., Joseph, S., Arun, N., Kumaravel, S., 2013. Optimization of biohydrogen production by Enterobacter species using artificial neural network and response surface methodology. J. Renew. Sustain. Energy 5. https://doi.org/10.1063/1.4803746

Kerman, C.O., Gaber, Y., Ghani, N.A., Lämsä, M., Hatti-Kaul, R., 2011. Clean

synthesis of biolubricants for low temperature applications using heterogeneous catalysts. J. Mol. Catal. B Enzym. 72, 263–269. https://doi.org/10.1016/j.molcatb.2011.06.014

Khawam, A., Flanagan, D.R., 2006. Solid-state kinetic models: Basics and mathematical fundamentals. J. Phys. Chem. B 110, 17315–17328. https://doi.org/10.1021/jp062746a

Khawam, A., Flanagan, D.R., 2005. Complementary use of model-free and modelistic methods in the analysis of solid-state kinetics. J. Phys. Chem. B 109, 10073–10080. https://doi.org/10.1021/jp050589u

Khodadadi, M.R., Malpartida, I., Tsang, C.W., Lin, C.S.K., Len, C., 2020. Recent advances on the catalytic conversion of waste cooking oil. Mol. Catal. 494. https://doi.org/10.1016/j.mcat.2020.111128

Khot, S.N., Lascala, J.J., Can, E., Morye, S.S., Williams, G.I., Palmese, G.R., Kusefoglu, S.H., Wool, R.P., 2001. Development and application of triglyceride-based polymers and composites. J. Appl. Polym. Sci. 82, 703–723. https://doi.org/10.1002/app.1897

Kim, S.S., Kim, J., Park, Y.H., Park, Y.K., 2010. Pyrolysis kinetics and decomposition characteristics of pine trees. Bioresour. Technol. 101, 9797–9802. https://doi.org/10.1016/j.biortech.2010.07.094

Kissinger, H.E., 1957. Reaction Kinetics in Differential Thermal Analysis. Anal. Chem. 29, 1702–1706. https://doi.org/10.1021/ac60131a045

Kleinová, A., Fodran, P., Brnčalová, L., Cvengroš, J., 2008. Substituted esters of stearic acid as potential lubricants. Biomass and Bioenergy 32, 366–371. https://doi.org/10.1016/j.biombioe.2007.09.015

Kodali, D.R., 2014. Development, properties and applications of high-performance biolubricants. Adv. Biorefineries Biomass Waste Supply Chain Exploit. 556–595. https://doi.org/10.1533/9780857097385.2.556

Koh, M.Y., Tinia, T.I., Idris, A., 2014. Synthesis of palm based biolubricant in an oscillatory flow reactor (OFR). Ind. Crops Prod. 52, 567–574. https://doi.org/10.1016/j.indcrop.2013.10.042

Kollias, S., Anastassiou, D., 1989. An Adaptive Least Squares Algorithm for the Efficient Training of Artificial Neural Networks. IEEE Trans. Circuits Syst. 36, 1092–1101. https://doi.org/10.1109/31.192419

Kollias, S., Anastassiou, D., 1988. Adaptive training of multilayer neural networks using a least squares estimation technique, in: IEEE International Conference on Neural Networks. IEEE, pp. 383–390. https://doi.org/10.1109/icnn.1988.23870

Kumar, A.N., Kishore, P.S., Raju, K.B., Ashok, B., Vignesh, R., Jeevanantham,

A.K., Nanthagopal, K., Tamilvanan, A., 2020. Decanol proportional effect prediction model as additive in palm biodiesel using ANN and RSM technique for diesel engine. Energy 213. https://doi.org/10.1016/j.energy.2020.119072

Lahiri, S.K., Ghanta, K.C., 2009. Development of a hybrid artificial neural network and genetic algorithm model for regime identification of slurry transport in pipelines. Chem. Prod. Process Model. 4. https://doi.org/10.2202/1934-2659.1343

Lahiri, S.K., Ghanta, K.C., 2008. Development of an artificial neural network correlation for prediction of hold-up of slurry transport in pipelines. Chem. Eng. Sci. 63, 1497–1509. https://doi.org/10.1016/j.ces.2007.11.030

Lathi, P.S., Mattiasson, B., 2007. Green approach for the preparation of biodegradable lubricant base stock from epoxidized vegetable oil. Appl. Catal. B Environ. 69, 207–212. https://doi.org/10.1016/j.apcatb.2006.06.016

Le, H.N.T., Imamura, K., Watanabe, N., Furuta, M., Takenaka, N., Boi, L. Van, Maeda, Y., 2018. Biodiesel Production from Rubber Seed Oil by Transesterification Using a Co-solvent of Fatty Acid Methyl Esters. Chem. Eng. Technol. 41, 1013–1018. https://doi.org/10.1002/ceat.201700575

Li, H., Niu, S., Lu, C., Wang, Y., 2015. Comprehensive Investigation of the Thermal Degradation Characteristics of Biodiesel and Its Feedstock Oil through TGA-FTIR. Energy and Fuels 29, 5145–5153. https://doi.org/10.1021/acs.energyfuels.5b01054

Li, W., Wang, X., 2015. Bio-lubricants Derived from Waste Cooking Oil with Improved Oxidation Stability and Low-temperature Properties. J. Oleo Sci. 64, 367–374. https://doi.org/10.1016/j.procbio.2010.09.020

Libor, M., 1991. Rheology of epoxy networks near the gel point. Polym. Bull. 116, 109–116.

Liu, H., Hong, R., Xiang, C., Wang, H., Li, Y., Xu, G., Chang, P., Zhu, K., 2020. Thermal decomposition kinetics analysis of the oil sludge using model-based method and model-free method. Process Saf. Environ. Prot. 141, 167–177. https://doi.org/10.1016/j.psep.2020.05.021

Lubricants market size [WWW Document], 2021. . Gd. View Res. https://doi.org/978-1-68038-123-8

Luna, F.M.T., Rocha, B.S., Rola, E.M., Albuquerque, M.C.G., Azevedo, D.C.S., Cavalcante, C.L., 2011. Assessment of biodegradability and oxidation stability of mineral, vegetable and synthetic oil samples. Ind. Crops Prod. 33, 579–583. https://doi.org/10.1016/j.indcrop.2010.12.012

Luque, R., Melero, J.A., 2012. Advances in biodiesel production: Processes and

technologies, Advances in Biodiesel Production: Processes and Technologies. https://doi.org/10.1533/9780857095862

Madankar, C.S., Dalai, A.K., Naik, S.N., 2013. Green synthesis of biolubricant base stock from canola oil. Ind. Crops Prod. 44, 139–144. https://doi.org/10.1016/j.indcrop.2012.11.012

Maity, U., Basu, J.K., Sengupta, S., 2014. Performance study of extraction and oxidation-extraction coupling processes in the removal of thiophenic compounds. Fuel Process. Technol. 121, 119–124. https://doi.org/10.1016/j.fuproc.2014.01.012

Mang, T., Wilfried, D., 2017. Lubricants and Lubrication. Wiley-VCH Verlag GmbH & Co. KGaA, Weinheim, Germany. https://doi.org/10.1002/9783527645565

Market volume of lubricants worldwide [WWW Document], 2021. . Statista. URL https://www.statista.com/statistics/821076/lubricants-global-market-volume-by-country/

Marques, J.P.C., Rios, Í.C., Parente, E.J.S., Quintella, S.A., Luna, F.M.T., Cavalcante, C.L., 2020. Synthesis and Characterization of Potential Bio-Based Lubricant Basestocks via Epoxidation Process. JAOCS, J. Am. Oil Chem. Soc. 97, 437–446. https://doi.org/10.1002/aocs.12317

Masood, H., Yunus, R., Choong, T.S.Y., Rashid, U., Taufiq Yap, Y.H., 2012. Synthesis and characterization of calcium methoxide as heterogeneous catalyst for trimethylolpropane esters conversion reaction. Appl. Catal. A Gen. 425–426, 184–190. https://doi.org/10.1016/j.apcata.2012.03.019

McNutt, J., He, Q.S., 2016. Development of biolubricants from vegetable oils via chemical modification. J. Ind. Eng. Chem. 36, 1–12. https://doi.org/10.1016/j.jiec.2016.02.008

Menkiti, M.C., Anaehobi, H.C., Onukwuli, O.D., 2016. Kinetics and parametric study of transesterification synthesis of biolubricant from melon-based methyl esters. Biofuels 7, 489–500. https://doi.org/10.1080/17597269.2016.1163212

Menkiti, M.C., Ocheje, O., Agu, C.M., 2017. Production of environmentally adapted lubricant basestock from jatropha curcas specie seed oil. Int. J. Ind. Chem. 8, 133–144. https://doi.org/10.1007/s40090-017-0116-1

Mobarak, H.M., Niza Mohamad, E., Masjuki, H.H., Kalam, M.A., Al Mahmud, K.A.H., Habibullah, M., Ashraful, A.M., 2014. The prospects of biolubricants as alternatives in automotive applications. Renew. Sustain. Energy Rev. 33, 34–43. https://doi.org/10.1016/j.rser.2014.01.062

Mohamed, M.S., Tan, J.S., Mohamad, R., Mokhtar, M.N., Ariff, A.B., 2013.

Comparative analyses of response surface methodology and artificial neural network on medium optimization for Tetraselmis sp. FTC209 grown under mixotrophic condition. Sci. World J. 2013. https://doi.org/10.1007/978-94-6300-154-0_14

Mohd, F.M.N., Juahir, H.H., Nuraainaa, R., Isahak, M., Nur, A.S., 2011. Artificial Neural Networks Combined with Sensitivity Analysis as a Prediction Model for Water Quality Index in Juru River, Malaysia. Int. J. Environ. Prot. 1, 1–8. https://doi.org/10.5963/ijep0103001

Mondal, B., Parhi, S.S., Rangaiah, G.P., Jana, A.K., 2021. Nano-catalytic heterogeneous reactive distillation for algal biodiesel production: Multi-objective optimization and heat integration. Energy Convers. Manag. 241. https://doi.org/10.1016/j.enconman.2021.114298

Mungroo, R., Pradhan, N.C., Goud, V. V., Dalai, A.K., 2008. Epoxidation of canola oil with hydrogen peroxide catalyzed by acidic ion exchange resin. JAOCS, J. Am. Oil Chem. Soc. 85, 887–896. https://doi.org/10.1007/s11746-008-1277-z

Muthusamy, S., Manickam, L.P., Murugesan, V., Muthukumaran, C., Pugazhendhi, A., 2019. Pectin extraction from Helianthus annuus (sunflower) heads using RSM and ANN modelling by a genetic algorithm approach. Int. J. Biol. Macromol. 124, 750–758. https://doi.org/10.1016/j.ijbiomac.2018.11.036

Naeem, A., Wali Khan, I., Farooq, M., Mahmood, T., Ud Din, I., Ali Ghazi, Z., Saeed, T., 2021. Kinetic and optimization study of sustainable biodiesel production from waste cooking oil using novel heterogeneous solid base catalyst. Bioresour. Technol. 328. https://doi.org/10.1016/j.biortech.2021.124831

Nagendramma, P., 2011. Study of pentaerythritol tetraoleate ester as industrial gear oil. Lubr. Sci. 23, 355–362. https://doi.org/10.1002/ls.161

Nagendramma, P., Kaul, S., 2012. Development of ecofriendly/biodegradable lubricants: An overview. Renew. Sustain. Energy Rev. https://doi.org/10.1016/j.rser.2011.09.002

Nik, W.B.W., Ani, F.N., Masjuki, H.H., 2005. Thermal stability evaluation of palm oil as energy transport media. Energy Convers. Manag. 46, 2198–2215. https://doi.org/10.1016/j.enconman.2004.10.008

Noorossana, R., Davanloo Tajbakhsh, S., Saghaei, A., 2009. An artificial neural network approach to multiple-response optimization. Int. J. Adv. Manuf. Technol. https://doi.org/10.1007/s00170-008-1423-7

Oh, J., Yang, S., Kim, C., Choi, I., Kim, J.H., Lee, H., 2013. Synthesis of

biolubricants using sulfated zirconia catalysts. Appl. Catal. A Gen. 455, 164–171. https://doi.org/10.1016/j.apcata.2013.01.032

Okpalaeke, K.E., Ibrahim, T.H., Latinwo, L.M., Betiku, E., 2020. Mathematical Modeling and Optimization Studies by Artificial Neural Network, Genetic Algorithm and Response Surface Methodology: A Case of Ferric Sulfate–Catalyzed Esterification of Neem (Azadirachta indica) Seed Oil. Front. Energy Res. 8. https://doi.org/10.3389/fenrg.2020.614621

Oladipo, B., Ojumu, T. V., Latinwo, L.M., Betiku, E., 2020. Pawpaw (Carica papaya) peel waste as a novel green heterogeneous catalyst for moringa oil methyl esters synthesis: Process optimization and kinetic study. Energies 13. https://doi.org/10.3390/en13215834

Olivieri, G. V., de Quadros, J. V., Giudici, R., 2020. Epoxidation Reaction of Soybean Oil: Experimental Study and Comprehensive Kinetic Modeling. Ind. Eng. Chem. Res. 59, 18808–18823. https://doi.org/10.1021/acs.iecr.0c03847

Onukwuli, D.O., Esonye, C., Ofoefule, A.U., Eyisi, R., 2021a. Comparative analysis of the application of artificial neural network-genetic algorithm and response surface methods-desirability function for predicting the optimal conditions for biodiesel synthesis from chrysophyllum albidum seed oil. J. Taiwan Inst. Chem. Eng. https://doi.org/10.1016/j.jtice.2021.06.012

Onukwuli, D.O., Umeuzuegbu, J.C., Nwobi-Okoye, C.C., 2021b. Computational Modeling and Multi-objective Optimization of Engine Performance with Waste Soya Oil-Based Biodiesel Using Genetic Algorithm and Utility Function. Process Integr. Optim. Sustain. https://doi.org/10.1007/s41660-021-00178-3

Opfermann, J., Kaisersberger, E., 1992. An advantageous variant of the Ozawa-Flynn-Wall analysis. Thermochim. Acta 203, 167–175. https://doi.org/10.1016/0040-6031(92)85193-Y

Oraegbunam, J.C., Oladipo, B., Falowo, O.A., Betiku, E., 2020. Clean sandbox (Hura crepitans) oil methyl esters synthesis: A kinetic and thermodynamic study through pH monitoring approach. Renew. Energy 160, 526–537. https://doi.org/10.1016/j.renene.2020.06.124

Oyeyemi, V.B., Keith, J.A., Carter, E.A., 2014. Accurate bond energies of biodiesel methyl esters from multireference averaged coupled-pair functional calculations. J. Phys. Chem. A 118, 7392–7403. https://doi.org/10.1021/jp412727w

Ozawa, T., 1965. A New Method of Analyzing Thermogravimetric Data. Bull. Chem. Soc. Jpn. 38, 1881–1886. https://doi.org/10.1246/bcsj.38.1881

Padmaja, K. V., Rao, B.V.S.K., Reddy, R.K., Bhaskar, P.S., Singh, A.K., Prasad,

R.B.N., 2012. 10-Undecenoic acid-based polyol esters as potential lubricant base stocks. Ind. Crops Prod. 35, 237–240. https://doi.org/10.1016/j.indcrop.2011.07.005

Pal, A.K., Katiyar, V., 2017. Theoretical and analyzed data related to thermal degradation kinetics of poly (L-lactic acid)/chitosan-grafted-oligo L-lactic acid (PLA/CH-g-OLLA) bionanocomposite films. Data Br. 10, 304–311. https://doi.org/10.1016/j.dib.2016.11.100

Paul, A.K., Borugadda, V.B., Bhalerao, M.S., Goud, V. V., 2018. In situ epoxidation of waste soybean cooking oil for synthesis of biolubricant basestock: A process parameter optimization and comparison with RSM, ANN, and GA. Can. J. Chem. Eng. 96, 1451–1461. https://doi.org/10.1002/cjce.23091

Pauline, J.M.N., Sivaramakrishnan, R., Pugazhendhi, A., Anbarasan, T., Achary, A., 2021. Transesterification kinetics of waste cooking oil and its diesel engine performance. Fuel 285. https://doi.org/10.1016/j.fuel.2020.119108

Pavlovicova, A., Cvengros, J., 1999. Lubricants based on vegetable oils. Pet. Coal 41, 99–102.

Pindit, K., Thanapimmetha, A., Saisriyoot, M., Srinopakun, P., 2021. Biolubricant basestocks synthesis using 5-step reaction from jatropha oil, soybean oil, and palm fatty acid distillate. Ind. Crops Prod. 166. https://doi.org/10.1016/j.indcrop.2021.113484

Pirro, D.M., Webster, M., Daschner, E., 2016. Lubrication Fundamentals, Revised and Expanded, 3rd ed. CRC Press, New York.

Prakash Maran, J., Priya, B., 2015a. Comparison of response surface methodology and artificial neural network approach towards efficient ultrasound-assisted biodiesel production from muskmelon oil. Ultrason. Sonochem. 23, 192–200. https://doi.org/10.1016/j.ultsonch.2014.10.019

Prakash Maran, J., Priya, B., 2015b. Modeling of ultrasound assisted intensification of biodiesel production from neem (Azadirachta indica) oil using response surface methodology and artificial neural network. Fuel 143, 262–267. https://doi.org/10.1016/j.fuel.2014.11.058

Pugazhendhi, A., Alagumalai, A., Mathimani, T., Atabani, A.E., 2020. Optimization, kinetic and thermodynamic studies on sustainable biodiesel production from waste cooking oil: An Indian perspective. Fuel 273. https://doi.org/10.1016/j.fuel.2020.117725

Puig-Arnavat, M., Bruno, J.C., 2015. Artificial Neural Networks for Thermochemical Conversion of Biomass. Recent Adv. Thermochem. Convers. Biomass 133–156. https://doi.org/10.1016/B978-0-444-63289-

0.00005-3

Quinchia, L.A., Delgado, M.A., Franco, J.M., Spikes, H.A., Gallegos, C., 2012. Low-temperature flow behaviour of vegetable oil-based lubricants. Ind. Crops Prod. 37, 383–388. https://doi.org/10.1016/j.indcrop.2011.12.021

Quinchia, L.A., Delgado, M.A., Valencia, C., Franco, J.M., Gallegos, C., 2010. Viscosity modification of different vegetable oils with EVA copolymer for lubricant applications. Ind. Crops Prod. 32, 607–612. https://doi.org/10.1016/j.indcrop.2010.07.011

Quinchia, L.A., Delgado, M.A., Valencia, C., Franco, J.M., Gallegos, C., 2009. Viscosity modification of high-oleic sunflower oil with polymeric additives for the design of new biolubricant formulations. Environ. Sci. Technol. 43, 2060–2065. https://doi.org/10.1021/es803047m

Razmi-Rad, E., Ghanbarzadeh, B., Mousavi, S.M., Emam-Djomeh, Z., Khazaei, J., 2007. Prediction of rheological properties of Iranian bread dough from chemical composition of wheat flour by using artificial neural networks. J. Food Eng. 81, 728–734. https://doi.org/10.1016/j.jfoodeng.2007.01.009

Reshad, A.S., Barman, P., Chaudhari, A.J., Tiwari, P., Kulkarni, V., Goud, V. V., Sahoo, N., 2015. Rubber Seed Oil Methyl Ester Synthesis, Engine Performance, and Emission Characteristics of Blends. Energy and Fuels 29, 5136–5144. https://doi.org/10.1021/acs.energyfuels.5b01033

Resul, M.F.M.G., Tinia, T.I., Idris, A., 2012. Kinetic study of jatropha biolubricant from transesterification of jatropha curcas oil with trimethylolpropane: Effects of temperature. Ind. Crops Prod. 38, 87–92. https://doi.org/10.1016/j.indcrop.2012.01.012

Romero, A., Cuesta, C., Sánchez-Muniz, F.J., 1998. Effect of oil replenishment during deep-fat frying of frozen foods in sunflower oil and high-oleic acid sunflower oil. JAOCS, J. Am. Oil Chem. Soc. 75, 161–167. https://doi.org/10.1007/s11746-998-0028-5

Roy, T., Sahani, S., Madhu, D., Chandra Sharma, Y., 2020. A clean approach of biodiesel production from waste cooking oil by using single phase BaSnO3 as solid base catalyst: Mechanism, kinetics & E-study. J. Clean. Prod. 265. https://doi.org/10.1016/j.jclepro.2020.121440

Rudnick, L.R., 2020. Synthetics, mineral oils, and bio-based lubricants : chemistry and technology.

Rudnick, L.R., Shubkin, R.L. (Eds.), 1999. Synthetic Lubricants And High-Performance Functional Fluids, Revised And Expanded, Synthetic Lubricants And High- Performance Functional Fluids, Revised And Expanded. CRC Press. https://doi.org/10.1201/9780203909898

Saalah, S., Abdullah, L.C., Aung, M.M., Salleh, M.Z., Biak, D.R.A., Basri, M., Jusoh, E.R., Mamat, S., 2017. Physicochemical Properties of jatropha oil-based polyol produced by a two steps method. Molecules 22. https://doi.org/10.3390/molecules22040551

Salih, N., Salimon, J., Yousif, E., 2011. The physicochemical and tribological properties of oleic acid based triester biolubricants. Ind. Crops Prod. 34, 1089–1096. https://doi.org/10.1016/j.indcrop.2011.03.025

Salimon, J., Salih, N., 2010. Chemical modification of oleic acid oil for biolubricant industrial applications, Australian Journal of Basic and Applied Sciences. INSinet Publications.

Salimon, J., Salih, N., Yousif, E., 2012. Improvement of pour point and oxidative stability of synthetic ester basestocks for biolubricant applications. Arab. J. Chem. 5, 193–200. https://doi.org/10.1016/j.arabjc.2010.09.001

Salimon, J., Salih, N., Yousif, E., 2011. Chemically modified biolubricant basestocks from epoxidized oleic acid: Improved low temperature properties and oxidative stability. J. Saudi Chem. Soc. 15, 195–201. https://doi.org/10.1016/j.jscs.2010.08.004

Salimon, J., Salih, N., Yousif, E., 2010. Biolubricants: Raw materials, chemical modifications and environmental benefits. Eur. J. Lipid Sci. Technol. 112, 519–530. https://doi.org/10.1002/ejlt.200900205

Salmasi, M.Z., Kazemeini, M., Sadjadi, S., 2020. Transesterification of sunflower oil to biodiesel fuel utilizing a novel K2CO3/Talc catalyst: Process optimizations and kinetics investigations. Ind. Crops Prod. 156. https://doi.org/10.1016/j.indcrop.2020.112846

Sammaiah, A., Padmaja, K.V., Prasad, R.B.N., 2014. Synthesis of epoxy jatropha oil and its evaluation for lubricant properties. J. Oleo Sci. 63, 637–643. https://doi.org/10.5650/jos.ess13172

Sbirrazzuoli, N., Girault, Y., Elégant, L., 1997. Simulations for evaluation of kinetic methods in differential scanning calorimetry. Part 3 - Peak maximum evolution methods and isoconversional methods. Thermochim. Acta 293, 25–37. https://doi.org/10.1016/s0040-6031(97)00023-3

Scala, J. La, Wool, R.P., 2005. Rheology of chemically modified triglycerides. J. Appl. Polym. Sci. 95, 774–783. https://doi.org/10.1002/app.20846

Schneider, M.P., 2006. Plant-oil-based lubricants and hydraulic fluids. J. Sci. Food Agric. 86, 1769–1780. https://doi.org/10.1002/jsfa.2559

Selvaraj, R., Moorthy, I.G., Kumar, R.V., Sivasubramanian, V., 2019. Microwave mediated production of FAME from waste cooking oil: Modelling and optimization of process parameters by RSM and ANN approach. Fuel 237,

40–49. https://doi.org/10.1016/j.fuel.2018.09.147

Shahabuddin, M., Masjuki, H.H., Kalam, M.A., Bhuiya, M.M.K., Mehat, H., 2013. Comparative tribological investigation of bio-lubricant formulated from a non-edible oil source (Jatropha oil). Ind. Crops Prod. 47, 323–330. https://doi.org/10.1016/j.indcrop.2013.03.026

Shancita, I., Masjuki, H.H., Kalam, M.A., Reham, S.S., Ruhul, A.M., Monirul, I.M., 2016. Evaluation of the characteristics of non-oxidative biodiesels: A FAME composition, thermogravimetric and IR analysis. RSC Adv. 6, 8198–8210. https://doi.org/10.1039/c5ra23963j

Shanmugaprakash, M., Sivakumar, V., 2013. Development of experimental design approach and ANN-based models for determination of Cr(VI) ions uptake rate from aqueous solution onto the solid biodiesel waste residue. Bioresour. Technol. https://doi.org/10.1016/j.biortech.2013.08.149

Sharma, B.K., Biresaw, G., 2016. Environmentally Friendly and Biobased Lubricants, Environmentally Friendly and Biobased Lubricants. https://doi.org/10.1201/9781315373256

Sharma, B.K., Doll, K.M., Erhan, S.Z., 2007. Oxidation, friction reducing, and low temperature properties of epoxy fatty acid methyl esters. Green Chem. 9, 469–474. https://doi.org/10.1039/B614100E

Sharma, U.C., Chandra, A.K., Sachan, S., 2019. Investigation on thermo-oxidative stability of karanja oil derived biolubricant base oil. Asian J. Chem. 31, 839–844. https://doi.org/10.14233/ajchem.2019.21762

Sharma, R. V., Dalai, A.K., 2013. Synthesis of bio-lubricant from epoxy canola oil using sulfated Ti-SBA-15 catalyst. Appl. Catal. B Environ. 142–143, 604–614. https://doi.org/10.1016/j.apcatb.2013.06.001

Sharma, R. V., Somidi, A.K.R., Dalai, A.K., 2015. Preparation and properties evaluation of biolubricants derived from canola oil and canola biodiesel. J. Agric. Food Chem. 63, 3235–3242. https://doi.org/10.1021/jf505825k

Sharma, Y.C., Singh, B., Upadhyay, S.N., 2008. Advancements in development and characterization of biodiesel: A review. Fuel 87, 2355–2373. https://doi.org/10.1016/j.fuel.2008.01.014

Shirneshan, A., Bagherzadeh, S.A., Najafi, G., Mamat, R., Mazlan, M., 2021. Optimization and investigation the effects of using biodiesel-ethanol blends on the performance and emission characteristics of a diesel engine by genetic algorithm. Fuel 289. https://doi.org/10.1016/j.fuel.2020.119753

Silva, M.A., Carvalho, C.A. de, Fonsêca, P.C. de A., Vieira, S.A., Ribeiro, A.Q., Priore, S.E., Franceschini, S. do C.C., 2015. Iron-deficiency anemia and vitamin A deficiency prevalence and associated factors among children under

one year. Cad. Saúde Coletiva 23, 362–367. https://doi.org/10.1590/1414-462X2015000100047

Singh, N.K., Singh, Y., Sharma, A., Rahim, E.A., 2020. Prediction of performance and emission parameters of Kusum biodiesel based diesel engine using neuro-fuzzy techniques combined with genetic algorithm. Fuel 280. https://doi.org/10.1016/j.fuel.2020.118629

Singh, Y., Kumar Singh, N., Sharma, A., Singla, A., Singh, D., Abd Rahim, E., 2021. Effect of ZnO nanoparticles concentration as additives to the epoxidized Euphorbia Lathyris oil and their tribological characterization. Fuel 285, 119148. https://doi.org/10.1016/j.fuel.2020.119148

Somidi, A.K.R., Sharma, R. V., Dalai, A.K., 2014. Synthesis of epoxidized canola oil using a sulfated-SnO2 Catalyst. Ind. Eng. Chem. Res. 53, 18668–18677. https://doi.org/10.1021/ie500493m

Soni, S., Agarwal, M., 2014. Lubricants from renewable energy sources – a review. Green Chem. Lett. Rev. 7, 359–382. https://doi.org/10.1080/17518253.2014.959565

Soriano, N.U., Migo, V.P., Matsumura, M., 2006. Ozonized vegetable oil as pour point depressant for neat biodiesel. Fuel 85, 25–31. https://doi.org/10.1016/j.fuel.2005.06.006

Soufi, M.D., Ghobadian, B., Najafi, G., Sabzimaleki, M., Jaliliantabar, F., 2015. Performance and Exhaust Emissions of a SI Two-stroke Engine with Biolubricants Using Artificial Neural Network. Energy Procedia 75, 3–9. https://doi.org/10.1016/j.egypro.2015.07.127

Souza, A.G., Danta, H.J., Silva, M.C.D., Santos, I.M.G., Fernandes, V.J., Sinfrônio, F.S.M., Teixeira, L.S.G., Novák, C., 2007. Thermal and kinetic evaluation of cotton oil biodiesel. J. Therm. Anal. Calorim. 90, 945–949. https://doi.org/10.1007/s10973-006-8199-5

Sreeprasanth, P.S., Srivastava, R., Srinivas, D., Ratnasamy, P., 2006. Hydrophobic, solid acid catalysts for production of biofuels and lubricants. Appl. Catal. A Gen. 314, 148–159. https://doi.org/10.1016/j.apcata.2006.08.012

Sripada, P.K., Sharma, R. V., Dalai, A.K., 2013. Comparative study of tribological properties of trimethylolpropane-based biolubricants derived from methyl oleate and canola biodiesel. Ind. Crops Prod. 50, 95–103. https://doi.org/10.1016/j.indcrop.2013.07.018

Srivastava, G., Paul, A.K., Goud, V. V., 2018. Optimization of non-catalytic transesterification of microalgae oil to biodiesel under supercritical methanol condition. Energy Convers. Manag. 156, 269–278.

https://doi.org/10.1016/j.enconman.2017.10.093

Stempfel, E.M., 1998. Practical experience with highly biodegradable lubricants, especially hydraulic oils and lubricating greases. NLGI Spokesm. 62, 8–23.

Sun, S., Ke, X., Cui, L., Yang, G., Bi, Y., Song, F., Xu, X., 2011a. Enzymatic epoxidation of Sapindus mukorossi seed oil by perstearic acid optimized using response surface methodology. Ind. Crops Prod. 33, 676–682. https://doi.org/10.1016/j.indcrop.2011.01.002

Sun, S., Yang, G., Bi, Y., Liang, H., 2011b. Lubricants from chemically modified vegetable oils. J. Am. Oil Chem. Soc. 88, 245–254. https://doi.org/10.1007/s11746-003-0777-y

Suryawanshi, P.G., Goud, V. V., 2021. Processing Thermogravimetric Analysis Data for Pyrolysis Kinetic Study of Microalgae Biomass 1415–1424. https://doi.org/10.1007/978-981-15-5955-6_134

Talaghat, M.R., Mokhtari, S., Saadat, M., 2020. Modeling and optimization of biodiesel production from microalgae in a batch reactor. Fuel 280. https://doi.org/10.1016/j.fuel.2020.118578

Talib, N.S.R., Halmi, M.I.E., Ghani, S.S.A., Zaidan, U.H., Shukor, M.Y.A., 2019. Artificial Neural Networks (ANNs) and Response Surface Methodology (RSM) Approach for Modelling the Optimization of Chromium (VI) Reduction by Newly Isolated Acinetobacter radioresistens Strain NS-MIE from Agricultural Soil. Biomed Res. Int. 2019. https://doi.org/10.1155/2019/5785387

Talkit, K.M., Mahajan, D.T., Masand, V.H., 2012. Study on physicochemical properties of vegetable oils and their blends use as possible ecological lubricant. J. Chem. Pharm. Res. 4, 5139–5144.

Tan, S.G., Chow, W.S., 2010. Biobased epoxidized vegetable oils and its greener epoxy blends: A review. Polym. - Plast. Technol. Eng. https://doi.org/10.1080/03602559.2010.512338

Tanveer, S., Sharma, U.C., Prasad, R., 2006. Rheology of multigrade engine oils. Indian J. Chem. Technol. 13, 180–184.

The DIN 51519 Table [WWW Document], n.d. . Widman Int. SRL. URL https://www.widman.biz/English/Tables/DIN-51519.html (accessed 1.12.21).

Ting, C.C., Chen, C.C., 2011. Viscosity and working efficiency analysis of soybean oil based bio-lubricants. Meas. J. Int. Meas. Confed. 44, 1337–1341. https://doi.org/10.1016/j.measurement.2011.04.005

Tinia, T.I., Resul, M.F.M.G., Idris, A., 2009. Bioenergy II: Production of biodegradable lubricant from jatropha curcas and trimethylolpropane. Int.

J. Chem. React. Eng. 7. https://doi.org/10.2202/1542-6580.1957

Todaka, M., Kowhakul, W., Masamoto, H., Shigematsu, M., Onwona-Agyeman, S., 2013. Thermal decomposition of biodiesel fuels produced from rapeseed, jatropha, and coffee oils with different alcohols. J. Therm. Anal. Calorim. 113, 1355–1361. https://doi.org/10.1007/s10973-013-3056-9

Tornero, V., Hanke, G., 2016. Chemical contaminants entering the marine environment from sea-based sources: A review with a focus on European seas. Mar. Pollut. Bull. 112, 17–38. https://doi.org/10.1016/j.marpolbul.2016.06.091

Valle, C.P. do, Rodrigues, J.S., Fechine, L.M.U.D., Cunha, A.P., Queiroz Malveira, J., Luna, F.M.T., Ricardo, N.M.P.S., 2018. Chemical modification of Tilapia oil for biolubricant applications. J. Clean. Prod. 191, 158–166. https://doi.org/10.1016/j.jclepro.2018.04.062

Vasishth, A., Kuchhal, P., Anand, G., 2014. Study of Rheological Properties of Industrial Lubricants. Conf. Pap. Sci. 2014, 1–5. https://doi.org/10.1155/2014/324615

Vuppaladadiyam, A.K., Memon, M.Z., Ji, G., Raheem, A., Jia, T.Z., Dupont, V., Zhao, M., 2019. Thermal Characteristics and Kinetic Analysis of Woody Biomass Pyrolysis in the Presence of Bifunctional Alkali Metal Ceramics. ACS Sustain. Chem. Eng. 7, 238–248. https://doi.org/10.1021/acssuschemeng.8b02967

Vyazovkin, S., Burnham, A.K., Criado, J.M., Pérez-Maqueda, L.A., Popescu, C., Sbirrazzuoli, N., 2011. ICTAC Kinetics Committee recommendations for performing kinetic computations on thermal analysis data. Thermochim. Acta 520, 1–19. https://doi.org/10.1016/j.tca.2011.03.034

Vyazovkin, S., Chrissafis, K., Di Lorenzo, M.L., Koga, N., Pijolat, M., Roduit, B., Sbirrazzuoli, N., Suñol, J.J., 2014. ICTAC Kinetics Committee recommendations for collecting experimental thermal analysis data for kinetic computations. Thermochim. Acta 590, 1–23. https://doi.org/10.1016/j.tca.2014.05.036

Vyazovkin, S., Clawson, J.S., Wight, C.A., 2001. Thermal dissociation kinetics of solid and liquid ammonium nitrate. Chem. Mater. 13, 960–966. https://doi.org/10.1021/cm000708c

Wagner, H., Luther, R., Mang, T., 2001. Lubricant base fluids based on renewable raw materials: Their catalytic manufacture and modification. Appl. Catal. A Gen. 221, 429–442. https://doi.org/10.1016/S0926-860X(01)00891-2

Wang, A., Chen, L., Jiang, D., Yan, Z., 2013. Vegetable oil-based ionic liquid microemulsions and their potential as alternative renewable biolubricant

basestocks. Ind. Crops Prod. 51, 425–429. https://doi.org/10.1016/j.indcrop.2013.09.039

Wang, E., Ma, X., Tang, S., Yan, R., Wang, Y., Riley, W.W., Reaney, M.J.T., 2014. Synthesis and oxidative stability of trimethylolpropane fatty acid triester as a biolubricant base oil from waste cooking oil. Biomass and Bioenergy 66, 371–378. https://doi.org/10.1016/j.biombioe.2014.03.022

Wu, X., Zhang, X., Yang, S., Chen, H., Wang, D., 2000. The Study of epoxidized rapeseed oil used as a potential biodegradable lubricant. JAOCS, J. Am. Oil Chem. Soc. 77, 561–563. https://doi.org/10.1007/s11746-000-0089-2

Xu, Y.Q., Qu, J.P., 2009. Mechanical and rheological properties of epoxidized soybean oil plasticized poly(lactic acid). J. Appl. Polym. Sci. 112, 3185–3191. https://doi.org/10.1002/app.29797

Yancey, B., Vyazovkin, S., 2015. The kinetics and mechanism of nanoconfined molten salt reactions: Trimerization of potassium and rubidium dicyanamide. Phys. Chem. Chem. Phys. 17, 10209–10217. https://doi.org/10.1039/c5cp01056j

Yen, H.Y., Yang, M.H., 2003. The effect of metal ions additives on the rheological behavior of polyacrylamide solution. Polym. Test. 22, 389–393. https://doi.org/10.1016/S0142-9418(02)00119-8

Yunus, R., Fakhru'l-Razi, A., Ooi, T.L., Omar, R., Idris, A., 2005. Synthesis of palm oil based trimethylolpropane esters with improved pour points. Ind. Eng. Chem. Res. 44, 8178–8183. https://doi.org/10.1021/ie050530

Zaher, F.A., El-Mallah, M.H., El-Hefnawy, M.M., 1989. Kinetics of oxirane cleavage in epoxidized soybean oil. J. Am. Oil Chem. Soc. 66, 698–700. https://doi.org/10.1007/BF02669955

Zhang, W., Ji, H., Song, Y., Ma, S., Xiong, W., Chen, C., Chen, B., Zhang, X., 2020. Green preparation of branched biolubricant by chemically modifying waste cooking oil with lipase and ionic liquid. J. Clean. Prod. 274. https://doi.org/10.1016/j.jclepro.2020.122918

Zwinselman, J., Pal, M., Singhal, S., 2000. Environmentally adapted lubricants, Part I. An overview. J. Synth. Lubr. 17, 135–143. https://doi.org/10.1002/jsl.3000170205

Appendix

Appendix

Typical M-File and Program output for ANN

```
%User defined Transfer Function (Input & Output Layers also)

clear;
clear all;
clc;

fprintf(' Artificial Neural Network');

inputs=load('in.txt'); % Create Input file in same folder and rename it in.txt
targets=load('tar.txt'); % Create Experimental output in same folder and rename
it tar.txt
inputs=inputs';
targets=targets';

fprintf('\n\n List of Transfer Functions \n\n 01. traingdm  : Gradient descent
with momontum backpropagation \n 02. traingda  : Gradient descent with
adaptive learning rate backpropagation \n 03. trainbfg  : BFGS quasi-Newton
backpropagation \n 04. traincgp  : Conjugate gradient backpropagation with
Polak-Ribiere updates \n');
fprintf(' 05. traingdx  : Gradient descent with momentum anad adaptive learning
rate backpropagation \n 06. trainbu  : Batch unsupervised weight/bias training
\n 07. trainoss  : One step secent backpropagation \n 08. trainlm  : Levenberg-
Marquardt backpropagation \n 09. trainr  : Random order incremental training
with learning functions \n 10. traincgb  : Conjugate gradient backpropagation
with Powell-Beale updates \n');
```

```
fprintf(' 11. trainrp  : Resilient backpropagation \n 12. trainc  : Cyclical order weight/bias training \n 13. traincgf  : Conjugate gradient backpropagation with Fletcher-Reeves updates \n 14. trainbfgc : BFGS quasi-Newton backpropagation for use with NN model reference adaptive controller \n 15. trainb  : Batch training with weight and bias learning rules \n');
fprintf(' 16. trainru  : Unsupervised random order weight/bias training \n 17. traingd  : Gradient descent backpropagation \n 18. trainscg  : Scaled conjugate gradient backpropagation \n 19. trainbr  : Bayesian regulation backpropagation \n\n');

% Programme

hiddenLayerSize = input ('\n Enter Number of nodes in hidden layer  : ');
net=fitnet(hiddenLayerSize);
net.divideParam.trainRatio=70/100;
net.divideParam.valRatio=15/100;
net.divideParam.testRatio=15/100;

%transferFunction = input('\n Write Name of Transfer Function : ', 's');

transferFunction = 'trainlm';

%fprintf('\n Input Layer Transfer Functions :\n 1. logsig : Log Sigmoid \n 2. tansig : Hyperbolic Tangent Sigmoid \n 3. radbas : Radial Basis \n 4. tribas : Triangular Basis');
%inTrFunction = input('\n\nWrite Name of the Input Layer Transfer Function : ','s');

inTrFunction = 'tansig';
```

```
%fprintf('\n\n Output Layer Transfer Functions :\n 1. purelin : Linear \n 2. tansig  : Hyperbolic Tangent Sigmoid \n 3. logsig  : Log Sigmoid \n');
%outTrFunction = input('\n\nWrite Name of the Output Layer Transfer Function : ','s');

outTrFunction = 'tansig';
net=newff(inputs,targets,hiddenLayerSize,{inTrFunction
outTrFunction},transferFunction);
%net=newff(inputs,targets,hiddenLayerSize,{},'traingdx');
[net,tr]=train(net,inputs,targets);
outputs=net(inputs);
errors=gsubtract(outputs,targets);
performance=perform(net,targets,outputs);% performance means mean square error
RMSE=sqrt(performance); % Root Mean Square Error
view(net)

IW = net.IW; % Cell containing the Input Weights;
b1 = net.b; % Cell containing the biases;
LW = net.LW; % Cell containing the layer weights;

% New Input
%ninputs=load('newin.txt'); % Create New inputs in same folder and rename it newin.txt
%ninputs=ninputs';
%noutputs=net(ninputs);
```

Table A1. Kinematic viscosity and viscosity index table.

Sample	Temperature (°C)	Density (kg/m³)	Dynamic Viscosity (Pa-s)	Kinematic Viscosity (cSt)	Viscosity Index
WSCO	25	788.5	0.04571	57.971	403.83
	40	780.2	0.02648	33.940	
	60	772.0	0.01707	22.111	
	80	765.7	0.01028	13.426	
	100	756.9	0.00995	13.146	
WSCOME	25	755.4	0.00391	5.177	372.29
	40	735.8	0.00332	4.512	
	60	730.9	0.00237	3.249	
	80	725.8	0.00181	2.493	
	100	720.4	0.00141	1.957	
EWSCO	25	802.1	0.28543	355.853	164.94
	40	792.7	0.21238	267.920	
	60	785.9	0.08847	112.572	
	80	774.2	0.04382	56.600	
	100	768.3	0.02501	32.552	
EWSCOME	25	773.8	0.01621	20.948	151.97
	40	765.0	0.00930	12.158	
	60	754.0	0.00544	7.210	
	80	741.0	0.00335	4.521	
	100	725.0	0.00240	3.317	

List of Publications

List of Publications

Journal Publications:

1. **Atanu Kumar Paul**, Swapan Kumar Achar, Swaroopa Rani Dasari, Venu Babu Borugadda, and Vaibhav V. Goud. 2017. "Analysis of Thermal, Oxidative and Cold Flow Properties of Methyl and Ethyl Esters Prepared from Soybean and Mustard Oils." *Journal of Thermal Analysis and Calorimetry* 130 (3): 1501–11. https://doi.org/10.1007/s10973-017-6424-z.

2. Garima Srivastava, **Atanu Kumar Paul**, and Vaibhav V. Goud. 2018. "Optimization of Non-Catalytic Transesterification of Microalgae Oil to Biodiesel under Supercritical Methanol Condition." *Energy Conversion and Management* 156: 269–78. https://doi.org/10.1016/j.enconman.2017.10.093.

3. **Atanu Kumar Paul**, Venu Babu Borugadda, Machhindra S. Bhalerao, and Vaibhav V. Goud. 2018. "In Situ Epoxidation of Waste Soybean Cooking Oil for Synthesis of Biolubricant Basestock: A Process Parameter Optimization and Comparison with RSM, ANN, and GA." *Canadian Journal of Chemical Engineering* 96 (7): 1451–61. https://doi.org/10.1002/cjce.23091.

4. Venu Babu Borugadda, **Atanu Kumar Paul**, Ashish J. Chaudhari, Vinayak Kulkarni, Niranjan Sahoo, and Vaibhav V. Goud. 2018. "Influence of Waste Cooking Oil Methyl Ester Biodiesel Blends on the Performance and Emissions of a Diesel Engine." *Waste and Biomass Valorization* 9 (2): 283–92. https://doi.org/10.1007/s12649-016-9749-0.

5. **Atanu Kumar Paul**, Venu Babu Borugadda, and Vaibhav V. Goud. 2021. "In-situ Epoxidation of Waste Cooking Oil and Its Methyl Esters for Lubricant Applications: Characterization and Rheology." *Lubricants* 9 (3): 27. https://doi.org/10.3390/lubricants9030027.

6. **Atanu Kumar Paul**, Venu Babu Borugadda, Ali Shemshedin, and Machhindra S. Bhalerao. 2021. "Comparative Study of Physicochemical and Rheological Property of Waste Cooking Oil, Castor Oil, Rubber Seed Oil, Their Methyl Esters and Blends with Mineral Diesel Fuel." *Materials Science for Energy Technologies*, 1–21. https://doi.org/10.1016/j.mset.2021.03.004.

7. **Atanu Kumar Paul**, Venu Babu Borugadda, Vaibhav V. Goud, "Optimization of the Waste Soybean Cooking Oil Methyl Ester Derived Biolubricant Basestock Via Response Surface Methodology, Artificial Neural Network and Genetic Algorithm". ***(Ready to submit)***

8. **Atanu Kumar Paul**, Pravin G. Suryawanshi, Vaibhav V. Goud, "Studies on Degradation Kinetics of waste soybean cooking oil (WSCO), waste soybean cooking oil methyl ester (WSCOME), epoxide of waste soybean cooking oil (EWSCO) and epoxide of waste soybean cooking oil methyl ester (EWSCOME)". ***(Ready to submit)***

Conference Presentations (National/International):

1. **Atanu Kumar Paul**, Vaibhav V. Goud, Study of Rheological Property of Waste Cooking Oil (WCO) with its Methyl Ester and Blends, Advances in Sustainable Polymers (ASP-15), Indian Institute of Technology Guwahati, Guwahati (India), Volume 2 (21-22 January 2015).

2. Garima Srivastava, **Atanu Kumar Paul**, Pushpita Das, Vaibhav V. Goud, Biodiesel production from microalgae. 68th Annual Session of Indian Institute of Chemical Engineers, Indian Chemical Engineering Congress (CHEMCON-2015), December 27-30, Indian Institute of Technology Guwahati, Guwahati, India. (2015)

3. **Atanu Kumar Paul**, Venu Babu Borugadda, Vaibhav V. Goud, Study of Rheological Property of Rubber Seed Oil (RSO) with its Methyl Ester and Blends, Science, Technology and Innovation: It's Impact on Communities of N.E. India, Department of Anthropology, Gauhati University, Assam, Volume: 1 (10-11 Sept. 2015).

4. Garima Srivastava, **Atanu Kumar Paul**, Pushpita Das, Vaibhav V. Goud, Sustainable fuel production from microorganism, Research Conclave-2016, March 18-21, Indian Institute of Technology Guwahati, Guwahati, India. (2016).

5. **Atanu Kumar Paul**, Venu Babu Borugadda, Vaibhav V. Goud, Comparative studies on rheological behaviour of waste cooking oil, its methyl ester and their blends, International Conference on Waste Management, "Recycle-2016", 1-2 April, Indian Institute of Technology Guwahati, Guwahati, India. (2016).

6. **Atanu Kumar Paul**, Venu Babu Borugadda, Machhindra Bhalerao, Vaibhav V. Goud, Optimization study of waste cooking oil biolubricant base stock via epoxidation by RSM, National Conference on Sustainable Advanced Technologies for Environmental Management (SATEM-2017), at Indian Institute of Engineering Science and Technology, Shibpur, Howrah, West Bengal 711103, India (2017)

7. **Atanu Kumar Paul**, Venu Babu Borugadda, Vaibhav V. Goud, Optimization of waste cooking oil lubricant base stock synthesis via epoxidation using homogeneous acidic catalyst, Fourth International Symposium on Advances in Sustainable Polymers 2017 (ASP 2017), 8-11 January 2018, at Indian Institute of Technology Guwahati, Guwahati, Assam, India.

8. **Atanu Kumar Paul**, Vaibhav V. Goud, Rheology Study of Waste Cooking Oil Methyl Ester and its Epoxide, International Conference on Renewable and Alternate Energy (ICRAE–2018), 4–6 December 2018, at Assam Science and Technology University, Guwahati, Assam, India.

Workshop/ Training/ Seminar/Webinar attended:

1. Participated in "National School on Sustainable Polymers and First Symposium on Advances in Sustainable Polymers (ASP-14)" held during January 6–11, 2014 at Indian Institute of Technology Guwahati, Assam.

2. Participated in "Technical Writing Workshop" held on 9th March 2014, during Reflux 2.0 – Annual Chemical Engineering Symposium, Department of Chemical Engineering, Indian Institute of Technology Guwahati, Assam.

3. Participated in "National Workshop on Molecular Modeling and Simulation of Sustainable Polymers and Nanocomposites (MSSP-14)" held during August 4-8, 2014 at Indian Institute of Technology Guwahati, Assam.

4. Participated in "IUCr Workshop on X-Ray diffraction systems and related applications" held during 11-12 September, 2014 at Indian Institute of Technology Guwahati (India).

5. Participated in the National Workshop on "Technical Writing" conducted under the Technical Education Quality Improvement Programme (TEQIP) sponsored by MHRD held on 6-7 December, 2014 at Indian Institute of Technology Guwahati (India).

6. Participated in the short term course on "Transport Processes and Optimization Techniques in Polymers" conducted by Department of Chemical Engineering and Knowledge Incubation Cell under the TEQIP (MHRD), held during December, 15-20, 2014 at Indian Institute of Technology Guwahati (India).

7. Participated in the "IITG-KIT Joint Symposium on Biobased Materials" held on January 20, 2015 at Indian Institute of Technology Guwahati (India).

8. Participated in the National Symposium on "IPR in Innovation and Entrepreneurship" conducted under the Technical Education Quality Improvement Programme sponsored by the Ministry of Human Resource Development, Government of India, held on 16th March, 2015 at Indian Institute of Technology Guwahati (India).

9. Attended and Participated in the short term course on "Recent Advances in Energy Research (RAER)" held at Indian Institute of Technology Guwahati, organized by the Department of Chemical Engineering during 23rd to 27th March, 2015.

10. Participated in "3D-Printing workshop" organized by AerotriX on 21st to 22nd March, 2015 at Indian Institute of Technology Guwahati during SEISMECH' 15.

11. Participated in the "Research Conclave 2015" from 23rd to 26th March, 2015 organized by the PhD Council of the Students' Academic Board (SAB) at Indian Institute of Technology Guwahati.

12. Participated in "EXHIBITION" held during Reflux 2015 – Annual Symposium organized by Department of Chemical Engineering, Indian Institute of Technology Guwahati on 27th to 29th March 2015.

13. Participated in the IEEE Workshop on "Amateur Radio Session" held on 19th to 20th December, 2015 at Indian Institute of Technology Guwahati.

14. Participated in "7th DAE-BRNS BIENNIAL SYMPOSIUM" jointly organized by Board of Research in Nuclear Sciences (BRNS) and Department of Chemical Engineering, Indian Institute of Technology Guwahati held on 17th to 20th May, 2016 at Indian Institute of Technology Guwahati.

15. Attended the full agenda of "ACS on Campus" organized by American Chemical Society on 16th January 2017 at Indian Institute of Technology Guwahati.

16. Participated in the Indo-Japan Bilateral Symposium on "Future Perspective of Bioresource Utilization in North-East India" held on 1st to 4th February 2018, jointly organized by Indian Institute of Technology Guwahati, India and Gifu University, Japan at Indian Institute of Technology Guwahati.

17. Conducted a workshop on "ImageJ" held on 9th March, 2018 during Research Conclave 2018, organized by Students' Academic Board, Indian Institute of Technology Guwahati.

18. Participated in the Industry-Academia Interface Seminar titled "Upstream Petroleum Engineering" held on 10th November, 2018 organized by Indian Institute of Chemical Engineers–Guwahati Regional Centre and the Department of Chemical Engineering, IIT Guwahati at Department of Chemical Engineering, Indian Institute of Technology Guwahati, Guwahati, Assam.

19. Attended the online seminar on "Basics of Rheology and Particle Characterization" organized by Anton Paar India Pvt. Ltd. on 8th April 2020 at Indian Institute of Technology Guwahati.

20. Attended ACS Webinars on "Fundamentals of Effective Scientific Writing: Manuscripts and Grants" organized by American Chemical Society - ACS Publications - ACS.org on 9th June 2020.

21. Attended the TEQIP sponsored six days online National Seminar on "Advances in Manufacturing, Materials and Modelling Process (AMMMP-2020)" organized by Mechanical Engineereing Department, Katihar Engineering College, Katrihar, Bihar-854109, India on 17-22 August, 2020.

22. Participated in the 3-Day online workshop on"Basic Oil and Gas Fieldm Development Lifecycle" jointly organized by Department of Petroleum Engineering, IIT(ISM) Dhanbad, Department of Chemical Engineering, NIT Durgapur and Department of Chemical Engineering, GMRIT, Rajam during 24-26 August, 2020.

23. Attended the TEQIP sponsored six days online National Seminar on "Advances in Manufacturing and Characterization Process (AMCP-2020)" organized by Mechanical Engineereing Department, Katihar Engineering College, Katrihar, Bihar-854109, India on 24-29 August, 2020.

24. Attended the TEQIP sponsored six days online National workshop on "Academia to Industry: Challenges & Opportunities (AICO-2020)" organized by Mechanical Engineereing Department, Katihar Engineering College, Katrihar, Bihar-854109, India on 31 August – 5 September, 2020.

25. Attended the online webinar on "Particle Size & Zeta Potential Measurement by Dynamic Light Scattering (DLS) & Electrophoretic Light Scattering (ELS) Techniques" organized by Anton Paar India Pvt. Ltd. on 15th March 2021 at Indian Institute of Technology Guwahati.

26. Attended the online webinar on "Latest techniques on BET surface area analysis: Gas Physisorption and Chemisorption" organized by Anton Paar India Pvt. Ltd. on 20th May 2021 at Indian Institute of Technology Guwahati.

27. Attended the online webinar on "Full Agenda of ACS on Campus - Graduate Student Summit" organized by American Chemical Society on 14th July 2021.

28. Attended the online webinar on "In-situ Electrochemical Studies with Bruker FT-IR Spectrometer" organized by Bruker India Scientific Pvt. Ltd. on 15th July 2021 at Indian Institute of Technology Guwahati.

29. Attended the online webinar on "In-situ Electrochemical Studies with Bruker FT-IR Spectrometer" organized by Bruker India Scientific Pvt. Ltd. on 15th July 2021 at Indian Institute of Technology Guwahati.

ATANU KUMAR PAUL

3D/34 S. N. Banerjee Road,
A-Zone, Durgapur, Paschim
Bardhaman, West Bengal,
India, PIN: 713204

Email: atanukpaul@outlook.com
atanu.kr.paul@gmail.com
DOB: 12 January 1990
Mob.: +91 8011027384
Website: https://iitg.ac.in/stud/atanu.2013
https://linkedin.com/in/atanukpaul
https://orcid.org/0000-0002-4307-2245

Career Objective

To continue my career with an organisation that will effectively use my talents, expertise, and opportunity to work with a team for betterment in the future, as well as one that offers promising career progression.

Education

Ph.D. (Chemical Engineering) **2022**
Indian Institute of Technology Guwahati, Guwahati CPI 6.5/10
Thesis: Synthesis of Bio-lubricant Base Stocks from Waste Oil

M.Tech. (Chemical Engineering) **2013**
National Institute of Technology Durgapur, Durgapur CGPA 7.36/10
Thesis: Study of Slurry Rheology and Pressure Drop with and without Additives

B.Tech. (Chemical Engineering) **2011**
Durgapur Institute of Advanced Technology and Management CGPA 7.43/10
West Bengal Maulana Abul Kalam Azad University of Technology, West Bengal
(Formerly Known as West Bengal University of Technology)
Thesis: Hydrodynamic Studies on Two Phase Inverse Fluidization Using Non Newtonian Fluid

Higher Secondary (Science) **2007**
'A' Zone Boys Multipurpose School 64.71 %
West Bengal Council of Higher Secondary Education (WBCHSE)

Secondary Examination **2005**
Durgapur Steel Plant A Zone High School 73.88 %
West Bengal Board of Secondary Education (WBBSE)

Membership in Professional Societies

- Graduate Student Member of the Institute of Electrical and Electronics Engineers (**IEEE**/Kolkata Section), Member ID: 93267582.
- Council Member of Indian Institute of Chemical Engineers Guwahati Regional Chapter (**IIChE-GRC**), 2014-2015.
- Life Associate Member of Indian Institute of Chemical Engineers (**IIChE**) since 2015 (LAM-54499).
- Member of International Association of Engineers. **IAENG** membership number is: 204276, (2017).

Skills/Teaching or Research Experiences

- I have eight years of teaching experience as a teaching assistant (TA) and almost eleven years of research experience. My job profile in IIT Guwahati is as a research scholar/teaching assistant.
- As for my strengths, I can state that I enjoy engaging with people from all walks of life and that I have the patience necessary to truly hear what they have to say.
- A multitasker, or someone who can handle multiple tasks at once, is a trait I have developed over time. During my time in college, I organised a number of cultural events and hostel-level tournaments in addition to my academic duties. I'm also eager to take on new projects.
- There is some analytical equipment that I am familiar with, and I'd like to expand my expertise. To emphasise this further, I can mention that I have excellent laboratory management skills, as I and my lab mates have established three new laboratories during my PhD study.
- I also have vast experience in organising seminars as well as workshops. From my B. Tech. studies to date, I am an organising team member of more than fifteen seminars/workshops conducted by us.
- In my course of study/program, I have a good grasp on the use of some educational or analytical software and having knowledge of laboratory processes and computer systems.
- Good written and verbal communication skills including good command of English, Hindi and Bengali language.
- A good technical handling expertise on analytical techniques such as Interfacial Rheometer, ATR-FTIR, NMR, GC-MS, DSC, TGA etc.
- Good technical handling of subcritical and hydrothermal reactors.

- Good command on Microsoft office tools, MATLAB, Design Expert and other modelling and simulations tools.
- I'm familiar with Machine Learning and Artificial Intelligence approaches.

Personal Details

Father: Asit Kumar Paul, retired service person at SAIL.
Mother: Rohita Paul, housewife.
Language Known: Bengali (Mother tongue), English, Hindi

Declarations

I do hereby declare that the particulars of information and facts stated herein above are true, correct and complete to the best of my knowledge and belief.

Place: Guwahati

Date: 28.02.2022

Atanu Kumar Paul

(ATANU KUMAR PAUL)